

*The most beautiful thing we can experience is the mysterious. It is the source of all true art and all science. He to whom this emotion is a stranger, who can no longer pause to wonder and stand rapt in awe, is as good as dead: his eyes are closed.*

— Albert Einstein

*The more that you read, the more things you will know. The more that you learn, the more places you'll go.*

— Theodor Geisel (Dr. Seuss)

University of Alberta

Diffusion Tensor Imaging of Human Brain Development

by

Catherine Alexandra Lebel

A thesis submitted to the Faculty of Graduate Studies and Research  
in partial fulfillment of the requirements for the degree of

Doctor of Philosophy

Medical Sciences — Biomedical Engineering

©Catherine Alexandra Lebel

Fall 2010

Edmonton, Alberta

Permission is hereby granted to the University of Alberta Libraries to reproduce single copies of this thesis and to lend or sell such copies for private, scholarly or scientific research purposes only. Where the thesis is converted to, or otherwise made available in digital form, the University of Alberta will advise potential users of the thesis of these terms.

The author reserves all other publication and other rights in association with the copyright in the thesis and, except as herein before provided, neither the thesis nor any substantial portion thereof may be printed or otherwise reproduced in any material form whatsoever without the author's prior written permission.

# Examining Committee

Christian Beaulieu, Department of Biomedical Engineering

Richard Thompson, Department of Biomedical Engineering

Linda Phillips, Canadian Centre for Research on Literacy

Alan Wilman, Department of Biomedical Engineering

Donald Gross, Department of Neurology

Andrew Alexander, Department of Medical Physics, University of Wisconsin

# Abstract

Structural brain changes occur in a complex manner throughout life, and understanding healthy brain development is crucial for the study of brain abnormalities in various conditions. Diffusion tensor imaging (DTI) is an advanced magnetic resonance imaging technique that provides information about tissue microstructure not accessible via conventional imaging methods. In this dissertation, DTI is used to assess typical brain development, brain abnormalities in fetal alcohol spectrum disorder (FASD), and relationships between cognition and brain structure in both populations.

Cross-sectional and longitudinal DTI studies were used to measure brain maturation from childhood to adulthood. Significant, nonlinear changes of diffusion parameters were noted across the brain, with regional variation in the timing and magnitude of development. Most regions experienced rapid maturation during childhood and adolescence, reached a developmental peak during adulthood, and then, during senescence, underwent a reversal of structural changes that occurred more gradually than the initial development. The genu and splenium of the corpus callosum had the earliest development, while frontal-temporal connections and the corticospinal tracts showed the most prolonged maturation trajectories.

DTI was also used to examine brain abnormalities in children with FASD, an acquired brain disorder associated with numerous cognitive, behavioural, and emotional difficulties. DTI revealed widespread differences in children with FASD when compared to healthy controls, suggesting extensive structural brain damage.

Finally, significant relationships between cognitive abilities and brain structure were observed in both populations. Brain lateralization of a frontal-

temporal pathway correlated with two specific cognitive abilities in typically-developing children. Additionally, a significant relationship between brain structure and mathematical ability was observed in the left parietal lobe of children with FASD. Preliminary results demonstrating reading-brain structure correlations in both healthy and FASD groups are also presented.

In conclusion, DTI has shown significant age-related changes in the typically-developing human brain, abnormalities in children with FASD, and correlations between brain structure and cognition in both populations. Normative DTI studies such as the ones presented here are important to establish healthy milestones of brain development and degradation, which may then be used to understand abnormalities in a variety of conditions, including FASD.

# Acknowledgements

Funding support for my graduate degree was provided by the Natural Sciences and Engineering Research Council (NSERC), the Alberta Heritage Foundation for Medical Research (AHFMR), the Department of Biomedical Engineering, and the University of Alberta. Thanks to the Canadian Language and Literacy Research Network (CLLRNet) and Canadian Institutes of Health Research (CIHR) for operating grants, and to the Canada Foundation for Innovation (CFI), Alberta Science and Research Authority, AHFMR, and the University Hospital Foundation for the MRI infrastructure that allowed me to conduct my research. Thanks also to the hundreds of volunteers from down the hall, across the country, and many places in between, who donated their time to provide me with data — this thesis would not exist without you.

I am deeply grateful for all of the advice, assistance, and encouragement provided to me over the years by so many different people. I have been blessed to have encouraging friends and family members, patient and supportive teachers and mentors, knowledgeable collaborators, sympathetic fellow students, and very helpful administrative staff; I do not have space to thank you all by name, but I appreciate all of your contributions.

I will specifically thank a few people — first, my supervisor Christian for guiding me in (what I hope is!) the right direction and for giving me so many exciting opportunities along the way. I have come to appreciate the barely-recognizable drafts of papers returned to me and I look forward to a few more to come! Thanks to the other members of my supervisory committee

— Richard Thompson and Linda Phillips — for useful discussions, advice, and numerous reference letters. Also thanks to the many other faculty, staff, and students in Biomedical Engineering and beyond who have helped me find my way through graduate school.

Thank you to my family and friends for listening to me drone on about research, sympathizing with me through the tough times, celebrating with me during the successes, and providing much-needed reality checks and distractions as appropriate. With a mix of support and humour, you've kept me grounded and made life inside and outside the lab quite enjoyable.

Finally, thanks most of all to my husband Marc — a fellow student, family member, and best friend rolled into one! Not only do you calm me down, perk me up, and cheer me on, you are a fantastic MR dictionary! Thanks for being there since the beginning of my foray into the world of MRI; I look forward to pestering you with questions for many more years to come!

– Catherine

July 2010

# Table of Contents

<b>Introduction</b>	<b>1</b>
<b>1 Introduction</b>	<b>1</b>
<b>2 Diffusion Imaging</b>	<b>5</b>
2.1 Diffusion . . . . .	5
2.2 Diffusion Imaging . . . . .	6
2.2.1 Diffusion Weighted Imaging . . . . .	6
2.2.2 The Diffusion Tensor . . . . .	9
2.3 Interpretation of Diffusion Parameters . . . . .	17
2.4 Analysis Techniques for Diffusion Tensor Images . . . . .	18
2.4.1 Region of Interest Analysis . . . . .	18
2.4.2 Tractography . . . . .	19
2.4.3 Voxel Based Morphometry . . . . .	21
<b>3 Human Brain Development</b>	<b>24</b>
3.1 Important Brain Features . . . . .	24
3.1.1 Brain Tissues . . . . .	24
3.1.2 The Cerebrum . . . . .	26
3.1.3 The Cerebellum . . . . .	27
3.1.4 The Limbic System . . . . .	27
3.1.5 The Corpus Callosum . . . . .	28
3.1.6 Projection Fibres . . . . .	29

3.1.7	Association Fibres . . . . .	30
3.1.8	Deep Gray Matter Structures . . . . .	32
3.2	Brain Development Across the Lifespan . . . . .	32
<b>4</b>	<b>Fetal Alcohol Spectrum Disorder</b>	<b>35</b>
4.1	Characteristics . . . . .	35
4.2	Diagnosis . . . . .	37
4.3	Common Brain Abnormalities . . . . .	38
	<b>Research</b>	<b>43</b>
<b>5</b>	<b>Normal Brain Maturation During Childhood and Adolescence</b>	<b>43</b>
5.1	Introduction . . . . .	44
5.2	Methods . . . . .	46
5.2.1	Subjects . . . . .	46
5.2.2	Image Acquisition . . . . .	46
5.2.3	Region-of-Interest Diffusion Measurements . . . . .	47
5.2.4	Fibre Tracking Diffusion Measurements . . . . .	47
5.2.5	Automated Fibre Tracking Reliability . . . . .	49
5.2.6	Curve Fitting . . . . .	49
5.2.7	Volume Measurements . . . . .	51
5.3	Results . . . . .	51
5.3.1	FA Increases with Age . . . . .	51
5.3.2	MD Decreases with Age . . . . .	54
5.3.3	Timing and Magnitude of Changes . . . . .	58
5.3.4	Volume . . . . .	58
5.4	Discussion . . . . .	58
5.5	Conclusion . . . . .	68

<b>6</b>	<b>Longitudinal Brain Development</b>	<b>69</b>
6.1	Introduction . . . . .	70
6.2	Methods . . . . .	71
6.2.1	Subjects . . . . .	71
6.2.2	Image Acquisition . . . . .	72
6.2.3	Tractography . . . . .	72
6.2.4	Diffusion Measurements . . . . .	73
6.2.5	Inter-Scan Reliability . . . . .	73
6.2.6	Statistical Analysis . . . . .	73
6.2.7	Diffusivities . . . . .	74
6.2.8	Brain Volume . . . . .	74
6.3	Results . . . . .	75
6.3.1	Inter-scan Reliability . . . . .	75
6.3.2	FA Increases with Age . . . . .	79
6.3.3	MD Decreases with Age . . . . .	79
6.3.4	Sex Differences . . . . .	79
6.3.5	Group Analysis of Age-Related Changes . . . . .	81
6.3.6	Magnitude of FA and MD changes . . . . .	81
6.3.7	Diffusivities . . . . .	82
6.3.8	Brain Volumes . . . . .	84
6.4	Discussion . . . . .	85
6.5	Conclusion . . . . .	89
<b>7</b>	<b>Age-Related Regional Variation of the Corpus Callosum</b>	<b>90</b>
7.1	Introduction . . . . .	91
7.2	Methods . . . . .	93
7.2.1	Subjects . . . . .	93
7.2.2	Image Acquisition . . . . .	93

7.2.3	Tractography . . . . .	93
7.2.4	Tract Volume . . . . .	96
7.2.5	Curve Fitting . . . . .	96
7.2.6	Parallel and Perpendicular Diffusivity . . . . .	97
7.2.7	Gender and Handedness . . . . .	97
7.2.8	Midline Corpus Callosum DTI Analysis . . . . .	97
7.3	Results . . . . .	99
7.3.1	Tract Volume . . . . .	99
7.3.2	Fractional Anisotropy Changes with Age . . . . .	99
7.3.3	Mean Diffusivity Changes with Age . . . . .	101
7.3.4	DTI Parameter Timing Differences . . . . .	101
7.3.5	Diffusivities . . . . .	105
7.3.6	Sex Differences . . . . .	105
7.3.7	Midline Corpus Callosum DTI Analysis . . . . .	107
7.4	Discussion . . . . .	108
7.5	Conclusion . . . . .	114
<b>8</b>	<b>Arcuate Fasciculus Lateralization and Cognition</b>	<b>115</b>
8.1	Introduction . . . . .	116
8.2	Methods . . . . .	118
8.2.1	Subjects . . . . .	118
8.2.2	Cognitive Assessment . . . . .	118
8.2.3	Image Acquisition . . . . .	119
8.2.4	Fibre Tracking Diffusion Measurements . . . . .	120
8.2.5	Statistical Analysis . . . . .	121
8.3	Results . . . . .	123
8.3.1	Lateralization Indices . . . . .	123
8.3.2	Age and Gender Differences . . . . .	126

8.3.3	Cognitive Assessments and Lateralization . . . . .	126
8.4	Discussion . . . . .	127
8.5	Conclusion . . . . .	132
<b>9</b>	<b>Brain Diffusion Abnormalities in Fetal Alcohol Spectrum Disorder</b>	<b>133</b>
9.1	Introduction . . . . .	134
9.2	Methods . . . . .	136
9.2.1	Subjects . . . . .	136
9.2.2	Cognitive Assessment . . . . .	137
9.2.3	Image Acquisition . . . . .	137
9.2.4	Region-of-Interest Diffusion Measurements . . . . .	138
9.3	Fibre Tracking Diffusion Measurements . . . . .	139
9.3.1	Volume Measurements . . . . .	140
9.3.2	Statistical Analysis . . . . .	140
9.4	Results . . . . .	140
9.4.1	Cognitive Testing . . . . .	140
9.4.2	Structural Imaging and Volume . . . . .	141
9.4.3	Diffusion Parameters . . . . .	144
9.5	Discussion . . . . .	146
9.6	Conclusion . . . . .	151
<b>10</b>	<b>Brain Structure and Mathematical Ability in Fetal Alcohol Spectrum Disorder</b>	<b>152</b>
10.1	Introduction . . . . .	153
10.2	Methods . . . . .	155
10.2.1	Subjects . . . . .	155
10.2.2	Cognitive Assessment . . . . .	157
10.2.3	Image Acquisition . . . . .	158

10.2.4	Voxel-Based Image Analysis . . . . .	158
10.2.5	Diffusivities . . . . .	159
10.2.6	Tractography . . . . .	159
10.3	Results . . . . .	160
10.3.1	Quantitative Concepts Scores . . . . .	160
10.3.2	Correlations of FA with Math Scores . . . . .	161
10.3.3	Right-handed Subjects Only . . . . .	162
10.3.4	Diffusivities . . . . .	162
10.3.5	White Matter Tracts Passing Through Clusters . . . . .	166
10.4	Discussion . . . . .	166
10.5	Conclusion . . . . .	172
<b>11</b>	<b>Ongoing Projects</b>	<b>173</b>
11.1	Brain Changes Across the Lifespan . . . . .	173
11.1.1	Introduction . . . . .	173
11.1.2	Methods . . . . .	175
11.1.3	Results . . . . .	178
11.1.4	Discussion . . . . .	184
11.1.5	Future Directions . . . . .	188
11.2	Reading Ability in Fetal Alcohol Spectrum Disorder . . . . .	189
11.2.1	Introduction . . . . .	189
11.2.2	Methods . . . . .	189
11.2.3	Results . . . . .	190
11.2.4	Discussion . . . . .	191
11.2.5	Future Directions . . . . .	192
	<b>Conclusions</b>	<b>195</b>
	<b>12 Limitations and Future Directions</b>	<b>195</b>

<b>13 Conclusions</b>	<b>203</b>
<b>Bibliography</b>	<b>229</b>
<b>Appendices</b>	<b>230</b>
<b>A Template Creation</b>	<b>230</b>
<b>B Tracking Fibres</b>	<b>232</b>
<b>C Semi-Automated Tractography: A step-by-step tutorial</b>	<b>238</b>
C.1 Preparation of Files . . . . .	238
C.2 Selection of Seeding, Target, and Exclusion Regions . . . . .	242
C.3 Tracking the Fibres . . . . .	242
C.4 Analyzing the Tracts . . . . .	244
C.5 Rejection of Tracts . . . . .	245
<b>D Automated Tractography</b>	<b>247</b>
D.1 Preparation of Files . . . . .	247
D.2 Tracking of Fibres . . . . .	249
<b>E Voxel-Based Analysis</b>	<b>251</b>
E.1 Normalization of Images . . . . .	251
E.2 Smoothing of Images . . . . .	252
E.3 Statistical Analysis . . . . .	253
<b>F Stereograms</b>	<b>258</b>

# List of Tables

5.1	Validation of semi-automated tractography . . . . .	50
5.2	Exponential fitting parameters for FA-age curves . . . . .	55
5.3	Exponential fitting parameters for MD-age curves . . . . .	59
6.1	Inter-scan reliability . . . . .	76
6.2	Longitudinal fitting parameters . . . . .	77
7.1	Fitting parameters for best fit equations . . . . .	100
7.2	Differences of peak and minimum ages among regions . . . . .	104
8.1	Cognitive assessments on 68 children . . . . .	119
8.2	Group lateralization characteristics . . . . .	125
9.1	FASD cognitive scores . . . . .	141
9.2	Diffusion abnormalities in FASD . . . . .	143
10.1	FASD subject characteristics . . . . .	156
10.2	Location of significant clusters . . . . .	160
11.1	Poisson curve fitting parameters for each tract . . . . .	179

# List of Figures

2.1	Stejskal-Tanner pulsed gradient spin echo sequence . . . . .	7
2.2	Diffusion ellipsoid . . . . .	10
2.3	Raw DTI images . . . . .	11
2.4	The diffusion tensor . . . . .	13
2.5	Mean diffusivity maps . . . . .	14
2.6	Fractional anisotropy maps . . . . .	15
2.7	FA and MD maps . . . . .	15
2.8	Colour maps . . . . .	16
2.9	Regions-of-interest measurements . . . . .	19
2.10	Diffusion tractography . . . . .	20
3.1	Tissue segmentation . . . . .	25
3.2	The human brain . . . . .	26
3.3	Limbic system fibres . . . . .	28
3.4	The corpus callosum . . . . .	29
3.5	Projection fibres . . . . .	30
3.6	Association fibres . . . . .	31
3.7	Tissue components at different ages . . . . .	34
4.1	Facial features of FAS . . . . .	36
4.2	Key brain abnormalities in FASD . . . . .	41
5.1	Age-related FA increases measured by tractography . . . . .	52

5.2	Age-related FA increases measured by ROI analysis . . . . .	53
5.3	Age-related changes of parallel and perpendicular diffusivities . . . . .	54
5.4	Age-related MD decreases measured by tractography . . . . .	56
5.5	Age-related MD decreases measured by ROI analysis . . . . .	57
5.6	Magnitude and timing of developmental changes . . . . .	60
5.7	Volume changes with age . . . . .	61
6.1	Reliability of tractography measures . . . . .	75
6.2	Age-related changes of fractional anisotropy . . . . .	78
6.3	Age-related changes of mean diffusivity . . . . .	80
6.4	Percent changes of FA and MD within age groups . . . . .	83
6.5	Age-related changes of parallel and perpendicular diffusivity . . . . .	84
6.6	Volume changes with age . . . . .	85
7.1	Corpus callosum parcellation by tractography . . . . .	94
7.2	Voxel proportions of corpus callosum subregions . . . . .	98
7.3	Fractional anisotropy and mean diffusivity versus age . . . . .	102
7.4	Best fit curves for fractional anisotropy and mean diffusivity versus age . . . . .	103
7.5	Parallel and perpendicular diffusivity . . . . .	106
7.6	Best fit Poisson curves of fractional anisotropy for midline . . . . .	107
8.1	Arcuate fasciculus fibre tracking methods . . . . .	122
8.2	Arcuate fasciculus lateralization index versus age . . . . .	124
8.3	Mean cognitive scores for lateralization groups . . . . .	126
8.4	Lateralization index versus PPVT and phonological processing scores . . . . .	127
9.1	Sample FA and MD maps . . . . .	138
9.2	Brain volume differences . . . . .	142

9.3	White matter abnormalities . . . . .	144
9.4	Gray matter abnormalities . . . . .	145
9.5	Changes of diffusion parameters with age . . . . .	149
10.1	Significantly correlated clusters of fractional anisotropy versus math ability in 21 children with FASD . . . . .	161
10.2	Correlations between math scores and fractional anisotropy . .	163
10.3	Parallel and perpendicular diffusivities . . . . .	164
10.4	White matter tracts passing through significant clusters . . . .	165
10.5	Parietal FA-math clusters in relation to the left IPS . . . . .	167
11.1	Plots of fractional anisotropy age-related changes across the lifespan. . . . .	180
11.2	Plots of mean diffusivity age-related changes across the lifespan.	181
11.3	Relative timing and magnitude of diffusion parameter changes	183
11.4	FA-reading clusters in control and FASD subjects . . . . .	191
11.5	FA-reading left parietal cluster in controls . . . . .	193
11.6	FA-reading right frontal cluster in FASD . . . . .	193
12.1	Image distortion in EPI . . . . .	196
12.2	Tract widths . . . . .	197
A.1	Colour maps for the semi-automated tractography template .	231
B.1	Fibre tracking: anterior limb of the internal capsule, body of the corpus callosum, cingulum . . . . .	233
B.2	Fibre tracking: corticospinal tracts, fornix, genu of the corpus callosum . . . . .	234
B.3	Fibre tracking: inferior fronto-occipital fasciculus, inferior lon- gitudinal fasciculus, splenium of the corpus callosum . . . . .	235

B.4	Fibre tracking: superior fronto-occipital fasciculus, superior longitudinal fasciculus, uncinate fasciculus . . . . .	236
B.5	Fibre tracking: fornix with CSF-suppressed data . . . . .	237
C.1	SPM: Normalise: Estimate . . . . .	240
C.2	SPM: Deformations . . . . .	241
E.1	SPM Normalise: Estimate & Write . . . . .	252
E.2	SPM: Smooth . . . . .	253
E.3	SPM: Specify 2nd-level . . . . .	254
E.4	SPM Results: Contrast . . . . .	255
E.5	SPM Results . . . . .	257
F.1	Tract stereogram . . . . .	258
F.2	Math clusters stereogram . . . . .	259
F.3	Corpus callosum stereogram . . . . .	259

# List of Abbreviations and Symbols

A	Anterior, page 122
ADC	Apparent diffusion coefficient, page 7
AF	Anterior frontal (corpus callosum), page 95
ALIC	Anterior limb of the internal capsule, page 176
b0	Non diffusion-weighted image, $b = 0 \text{ s/mm}^2$ , page 10
bCC	Body of the corpus callosum, page 176
C	Celsius, page 6
CC	Corpus callosum, page 143
CREVT	Comprehensive Receptive & Expressive Vocabulary Test, page 137
CSF	Cerebrospinal fluid, page 12
CST	Corticospinal tract, page 49
DTI	Diffusion tensor imaging, page 1
EPI	Echo-planar imaging, page 158
FA	Fractional anisotropy, page 12
FAS	Fetal alcohol syndrome, page 35
FASD	Fetal alcohol spectrum disorder, page 2

FLAIR	Fluid-attenuated inversion recovery, page 46
FWE	Family-wise error, page 256
FWHM	Full-width at half maximum, page 253
gCC	Genu of the corpus callosum, page 176
IFO	Inferior fronto-occipital fasciculus, page 49
ILF	Inferior longitudinal fasciculus, page 49
IPS	Intraparietal sulcus, page 168
L	Left, page 122
LI	Lateralization index, page 121
MANCOVA	Multiple analysis of covariance, page 140
MANOVA	Multiple analysis of variance, page 96
MD	Mean diffusivity, page 12
MPRAGE	Magnetization-prepared gradient echo, page 46
MRI	Magnetic resonance imaging, page 1
NAA	N-acetyl aspartate, page 39
NBD:AE	Neurobehavioural disorder: alcohol exposed, page 37
NEPSY	Neuropsychological assessment tool, page 118
NMR	Nuclear magnetic resonance, page 6
Occ	Occipital (corpus callosum), page 95
OF	Orbital frontal (corpus callosum), page 95
P	Posterior, page 122
pFAS	Partial fetal alcohol syndrome, page 37

PP	Posterior parietal (corpus callosum), page 95
PPVT	Peabody Picture Vocabulary Test, page 119
R	Right, page 122
ROI	Region of interest, page 18
sCC	Splenium of the corpus callosum, page 176
SE:AE	Static encephalopathy: alcohol exposed, page 37
SF	Superior frontal (corpus callosum), page 95
SFO	Superior fronto-occipital fasciculus, page 49
SLF	Superior longitudinal fasciculus, page 49
SNR	Signal to noise ratio, page 10
SP	Sentinel physical findings, page 156
SP	Superior parietal (corpus callosum), page 95
SPM	Statistical parametric mapping, page 51
T	Tesla (SI unit of magnetic flux density), page 8
T1	Transverse relaxation time, page 24
TBSS	Tract-based spatial statistics, page 22
TE	Echo time, page 46
Temp	Temporal (corpus callosum), page 95
TI	Inversion time, page 46
TONI	Test of Nonverbal Intelligence, page 119
TR	Recovery time, page 46
UF	Uncinate fasciculus, page 49

VBM	Voxel based morphometry, page 21
WJ	Woodcock-Johnson, page 137
WMTB-C	Working Memory Test Battery for children, page 137
WRMT	Woodcock Reading Mastery Test, page 137
$b$	Diffusion weighting, page 8
$D$	Diffusion coefficient, page 5
$\Delta$	Separation of diffusion-sensitizing gradients, page 7
$\delta$	Duration of diffusion-sensitizing gradients, page 7
$\gamma$	Gyromagnetic ratio (42.6 MHz/T for protons), page 8
$G$	Strength of diffusion-sensitizing gradients, page 7
$\lambda_1, \lambda_2, \lambda_3$	Eigenvalues 1, 2, and 3 (in descending order), page 12
$\lambda_{\parallel}$	Parallel diffusivity (equivalent to $\lambda_1$ ), page 16
$\lambda_{\perp}$	Perpendicular diffusivity (average of $\lambda_2$ and $\lambda_3$ ), page 16
$n$	Number of dimensions, page 5
$\langle r^2 \rangle$	Mean squared displacement, page 5
$S$	Signal from diffusion-weighted image, page 7
$S_0$	Signal from non diffusion-weighted image, page 7
$t$	Diffusion time, page 5

# Chapter 1

## Introduction

Structural brain changes involve complex processes that occur throughout life, and are linked to cognitive, behavioural, and emotional maturation. There are many conditions considered developmental disorders (e.g., autism, attention-deficit hyperactivity disorder, Williams syndrome) and others considered aging diseases (e.g., Alzheimer’s Disease, dementia) that are related to altered brain structure. In order to properly study the progression of brain changes in these abnormal diseases and conditions, there must first exist a thorough understanding of healthy or “normal” brain development. Several key autopsy studies provided early insight into healthy brain changes (Benes, 1989; Yakovlev and Lecours, 1967), but it was the advent of in vivo neuroimaging methods that allowed for investigation of much larger and more diverse populations.

Diffusion tensor imaging (DTI), in particular, is an advanced, quantitative magnetic resonance imaging (MRI) technique for measuring the microstructural properties of tissues. DTI is sensitive to the Brownian motion of water molecules and is thus able to probe tissue microstructure, providing measures typically associated with myelination and axonal packing of white matter structures. Furthermore, diffusion tractography is a DTI analysis tool that allows for virtual reconstruction, visualization and assessment of white matter connections in vivo.

DTI is an attractive method for investigating age-related brain changes because it provides a more sensitive measure than conventional imaging methods

(Basser et al., 1994; Beaulieu, 2002; Le Bihan, 2003). DTI has been widely used to study brain abnormalities in various diseases and conditions, including obsessive-compulsive disorder (White et al., 2008), autism (Alexander et al., 2007a), schizophrenia (Kyriakopoulos et al., 2008), Alzheimer’s disease (Chua et al., 2008), and many more. DTI has also been used by multiple studies to investigate age-related changes in healthy subjects, demonstrating development through infancy, childhood, and adolescence (Barnea-Goraly et al., 2005b; Dubois et al., 2006; Hermoye et al., 2006; Schmithorst et al., 2002), and demonstrating opposite trends occurring later in life during the aging process (Hsu et al., 2010; Ota et al., 2006; Pfefferbaum et al., 2000).

When this thesis was started, most studies examining healthy brain development had small sample sizes, limited age ranges, and/or only analyzed a few brain structures. One of the original goals of this thesis was to address these issues by generating a large sample of healthy subjects across a wide age range, and performing a comprehensive analysis of age-related structural changes in the brain. Chapters 5, 6, 7, and the ongoing work presented in Section 11.1 attempt to address these issues by examining development across wide age ranges in large numbers of subjects. Chapter 5 focuses on cross-sectional development from childhood to adulthood (subjects aged 5–30 years), examining 20 different brain structures, and Chapter 6 extends this work to a longitudinal study across the same age span. Development of the corpus callosum and its subdivisions are described across a larger age range (5–59 years) in Chapter 7, and Section 11.1 details the development of 12 major white matter tracts across most of the lifespan (5–83 years).

The secondary purpose of this thesis was to investigate brain development under abnormal conditions, specifically fetal alcohol spectrum disorder (FASD). FASD is a developmental disorder attributed to prenatal alcohol exposure that can lead to many behavioural and neurological impairments, including structural brain damage (Jacobson and Jacobson, 2002; Riley and McGee, 2005). At the time of conception of this project, only two previous studies had used DTI to investigate FASD, both examining only the corpus callosum (Ma et al., 2005; Wozniak et al., 2006). Therefore, the question remained: which

other brain structures are affected by prenatal alcohol exposure? Chapter 9 addresses this question by examining ten major white matter tracts and four deep gray matter structures in children with FASD compared to a group of healthy controls.

From these original goals came several additional projects exploring the relationship between brain structure and cognition. Structural lateralization of language has long been known (Broca, 1861; Wernicke, 1874), yet the relationship between structural asymmetry and cognition remains poorly understood. In 2007, another group published a paper outlining the effects of lateralization of the arcuate fasciculus, a major white matter tract involved in language and intelligence, on cognitive ability in adults (Catani et al., 2007). With our large data set, including cognitive scores from many of the children aged 5–13 years, we were able to complete a study exploring lateralization and its relationship to cognitive abilities in children (Chapter 8).

Another secondary project that developed was related to mathematical abilities in children with FASD. Although individuals with FASD have trouble with many cognitive domains, mathematics is often considered a particular difficulty (Howell et al., 2006). Mathematical disability is relatively common in the general population, at approximately 5–6% (Shalev, 2004), but had only been investigated by two previous DTI studies, one in a rare genetic disorder (Barnea-Goraly et al., 2005a), and one in healthy children (van Eimeren et al., 2008). Children with FASD provide an interesting group to study due to their wide range of mathematical ability and brain abnormalities. Therefore, using the mathematics scores obtained on the children with FASD, we examined correlations between brain structure and cognitive performance in 21 subjects; this work is presented in Chapter 10. Section 11.2 describes ongoing work measuring correlations between reading ability and brain structure in children and adolescents with FASD, as well as healthy controls. Preliminary results and future directions with respect to this project are discussed.

Appendices A through E present a more detailed explanation of the methods used in this thesis than are given in each individual methods section. Specifically, detailed instructions for both manual and semi-automated trac-

tography, as well as voxel-based analysis are provided.

As stated by Dr. Seuss in the quote provided at the beginning of this thesis, “The more you read... the more places you’ll go”. Therefore, I have provided over 250 pages for your reading pleasure and any world-traveller aspirations you may have. The last chapter, Appendix F, has some stereograms (like Magic Eyes) for added enjoyment, so if you get bored, just skip straight to the pretty pictures.

# Chapter 2

## Diffusion Imaging

### 2.1 Diffusion

Diffusion refers to the constant, random motion of particles suspended in a liquid or a gas. Although there are several earlier reports describing diffusion, the discovery of this irregular motion is typically attributed to observations made by Robert Brown in 1827, and this type of motion now bears his name — Brownian motion (Brown, 1828, 1829; Lemons, 2002; Nelson, 2001). Brown observed and described the rapid, irregular movement of both pollen and dust molecules in water, and illustrated the importance of this phenomenon to the wider scientific community.

Almost 100 years later, in the early 20th century, Albert Einstein further described and quantified molecular diffusion, representing Brown's observations as a mathematical relationship between time and distance for diffusion in a medium with no concentration gradient (Einstein, 1905). This relationship in one dimension gives:

$$\langle r^2 \rangle = 2Dt \tag{2.1}$$

where  $\langle r^2 \rangle$  represents the mean squared displacement,  $D$  is the diffusion coefficient, and  $t$  is the time of diffusion. Therefore, in free space, particles move an average distance of  $\sqrt{2Dt}$  in one dimension during time  $t$ . This equation can be generalized to  $\langle r^2 \rangle = 2Dtn$  for  $n$  dimensions, from which it can be determined that average displacement in three dimensions is  $\sqrt{6Dt}$ .

Although the average distance travelled by molecules increases with time or with the diffusion coefficient, it is important to note that the average displacement remains constant at zero, since diffusion is equally likely to occur in all directions.

If the time and mean distance are known, it is easy to solve for the diffusion coefficient,  $D$ . The diffusion coefficient varies with temperature, pressure, and viscosity of the medium, as well as the size of the molecule diffusing; however, for diffusion imaging, these are assumed constant for the duration of the experiment. In the case of water, the medium and the molecule are the same, and the process is technically known as self-diffusion, although it is commonly referred to as diffusion. The diffusion coefficient of water at 25°C is approximately  $2.4 \times 10^{-3}$  mm<sup>2</sup>/s, and at body temperature (37°C) it is  $3.0 \times 10^{-3}$  mm<sup>2</sup>/s (Mills, 1973).

## 2.2 Diffusion Imaging

### 2.2.1 Diffusion Weighted Imaging

During a nuclear magnetic resonance (NMR) experiment, water diffusion reduces the signal available for measurement because molecules are moving among different local fields. This effect was first noted by Hahn in his 1950 analysis of spin echoes (Hahn, 1950). In some cases, this phenomenon is a nuisance, but in others, it is useful because it makes measurement of diffusion coefficients possible using NMR. The effects of diffusion on the NMR signal were further described by Carr and Purcell, who used NMR to measure the diffusion coefficient of water in the early 1950s (Carr and Purcell, 1954). Around the same time, Torrey added a diffusion term accounting for additional signal loss to the Bloch equations, which describe the behaviour of magnetization in an NMR experiment over time (Torrey, 1956). One problem with the early diffusion measurements was the use of a constant field gradient, which increases noise as one tries to measure smaller diffusion coefficients; this makes it difficult to distinguish signal loss due to diffusion from that due to transverse relaxation.

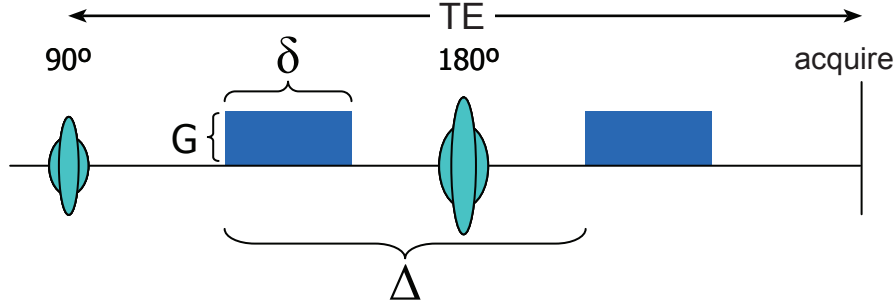


Figure 2.1: The Stejskal-Tanner pulsed gradient spin echo sequence uses two equal gradients of strength  $G$  and duration  $\delta$ , separated by time  $\Delta$ , on either side of the  $180^\circ$  refocusing pulse. These gradients fully refocus any spins that have not moved in the same direction as the diffusion gradients during the diffusion time; any spins that have moved are not completely refocused, resulting in signal loss.

In 1965, Stejskal and Tanner introduced a pulsed gradient spin echo method for measuring diffusion that overcame the problems associated with the constant gradient. Their approach uses the spin echo method, with two equal diffusion-sensitizing gradients placed on either side of the  $180^\circ$  refocusing pulse (see Figure 2.1). The gradients are of equal strength ( $G$ ) and equal duration ( $\delta$ ), separated by time  $\Delta$ , and can be applied in any Cartesian direction, as long as the direction is the same for both gradients. The diffusion time is calculated as  $\Delta - \delta/3$ , which accounts for diffusion that occurs between the gradients and while they are applied. Any spins that do not move in the direction of the diffusion-sensitizing gradients during the diffusion time will be completely refocused by the equal gradient after the refocusing pulse. However, when spins move in the direction of the diffusion gradient, they experience different fields and will not be completely refocused. By assuming that local background gradients are negligible and that applied gradients are linear, the Bloch-Torrey equations can be solved to give an expression relating the measured signal ( $S$  for the diffusion-weighted image;  $S_0$  for the non diffusion-weighted image) to the apparent diffusion coefficient (ADC):

$$\ln \left( \frac{S}{S_0} \right) = -\gamma^2 \delta^2 G^2 \left( \Delta - \frac{\delta}{3} \right) ADC \quad (2.2)$$

The diffusion coefficient measured in MRI is properly referred to as the apparent diffusion coefficient rather than simply the diffusion coefficient, because

it is not measured directly, and the water molecules are not diffusing freely. In fact, the measured ADC will vary depending on the interactions of the water molecules with their local environment, thus providing valuable information about the structure of the tissue being measured. Equation 2.2 is generally simplified to:

$$\frac{S}{S_0} = e^{-bADC} \quad (2.3)$$

where the diffusion sensitivity,  $b$ , depends on the gyromagnetic ratio and the sequence parameters according to:

$$b = \gamma^2 G^2 \delta^2 \left( \Delta - \frac{\delta}{3} \right) \quad (2.4)$$

Equations 2.2 and 2.4 show that diffusion sensitivity and the resulting signal loss depend on  $G$ ,  $\delta$ , the gyromagnetic ratio  $\gamma$ , and the diffusion time  $\Delta - \delta/3$ . With the exception of  $\gamma$ , which is constant for any species ( $\gamma = 42.6$  MHz/T for protons), these parameters can be manipulated to change the diffusion sensitivity of the sequence. Higher diffusion sensitivity of a sequence will cause greater signal loss.

Due to barriers such as cell membranes, diffusion in the human brain does not occur freely. Since the orientation and density of barriers varies within the brain itself and depends on (among other things) tissue type, age, and pathology, diffusion coefficients calculated at different locations within the brain will be different. Since temperature and pressure are assumed constant, differences in the ADC values calculated at various locations in the brain are assumed to reflect differences of tissue microstructure.

Diffusion-weighted images of the brain can be achieved by using any type of diffusion encoding gradients designed to decrease signal in proportion to the amount of diffusion occurring. Measurements of ADC, however, require a minimum of two images with different b-values (diffusion sensitivities) in order to solve Equation 2.3 for ADC. Typically, one of these images will have no diffusion weighting (i.e.  $b = 0$  s/mm<sup>2</sup>) and the other will have a b-value in the range of 700–1500 s/mm<sup>2</sup>. It is important to keep in mind when mea-

suring ADC using this type of sequence, that one is only measuring ADC in the direction of the applied diffusion-sensitizing gradients; diffusion-weighted images are insensitive to motion occurring in other directions. As explained in Section 2.2.2, ADC may vary quite substantially with direction.

## 2.2.2 The Diffusion Tensor

Several definitive papers in the early 1990s demonstrated that the measured diffusivity of water molecules in human brain white matter depends on the direction of the applied diffusion sensitizing gradients (Chenevert et al., 1990; Doran et al., 1990; Douek et al., 1991). It was noted in these studies that diffusion was higher when diffusion-sensitizing gradients and nerve fibres were oriented parallel to each other rather than when they were perpendicular. It is easy to orient diffusion gradients parallel and perpendicular to fibres in excised nerves to measure anisotropy; however, it is much more difficult to orient the diffusion sensitizing gradients parallel and perpendicular to in vivo human brain neurons due to their complex orientations. Therefore, another method is needed in order to fully assess anisotropy in vivo. This technique is diffusion tensor imaging (DTI) (Basser et al., 1994), and it uses multiple diffusion encoding directions to estimate the diffusion tensor, which characterizes diffusion in three dimensions. Equation 2.3 can be rewritten for three dimensions as:

$$\ln\left(\frac{S}{S_0}\right) = -\sum_{i=1}^3 \sum_{j=1}^3 b_{ij} ADC_{ij} \quad (2.5)$$

which is expanded for x, y, and z to give:

$$\begin{aligned} \ln\left(\frac{S}{S_0}\right) = & - (b_{xx}ADC_{xx} + 2b_{xy}ADC_{xy} + 2b_{xz}ADC_{xz} \\ & + b_{yy}ADC_{yy} + 2b_{yz}ADC_{yz} + b_{zz}ADC_{zz}) \end{aligned} \quad (2.6)$$

The tensor can now be calculated from the three-dimensional signal equation, and is represented mathematically by a  $3 \times 3$  symmetric, positive definite matrix of the form:

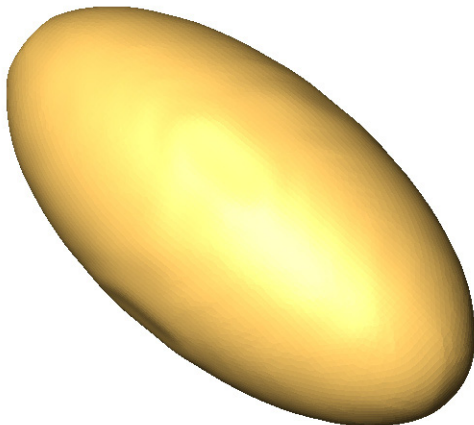


Figure 2.2: An example of an ellipsoid representing diffusion in all directions

$$ADC = \begin{bmatrix} ADC_{xx} & ADC_{xy} & ADC_{xz} \\ ADC_{yx} & ADC_{yy} & ADC_{yz} \\ ADC_{zx} & ADC_{zy} & ADC_{zz} \end{bmatrix} \quad (2.7)$$

An intuitive way to visualize the diffusion tensor is as an ellipsoid (see Figure 2.2), which represents the diffusivity in each direction. Using DTI, we are able to measure the diffusion tensor, and thus characterize diffusion in every direction.

With six unique elements, at least six equations are needed to solve the tensor, so diffusion must be measured using a minimum of six different gradient directions. At least one non diffusion-weighted image ( $b = 0$  s/mm<sup>2</sup>, often referred to as “b0”) is also required. The diffusion sensitizing gradients may be applied in any particular direction, but the multiple directions must be non-collinear and non-coplanar in order to solve for the tensor. In practice, DTI is often performed with many more than six directions (even more than 100 in some cases), although six are sufficient. Studies have shown that with signal-to-noise (SNR) ratios below approximately 15 (Jones, 2004), the use of 30 or more diffusion-encoding directions is beneficial for robust estimates of diffusion parameters. However, the problems associated with fewer directions diminish greatly with higher SNR values (approximately 30 or higher), and there is likely little difference between studies using six directions or those using more in terms of ability to detect group differences in diffusion parameters, as long as SNR is high (Landman et al., 2007; Ni et al., 2006). Figure 2.3

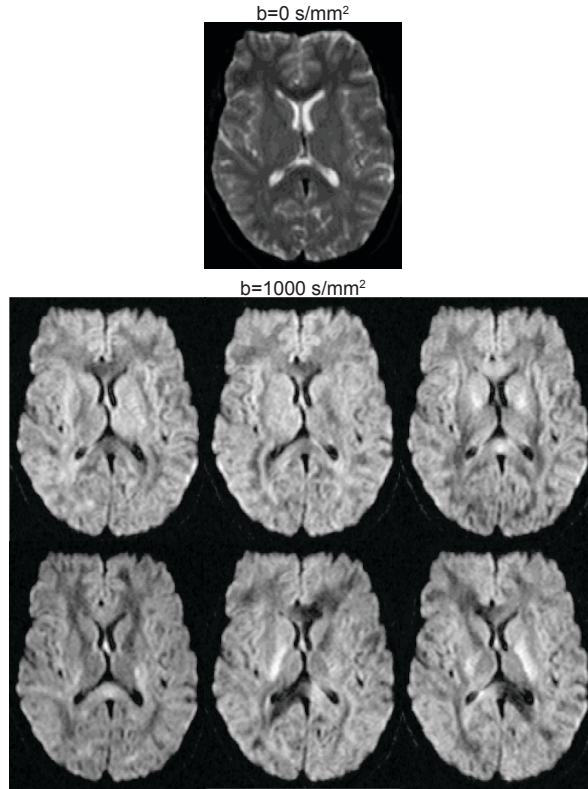


Figure 2.3: Raw DTI Images acquired using 6 diffusion-sensitizing gradient directions and a b-value of  $1000 \text{ s/mm}^2$ . The non diffusion-weighted image ( $b_0$ ) is shown on top, with the 6 diffusion-weighted images below.

demonstrates the raw data acquired when 6 diffusion sensitizing gradients and one  $b_0$  acquisition are used. The  $b_0$  image on top has no diffusion weighting, while the six lower images all have a diffusion weighting of  $b = 1000 \text{ s/mm}^2$  in six different directions. Because diffusion weighting reduces the signal in proportion to the amount of diffusion occurring, areas with more diffusion appear dark in the raw images, while bright areas have little diffusion in the direction of that acquisition gradient. Note the directional dependence in the images, particularly in white matter regions such as the corpus callosum and internal capsule, which appears bright and dark in different images.

The images in Figure 2.3 may be used to calculate the tensor shown in Figure 2.4. Recall that the tensor is a symmetric, positive definite matrix with six unique elements. The diagonal elements of the tensor represent diffusivity in the x, y, and z directions, respectively, according to the applied diffusion

gradients. The off-diagonal elements of the tensor are the cross-correlation terms between directions and they are symmetric. In the case of perfectly isotropic diffusion, the off-diagonal elements are zero. Although slightly more informative than the raw DTI images, the tensor is still difficult to interpret, especially since the x, y, and z gradient directions are unlikely to line up with the orientation of the tissues of interest. Diagonalization of the tensor, however, gives a much more intuitive feel for diffusion. Diagonalization of the tensor involves solving for the eigenvectors and eigenvalues of the tensor, and is equivalent to rotating the axes of the reference frame to match the orientation of the ellipsoid for each voxel. Through this process, the off-diagonal elements become zero, and the diagonal elements now represent diffusion in the primary diffusion direction (the longest axis of the ellipsoid,  $\lambda_1$ ), the second largest diffusion direction orthogonal to the first (the second axis of the ellipsoid,  $\lambda_2$ ), and the final orthogonal direction ( $\lambda_3$ ). The new diagonal elements are termed the diffusion eigenvalues; the eigenvectors resulting from diagonalization give the primary, secondary, and tertiary directions of diffusion. Since the tensor is calculated separately for each voxel, the eigenvectors and eigenvalues will also vary by voxel. The diagonalized tensor now has the form:

$$ADC = \begin{bmatrix} \lambda_1 & 0 & 0 \\ 0 & \lambda_2 & 0 \\ 0 & 0 & \lambda_3 \end{bmatrix} \quad (2.8)$$

In addition to the eigenvalues obtained by diagonalization of the diffusion tensor, several measures may be used to assess DTI data; mean diffusivity (MD) and fractional anisotropy (FA) are by far the most common. MD is simply the average of the three diagonal elements of the tensor (before or after diagonalization) and is given by:

$$\begin{aligned} MD &= \frac{(ADC_{xx} + ADC_{yy} + ADC_{zz})}{3} \\ &= \frac{(\lambda_1 + \lambda_2 + \lambda_3)}{3} \end{aligned} \quad (2.9)$$

MD tends to be relatively uniform across the brain parenchyma (both white and gray matter have MD values in the range of  $0.7\text{--}0.9 \times 10^{-3}$  mm<sup>2</sup>/s), while cerebrospinal fluid (CSF) has much higher values of MD, at approximately

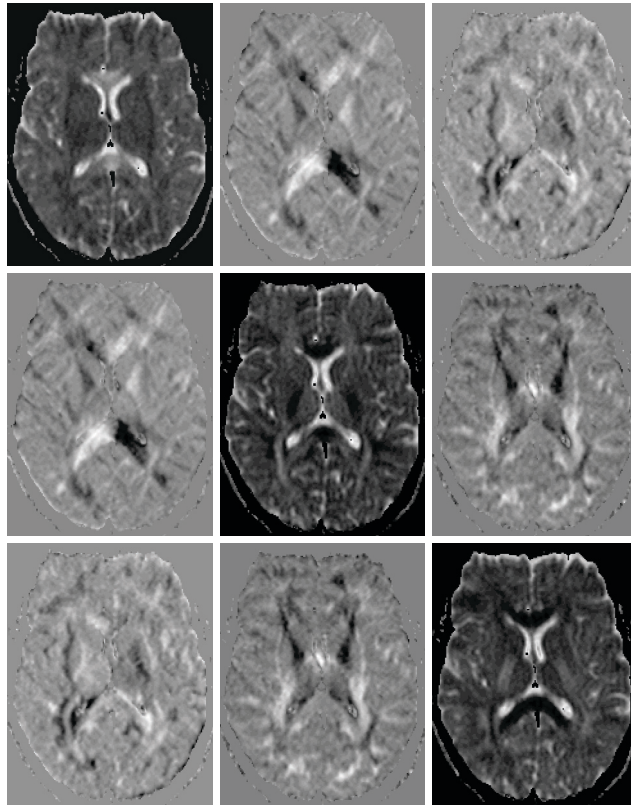


Figure 2.4: The diffusion tensor: images from each tensor element are shown. The diagonal elements are the diffusion-weighted images for the  $x$ ,  $y$ , and  $z$  directions. The off-diagonal elements are symmetric and represent the covariance terms.

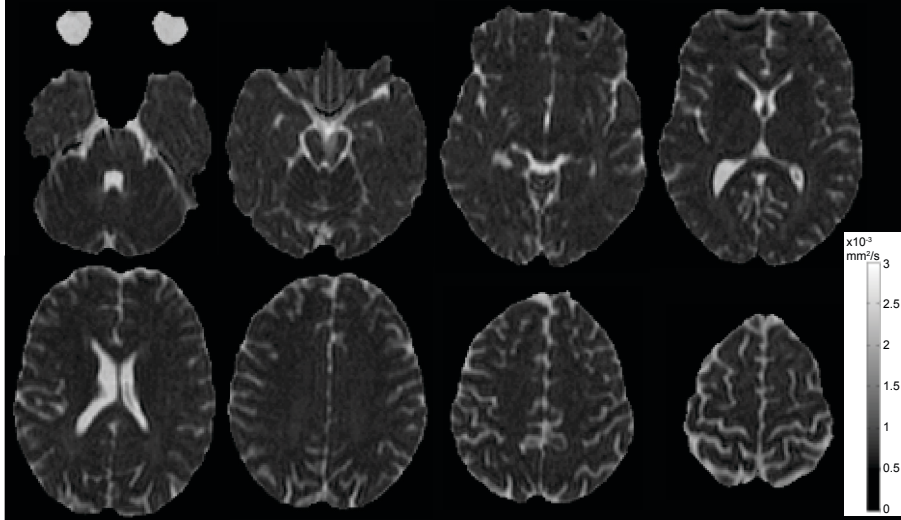


Figure 2.5: Several slices of a mean diffusivity (MD) map are shown for a human brain.

$2.5\text{--}3 \times 10^{-3} \text{ mm}^2/\text{s}$ . This can be seen on the MD maps from a human brain shown in Figure 2.5.

FA is the first moment of the diffusion tensor and relates to the variance of the eigenvalues. FA ranges from zero (completely isotropic diffusion) to 1 (highly anisotropic diffusion), and is calculated according to:

$$FA = \sqrt{\frac{3}{2}} \sqrt{\frac{(\lambda_1 - MD)^2 + (\lambda_2 - MD)^2 + (\lambda_3 - MD)^2}{\lambda_1^2 + \lambda_2^2 + \lambda_3^2}} \quad (2.10)$$

Figure 2.6 shows FA maps of a human brain. It can be seen from the images that FA, unlike MD, varies greatly across the brain. The high FA values ( $\sim 0.4\text{--}0.8$ ) in white matter structures are evident on FA maps; deep gray matter structures such as the thalamus, with lower values of FA, are still visible on FA maps (but are not as bright as white matter structures), and the low FA values make cortical gray matter and CSF appear mostly black.

Figure 2.7 shows FA and MD maps of the brain, as well as diffusion ellipsoids and FA and MD values for several structures. It can be appreciated that some structures, such as the corpus callosum and anterior limb (white matter), have high FA values and elongated ellipsoids, while the thalamus and other deep gray matter structures have lower FA values and less elongated ellipses. The cortical gray matter and cerebrospinal fluid (CSF) have very low FA, and

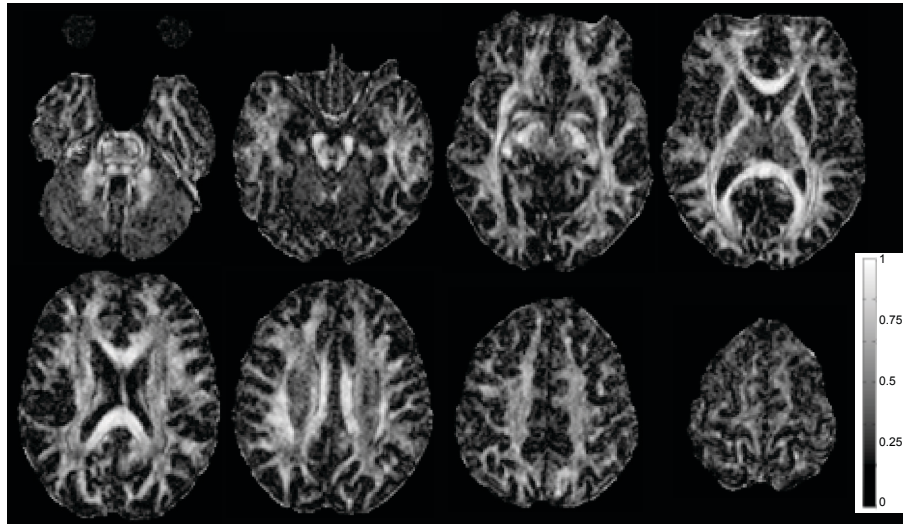


Figure 2.6: Several slices of a fractional anisotropy (FA) map are shown for the same individual as in Figure 2.5.

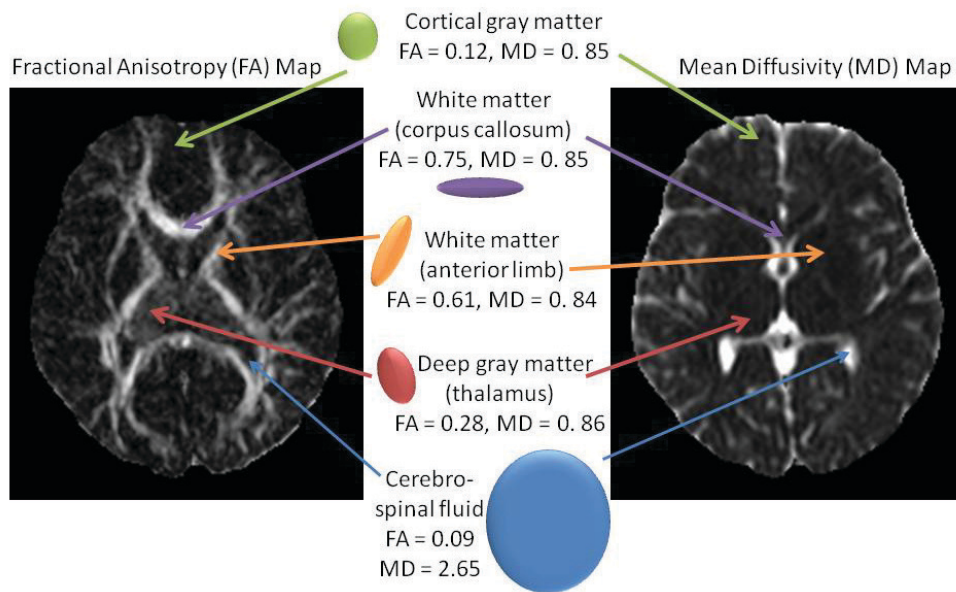


Figure 2.7: A fractional anisotropy (FA) map and mean diffusivity (MD) map from the same slice of the same brain are shown along with diffusion ellipsoids and FA and MD values for several brain regions.

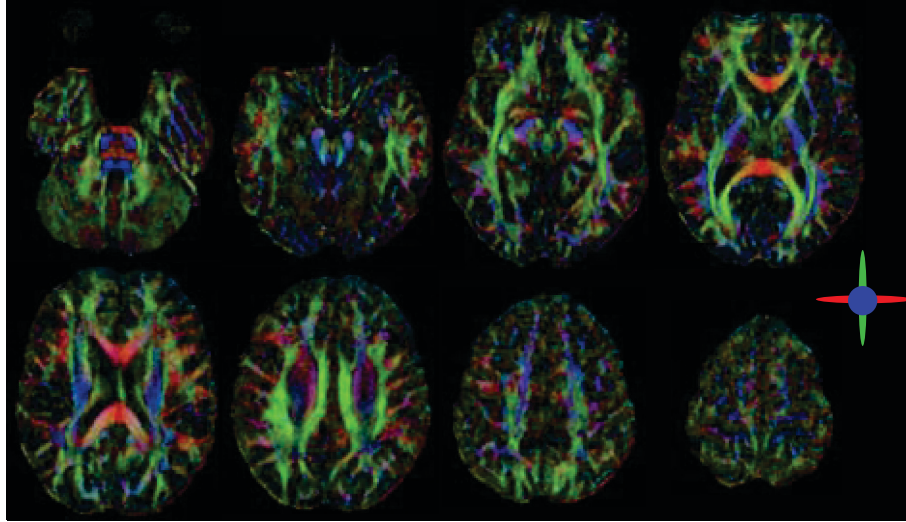


Figure 2.8: Several slices of a colour map coded by primary diffusion direction (red=left-right, blue=inferior-superior, green=anterior-posterior) are shown for the same individual as in Figures 2.5 and 2.6.

their diffusion ellipsoids appear almost as spheres. At the same time, MD is relatively uniform across the brain parenchyma, with white and gray matter structures having very similar MD values. CSF, however, has much higher MD values than the rest of the brain, as can be appreciated by the size of its ellipsoid.

In addition to FA and MD, the eigenvalues of the diffusion tensor can be useful to examine diffusion properties, as they provide additional information. The secondary and tertiary eigenvalues,  $\lambda_2$  and  $\lambda_3$ , are often averaged to provide one measure called perpendicular or radial diffusivity ( $\lambda_{\perp}$ ), while primary diffusivity ( $\lambda_1$ ) may also be referred to as parallel or axial diffusivity ( $\lambda_{\parallel}$ ). In white matter,  $\lambda_{\parallel}$  represents diffusion along the length of the axon and is often associated with neuronal integrity, while changes in  $\lambda_{\perp}$  are generally attributed to myelination and axonal packing changes.

An additional way of looking at DTI data is using a colour map (see Figure 2.8). A colour map uses intensity to represent FA values and colour to show the primary diffusion direction (given by the eigenvector) in each voxel. Blue represents diffusion in the inferior-superior direction; green is the anterior-posterior direction, and red represents left-right. Since intensity is determined by FA values, only structures with relatively high FA (and thus one direction in

which diffusion occurs preferentially) are brightly coloured; structures without a dominant diffusion direction appear darker in the background due to low FA values. The major advantage of colour maps is the information added by the primary diffusion direction, which allows for easy delineation of structures with similar FA values but different orientations (for example, the anterior and posterior limbs of the internal capsule).

## 2.3 Interpretation of Diffusion Parameters

The two most commonly used diffusion parameters, FA and MD, are sensitive to tissue microstructure changes, but they are not always specific. FA is typically attributed to “white matter integrity”, and is generally lower in patient populations than in controls. MD is related to the magnitude of diffusion occurring, and is often, although certainly not always, higher in patients than in controls. However, changes in these parameters do not necessarily provide specific information about tissue changes, because they are influenced by multiple factors.

The factors of greatest relevance to the work presented in this thesis are axonal density and myelination. Anisotropic diffusion in nerves is primarily driven by the presence of axonal membranes (Beaulieu, 2002), because the membranes greatly hinder diffusion perpendicular to nerve fibres and result in greater diffusion along the length of the axon rather than parallel to it. Because of this important contribution from axonal membranes, anisotropy is modulated by axonal packing, with denser and more coherent arrangements of axons leading to higher anisotropy and lower diffusivity (Concha et al., 2010; Golabchi et al., 2010). Myelination also modulates anisotropy values, and higher anisotropy is found in myelinated nerves than non-myelinated ones (Gulani et al., 2001). Interestingly, myelination affects almost exclusively perpendicular diffusivity ( $\lambda_{\perp}$ ), which increases or decreases with demyelination and remyelination, respectively (Song et al., 2002, 2003, 2005). Increased or decreased myelination will result in corresponding changes to FA (increases and decreases, respectively) and MD values (decreases and increases, respec-

tively). Brain water content is another factor that may influence diffusivity values, with reduced brain water leading to reduced diffusivity during childhood (Mukherjee et al., 2002).

Although they are less relevant in normal, healthy brain tissue, numerous other factors influence measurements of anisotropy and diffusivity. While  $\lambda_{\perp}$  is a marker of myelination,  $\lambda_{\parallel}$  is a marker of axonal integrity. Axonal degradation leads to significantly reduced  $\lambda_{\parallel}$ , but leaves  $\lambda_{\perp}$  largely unchanged. Thus, decreased axonal integrity will reduce both FA and MD values. Ischemia, such as caused by stroke, typically leads to decreased diffusivity and increased anisotropy immediately following insult; anisotropy drops and diffusivity becomes elevated in the chronic stages of ischemia (Sotak, 2002). Inflammation and edema of tissue both cause increased diffusivity and decreased anisotropy (Alexander et al., 2007b; Assaf and Pasternak, 2008).

## 2.4 Analysis Techniques for Diffusion Tensor Images

There are three commonly used methods for analyzing diffusion tensor imaging data: region-of-interest analysis, tractography, and voxel-based morphometry. Each has inherent advantages and disadvantages, but all are widely used as analysis techniques throughout the literature. These three methods are briefly described in the following sections.

### 2.4.1 Region of Interest Analysis

Regions-of-interest (ROIs) are two-dimensional areas drawn on an image that can be used to examine the diffusion parameters of various brain structures. ROIs are generally drawn by hand on two-dimensional slices from colour maps, FA maps, MD maps, or non diffusion-weighted ( $b_0$ ) images, whichever makes the structure of interest most easily delineated from surrounding structures. Once a region has been selected and traced, diffusion parameters (e.g., FA, MD) from each voxel within the area are averaged to provide an overall value. ROIs can be used to examine any structure that is readily visible on a two-

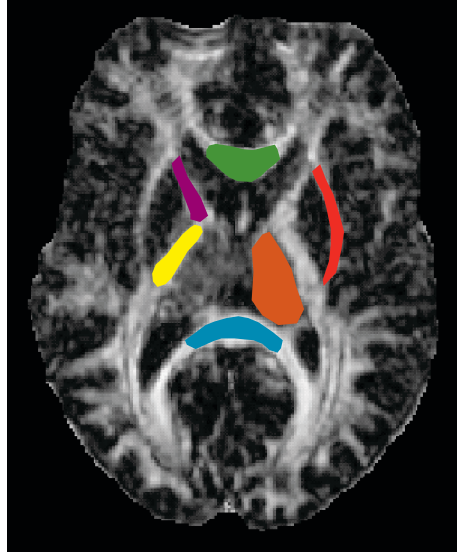


Figure 2.9: Several examples of ROIs are drawn on an FA map: genu and splenium of the corpus callosum (green, blue), anterior and posterior limbs of the internal capsule (purple, yellow), thalamus (orange), and external capsule (red).

dimensional image, but they are particularly useful for assessing subsections of structures or for measuring gray matter and subcortical white matter (which are difficult to analyze using other methods because their FA values are low). Figure 2.9 shows some examples of ROIs drawn on FA maps.

A major advantage of ROI analysis is that it does not require normalization of images, but one of the problems is its user-dependence. To provide consistency across subjects, all analysis should be done by the same rater, and strict rules about where and how to draw ROIs should be followed for all subjects; however, it is still difficult to keep the ROIs equivalent in all individuals. The consistency is especially important for small ROIs, which are sensitive to small changes in placement because every voxel within the ROI is counted. Nonetheless, ROI analysis is a useful, simple technique that can be learned and performed relatively easily.

## 2.4.2 Tractography

Diffusion tractography is an advanced method that allows for virtual reconstruction and visualization of white matter pathways in vivo (Basser et al., 2000; Conturo et al., 1999; Jones et al., 1999; Mori et al., 1999). Tractography

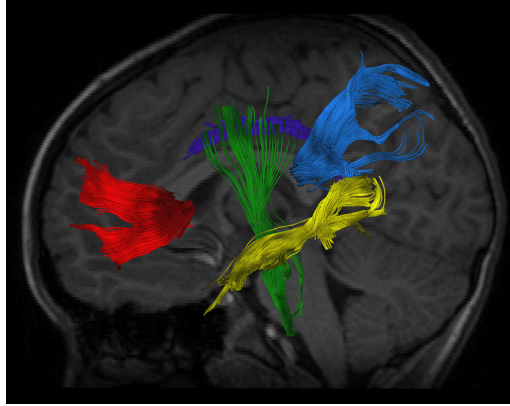


Figure 2.10: Several examples of white matter tracts delineated using tractography are shown: genu and splenium of the corpus callosum (red, blue), corticospinal tracts (green), inferior longitudinal fasciculus (yellow) and cingulum (purple).

uses the primary diffusion direction and anisotropy within each voxel to trace out white matter pathways. By following the primary diffusion direction from voxel to voxel (essentially a sophisticated method of connect the dots), the pathway of diffusion is traced and assumed to represent the actual trajectory of a particular white matter tract in vivo. There are several algorithms for tractography, but they can generally be grouped into two categories: deterministic and probabilistic. Figure 2.10 shows examples of several white matter tracts delineated using deterministic tractography. All of these tracts are easily traced using tractography, but are sometimes difficult to delineate using other methods (e.g., there is overlap between the inferior longitudinal fasciculus and the inferior fronto-occipital fasciculus so it can be difficult to tell which is which on two-dimensional images using either ROI analysis or VBM).

Deterministic tractography (Basser et al., 2000; Conturo et al., 1999; Jones et al., 1999; Mori et al., 1999) begins at a seed point in one voxel (or multiple voxels at the same time) and follows the direction of the primary diffusion vector from voxel to voxel, tracing the path that is likely to represent a white matter fibre bundle. A specific FA threshold is set to ensure that pathways are not tracked through areas of low FA where fibre tracts are unlikely to go (generally approximately  $FA > 0.2$ ); an angle threshold (generally at least  $30^\circ$ ) is set to prevent unlikely turns from occurring. If the FA drops below the threshold or the angle between adjacent vectors is too high, tracking stops.

Resulting fibres can then be visualized in three dimensions, or used to form volumes of interest for further analysis. Deterministic tractography can be prone to errors, particularly in regions of crossing fibres, such as the parietal region where the superior longitudinal fasciculus, corticospinal tracts, and lateral projections of the corpus callosum intersect. In areas of crossing fibres such as this, FA values become artificially low and fibre tracking may stop even though the actual white matter pathways continue. Furthermore, deterministic tractography provides no estimate of the confidence in a given pathway, but merely provides a reconstructed tract. Nonetheless, deterministic tractography is an excellent method for tracing the trajectories of known fibre bundles and for creating three-dimensional volumes of interest for assessing white matter structures.

Probabilistic tractography attempts to deal with some of the shortcomings of deterministic tractography using a bootstrapping method to estimate the uncertainty in each voxel and to provide a range of possible pathways from each voxel and their likelihood (Behrens et al., 2003; Jones and Pierpaoli, 2005; Lazar and Alexander, 2005). Probabilistic tractography can be especially useful for exploring all possible connections between regions, and identifying new pathways. Deterministic tractography, however, may be more useful for measuring diffusion parameters along fibre pathways that follow well-known trajectories.

Tractography overcomes some of the problems associated with ROI analysis, and has been shown to be more reproducible and less user-dependent (Kanaan et al., 2006; Partridge et al., 2005). Semi-automated (see Appendix C for details on the method used throughout this thesis) or atlas-based tractography methods are even less user-dependent and are beginning to be more widely used (O'Donnell and Westin, 2007; Zhang et al., 2008a).

### **2.4.3 Voxel Based Morphometry**

Voxel based morphometry (VBM, or voxel based analysis) is a useful technique for analyzing data across the whole brain (Ashburner and Friston, 2000). While ROI analysis and tractography segment the brain into specific structures

and average diffusion parameters across a region, VBM allows for examination of each voxel individually. The two main strengths of voxel based analysis are that it is operator-independent (although it does depend on parameter choices), and it examines the entire brain without any need for a priori hypotheses about which structures may be affected. Voxel based analysis can detect small areas of correlation or differences between groups of subjects that may not be apparent when examining a much larger portion of a structure using tractography or ROIs.

VBM is generally performed in three steps, the first of which is to normalize data to a template. Several standard templates are available (for example the ICBM-152 template), or one can create a template specific to the subject group. With DTI data, either the FA maps or the b0 images are usually normalized to a template. The goal of normalization is to align all subject brains so that equivalent structures overlap among all individuals. However, due to the great variation among subjects, normalization is never perfect, and this is one of the difficulties associated with VBM.

The second step of VBM is smoothing, which helps to mitigate normalization errors. Choice of an appropriate smoothing kernel is crucial, since the use of different smoothing procedures has been shown to alter results (Jones et al., 2005). The third step is analysis of each voxel for group differences or correlation with a certain parameter such as age or a cognitive score. Generally, strict statistical thresholds are set for significance value and for cluster size in order to avoid multiple comparison problems (since thousands of voxels are being examined simultaneously).

Tract-based spatial statistics (TBSS) is a relatively new form of VBM designed specifically for analysis of DTI data (Smith et al., 2006). With TBSS, a white matter skeleton is used, representing only the central portion of white matter pathways. After normalization of each subject's FA map, the maximal FA value within the tract perpendicular to each section of the skeleton is projected onto the skeleton. Then, the skeleton is analyzed voxel-by-voxel in the same way as VBM, except that only central white matter areas are examined. TBSS addresses some of the problems associated with normal VBM

by measuring only the central portion of the white matter tract, mitigating some of the normalization issues and restricting the analysis to known white matter areas.

# Chapter 3

## Human Brain Development

The human brain undergoes remarkable changes across the lifespan. Brain development begins in utero and continues during childhood and adolescence, and even into young adulthood. During later adulthood and senescence, many of the processes that occurred during development begin to reverse, and structural degradation and other changes associated with aging take place. In order to understand the changes that are occurring, a basic overview of brain anatomy and the important features of the brain is needed. The next section outlines some of the key brain structures and their primary functions. Following that, a basic description of brain development and aging is provided.

### 3.1 Important Brain Features

#### 3.1.1 Brain Tissues

The human brain consists of many components, the three largest of which are gray matter, white matter, and cerebrospinal fluid (CSF). The proportions of these components change significantly with age, although total brain volume remains relatively constant (usually in the range of 1–2 litres, depending on the individual) after approximately 5 years of age (Giedd et al., 1999a; Good et al., 2001b). Figure 3.1 shows the brain of a healthy 12 year old female in a T1-weighted image, along with binary maps of the gray matter, white matter, and CSF components.

The gray matter in the brain consists of the neuronal cell bodies and glial cells in the brain, and is often considered to be the brain’s “computers”. Gray

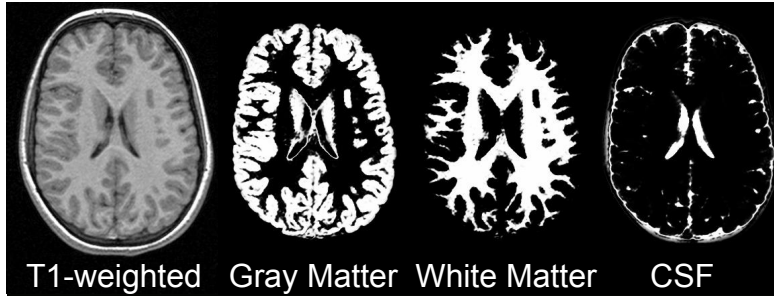


Figure 3.1: A raw T1-weighted image (far left) along with the segmentation results showing probability maps for gray matter (middle left), white matter (middle right), and CSF (far right) in the brain of a healthy 12 year old girl. Voxels with a high probability of the listed tissue type are shown in white, while those with a low probability are shown in black.

matter can be divided into cortical gray matter, which lines the outside of the cerebrum and cerebellum, and deep gray matter structures, which are located near the centre of the brain and serves as relay stations to integrate incoming sensory and motor signals (see Section 3.1.8 for more on deep gray matter structures). Gray matter forms more than 50% of the total brain volume at birth, but decreases across the lifespan, and makes up approximately 40–45% of brain volume during old age.

White matter is composed of the neuronal axons, and appears white (or at least white-ish) on visual inspection (not necessarily on MRI) due to the presence of the fatty myelin sheaths wrapped around the axons. Axons are bundled together to form a variety of white matter connections throughout the brain, which serve to transmit information between spatially segmented brain regions. White matter connections are necessary for proper cognitive function, and are often thought of as the brain’s “wiring”. The total volume of white matter in the brain increases during childhood and adolescence, then decreases during adulthood, but remains within the range of approximately 25–30% of total brain volume.

CSF is a protective fluid that fills the ventricles deep within the brain as well as the subarachnoid space, providing a buffer between the brain and the skull. CSF forms approximately 20% of total brain volume during childhood; this proportion increases throughout life, and is in the range of 30–35% during

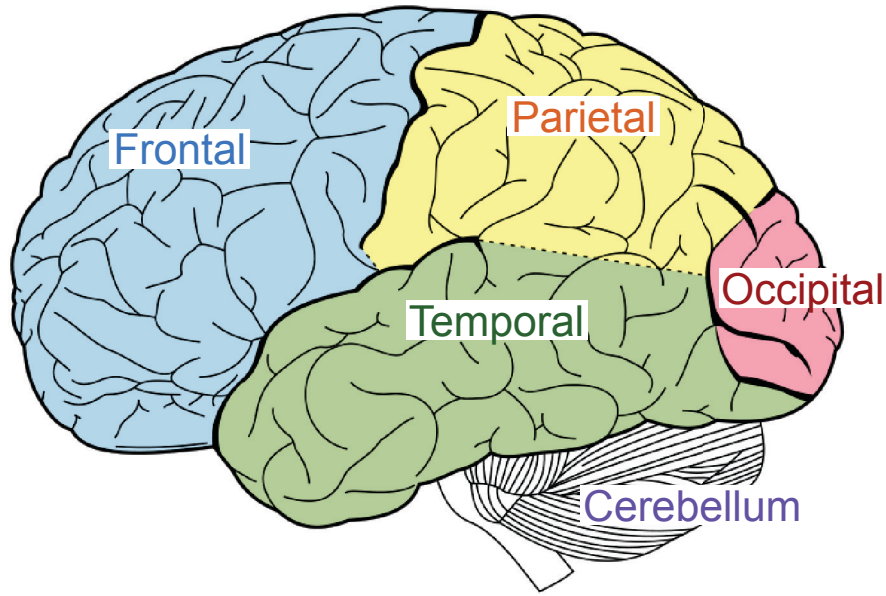


Figure 3.2: The human brain: the cerebrum can be divided into four lobes, as shown above. The cerebellum is located just inferior to the cerebrum. Figure adapted from Gray's Anatomy (20th edition), public domain.

old age.

### 3.1.2 The Cerebrum

The brain is divided into two main compartments: the cerebellum (see Section 3.1.3) and the cerebrum. The cerebrum can be further divided into four lobes (each with a left and right component): the frontal, parietal, temporal, and occipital lobes (see Figure 3.2). The frontal lobe, at the anterior end of the brain, is primarily involved in executive functioning (higher cognitive processes including reward, consequence, inhibition, etc.). The parietal lobe, located behind the frontal lobe, deals with sensory information, while the occipital lobe, at the posterior end of the cerebrum, contains the visual cortex and is the primary vision processing center of the brain. The temporal lobe, located beneath the parietal lobe on either side of the brain, is involved in a variety of functions including memory, auditory perception, and semantic processing. Although each lobe has processes that are typically associated with it, brain function is complex and generally involves multiple brain regions.

### 3.1.3 The Cerebellum

The cerebellum is a structure located inferior to the cerebrum at the posterior end of the brain (see Figure 3.2). It contains many folds and layers, and is formed of both white and gray matter. Several white matter pathways link the cerebellum to the cerebrum, including the inferior, middle, and superior cerebellar peduncles.

The cerebellum was traditionally thought to be a fairly primitive structure responsible for regulating motor coordination and balance. Although it is most certainly involved in those processes, recent studies suggest it also plays a role in higher cognition. Cerebellar volume correlates positively with intelligence in healthy young adults (Andreassen et al., 1993) and preterm adolescents (Parker et al., 2008), cerebellar abnormalities are associated with a variety of intellectual deficits (Steinlin, 2008), and the cerebellum is often activated during cognitive tasks in functional imaging studies (Baillieux et al., 2008). The cerebellum also plays an important role in learning processes, and it is hypothesized that the earlier cerebellar abnormalities are present, the more severe the cognitive deficits (Steinlin, 2008).

### 3.1.4 The Limbic System

The limbic system is a set of brain structures involved in emotion, memory, and behaviour (among other tasks). It consists of deep gray matter structures including the hippocampus, mammillary bodies, thalamus, and amygdala, olfactory bulb, and parahippocampal and cingulate gyrus, as well as the white matter fibre tracts connecting these regions. The two hippocampi are located one in each hemisphere in the medial temporal lobe, while the amygdala is actually a group of nuclei located adjacent to the hippocampus in each hemisphere.

Figure 3.3 shows two major white matter connections of the limbic system: the fornix and cingulum. The fornix projects from the hippocampus on either side of the brain to the mammillary bodies, by arching over the thalamus. At the hippocampal end (the crus of the fornix), the fornix has two branches,

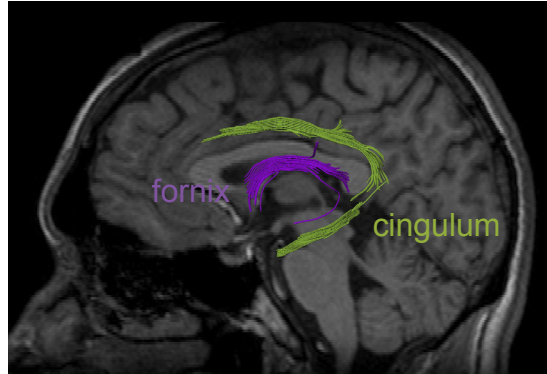


Figure 3.3: Limbic system fibres: The fornix (purple) and the cingulum (green) are two major limbic system white matter connections. Both can be difficult to delineate using tractography, and may need to be tracked in several parts, as the cingulum is shown here.

which come together as they approach the septal region (body of the fornix), and may separate again as they reach the mammillary bodies (columns of the fornix). The cingulum connects the temporal and frontal lobes by arching around the corpus callosum. These two fibres are known to be abnormal in epilepsy (Concha et al., 2005a), Alzheimer’s disease (Mielke et al., 2009), and schizophrenia (Kubicki et al., 2005) among other diseases and conditions.

### 3.1.5 The Corpus Callosum

The corpus callosum (see Figure 3.4) is the largest white matter structure in the human brain, and serves primarily, though not exclusively, to connect homologous regions across hemispheres. It is a complex and heterogeneous structure unique to placental mammals, and it undergoes important structural changes throughout life (Aboitiz and Montiel, 2003; Doron and Gazzaniga, 2008; Pfefferbaum et al., 2000). Its structure is associated with motor skills (Rademaker et al., 2004; van Kooij et al., 2008), numerous cognitive abilities (Fine et al., 2007; Hutchinson et al., 2009; Westerhausen et al., 2006), and the corpus callosum is often malformed and may even be absent in various conditions (Bookstein et al., 2001; Egaas et al., 1995; Luders et al., 2009; Paul et al., 2007; Walterfang et al., 2008).

The corpus callosum is such a large structure that it is often subdivided into

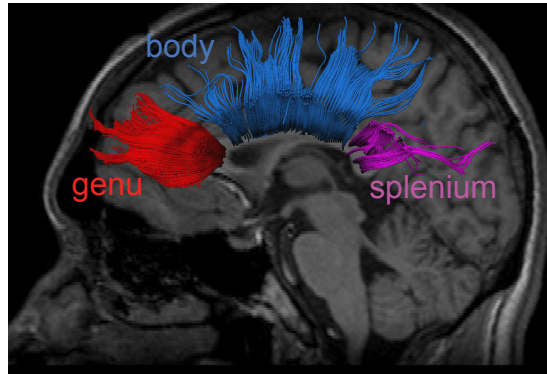


Figure 3.4: The corpus callosum is the largest white matter tract in the human brain. It is a commissural fibre, connecting homologous regions between the two hemispheres. It is often subdivided into regions such as the genu, body, and splenium.

anywhere from 2 to 8 different regions for analysis purposes. There are many different methods of segmenting the corpus callosum, using 2-dimensional or 3-dimensional landmarks and following various rules about length and distance (Chao et al., 2009; Hofer and Frahm, 2006; Huang et al., 2005; Witelson, 1989). Most studies segment the corpus callosum into at least two or three distinct sections; the genu (the most anterior portion, which projects to the frontal lobe), splenium (the most posterior portion, projecting to the occipital lobe), and body (the middle section, which projects upward into the frontal and parietal lobes) are the most commonly analyzed. Although the corpus callosum is by far the largest and most important of the commissural fibres, the anterior and posterior commissures are additional white matter tracts that provide connections between homologous regions in the two hemispheres.

### 3.1.6 Projection Fibres

Projection fibres are the white matter bundles that run from the cortex through the brainstem to relay sensory and motor information between the brain and the rest of the body. Projection fibres can be divided in many different ways, which may include the external capsule, and the anterior and posterior limbs of the internal capsule. The anterior limb of the internal capsule contains fibres of the anterior thalamic radiation, and connects the frontal brain regions

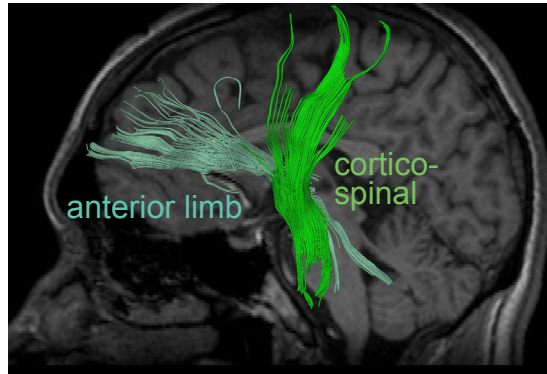


Figure 3.5: Projection fibres: The anterior limb of the internal capsule (teal green) projects from the frontal lobe, while the corticospinal tracts (bright green) occupy the posterior third of the posterior limb of the internal capsule and project from the motor cortex. Other projection fibres include the corticobulbar tracts and thalamic radiations (not shown).

with the brain stem, while the external capsule connects parietal regions, including the motor cortex, to the brainstem. The posterior limb of the internal capsule contains the corticospinal tracts, which occupy the posterior third, as well as corticobulbar tracts and thalamocortical somatosensory radiations (Kretschmann, 1988; Wakana et al., 2004). Figure 3.5 shows both the anterior limb of the internal capsule and the corticospinal tracts. Projection fibres may be affected in a variety of conditions, including cerebral palsy (Hoon et al., 2009) and paraplegia (Hourani et al., 2009).

### 3.1.7 Association Fibres

Association fibres are the white matter bundles that connect separate brain regions within a hemisphere. Short-range association fibres are the cortical U-fibres that connect adjacent regions throughout the brain. Long-range association fibres include the superior and inferior longitudinal fasciculi, superior and inferior fronto-occipital fasciculi, and the uncinate fasciculus (see Figure 3.6).

The superior longitudinal fasciculus is a well-studied tract that connects Broca’s area in the frontal lobe with Wernicke’s area in the temporal lobe. It is known to be involved in a variety of tasks including language, intelligence,

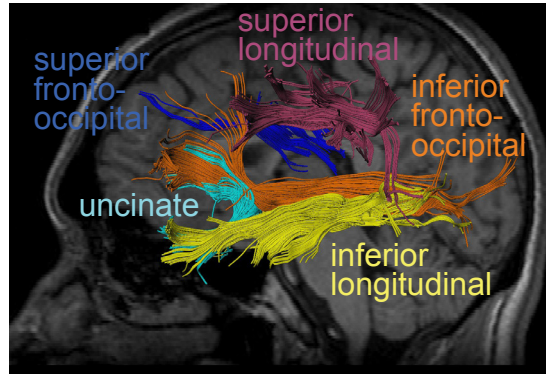


Figure 3.6: Association fibres: The superior and inferior longitudinal fasciculi (pink and orange, respectively), the superior and inferior front-occipital fasciculi (blue and yellow, respectively), and the uncinate fasciculus (cyan) are all major white matter association fibres.

and reasoning tasks (Ashtari et al., 2007; Breier et al., 2008; Jung and Haier, 2007; Schmithorst et al., 2005; Turken et al., 2008). The superior longitudinal fasciculus is often subdivided into direct (a pathway connecting Broca’s and Wernicke’s regions directly, also known as the arcuate fasciculus) and indirect segments (connecting Broca’s and Wernicke’s regions via Geschwind’s area in the parietal lobe). The inferior longitudinal fasciculus is an occipital-temporal connection likely involved in secondary visual processing (Catani et al., 2003).

The superior and inferior fronto-occipital fasciculi are both very long range tracts connecting the frontal and occipital lobes (surprise!). The inferior fronto-occipital fasciculus connects auditory and visual areas in the posterior brain to the prefrontal cortex (Kier et al., 2004). The superior fronto-occipital fasciculus is the only association fibre that projects medially to the thalamus and along the ventricle, and is not often mentioned in the literature, likely due to the difficulty of delineating it with tractography through crossing fibre and partial volume regions.

The uncinate fasciculus connects the anterior temporal lobe to the frontal cortex. It has been implicated in schizophrenia (Kubicki et al., 2002), and is involved in higher cognitive processes such as language (Parker et al., 2005).

### 3.1.8 Deep Gray Matter Structures

Deep gray matter structures are distinct from the cortical gray matter in that they are located within brain, subcortically. The deep gray matter structures act as relay stations to integrate incoming sensory and motor information before it passes to the cortex.

Deep gray matter structures include the hippocampus and amygdala, which are part of the limbic system (see Section 3.1.4), as well as the thalamus and the basal ganglia. The term basal ganglia refers to a group of deep gray matter nuclei, consisting of the putamen and caudate nucleus (which together make up the striatum), the globus pallidus, the subthalamic nucleus, and the substantia nigra. Together, all of these structures are involved in emotion, learning and memory, cognition, and motor control.

The deep gray matter structures are often disproportionately affected in conditions and diseases, such as fetal alcohol spectrum disorder, in which their volumes are considerably reduced, even compared to total brain volume (Archibald et al., 2001), and in Alzheimer’s disease and Parkinson’s disease, in which iron accumulates in specific deep gray matter structures (Brass et al., 2006).

## 3.2 Brain Development Across the Lifespan

Throughout life, the brain undergoes marked changes. At birth, the brain is only approximately 25–30% the size of an adult brain, but increases in brain volume are nearly complete by age 5 years (Giedd et al., 1999a; Good et al., 2001a). Despite this fact that total brain volume remains relatively constant after approximately age 5 years, the individual brain structures themselves change quite significantly across the age span, and this structural brain development involves complex processes that are linked with behavioural, emotional, cognitive, and overall maturation.

Myelination of white matter tracts begins in utero and progresses throughout childhood and adolescence, even into the third decade of life (Benes, 1989; Yakovlev and Lecours, 1967). Increases of “white matter density” have also

been demonstrated during childhood and adolescence using T1-weighted MRI (Paus et al., 1999). DTI studies provide further information about white matter changes, including indirect measures of myelination and axonal growth, and they demonstrate increases of FA and decreases of MD in most brain structures throughout infancy, childhood and adolescence, and even into the twenties (Ashtari et al., 2007; Barnea-Goraly et al., 2005b; Ben Bashat et al., 2005; Mukherjee et al., 2001; Schmithorst et al., 2002; Snook et al., 2005). Later in life, DTI demonstrates a reversal of these trends, showing decreasing FA and increasing MD (Bhagat and Beaulieu, 2004; Hsu et al., 2010; Pfefferbaum et al., 2000).

Significant cortical gray matter development occurs in utero (Neil et al., 2002), and cortical gray matter thickness changes across the lifespan, with distinct areas developing at different rates (Lerch et al., 2006; Sowell et al., 2004; Whitford et al., 2007). Deep gray matter structures also undergo changes in volume and microstructure, showing increased diffusion parameters during childhood and adolescence (Snook et al., 2005), and decreases of these same measures during old age (Pfefferbaum et al., 2000).

The volume of the brain tissue components changes throughout the lifespan, with gray matter volume decreasing, white matter volume increasing then decreasing, and CSF volume steadily increasing throughout life (Giedd et al., 1999a; Good et al., 2001b). Some changes, such as the amount of gray matter, white matter, and CSF are even appreciable in Figure 3.7, which shows T1-weighted images from three male subjects, aged 6, 27, and 51 years. Even in these images, the decreased gray matter and increased white matter from 6 to 27 years can be observed and there is noticeably more CSF in the 51 year old brain than in the younger two subjects.

Significant volume changes of different brain lobes and structures also occur, with considerable regional variation in the timing of these increases and decreases (Giedd et al., 1999a). White matter structures tend to increase in volume during childhood and adolescence. During later life, reductions in the size of many brain structures are noted (Smith et al., 2007; Suganthy et al., 2003).



Figure 3.7: Tissue components change with age. During childhood and adolescence, gray matter thins and white matter increases in volume. During the aging process, the proportion of cerebrospinal fluid increases and the volume of gray and white matter declines. These changes are evident on the three examples shown above.

# Chapter 4

## Fetal Alcohol Spectrum Disorder

### 4.1 Characteristics

Fetal alcohol spectrum disorder (FASD) is an umbrella term referring to the various developmental disorders associated with prenatal alcohol exposure. FASD is the leading known cause of mental retardation, and is entirely preventable (Abel and Sokol, 1986). The most recognizable disorder falling under the umbrella term FASD is fetal alcohol syndrome (FAS), a condition describing a specific set of brain, cognitive, behavioural and facial abnormalities attributed to alcohol exposure in utero. FAS was first described in the late 1960s and early 1970s (Jones and Smith, 1973; Lemoine et al., 1968). It is estimated to affect anywhere from 0.3–3 individuals per 1000 live births in the general population (Abel and Sokol, 1987, 1991; May and Gossage, 2001; Sampson et al., 1997), and its incidence is often much higher in specific populations (Astley, 2004). Individuals with FAS demonstrate characteristic facial abnormalities such as a smooth philtrum, short palpebral fissures, and a thin upper lip (Astley, 2004; Sampson et al., 1997), as shown in Figure 4.1. Common brain malformations revealed by postmortem studies include microcephaly, ventriculomegaly, a small cerebellum, and malformations or agenesis of the corpus callosum (Clarren et al., 1978; Jones and Smith, 1973; Peiffer et al., 1979). Children and adults with FAS may also demonstrate a wide variety of cognitive and behavioural problems including motor delays, and deficits of ex-

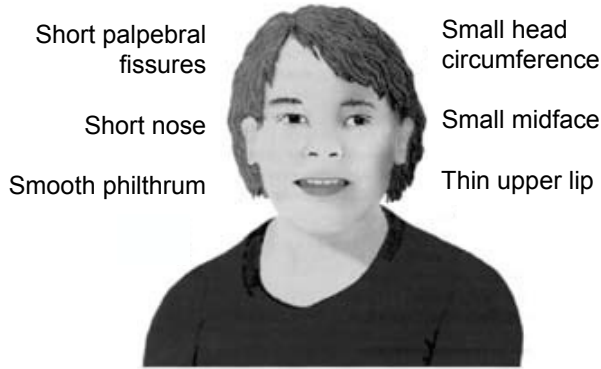


Figure 4.1: Characteristic facial features of fetal alcohol syndrome (FAS) include short palpebral fissures (eye openings), small head circumference, short nose, small midface, smooth philtrum and thin upper lip. Facial abnormalities are always present to some degree in FAS, but may or may not appear in other individuals with prenatal alcohol exposure. Figure was adapted from the National Institute on Alcohol Abuse and Alcoholism (public domain).

ecutive functioning, attention, memory, reading, and mathematics (Jacobson and Jacobson, 2002; Kalberg et al., 2006; Mukherjee et al., 2006).

Not all children with prenatal alcohol exposure demonstrate the same extent of symptoms, and it is now known that there is a wide range of outcomes beyond FAS associated with drinking during pregnancy (Astley, 2004). Although poorly understood, the extent and timing of prenatal alcohol consumption likely play major roles in creating this spectrum. In addition, there are differences in genetic susceptibility that may affect outcomes (Streissguth and Dehaene, 1993). Many individuals with known prenatal alcohol exposure demonstrate some, but not all of the characteristics of FAS. FASD is the term used to describe the full range of developmental disorders associated with prenatal alcohol exposure, and its prevalence is estimated at up to 1% of live births in North America (May and Gossage, 2001; Sampson et al., 1997).

The cognitive, behavioural and emotional deficits associated with FASD may change with time and manifest themselves in different ways, however, they are often sufficient to reduce the quality of life of those with FASD and prevent them from leading fully independent lives (Spohr et al., 2007; Streissguth et al., 2004). Individuals with FASD are more likely to have mental health problems, addictions, and trouble with the law than the non-FASD population (Astley

et al., 2009b; Baer et al., 2003; Barr et al., 2006; Streissguth et al., 2004). In Canada, the estimated lifetime cost per individual with FASD is over one million dollars (Stade et al., 2009; Thanh and Jonsson, 2009), and this disorder has serious consequences for the individuals diagnosed with it, their families, communities, and society.

## 4.2 Diagnosis

Accurate assessment of individuals with FASD is important to ensure that adequate treatment and necessary resources are provided. Therefore, a consistent, objective diagnostic tool is highly desirable. Several methods exist for assessing the effects of prenatal alcohol exposure and diagnosing the associated disorders; however, the 4-digit diagnostic code is becoming an increasingly popular method due to its consistency and reliability (Astley, 2004). Diagnosis is typically performed by a multidisciplinary team using the Diagnostic Guide for Fetal Alcohol Spectrum Disorders: The 4-Digit Diagnostic Code (Astley, 2004) to rank information in the areas of growth deficiency, facial phenotype, brain dysfunction, and alcohol use. The magnitude of expression of each feature is ranked independently on a 4-point Likert scale, with 1 reflecting complete absence of the typical FAS feature and 4 reflecting a strong “classic” presence of the FAS feature. As part of the diagnostic process, individuals are given a 4-digit code reflecting the growth, facial features, brain dysfunction and alcohol use, respectively. Based on this code, possible results can vary from FAS to “no physical findings or central nervous system abnormalities detected”. In order for a diagnosis to fall under the umbrella of FASD, an individual must have a brain code of 2 or higher (reflecting the presence of brain dysfunction) and confirmed alcohol exposure, as indicated by alcohol use scores of 3 (some risk) or 4 (high risk). Diagnoses falling under the FASD umbrella can be grouped into four broad categories, which are (in order of most severe to least severe): FAS, partial FAS (pFAS), static encephalopathy: alcohol-exposed (SE:AE), and neurobehavioural disorder: alcohol-exposed (NBD:AE).

Individuals diagnosed with FAS, the most severe end of the FASD spec-

trum, display serious, permanent, structural and functional brain abnormalities (brain code of 3 or 4), growth deficiencies (rank 2–4), and the full FAS phenotype of thin upper lip, smooth philtrum, and short palpebral fissures (facial code of 4, see Figure 4.1). SE:AE (meaning permanent, unchanging brain abnormalities) is the diagnosis given to subjects who have significant structural and/or functional brain abnormalities at a level of 3 or 4, but are lacking the growth deficiencies and facial features of FAS. When individuals meet the criteria for static encephalopathy and display most, but not all, of the growth deficiencies and facial features of FAS, they are given the diagnosis of pFAS. Subjects with NBD:AE have confirmed brain abnormalities (brain code of 2), but they are less severe than for those with static encephalopathy. The term “sentinel physical finding(s)” is placed at the end of the diagnosis if growth or facial abnormalities are present at rank 3 or 4; this term is omitted for diagnoses of FAS or pFAS, since growth and facial abnormalities are requirements for these diagnoses. There are many individuals with confirmed prenatal alcohol exposure who do not meet the brain dysfunction criteria for an FASD diagnosis; however, these individuals may still have cognitive, functional, and/or structural brain abnormalities.

### **4.3 Common Brain Abnormalities**

Early studies of children with prenatal alcohol exposure used autopsies to identify several structural brain abnormalities caused by neuronal and glial migration errors (Clarren et al., 1978; Jones and Smith, 1973; Peiffer et al., 1979). These malformations include microcephaly, a small cerebellum, agenesis or severe malformations of the corpus callosum, and ventriculomegaly, although no consistent abnormalities were identified by these early studies (Roebuck et al., 1998). However, autopsy studies are limited by the number of available subjects and represent a skewed sample, since only the most severely alcohol-affected subjects die during infancy or childhood. Studies with much larger sample sizes and a wider range of subjects have more recently been made possible by brain imaging techniques such as MRI, which are able to

non-invasively assess the teratogenic effects of alcohol in-vivo.

MRI and other neuroimaging studies have shown many different structural brain abnormalities in individuals with FASD, some of which are relatively consistent findings. The corpus callosum, the largest white matter structure in the human brain, has been repeatedly implicated as abnormal across autopsy and imaging studies, with a variety of malformations reported, including complete agenesis in some cases (Bookstein et al., 2001; Jones and Smith, 1973; Peiffer et al., 1979). Individuals with FASD demonstrate total brain volume reductions, as well as reductions of many major tissue components (Archibald et al., 2001; Astley et al., 2009a). These volume reductions are particularly prominent in the parietal lobe and in deep gray matter structures such as the caudate nucleus (Archibald et al., 2001; Astley et al., 2009a; Cortese et al., 2006; Mattson et al., 1996). Children with FASD tend to have thicker cortical gray matter than healthy children, especially in the parietal and temporal lobes (Sowell et al., 2008b).

Functional and metabolic abnormalities have also been noted in FASD. Subjects with FASD demonstrate significant differences for metabolite ratios of choline, creatine, and N-acetyl-aspartate (NAA) in frontal white matter, the corpus callosum, and deep gray matter structures (Astley et al., 2009c; Cortese et al., 2006; Fagerlund et al., 2006). Furthermore, functional brain abnormalities have been reported in children with FASD, with different patterns of brain activation for a variety of tasks including spatial working memory, inhibition, verbal learning, and arithmetic tasks (Santhanam et al., 2009; Fryer et al., 2007; Sowell et al., 2007; Spadoni et al., 2009).

DTI, because of its increased sensitivity compared to conventional imaging techniques, has added knowledge of brain damage in FASD. DTI studies have demonstrated widespread brain abnormalities in children, adolescents, and young adults with prenatal alcohol exposure (Fryer et al., 2009; Li et al., 2009; Ma et al., 2005; Sowell et al., 2008a; Wozniak et al., 2006, 2009). One of the most common abnormalities across DTI studies of prenatal alcohol exposure is the corpus callosum, which has been shown to be abnormal in all previous DTI studies of FASD. The posterior corpus callosum (splenium and isthmus) seems

to be particularly affected. In addition to the corpus callosum, the temporal lobes in both hemispheres and their associated white matter connections (superior and inferior longitudinal fasciculi, cingulum, uncinate fasciculus) show abnormally low white matter integrity in multiple DTI studies.

Some of the key abnormalities observed in FASD are highlighted in Figure 4.2. With many non-invasive imaging studies over the past few years, a much clearer picture of brain abnormalities in FASD is emerging. Key areas include the corpus callosum, which demonstrates a variety of malformations and shows consistently reduced white matter integrity than in healthy subjects (Bookstein et al., 2001; Jones and Smith, 1973; Ma et al., 2005), and the temporal lobes, which are smaller (even when total brain volume is considered), have thicker cortices, and lower white matter integrity than in healthy subjects (Archibald et al., 2001; Sowell et al., 2008a,b). The right hemisphere also is more commonly abnormal than the left when compared to control subjects, particularly in DTI studies. The deep gray matter structures show particularly reduced volumes and have abnormal metabolite ratios compared to healthy controls (Cortese et al., 2006; Fagerlund et al., 2006).

Studies of FASD are often complicated by several factors. It is usually difficult (if not impossible) to obtain an accurate history of alcohol intake during pregnancy, and there are often other substance exposures (e.g. cocaine, methamphetamine, tobacco), which can lead to structural brain damage as well (Warner et al., 2006; Cloak et al., 2009; Jacobsen et al., 2007). In some cases, children may have suffered, in utero or after birth, from malnutrition, neglect and/or abuse. Obtaining accurate histories is often further complicated because many children diagnosed with FASD are in foster or adoptive families and may not have continued contact with the birth mother. Comorbidities such as attention deficit hyperactivity disorder (ADHD), obsessive compulsive disorder (OCD), or oppositional defiant disorder (ODD) may also affect children with FASD, further confounding the interpretation of brain abnormalities. Therefore, it is important to consider that factors other than prenatal alcohol exposure may be influencing any brain abnormalities noted in studies of FASD.

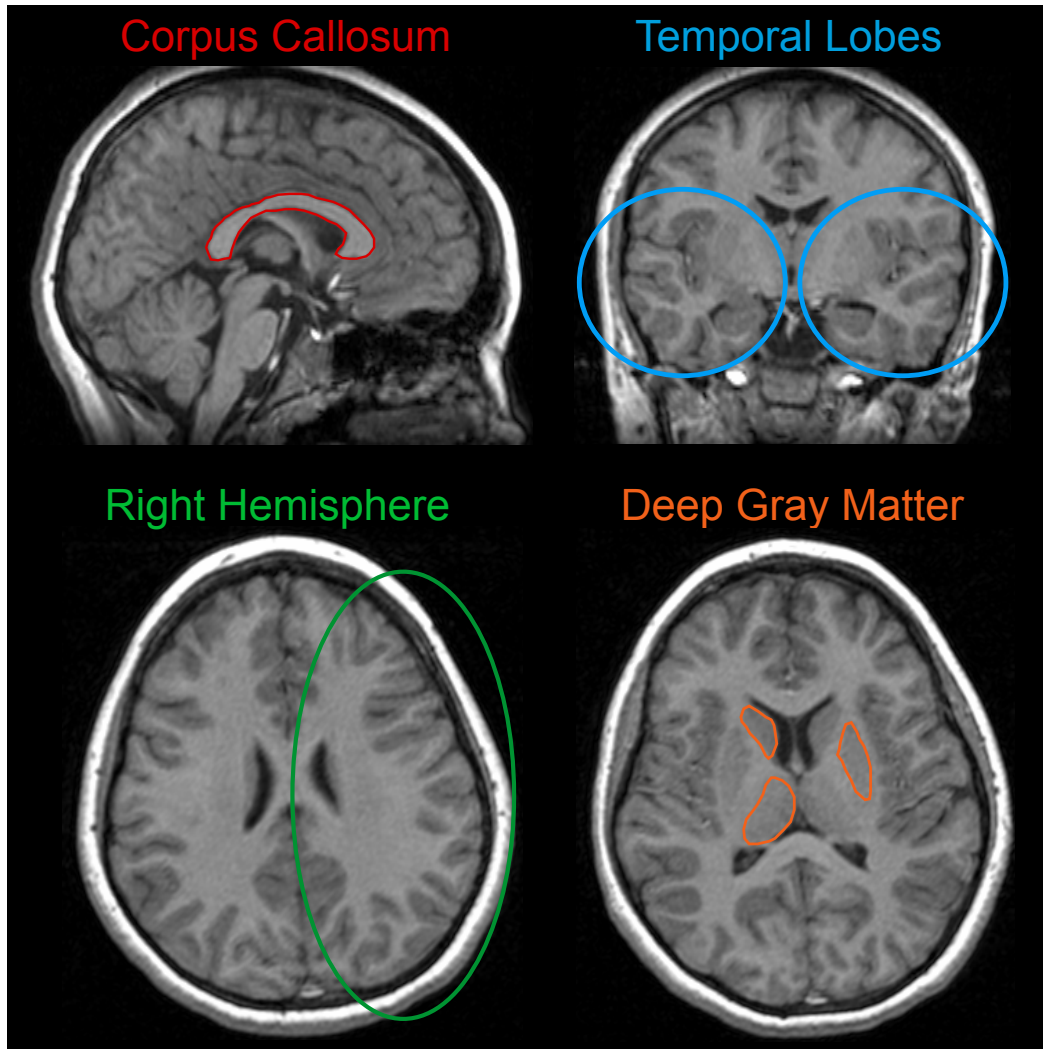


Figure 4.2: Several areas are consistently highlighted as abnormal in individuals with FASD: the corpus callosum, which is often malformed and in some cases even absent; the temporal lobes, which are particularly reduced in volume, have abnormal cortical thickness and lower white matter integrity than in controls; the right hemisphere, which shows up as abnormal more often than the left; and the deep gray matter structures (e.g., thalamus, caudate nucleus, globus pallidus, putamen), which are reduced in volume, show abnormal metabolite ratios and lower structural integrity than in controls.

Disorders falling under the FASD umbrella are serious, permanent conditions that require lifelong treatment and adaptation, and have major consequences. A more thorough understanding of the numerous brain abnormalities in FASD, how they relate to each other, and how they relate to the diverse cognitive, behavioural and emotional problems, may help lead to earlier identification and better treatment of individuals with FASD, thus improving outcomes for all involved.

# Chapter 5

## Normal Brain Maturation During Childhood and Adolescence<sup>1</sup>

### Abstract

Brain maturation is a complex process that continues well beyond infancy, and adolescence is thought to be a key period of brain rewiring. To assess structural brain maturation from childhood to adulthood, we charted brain development in subjects aged 5 to 30 years using diffusion tensor magnetic resonance imaging, a novel brain imaging technique that is sensitive to axonal packing and myelination and is particularly adept at virtually extracting white matter connections. Age-related changes were seen in major white matter tracts, deep gray matter, and subcortical white matter, in our large (n=202), age-distributed sample. These diffusion changes followed an exponential pattern of maturation with considerable regional variation. Differences observed in developmental timing suggest a pattern of maturation in which fronto-temporal connections develop more slowly than other regions. These in vivo results expand upon previous postmortem and imaging studies and provide quantitative measures indicative of the progression and magnitude of regional human brain maturation.

---

<sup>1</sup>A version of this chapter has been published. C. Lebel, L. Walker, A. Leemans, L. Phillips, and C. Beaulieu, 2008. Microstructural Maturation of the Human Brain from Childhood to Adulthood. *NeuroImage* 40: 1044–55.

## 5.1 Introduction

Brain development is a complex process linked with behavioural, emotional, cognitive, and overall maturation that progresses throughout childhood, adolescence, and into adulthood. A thorough knowledge of structural brain development during adolescence is crucial for understanding the extensive cognitive and behavioural advances that occur during the same period, and for linking brain structure with brain function in both healthy and disease states. Post-mortem studies have provided valuable insight into white matter development, demonstrating continued myelination of white matter tracts into the second and third decades of life (Benes, 1989; Yakovlev and Lecours, 1967). However, these studies are limited by the availability of young, previously healthy subjects.

Magnetic resonance imaging (MRI) is a powerful tool that has made it possible to investigate healthy brain development in vivo, demonstrating both global brain development, as well as more specific brain maturation. MRI has been used extensively to study brain and tissue volume changes, and has demonstrated that though total brain volume remains approximately constant after early childhood, the volume of the individual tissue components changes throughout the life span (Giedd et al., 1999a; Good et al., 2001b). Studies of cortical gray matter development have shown regional patterns of brain maturation, with distinct areas developing at different rates (Lerch et al., 2006; Sowell et al., 2004; Whitford et al., 2007).

Despite the fact that adolescence is considered a crucial period of brain re-wiring, relatively little is known about the development of the white matter tracts that form this wiring or the deep gray matter structures that provide the relay stations. Previous studies using T1-weighted anatomical MRI have shown various brain white matter changes during adolescence, including an overall volume increase (Giedd et al., 1999a), and increases of “white matter density” in the internal capsule and the left arcuate fasciculus (Paus et al., 1999). Diffusion tensor MRI (DTI) is a non-invasive tool that provides unique information about tissue microstructure, including indirect measures

of myelination and axonal growth, and may be more sensitive than conventional imaging (Basser et al., 1994; Beaulieu, 2002; Le Bihan, 2003). DTI has demonstrated more widespread white matter and deep gray matter development with age during childhood and adolescence (Ashtari et al., 2007; Barnea-Goraly et al., 2005b; Ben Bashat et al., 2005; Mukherjee et al., 2001; Schmithorst et al., 2002; Snook et al., 2005) than is observed on T1-weighted scans. However, previous DTI studies of adolescence were limited by small sample sizes (Eluvathingal et al., 2007; Morriss et al., 1999), limited brain regions analyzed (Ben Bashat et al., 2005; McLaughlin et al., 2007), narrow age ranges (Schneider et al., 2004; Snook et al., 2005), and/or assumptions of linear development (Barnea-Goraly et al., 2005b; Giorgio et al., 2008; Schmithorst et al., 2002). Since nonlinear patterns of development have been shown in some cognitive abilities during adolescence (Kail, 1993; Luna et al., 2004), it is probable that DTI measures of specific brain white matter and deep gray matter structures may also deviate from a linear trajectory of development through adolescence.

Here, we use DTI to characterize the trajectory of microstructural brain development from childhood to adulthood, showing regionally specific changes in both timing and relative magnitude. We measured fractional anisotropy (FA), an indicator of white matter coherence and axonal organization, and mean diffusivity (MD), the average magnitude of water diffusion, to assess brain development in a large, age distributed sample. Subjects were 202 individuals ranging from 5–30 years, with no history of neurological/psychiatric disease or brain injury. Twenty distinct brain regions were analyzed, including major white matter tracts, subcortical white matter in gyri, and deep gray matter. Ten structures were examined using region-of-interest analysis, and ten structures were analyzed using diffusion tensor tractography, a novel method of virtually reconstructing and visualizing white matter tracts in vivo (Basser et al., 2000; Conturo et al., 1999; Jones et al., 1999; Mori et al., 1999). These two complementary methods provide a means of assessing three dimensional white matter tracts, as well as structures such as deep gray matter and subcortical white matter in gyri, which cannot be examined using tractography.

## 5.2 Methods

### 5.2.1 Subjects

This study included 202 healthy volunteers with no self-reported history of neurological or psychiatric disease or brain injury. Subjects were aged 5.6 to 29.2 years (mean age  $\pm$  standard deviation:  $15.2 \pm 6.1$ , 98 female, 104 male, 187 right-handed, 13 left-handed, 2 no preference). Subjects were approximately equally distributed across the age range, with a minimum of 3 males and 3 females for each year from 6-22 years. Health was verified by asking participants a series of questions to ensure there was no history of neurological or psychiatric disease or brain injury. All subjects provided informed consent; child assent and parent/guardian consent was obtained for volunteers under 18 years.

### 5.2.2 Image Acquisition

All data was acquired on the exact same 1.5 T Siemens Sonata MRI scanner using identical methods. Total acquisition time was approximately 26 minutes and included anatomical imaging and both standard and cerebrospinal fluid (CSF) suppressed DTI<sup>1</sup>. Standard DTI was acquired using a dual spin-echo, single shot echo-planar imaging sequence with the following parameters: 40 3 mm thick slices with no inter-slice gap, TR=6400 ms, TE=88 ms, 6 non-collinear diffusion sensitizing gradient directions with  $b=1000$  s/mm<sup>2</sup>, 8 averages, field-of-view  $220 \times 220$  mm<sup>2</sup>, matrix of  $96 \times 128$  zero-filled to  $256 \times 256$ . Total DTI acquisition time was 6:06 minutes. CSF-suppressed DTI was also acquired in 173 subjects and used a dual spin-echo, echo planar imaging sequence with inversion time=2200 ms, TR=8600 ms, TE=88 ms, with 26 slices, and all other parameters the same as the standard DTI. Total acquisition time for FLAIR DTI was 8:12 minutes. High resolution ( $1 \times 1 \times 1$  mm<sup>3</sup>) T1-weighted images were also acquired using MPRAGE with TE=4.38 ms, TR=1870 ms, TI=1100 ms, and scan time of 4:29 minutes.

---

<sup>1</sup>CSF-suppressed DTI was acquired to facilitate tracking of the fornix, which is susceptible to partial voluming with the neighbouring CSF (Concha et al., 2005b)

### 5.2.3 Region-of-Interest Diffusion Measurements

Using the standard DTI scans, average mean diffusivity (MD) and fractional anisotropy (FA) values were calculated for 10 brain regions using region-of-interest (ROI) analysis by the same investigator (L.W.), including the anterior and posterior limbs of the internal capsule, external capsule, corona radiata, centrum semiovale, subcortical white matter in gyri (right superior frontal gyrus, right supra marginal gyrus, right middle occipital gyrus, left superior temporal gyrus, and the left postcentral gyrus), and four deep gray matter structures (thalamus, globus pallidus, putamen, and head of the caudate nucleus), according to previously described methods (Snook et al., 2005). A previous intra-rater reliability study by the individual who performed all of the ROI analysis in this paper showed good reliability of ROI measurements (Snook et al., 2005). Three individuals were scanned on four separate occasions, and FA was measured in four regions (genu of the corpus callosum, corona radiata, thalamus and head of the caudate nucleus); standard deviations were 0.02 or smaller for FA values within the same individual. Where appropriate, left and right measurements were made separately and averaged for further analysis, since although some regions showed significant asymmetry, the absolute FA and MD differences were quite small (0.01 or less for FA and less than  $0.02 \times 10^{-3}$  mm<sup>2</sup>/s for MD). The FA and MD values from each of the five ROIs drawn in subcortical white matter in gyri were averaged to give one value for each individual, in order to improve the fits of the subcortical white matter in gyri. The five subcortical white matter regions had poor individual fits, likely due to partial volume effects of averaging with CSF. Eigenvalues were not analyzed for the regions measured using ROI analysis.

### 5.2.4 Fibre Tracking Diffusion Measurements

A novel, semi-automated tractography method was developed specifically for this project to logistically permit the extraction of ten tracts in 202 individuals. A template was created based on 20 scans of one 25 year old male. The images from these 20 scans were normalized to each other using an affine

transformation and averaged to create the template. Non diffusion-weighted images ( $b=0$  s/mm<sup>2</sup>) were registered to the template using an affine transformation followed by tensor reorientation. For each tract, seeding, target, and exclusion regions were selected manually on the template colour map and automatically copied to each normalized brain. All voxels within the seeding region were used as seed points for fibre tracking for each of the 202 subjects, and the target and exclusion regions served to include or exclude fibres passing through specific areas. Fibre tracking was performed in ExploreDTI using a deterministic streamline method. FA thresholds were set to 0.25 to initiate and continue tracking, while the angle threshold was set to 60 for the uncinate fasciculus and the superior longitudinal fasciculus and 30 for all other tracts. An FA threshold of 0.25 was chosen to avoid voxels that are not part of the white matter tract (cortex has FA  $\sim 0.2$ ), minimize the inclusion of voxels with a higher degree of partial volume contamination, and limit the presence of spurious tracts. Tractography was used to identify the genu and splenium of the corpus callosum, the inferior and superior longitudinal fasciculi, the inferior and superior fronto-occipital fasciculi, fornix, cingulum, uncinate fasciculus, and corticospinal tract, according to a priori information on tract location (Wakana et al., 2004). Standard DTI data was used to track all fibres except the fornix, for which we used FLAIR-DTI data due to deleterious partial volume effects in the standard (non-CSF suppressed) DTI data (Concha et al., 2005b). Where appropriate, left and right fibres were measured separately and averaged for further analysis, since although some regions showed significant asymmetry, the absolute FA and MD differences were quite small (0.01 or less for FA and less than  $0.02 \times 10^{-3}$  mm<sup>2</sup>/s for MD). Eigenvalues of the ten tractography-derived tracts were measured to determine what was driving any FA changes. Parallel diffusivity was measured by the first eigenvalue ( $\lambda_{\parallel} = \lambda_1$ ), while perpendicular diffusivity was calculated by averaging the second and third eigenvalues ( $\lambda_{\perp} = (\lambda_2 + \lambda_3)/2$ ).

### 5.2.5 Automated Fibre Tracking Reliability

Validity of the semi-automated fibre tracking method was ensured by manually tracking each of the ten white matter tracts in 15 randomly selected individuals. The results of the paired t-tests comparing the manual and semi-automated methods are shown in Table 5.1. While some tracts showed very small significant differences (all differences of FA were less than 0.015 and differences of MD were  $0.02 \times 10^{-3}$  mm<sup>2</sup>/s or smaller), these differences are smaller than the standard deviation of ROI measurements made from multiple scans of the same individual (Snook et al., 2005). All correlations between manual and semi-automated methods were highly significant (all correlations were greater than 0.836 with  $p < 0.001$ ). Furthermore, the semi-automated method of tractography is fairly robust to errors of spatial normalization, because the FA thresholds used for tracking help eliminate spurious fibres and allow seeding and target regions to be larger than the actual structure of interest, accommodating for misaligned structures due to poor normalization.

### 5.2.6 Curve Fitting

Average values of FA and MD for each ROI and over the entirety of each tract for tractography were correlated with subject age using linear and non-linear regression. Linear, monoexponential and biexponential fits were compared using F-tests and the Akaike information criterion (AIC). Negative values of the AIC were considered to mean the exponential fit offered substantial improvements over the linear fit, while a threshold of  $p < 0.05$  was used for the F-test between mono- and bi-exponential fits. Exponential fitting equations of the form  $FA$  (or  $MD$ ) =  $C + Ae^{-age/t}$  yielded time constants ( $t$ ) indicating the rate of development, as well as correlation coefficients and asymptotic standard error values indicating the quality of the fits. To compare developmental timing parameters, maximum development was defined as the FA and MD values at the asymptotes of the exponential curves, and the time to reach 90% of this maximum development from 5 years was calculated for each tract. Male and female fits were calculated separately and the timing parameters were com-

Table 5.1: Validation of semi-automated tractography versus manual tracking of all ten tracts in 15 individuals

Tract	Measure	Correlation (R)	Correlation p-value	Difference <sup>a</sup> FA: unitless MD: $10^{-3}\text{mm}^2/\text{s}$	Paired t-test p-value
Cingulum	FA	0.903	<0.001	-0.006	0.123
	MD	0.983	<0.001	-0.001	0.639
CST	FA	0.838	<0.001	-0.012	0.047
	MD	0.839	<0.001	0.020	0.002
Fornix	FA	0.836	<0.001	-0.013	0.007
	MD	0.863	<0.001	-0.020	0.064
Genu	FA	0.968	<0.001	-0.004	0.044
	MD	0.957	<0.001	0.001	0.759
IFO	FA	0.972	<0.001	0.014	0.000
	MD	0.961	<0.001	0.012	0.001
ILF	FA	0.935	<0.001	-0.011	0.000
	MD	0.959	<0.001	-0.007	0.011
Splenium	FA	0.830	<0.001	-0.000	0.995
	MD	0.874	<0.001	-0.020	0.004
SFO	FA	0.836	<0.001	0.009	0.007
	MD	0.871	<0.001	-0.015	0.004
SLF	FA	0.939	<0.001	-0.007	0.003
	MD	0.981	<0.001	-0.001	0.572
UF	FA	0.861	<0.001	-0.000	0.940
	MD	0.975	<0.001	-0.003	0.181

<sup>a</sup> Negative mean differences indicate that manual method has higher values than automated method

pared to see if they overlapped, given the standard error from the exponential fits. For FA values, the timing parameter differences between genders were less than one standard error and considered not to be significant. For MD values, the differences were larger, with five structures showing timing differences greater than two standard errors of the fit. However, the fits for all structures were considerably poorer when separated by gender, and no gender differences of FA timing were present, so data was combined to simplify interpretation and improve confidence in the fits; therefore, all data shown is combined male and female data.

### **5.2.7 Volume Measurements**

T1-weighted MPRAGE images were segmented using SPM5 (Wellcome Trust Centre for Neuroimaging, London, UK), after normalization to the T1 template provided as part of the software package. Total gray matter and white matter volumes were measured, and total brain volume was calculated. CSF was not included in total brain volume measurements. Linear regression was used to determine whether significant age-related changes existed in gray matter, white matter, and total brain volume.

## **5.3 Results**

### **5.3.1 FA Increases with Age**

For almost all structures, an exponential curve best represented the cross-sectional age-related increases of FA; only the uncinate fasciculus showed linear increases of FA. The increases occurred rapidly initially, then slowed and reached a plateau; for most structures, the plateau was reached during the late teens or twenties. FA increased significantly in 17 of 20 structures measured; however, no significant age-related changes were observed in the fornix, corona radiata or centrum semiovale. As shown in Figures 5.1 and 5.2, regional differences in the rate of development were observed for FA, with some brain regions, such as the corpus callosum and the inferior longitudinal fasciculus, increasing in FA (and presumably developing) faster and earlier than other

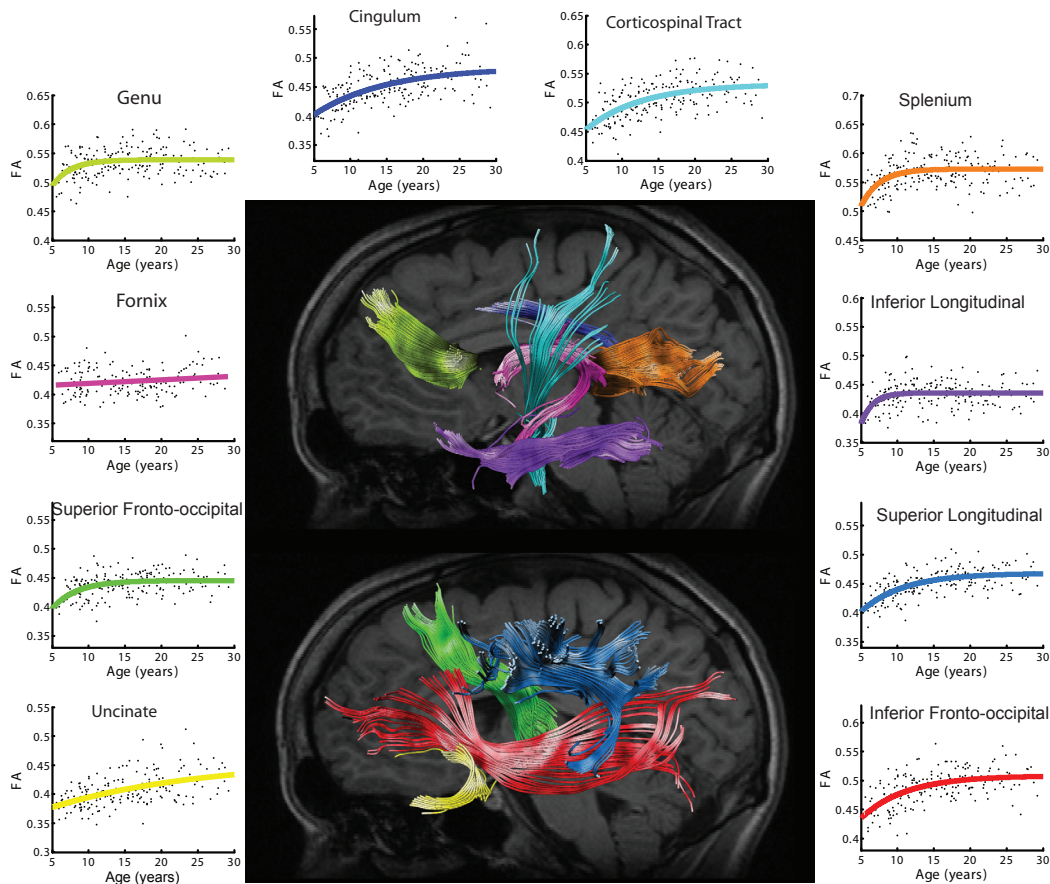


Figure 5.1: Considerable variation was seen in age-related fractional anisotropy (FA) changes in nine of ten white matter tracts measured using fibre tractography. These results suggest a hierarchical pattern of maturation in which areas with frontal-temporal connections develop more slowly than others. Here, tracts are shown in a 23 year old male with corresponding FA-age plots (colour of tract matches colour of curve in plot). Rapid development can be seen in the splenium and genu of the corpus callosum, while the cingulum and uncinate fasciculus demonstrate more gradual maturation. The fornix, a very basic tract involved in memory and emotion, shows no age-related changes at all. These structures showed similar age-related decreases of mean diffusivity, as shown in Fig. 5.4.

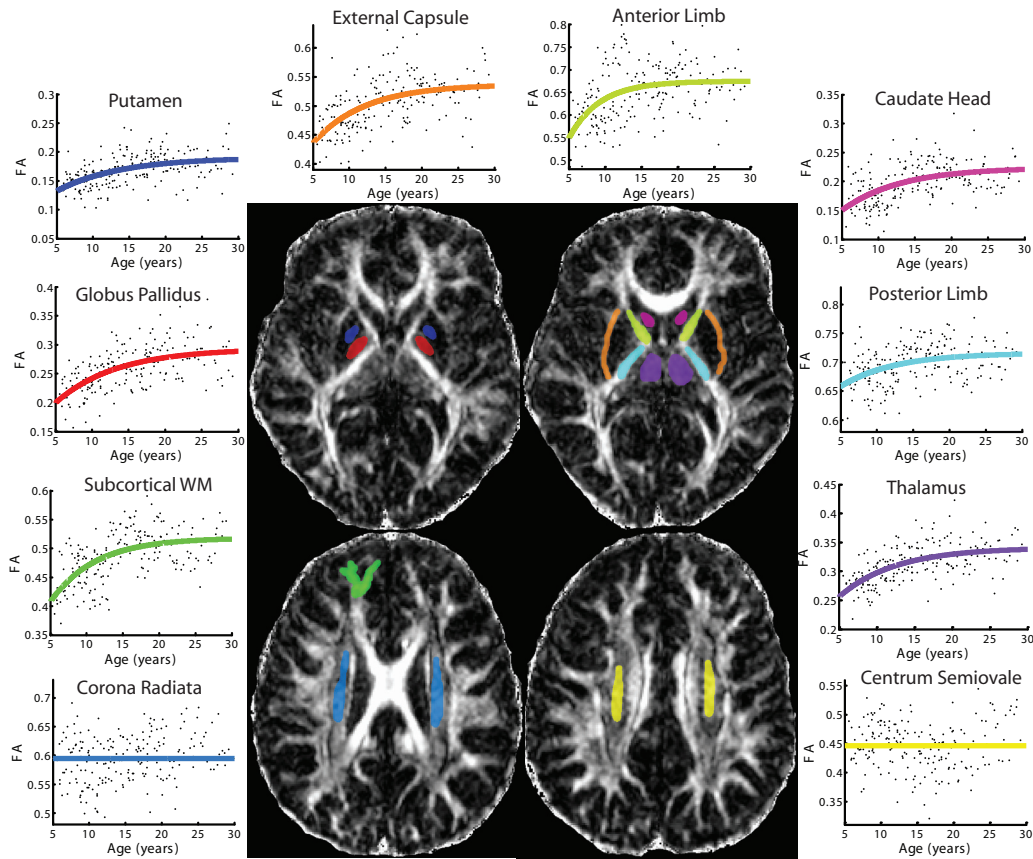


Figure 5.2: Variation was seen in age-related fractional anisotropy (FA) changes for 8 of 10 structures measured using region-of-interest analysis; this data also suggests hierarchical maturation. Here, regions are shown on the FA map of a 6 year old male with corresponding FA-age plots (colour of ROI matches colour of curve in plot). Considerable variation is seen in the amount of FA change, with deep gray matter structures such as the thalamus and caudate head showing very large percent changes and the white matter structures showing smaller, but still significant, changes. These structures showed similar age-related decreases of mean diffusivity, as shown in Fig. 5.5. Subcortical white matter curve was obtained by averaging FA values from five separate regions; only one region is shown above.

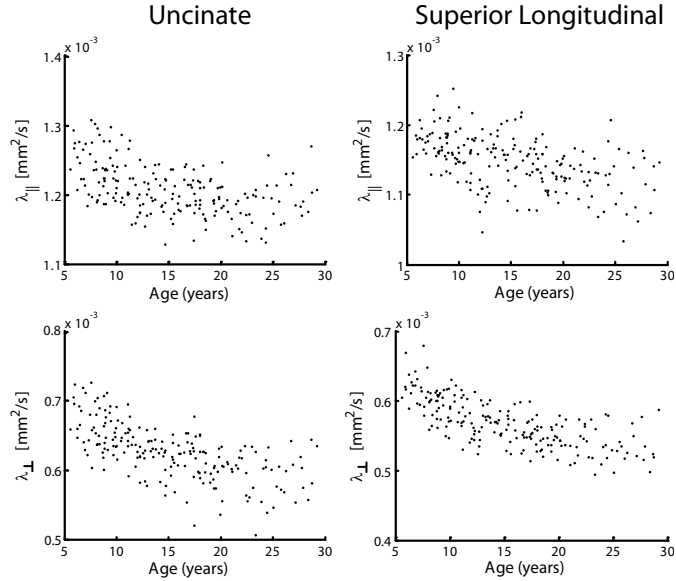


Figure 5.3: Parallel diffusivity ( $\lambda_{\parallel}$ ) remained constant or declined slightly in all white matter tracts analyzed with tractography, while perpendicular diffusivity ( $\lambda_{\perp}$ ) declined more than parallel diffusivity, driving the age-related increase of fractional anisotropy. The superior longitudinal fasciculus and uncinate fasciculus are shown here as examples.

tracts that appear to mature more slowly, such as the fronto-temporal connections. An analysis of the eigenvalues revealed a consistent pattern among the white matter tracts measured with tractography, with perpendicular diffusivity ( $\lambda_{\perp}$ ) decreasing in all tracts, while parallel diffusivity ( $\lambda_{\parallel}$ ) remained the same or decreased only slightly. Figure 5.3 shows the age-related changes of the eigenvalues for the superior longitudinal fasciculus and the uncinate fasciculus, for example.

### 5.3.2 MD Decreases with Age

An exponential fit best represented the age-related decreases of MD for most structures, with only the corticospinal tract demonstrating linear decreases of MD. For most structures, rapid decreases of MD occurred at younger ages, slowed, and gradually reached a plateau during the late teens or early twenties, as shown in Figures 5.4 and 5.5. Significant differences of MD with age were seen in all measured structures, including those that showed no age-related FA changes. Like FA changes, regional differences of the timing of MD changes

Table 5.2: Correlation (R) and time constant (t) of the exponential fits, as well as absolute and relative increases of FA over the age span of 5–30 years. Regions are sorted from earliest to latest developing

Region <sup>a</sup>	R	t <sup>b</sup>	Absolute change (5–30 years)	Percent change (5–30 years)
ILF	0.285	1.62	0.05	14
Splenium	0.382	2.57	0.06	13
Genu	0.355	2.58	0.05	9.0
SFO	0.453	3.47	0.05	12
Anterior limb	0.435	4.29	0.13	23
SLF	0.640	5.86	0.07	16
IFO	0.580	6.19	0.07	17
Subcortical WM	0.593	6.20	0.07	27
External capsule	0.543	7.20	0.10	23
Posterior limb	0.397	7.48	0.06	8.5
Thalamus	0.600	7.49	0.08	32
CST	0.591	7.70	0.08	17
Caudate head	0.511	7.97	0.07	47
Globus pallidus	0.591	8.33	0.09	45
Putamen	0.488	8.79	0.06	41
Cingulum	0.560	9.86	0.08	19
UF	0.514	- <sup>c</sup>	0.06	15

<sup>a</sup> No fits for FA changes were obtained for the corona radiata, centrum semiovale, and fornix, so no data is shown

<sup>b</sup> obtained from the exponential fit according to the equation  $FA=C + Ae^{-age/t}$

<sup>c</sup> FA changes in the uncinate fasciculus were best represented by a linear fit, so no t parameter is shown

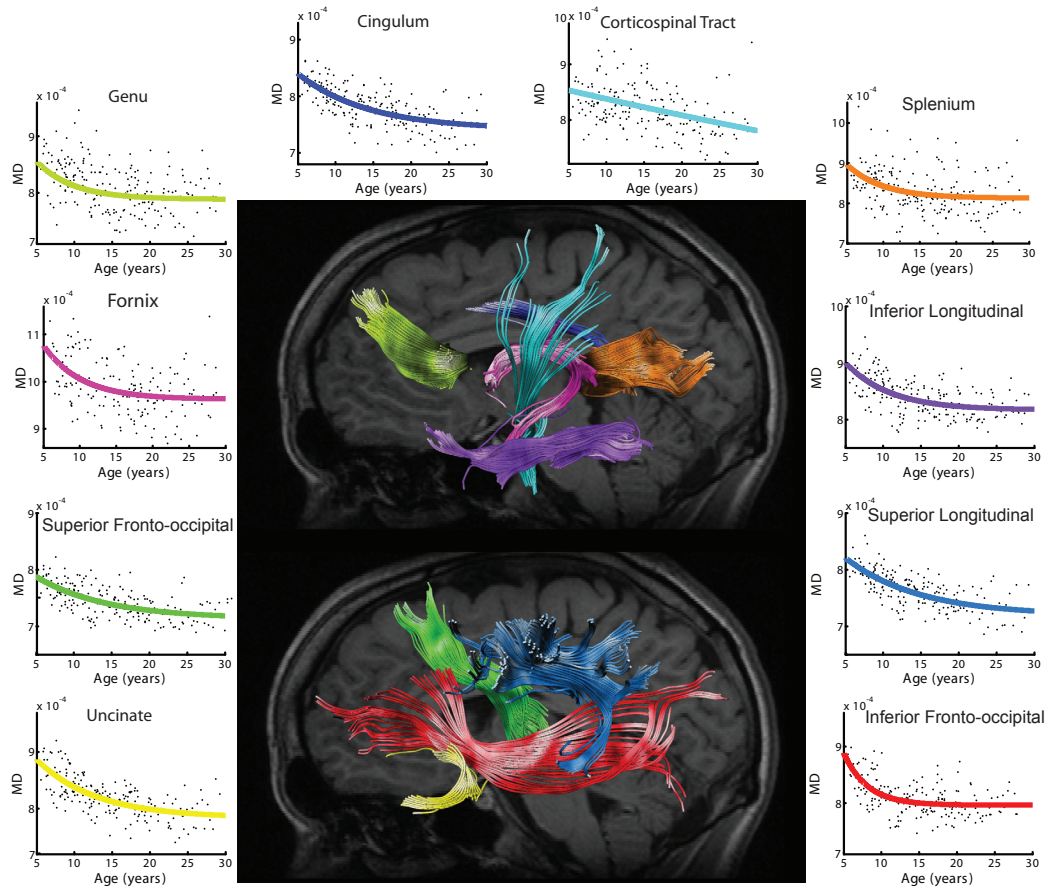


Figure 5.4: Significant decreases of mean diffusivity ( $\text{mm}^2/\text{s}$ ) were observed for all ten structures measured using tractography. Here, all ten white matter tracts are shown in a 23 year old male with corresponding mean diffusivity-age plots (colour of tract matches colour of curve in plot). The rate of decrease varies regionally, with frontal connections, such as the superior longitudinal fasciculus, superior fronto-occipital fasciculus, cingulum and uncinate fasciculus tending to mature later than other tracts such as the corpus callosum, fornix and inferior longitudinal fasciculus.

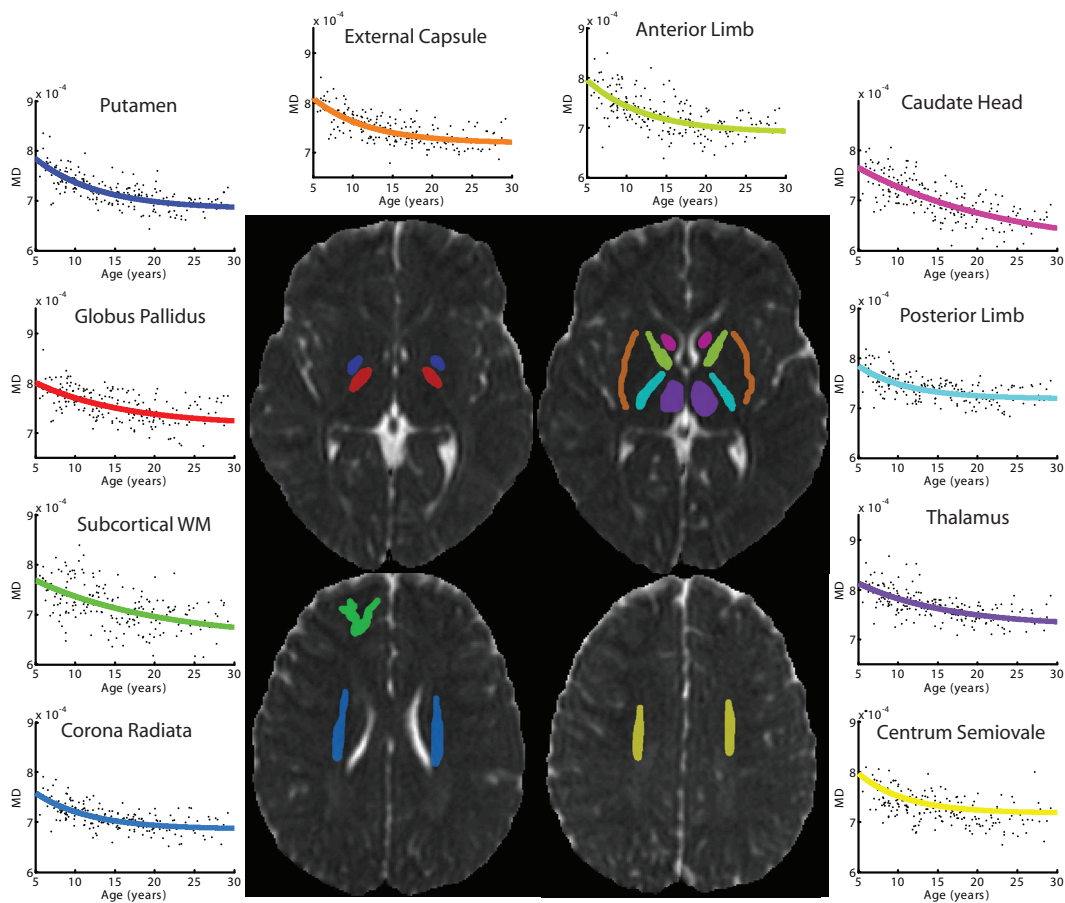


Figure 5.5: Significant decreases of mean diffusivity ( $\text{mm}^2/\text{s}$ ) were seen in all structures measured using region-of-interest analysis. Here, regions are shown here on the MD map of a 6 year old male with corresponding mean diffusivity-age plots (colour of ROI matches colour of curve in plot). Regional variation can be seen in the rate of the changes. Subcortical white matter curve was obtained by averaging MD values from five separate regions; only one region is shown above.

were observed; however, the range of exponential time constants was more uniform for MD decreases than for FA increases.

### 5.3.3 Timing and Magnitude of Changes

Figure 5.6 shows the relative timing and magnitude of development in all measured brain regions; these are also summarized in Tables 5.2 and 5.3. Error bars in Figure 5.6 represent the standard error and indicate the reliability of the timing parameter obtained from the exponential fit. As can be seen from Figure 5.6 and Tables 5.2 and 5.3, by age 20, approximately half of measured structures have reached 90% of their maximum FA values. At age 25, three structures have still not reached their plateau, with the uncinate fasciculus appearing to continue development beyond 30 years. MD decreases continue slightly later than FA increases, with only one structure having reached the 90% mark by age 15. Two structures, the head of the caudate nucleus and the corticospinal tracts, appear to continue undergoing MD changes past 30 years of age. In addition, the greatest magnitude of changes occurs in the deep gray matter, which shows up to 50% increases of FA and 16% decreases of MD.

### 5.3.4 Volume

Total brain volume, as well as white and gray matter volume, was measured for each subject using T1-weighted images. As shown in Figure 5.7, total brain volume is relatively constant throughout our sample, from age 5–30 years; however, the major tissue classes within the brain changed in opposite directions. A significant linear decrease of total gray matter was observed with a corresponding linear increase in total white matter volume.

## 5.4 Discussion

Although DTI has demonstrated that much of brain development occurs during the first few years of life (Dubois et al., 2008; Hermoye et al., 2006; Provenzale et al., 2007), our results illustrate that this process continues well beyond infancy. Tractography and ROI analyses have provided direct evidence that

Table 5.3: Correlation (R) and time constant (t) of the exponential fits, as well as absolute and relative reductions of MD over the age span of 5–30 years. Regions are sorted from earliest to latest developing.

Region	R	t <sup>a</sup>	Absolute change (5–30 years)	Percent change (5–30 years)
Corona radiata	0.354	6.68	-0.07	-9.3
Centrum semiovale	0.602	6.03	-0.08	-10
Fornix	0.426	5.23	-0.11	-11
ILF	0.592	5.88	-0.09	-9.2
Splenium	0.350	4.87	-0.08	-9.2
Genu	0.453	6.09	-0.08	-9.3
SFO	0.625	9.31	-0.07	-8.8
Anterior limb	0.633	6.69	-0.10	-13
SLF	0.724	9.80	-0.10	-11
IFO	0.560	3.15	-0.09	-10
Subcortical WM	0.717	7.919	-0.11	-13
External capsule	0.704	6.62	-0.09	-11
Posterior limb	0.600	5.63	-0.07	-8.2
Thalamus	0.651	9.62	-0.08	-9.3
CST	0.723	- <sup>b</sup>	-0.07	-15
Caudate head	0.407	7.97	-0.12	-8.6
Globus pallidus	0.575	8.49	-0.07	-9.1
Putamen	0.729	6.81	-0.10	-12
Cingulum	0.673	9.28	-0.09	-11
UF	0.697	7.82	-0.10	-11

<sup>a</sup> obtained from the exponential fit according to the equation  $MD=C + Ae^{-age/t}$

<sup>b</sup> The MD changes in the corticospinal tract were best represented by a linear fit, so no t parameter is shown.

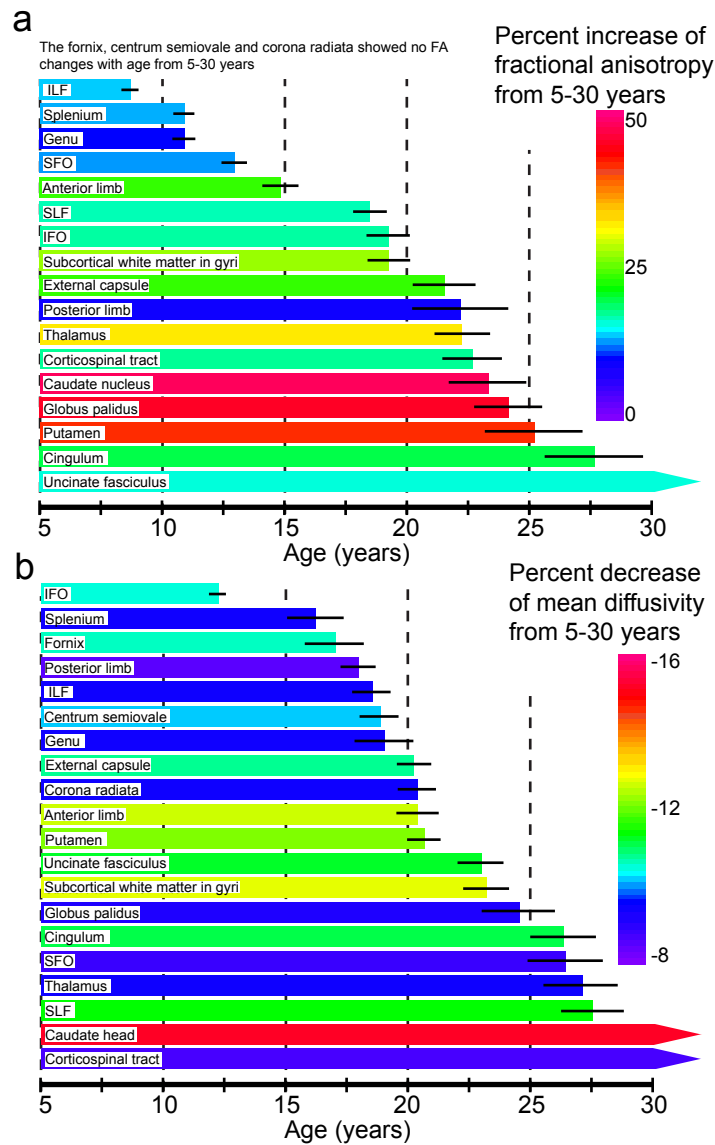


Figure 5.6: Magnitude and timing of development vary by brain region. The length of the coloured bars indicates the age at which regions reached 90% of their development plateau; the colour represents (a) the percent increase of FA or (b) decrease of MD from 5–30 years. The small black bars show the standard error of the timing parameter (error bars not included for regions with development extending beyond 25 years). The fornix, centrum semiovale and corona radiata showed no changes of FA; data not shown. Note the tendency of fronto-temporal connections (e.g., cingulum, uncinate fasciculus) to mature later than other structures, and that deep gray matter undergo the largest percent changes. FA increases for the uncinate fasciculus in (a) and decreases of MD for the caudate head and corticospinal tract in (b) extend beyond 30 years.

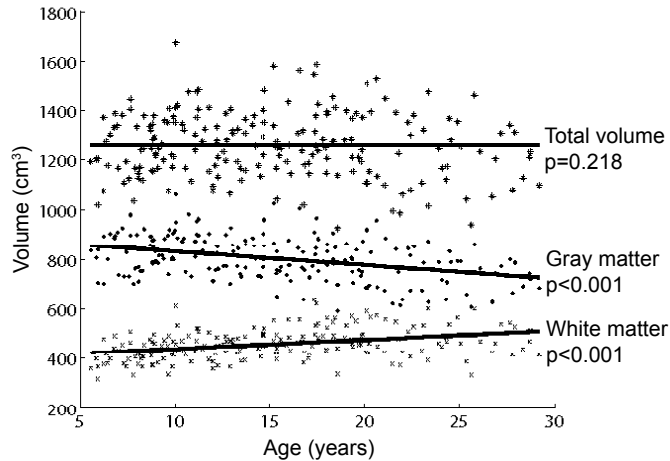


Figure 5.7: Total brain volume from T1-weighted scans, excluding cerebrospinal fluid, remains constant after age 5, despite major internal changes taking place throughout adolescence. Total white matter volume increases significantly, while total gray matter volume decreases over this age range of 5 to 30 years.

maturation of brain white matter and deep gray matter is widespread throughout the brain and continues throughout adolescence and, in some structures, into the twenties.

The putative rate of development, as implied by changes of diffusion parameters, can be obtained for each brain region from the exponential fit for that particular structure. There is considerable variation in the development curves, suggesting that white matter tracts with fronto-temporal connections, as well as deep gray matter areas, tend to mature more slowly than other regions. Brain structures can be categorized based on the age at which their curve reached 90% of its limit, as measured from 5 years (see Fig. 5.6). The fornix, a white matter connection involved in very basic processing such as memory and emotion, showed no significant changes of FA with age. DTI has demonstrated that, during infancy, the fornix appears to be more developed than other brain regions (Dubois et al., 2006, 2008), suggesting that its development may be complete by age 5. Two other areas, the corona radiata and the centrum semiovale, also showed no age-related FA changes; however, these are complex crossing fibre regions that are difficult to measure using the standard tensor model. The splenium and genu of the corpus callosum, crucial

left-right hemispheric connections, and the inferior longitudinal fasciculus, an important occipital-temporal tract involved in visual processing (Catani et al., 2003), show the earliest and most rapid changes of FA with age, all reaching 90% of their maximum FA value by 11 years of age. Most association fibres, such as the superior longitudinal fasciculus, the superior and inferior fronto-occipital fasciculi, and the anterior limb of the internal capsule reach the 90% milestone between 13 and 20 years of age. The external capsule, posterior limb of the internal capsule, corticospinal tract, all three of which are projection fibres, as well as two deep gray matter structures, the thalamus and the caudate head, all reach the 90% mark between the ages of 21 and 24 years. The globus pallidus and putamen, two deep gray matter structures, as well as the cingulum and uncinate fasciculus, important fronto-temporal connections, matured much later, reaching 90% of development only after 25 years of age.

Reductions of mean diffusivity demonstrate less timing variation amongst regions, and the changes, in general, occur later than the increases of FA. Visual and hemispheric connections, such as the inferior longitudinal fasciculus, and genu and splenium of the corpus callosum, undergo 90% of their MD developmental changes by 20 years of age. According to the MD time course, most frontal connections, gray matter structures, and the corticospinal tracts do not mature to this extent until age 24 or later. Although differences exist in the order of development, patterns of change similar to those observed with FA were seen, with the commissural fibres developing early and the fronto-temporal and gray matter structures maturing later. All structures showed significant decreases of MD, including the three structures that failed to show significant changes of FA with age. Although the FA development profiles for the posterior limb and the corticospinal fibres were quite similar (see Figure 5.6), the MD profiles differed substantially, with the corticospinal tract leveling off much later than the posterior limb. While the posterior limb of the internal capsule contains the corticospinal tract, it also contains fibres belonging to the corticobulbar fibres and thalamocortical somatosensory radiations, with the corticospinal tract occupying only the posterior third (Kretschmann, 1988).

Analysis of the eigenvalues for the tractography data revealed that the FA increases are due to age-related decreases of perpendicular diffusivity accompanied by either a modest decrease or no change at all in the parallel diffusivity for each tract (see Fig. 5.3). Remyelination in the mouse brain is characterized by decreases of perpendicular diffusivity without corresponding changes of parallel diffusivity (Song et al., 2005), suggesting that increasing myelination with age may be the cause of the drop of perpendicular diffusivity in our population. Other studies have also shown that developmental increases of FA are primarily driven by decreasing perpendicular diffusivity (Giorgio et al., 2008; Snook et al., 2005).

Absolute changes of FA and MD varied across the brain, as shown in Tables 5.2 and 5.3, with deep gray matter regions and frontal association fibres showing slightly larger increases of FA and decreases of MD than other regions. The percent changes of FA and MD, however, reveal large differences, and the greater magnitude of age-related diffusion parameter differences in the brain is interpreted as regions undergoing more development during childhood and adolescence. The deep gray matter structures examined, i.e., the thalamus, caudate nucleus, putamen, and globus pallidus, showed by far the largest percent changes of FA, increasing between 30–50% from 5 to 30 years of age. These large differences, particularly with respect to more moderate changes across the white matter, likely indicate that tracts emanating from or arriving at these gray matter structures are becoming better organized or more myelinated, perhaps undergoing so-called “rewiring”. Similarly, white matter may be extending into the deep gray matter structures from which they originate or terminate, resulting in an increase of FA. The subcortical white matter in gyri also showed relatively large age-related increases of FA of approximately 25%, and this suggests that as the brain develops, myelinated axons extend further into the cortex, causing this rise of FA of subcortical white matter. Major white matter tracts showed smaller increases of FA, between approximately 8–19%, indicating that myelination is still occurring during adolescence, but the changes are not quite as dramatic as in the subcortical white matter and deep gray matter. One interpretation of these marked differences in relative

changes, as well as timing, could be that the white matter wiring is laid down earlier, followed by “reprogramming” of the deep gray matter relay stations.

Despite total brain volume remaining constant after age 5 (see Fig. 5.7), major internal remodeling is occurring within the brain. Total gray matter volume declines, while white matter undergoes a corresponding increase in volume. Adolescence is thought to be a time of cortical pruning (Toga et al., 2006), and previous studies of cortical gray matter volume have shown inverted U-shaped curves representing age-volume changes, with age of peak volume depending on brain region (Giedd et al., 1999a). The timing parameters for maturation seem to indicate that white matter development (i.e. myelination and/or axonal packing) and deep gray matter reorganization occur in tandem with cortical changes, although cortical gray matter was not measured in this study. Total gray matter volume decreases in a linear manner across our age range while total white matter volume increases; one possible explanation is that increased myelination and advancing axons are causing tissue previously classified as gray matter to be newly classified as white matter and accounting for the tissue volume changes that occur despite constant total brain volume.

During infancy and early childhood, the brain undergoes rapid microstructural changes; between birth and 5 years of age, FA values increase by up to 200% and MD values decrease by approximately 40%, with the bulk of these changes occurring during the first 24 months of life (Dubois et al., 2006, 2008; Hermoye et al., 2006; Mukherjee et al., 2001; Partridge et al., 2005). These relative FA and MD changes are much larger than the ones reported in our study. Nonetheless, although the most rapid development occurs in infancy, we show that brain maturation continues well beyond that period, and most brain wiring is not fully established until the teenage years and even the twenties. By age 12, only three of 20 structures measured have undergone 90% of their FA changes (recall 90% relative to age 5); by age 20, an additional five structures have reached this 90% milestone, including most of the association tracts and subcortical white matter. By age 25 years, only the cingulum and the uncinate fasciculus, two important fronto-temporal connections, have yet to reach a plateau.

In agreement with our findings, previous studies have consistently reported brain maturation during adolescence in the internal capsule, arcuate fasciculus, and corticospinal tracts (Barnea-Goraly et al., 2005b; Ben Bashat et al., 2005; Paus et al., 1999; Schmithorst et al., 2002). Developmental changes have also been reported in a large number of other brain areas where we also found age-related changes, including the corpus callosum and subcortical white matter (Ben Bashat et al., 2005), occipital pathways (Barnea-Goraly et al., 2005b) and the inferior longitudinal fasciculus (Schmithorst et al., 2002). We observed more widespread brain maturation, however, with all brain regions measured demonstrating decreases of MD, and most areas demonstrating FA increases during adolescence. Timing parameters of non-linear development have been previously reported in only one study of adolescents (Ben Bashat et al., 2005); however, their cohort included much younger subjects (as young as 4 months), making comparisons difficult due to the rapid development of infant brains. Our observations of exponential brain maturation during adolescence may be a continuation of the exponential patterns of development that are observed during infancy and early childhood in many of the same structures (Hermoye et al., 2006; Mukherjee et al., 2001), or they may represent different and separate developmental time courses; further studies over the entire age range with the same imaging parameters and analysis methods may be able to settle this question.

Several postmortem studies (Benes, 1989; Yakovlev and Lecours, 1967) have described a general pattern of posterior to anterior myelination. The opposite pattern was observed in the corpus callosum using sophisticated image processing of anatomical MRI scans as a rostral to caudal wave of growth (Thompson et al., 2000). Using DTI, we observed the splenium developing slightly before the genu, as evidenced by MD changes; however, the timing of FA increases in these two structures is similar. More generally, our data seem to indicate that some frontal connections, particularly fronto-temporal connections such as the uncinate fasciculus and the cingulum, mature later and more slowly than other connections, such as the commissural connections of the corpus callosum. Some frontal connections, however, such as the inferior

and superior fronto-occipital fasciculi, display relatively early maturation compared to other structures. In addition, the deep gray matter structures and the projection fibres seem to exhibit relatively slow maturation, perhaps indicating the ongoing development of these structures. These patterns are also similar to DTI studies of preterm infant brain maturation that show frontal areas tend to mature later than others (Deipolyi et al., 2005; McKinstry et al., 2002). The temporal lobe demonstrates later maturation than other regions, as evidenced by continued cortical thickening into the thirties and later volumetric changes than other cortices (Giedd et al., 1999a; Sowell et al., 2003), supporting our findings of slow maturation of fronto-temporal connections.

Our large, age-distributed sample relative to previous studies allows for increased sensitivity to non-linear developmental changes, and our findings challenge earlier DTI findings suggesting a linear increase (Barnea-Goraly et al., 2005b; Schmithorst et al., 2002). These two studies used voxel-based analysis methods, which assume linear development. Our observed non-linear pattern of maturation was consistent across the brain, with only the uncinate fasciculus showing linear development of FA with age and the corticospinal tract demonstrating a linear reduction of MD with age. Given a larger age range, these tracts would likely show non-linear changes that level off during the thirties or later. For most brain areas, the exponential model was superior to the linear model, indicating the robustness of these non-linear findings.

While several studies have observed asymmetry of brain anisotropy (Buchel et al., 2004; Gong et al., 2005) and sex differences during development (Giedd et al., 1999a; Lenroot et al., 2007; Schmithorst et al., 2008; Schneiderman et al., 2007), we observed only very small asymmetries and gender differences in our cohort, and elected to combine all data for the final analysis. Asymmetry of anisotropy has been reported in the cingulum (Gong et al., 2005) and the superior longitudinal fasciculus (Buchel et al., 2004), both showing left greater than right asymmetry. While we also observed leftward asymmetry in both of these white matter tracts, the actual differences of FA were very small, only 0.01 for each tract. Asymmetry was observed in several other structures, but in all cases asymmetry of FA was 0.01 or less, and differences

of MD were smaller than  $0.02 \times 10^{-3}$  mm<sup>2</sup>/s. Since these differences are very small and separating them would add unnecessary complexity, all values from left and right hemispheres were averaged in this paper. Similarly, male and female data were combined, due to only minor differences in developmental trajectories. Since we were interested in the relative timings of development, we looked for differences between male and female timing parameters, rather than absolute FA or MD differences. For age-related FA changes, all gender differences of the timing parameter were smaller than the standard error of the measurement. Furthermore, fits were greatly improved by combining males and females (effectively doubling the data set). Therefore, males and females were combined for all of our analyses, as has been done in many developmental studies (Barnea-Goraly et al., 2005b; Mukherjee et al., 2001; Snook et al., 2005; Sowell et al., 2003).

Deterministic tractography methods require threshold values of FA to define each tract, although this practice may influence the resulting FA values calculated from the tract. For this study, the threshold was set to voxels with FA values greater than 0.25, to minimize inclusion of voxels with a high degree of partial volume contamination, and to avoid spurious tracts. Choosing a threshold is unlikely to substantially affect the age-related FA and MD changes with respect to the relative differences between structures. FA values derived from tractography are, in general, lower than FA values derived from ROI analysis due partly to this floor value, but primarily to variability of FA along the tracts themselves. ROI analysis defines structures on two-dimensional maps and generally includes the areas of higher FA in a particular tract. Tractography, however, include a much larger portion of the tract, including the lower FA values near the ends, and obtains values that are lower overall. This variability in FA measures means that values obtained using identical methods can be compared, while it is difficult to compare absolute FA measures from different procedures.

## 5.5 Conclusion

We used diffusion parameters as surrogate markers for microstructural development to extract the magnitude and timing of developmental changes in 20 brain regions that included major white matter tracts, subcortical white matter, and deep gray matter. We examined maturation of these structures over a wide age range of 5 to 30 years in a large sample of 202 healthy subjects. Both ROI analysis and tractography revealed development trajectories for all structures which, if compared to those in a patient population, could highlight the presence and timing of specific brain abnormalities associated with a particular disease.

## Chapter 6

# Longitudinal Diffusion Tensor Imaging of Human Brain Maturation from Childhood to Adulthood<sup>1</sup>

### Abstract

Brain development is a complex process that begins in utero and continues during childhood and adolescence. Longitudinal studies provide increased sensitivity over cross-sectional studies and the ability to measure changes within individuals, yet there have been very few looking at healthy brain development. We examined longitudinal brain maturation using diffusion tensor tractography in 103 healthy subjects initially aged 5–29 years. Each volunteer was scanned at least twice, with an average age gap of 3.8 years. Fractional anisotropy (FA) and mean diffusivity (MD) were assessed in eleven different white matter pathways. All tracts showed significant changes of both FA and MD across the age range, with most tracts demonstrating non-linear increases of FA that slowed and, in some cases, reversed at the upper end of the age range; most tracts also showed non-linear decreases of MD. Average changes within individuals ranged from 1–5% increases of FA and 0–4% MD decreases

---

<sup>1</sup>A version of this chapter has been published. C. Lebel and C. Beaulieu, 2009. Longitudinal Diffusion Tensor Imaging of Healthy Brain Development in Children, Abstract #3421. Proceedings of the International Society for Magnetic Resonance in Medicine, 17th Annual Meeting, Honolulu, Hawaii, USA.

in the youngest subjects to changes ranging from -2 to +2% for FA and -1 to +1% for MD in the oldest subjects. Overall, the frontal-temporal connections (uncinate fasciculus, cingulum, superior longitudinal fasciculus) had the most prolonged development, while the genu and splenium of the corpus callosum demonstrated the earliest changes.

## 6.1 Introduction

Childhood and adolescence are periods of significant change, with behavioural, emotional, hormonal and cognitive processes undergoing maturation. Brain structure is no different, and brain development progresses throughout childhood and adolescence and into young adulthood. Longitudinal studies are valuable because they can measure structural changes within individuals and have increased sensitivity over cross-sectional studies. Longitudinal brain development studies using conventional magnetic resonance imaging (MRI) have shown regional variation in development trajectories of white and gray matter volume (Giedd et al., 1999a,b; Giorgio et al., 2010; Lenroot et al., 2007), as well as gender differences (Giedd et al., 1999a; Lenroot et al., 2007).

Diffusion tensor imaging (DTI) is an excellent way of studying structural brain changes as it provides a more sensitive measure of tissue microstructure than conventional imaging. Many cross-sectional studies have used DTI to investigate age-related changes of brain structure during childhood, adolescence and young adulthood. These studies consistently show increasing fractional anisotropy (FA), a measure of white matter integrity, and decreasing mean diffusivity (MD), a measure of the overall water diffusion (Ashtari et al., 2007; Barnea-Goraly et al., 2005b; Bonekamp et al., 2007; Eluvathingal et al., 2007; Lebel et al., 2008b; Mukherjee et al., 2001; Schmithorst et al., 2002). Although informative, cross-sectional studies are limited because they cannot provide information about change within individual subjects. Longitudinal studies, with increased sensitivity, are needed to more accurately examine gender and hemispheric differences of white matter development. Only one DTI study has examined longitudinal FA changes during adolescence, using voxel-based

analysis to show significant age-related increases of FA throughout most of the brain white matter in 24 adolescents (Giorgio et al., 2010). However, this study had a relatively small sample size and used voxel-based methods that assume linear FA changes. While age-related changes can be approximated as linear over small age ranges, they are non-linear over larger ranges (Ben Bashat et al., 2005; Lebel et al., 2008b; Mukherjee et al., 2001), and nonlinear development models provide additional information about relative timing of development and regional variations throughout the brain.

The goal of this study was to extend previous cross-sectional work by examining longitudinal development of brain white matter using DTI tractography in a large group of 103 healthy subjects from childhood to adulthood (5–32 years). Longitudinal studies, especially with this many subjects, provide a large amount of data that can be examined in many different ways. In this study, we measure the trajectories of FA and MD with age, but also closely look at brain development within individual subjects.

## 6.2 Methods

### 6.2.1 Subjects

Subjects for this study were 103 healthy volunteers with no self-reported history of neurological or psychiatric disease or brain injury. Subjects were initially aged 5.6 to 29.3 years (mean age  $\pm$  standard deviation:  $14.8 \pm 6.4$ , 52 female/51 male, 97 right-handed/6 left-handed). A total of 221 scans were obtained on these subjects: 92 volunteers were scanned exactly twice, 7 subjects received three scans, and 4 subjects were scanned four times. The mean age gap between first and second scans was 3.8 years. The first scans for many of these subjects (94) were included in a previous cross-sectional study of brain development from age 5–30 years (Lebel et al., 2008b). All subjects gave informed consent; child assent and parent/guardian consent was obtained for volunteers under 18 years.

## 6.2.2 Image Acquisition

All data was acquired on the same 1.5 T Siemens Sonata MRI scanner with identical methods. DTI acquisition used a dual spin-echo, single shot echo-planar imaging sequence with the following parameters: 40 3 mm thick slices with no inter-slice gap, TR=6400 ms, TE=88 ms, 6 non-collinear diffusion sensitizing gradient directions with  $b=1000$  s/mm<sup>2</sup>, 8 averages, field-of-view 220×220 mm<sup>2</sup>, matrix of 128×128 with 75% phase partial Fourier, zero-filled to 256×256. Total DTI acquisition time was 6:06 minutes. Cerebrospinal fluid (CSF)-suppressed DTI was acquired for at least two time points in 80 subjects and used a dual spin-echo, echo planar imaging sequence with inversion time=2200 ms, TR=8600 ms, TE=88 ms, 26 slices, all other parameters the same as standard DTI. CSF-suppressed DTI was not successfully acquired in other subjects due to time constraints or motion artifacts. High resolution (1×1×1 mm<sup>3</sup>) T1-weighted images were acquired using MPRAGE with TE=4.38 ms, TR=1870 ms, TI=1100 ms, scan time was 4:29 minutes. T1-weighted images were successfully acquired for 215 of the 221 scans; there were 99 subjects with MPRAGE images at multiple time points.

## 6.2.3 Tractography

A previously described semi-automated tractography method (Lebel et al., 2008a) was used to delineate eleven major white matter tracts in each individual, according to a priori information on tract location (Catani et al., 2002; Wakana et al., 2004). The tracts delineated were the genu, body, and splenium of the corpus callosum (CC), superior and inferior longitudinal fasciculi, superior and inferior fronto-occipital fasciculi, uncinate fasciculus, corticospinal tracts, cingulum, and the fornix. Fibre tracking was performed using Matlab code modified from ExploreDTI (A. Leemans, Utrecht, Netherlands), using a deterministic streamline method. FA thresholds were set to 0.25 to initiate and continue tracking, while the angle threshold was set to 60° for the uncinate fasciculus, superior longitudinal fasciculus, and fornix and 30° for all other tracts. An FA threshold of 0.25 was chosen to avoid voxels that are

not part of the white matter tract (cortex has FA  $\sim 0.2$ ), minimize the inclusion of voxels with a higher degree of partial volume contamination, and limit the presence of spurious tracts. Where appropriate, left and right fibres were measured separately.

#### **6.2.4 Diffusion Measurements**

Fractional anisotropy (FA) and mean diffusivity (MD) were measured for each individual scan for each tract by averaging all voxels along the tract; each voxel was counted only once. Eigenvalues were also measured to determine what was driving any FA or MD changes. Parallel diffusivity was measured by the first eigenvalue ( $\lambda_{\parallel} = \lambda_1$ ), while perpendicular diffusivity was calculated by averaging the second and third eigenvalues ( $\lambda_{\perp} = (\lambda_2 + \lambda_3)/2$ ).

#### **6.2.5 Inter-Scan Reliability**

To test the inter-scan reliability of FA and MD measurements, seven individuals aged 7, 9, 10 (2 subjects), 17, 21 and 23 years were scanned 3–4 times each within six months. FA and MD values were calculated for each tract according to the semi-automated methods described above. The mean, standard deviation, and spread of FA and MD values were calculated for each individual, and the average spread and standard deviation of values for each tract were computed to provide estimates of accuracy of the longitudinal FA and MD measurements. CSF-suppressed DTI was not acquired in these reliability subjects.

#### **6.2.6 Statistical Analysis**

Age-related changes of FA and MD were analyzed using linear mixed models to account for the repeated measurements on each individual. The following equation was fit to the data: FA (or MD) =  $A \cdot \text{age}^2 + B \cdot \text{age} + C + D \cdot \text{sex}$ . If terms were not significant, they were eliminated and a new fit was calculated. For fits where the quadratic term was significant, age of peak FA value and minimum MD value was calculated. Initially, separate fits were calculated for

the left and right hemisphere tracts, where appropriate. If the age and age<sup>2</sup> fitting parameters were not significantly different between hemispheres (using F-tests), average values were computed and one fit was done for both left and right sides combined.

To further evaluate changes, subjects were divided into 6 groups according to age: 5–11 years (15 subjects initially aged 5–8 years and aged 7–11 years at their final scan), 8–15 years (8–10 years to 12–15 years; n=23), 11–18 years (11–14 years to 15–18 years; n=16), 15–22 years (15–18 years to 19–22 years; n=18), 19–25 years (19–21 years to 22–25 years; n=16), and 22–32 years (22–29 years to 24–32 years; n=15). For subjects with only two scans, the change of FA or MD within each region was measured as the value at the second scan minus the value at the first. For subjects with more than two scans, best fit lines were calculated, and the total diffusion parameter changes were measured as the difference between the best fit line at the final age and the initial age. Within each age group, the number of subjects who had FA or MD increases or decreases greater than the average standard deviation for that tract (as computed by the reliability tests described above) were tabulated. Subjects who had FA or MD changes within one standard deviation were considered not to change. As CSF-suppressed DTI was not acquired in the reliability subjects, the mean standard deviation from the other tracts was used for the fornix. In addition, percent changes were calculated for each subject and averaged across each age group.

### **6.2.7 Diffusivities**

To investigate the causes of any changes of FA or MD across the age span, the parallel ( $\lambda_{\parallel}$ ), and perpendicular ( $\lambda_{\perp}$ ) diffusivities (eigenvalues) were examined using a mixed models approach in the same way as FA and MD values, using an equation of the form  $\lambda_{\parallel}$  (or  $\lambda_{\perp}$ ) = A\*age<sup>2</sup> + B\*age + C.

### **6.2.8 Brain Volume**

Gray matter and white matter volume, as well as total brain volume were measured using FreeSurfer (Athinoula Martinos Center for Biomedical Imag-

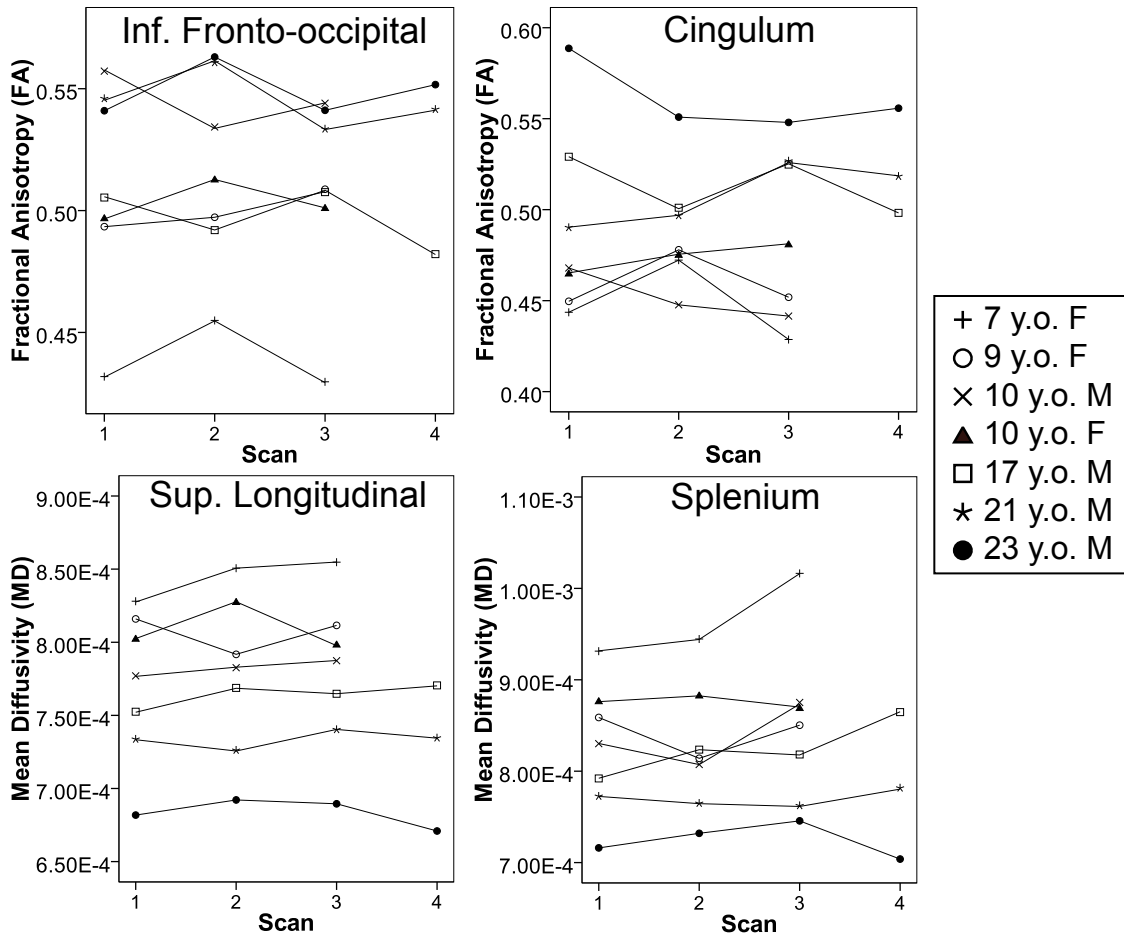


Figure 6.1: FA and MD values are shown in 7 individuals for several tracts (each individual is marked with a different symbol). All 7 individuals were scanned 3–4 times over a period of less than 6 months. Overall, diffusion parameter measurements from tractography were fairly stable across these short periods of time, with some small variation due to random error (approximately 1–3% on average).

ing, Charlestown, Massachusetts). Total brain volume did not include cerebrospinal fluid (CSF). Changes in brain volumes were modeled using the same linear mixed models methods described above for FA and MD changes.

## 6.3 Results

### 6.3.1 Inter-scan Reliability

There was variation in FA and MD values measured within seven individuals across time points (as seen in Figure 6.1). However, this variation was relatively small: the average standard deviations across all 7 subjects for the

Table 6.1: Seven subjects were scanned 3–4 times each over a period of less than six months. Their FA and MD values were measured for 10 major white matter tracts and the spread and standard deviation calculated. The average spread and standard deviation of values across subjects are given below for each tract.

Tract	FA spread	FA standard deviation	MD spread ( $\times 10^{-3}$ mm <sup>2</sup> /s)	MD standard deviation ( $\times 10^{-3}$ mm <sup>2</sup> /s)
bCC	0.0251	0.0125	0.0215	0.0421
Cingulum	0.0316	0.0160	0.0242	0.0118
CST <sup>a</sup>	-	-	0.0502	0.0253
Left CST <sup>a</sup>	0.0368	0.0287	-	-
Right CST <sup>a</sup>	0.0373	0.0187	-	-
gCC	0.0248	0.0121	0.0339	0.0173
IFO	0.0223	0.0109	0.0226	0.0118
ILF	0.0143	0.0069	0.0252	0.0117
sCC	0.0251	0.0115	0.0487	0.0237
SFO	0.0180	0.0090	0.0234	0.0112
SLF	0.0180	0.0085	0.0209	0.0104
UF	0.0221	0.0104	0.0248	0.0119

<sup>a</sup> The CST was assessed separately for each hemisphere for FA measures, where there were significant differences in the age and age<sup>2</sup> parameters; for MD there were no significant differences, so hemisphere were combined.

Table 6.2: Fitting parameters for age-related changes of fractional anisotropy (FA) and mean diffusivity (MD) for all tracts are given, with significance values in parentheses. \* $p < 0.001$ ; n.s.=not significant

	Fractional Anisotropy				Mean Diffusivity (mm <sup>2</sup> /s)			
	Intercept	Age ( $\times 10^{-2}$ )	Age <sup>2</sup> ( $\times 10^{-3}$ )	Sex <sup>a</sup> ( $\times 10^{-2}$ )	Intercept ( $\times 10^{-3}$ )	Age ( $\times 10^{-5}$ )	Age <sup>2</sup> ( $\times 10^{-6}$ )	Sex <sup>a</sup> ( $\times 10^{-2}$ )
bCC	0.48 *	0.60 *	-0.14 *	n.s.	0.97 *	-0.97 *	0.16 (0.004)	n.s.
Cing	0.43 *	0.33 *	-0.07 (0.038)	-1.4*	0.88 *	-0.94 *	0.17 *	0.89 0.021
CST <sup>b</sup>					0.86 *	-0.20	n.s.	1.2 (0.007)
L CST <sup>b</sup>	0.43 *	1.03 *	-0.24 *	-0.9 (0.004)				
R CST <sup>b</sup>	0.46 *	0.60 *	-0.13 *	-1.1 (0.001)				
Fornix	0.37 *	0.15 (0.001)	n.s.	-1.4*	1.00 *	-1.24 (0.003)	0.30 (0.007)	n.s.
gCC	0.52 *	0.51 *	-0.13 *	n.s.	0.88 *	-0.87 *	0.18 *	n.s.
IFO	0.45 *	0.68 *	-0.13 *	n.s.	0.88 *	-0.68 *	0.15 *	n.s.
ILF	0.41 *	0.47 *	0.01 (0.001)	n.s.	0.93 *	-0.79 *	0.16 *	n.s.
sCC	0.53 *	0.52 (0.001)	-0.11 (0.013)	1.3 (0.001)	0.93 *	-1.36 *	0.31 *	n.s.
SFO	0.41 *	0.53 *	-0.13 *	n.s.	0.82 *	-0.62 *	0.11 (0.002)	0.81 (0.017)
SLF	0.42 *	0.67 *	-0.14 *	-0.5 (0.027)	0.85 *	-0.89 *	0.17 *	n.s.
UF	0.37 *	0.44 *	-0.08 (0.011)	-0.9 (0.002)	0.90 *	-0.58 *	0.10 *	n.s.

<sup>a</sup> Positive values for sex differences indicate higher FA or MD values in females.

<sup>b</sup> The CST was assessed separately for each hemisphere for FA measures, where there were significant differences in the age and age<sup>2</sup> parameters; for MD there were no significant differences, so hemisphere were combined.

tracts were less than 0.019 for FA and less than  $0.026 \times 10^{-3}$  mm<sup>2</sup>/s for MD values. The average spread of values was approximately double the standard deviation for most tracts (Table 6.1). The superior and inferior longitudinal fasciculi, superior and inferior fronto-occipital fasciculi, and the uncinate fasciculus had the lowest standard deviations for FA and MD values, while the corticospinal tracts, and corpus callosum had higher standard deviations.

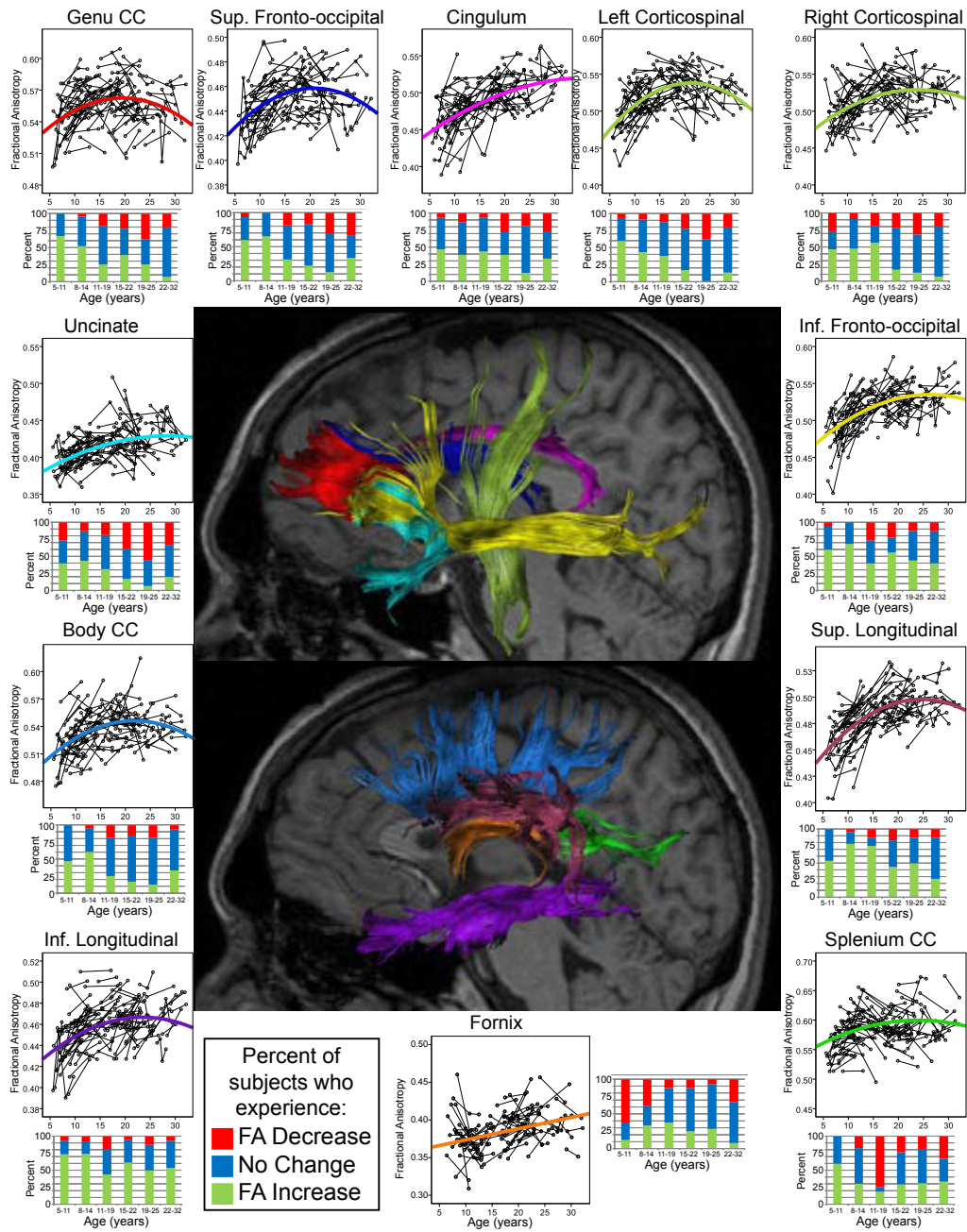


Figure 6.2: All eleven tracts showed significant age-related changes of fractional anisotropy (FA); all but the fornix demonstrated quadratic trends with increases of FA during childhood which slow during adolescence and young adulthood. The fornix showed linear increases of FA.

### 6.3.2 FA Increases with Age

There were significant age-related increases of FA in all eleven tracts measured (see Figure 6.2, Table 6.2). All tracts except the fornix had significant age and age<sup>2</sup> terms, indicating non-linear development, with the most rapid FA increases at the youngest ages, slowing and in some cases reversing at the upper end of the age range. The fornix had linear increases of FA across the age range. The corticospinal tracts had significant differences between left and right sides, and therefore they were kept separate; fits for both sides were significant. The uncinate, cingulum, superior longitudinal, inferior fronto-occipital fasciculus, and fornix had the most prolonged increases of FA, while the genu, and superior fronto-occipital fasciculus had the earliest FA peaks.

### 6.3.3 MD Decreases with Age

All eleven tracts measured showed significant age-related decreases of MD: ten had significant nonlinear trajectories and one, the corticospinal tract, had a linear trajectory (see Figure 6.3, Table 6.2). The non-linear trends showed decreasing MD at first, then slowed and sometimes reversed, with small increases of MD at the upper end of the age range. The corticospinal tracts had significant linear decreases of MD across the age range. The genu, splenium, fornix, and inferior fronto-occipital fasciculus showed the earliest reversals of MD trajectories; most of the other tracts with significant non-linear fits showed more gradual decreases at the upper ages rather than MD increases. None of the tracts showed differences in trajectories between hemispheres.

### 6.3.4 Sex Differences

Six tracts had significant gender differences in the FA parameters, while only three showed sex differences of MD values (two tracts had sex differences of both FA and MD values; see Table 6.2). Females had significantly higher FA values in the splenium of the corpus callosum, while males had significantly higher FA in the cingulum, fornix, corticospinal tracts (both left and right sides), superior longitudinal fasciculus, and uncinate fasciculus. In terms

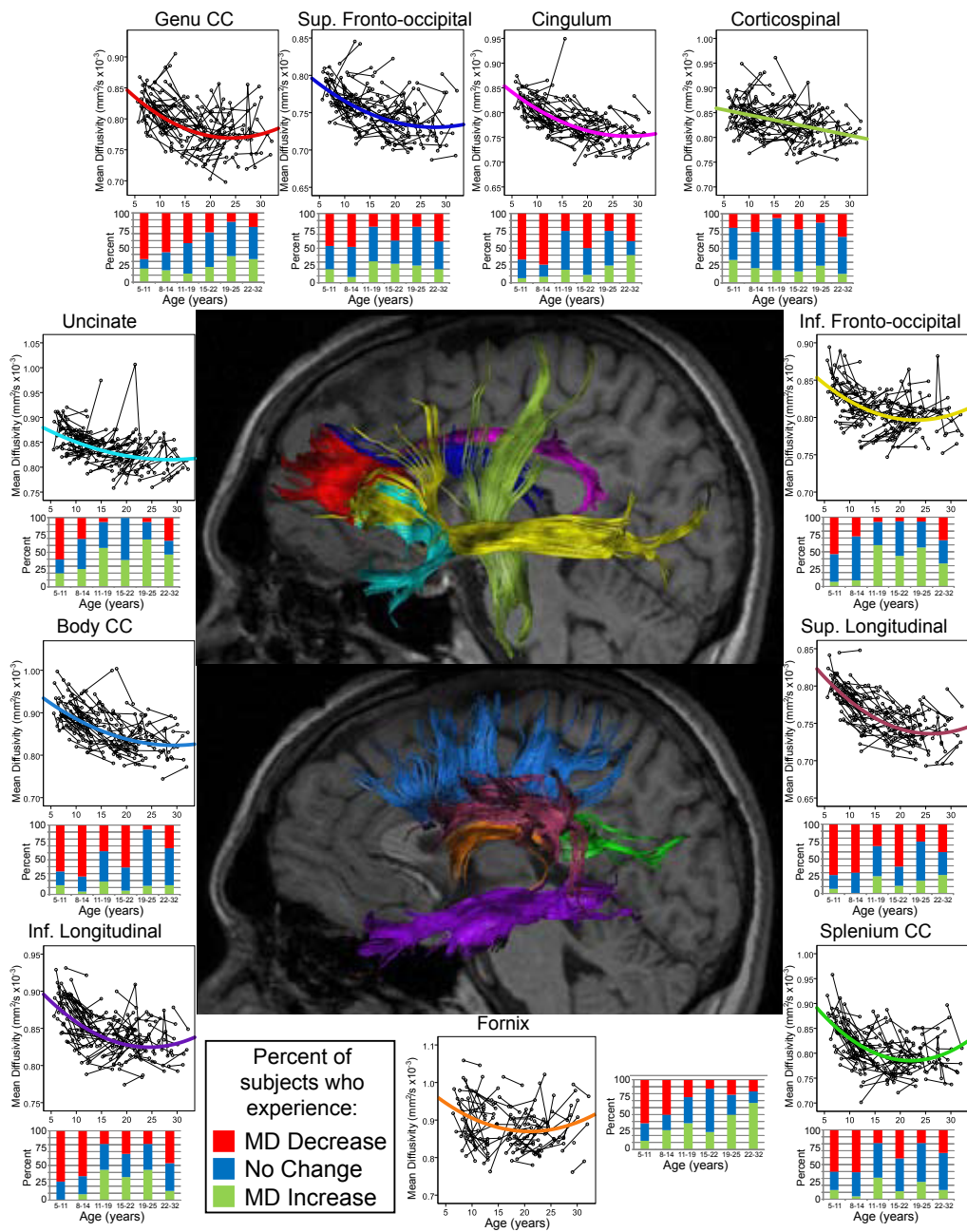


Figure 6.3: All eleven tracts measured showed significant age-related decreases of mean diffusivity (MD); the corticospinal tract had a linear decrease, while the other tracts showed quadratic changes.

of MD, females had higher values in the cingulum, corticospinal tracts, and superior fronto-occipital fasciculus.

### **6.3.5 Group Analysis of Age-Related Changes**

The total FA or MD change for each subject between their first and last scans was calculated and compared to the standard deviation value (from the reliability analysis) for that particular tract. If the change was greater than the standard deviation in either direction, the subject was considered to have an “increase” or a “decrease” between scans. If the change was less than the standard deviation, the subject was considered not to change. The number and percent of subjects increasing, decreasing, and staying the same are shown in Figure 6.2 for FA and Figure 6.3 for MD values. The majority of tracts showed a pattern in which the proportion of subjects with increasing FA started high, at 50–75%, and decreased steadily across groups such that in the oldest age group, most subjects had decreases (20–30%) or no change (30–70%) and only 10–30% were showing increasing FA. The superior and inferior longitudinal fasciculi, and the inferior fronto-occipital fasciculus had more steady patterns, with 40–70% of young subjects and 20–55% of older subjects showing increased FA values. The fornix had a unique pattern in which most of the youngest (60%) and oldest (40%) subjects had decreases, but more were increasing (25–45%) than decreasing (10–30%) in the middle age groups.

In terms of MD, most subjects in the youngest group (50–75%) and still many in the oldest group (20–50%) had decreasing MD values. The corticospinal tract and superior fronto-occipital fasciculus had relatively consistent numbers of subjects with increasing and decreasing MD across the age range.

### **6.3.6 Magnitude of FA and MD changes**

Figure 6.4 shows the percent changes of FA and MD in each age group for each tract. In the two youngest age groups, all tracts except the fornix have increases of FA. For the third and fourth age groups, most tracts are still increasing, but to a lesser extent, and in the oldest two age groups, approximately

half of the tracts are increasing and half are decreasing. The largest increases are observed in the inferior fronto-occipital fasciculus, inferior longitudinal fasciculus and the cingulum, while the smallest increases/largest decreases are in the splenium of the corpus callosum, uncinate fasciculus, and corticospinal tracts.

For MD, most regions have decreasing values in the youngest groups (the corticospinal tracts and the uncinate have slight increases in the youngest and second youngest groups, respectively). In the oldest four groups, approximately half of the tracts are increasing and half are decreasing. Across all groups, the fornix, uncinate, and inferior longitudinal fasciculus have the smallest decreases/largest increases, and the cingulum, body and splenium of the corpus callosum have the largest decreases.

### 6.3.7 Diffusivities

Out of the eleven white matter pathways examined, ten had significant age-related changes of parallel diffusivity ( $\lambda_{\parallel}$ ). The cingulum, superior longitudinal fasciculus, fornix, and genu and splenium of the corpus callosum had nonlinear trends for  $\lambda_{\parallel}$ , with significant decreases at first, followed by a slowing, a minimum, and then increases. The body of the corpus callosum, inferior longitudinal, superior fronto-occipital, and uncinate fasciculi had significant linear decreases of  $\lambda_{\parallel}$  across the range. Interestingly, the corticospinal tract had significant increases of  $\lambda_{\parallel}$  at first; however, it a significant quadratic term, and demonstrated decreasing of  $\lambda_{\parallel}$  across the second half of the age range. The inferior fronto-occipital fasciculus had no significant changes of  $\lambda_{\parallel}$  (linear or quadratic).

For perpendicular diffusivity ( $\lambda_{\perp}$ ), all eleven tracts displayed significant quadratic trajectories, which decreased initially, slowed, reached a minima and in some cases, had slight increases at the upper end of the age range.

The diffusivity results can be divided into two main categories: tracts with linearly decreasing  $\lambda_{\parallel}$ , and a quadratic trajectory of  $\lambda_{\perp}$  (body of the corpus callosum, inferior longitudinal fasciculus, superior fronto-occipital fasciculus, fornix, and uncinate fasciculus); and those that have quadratic trajectories for

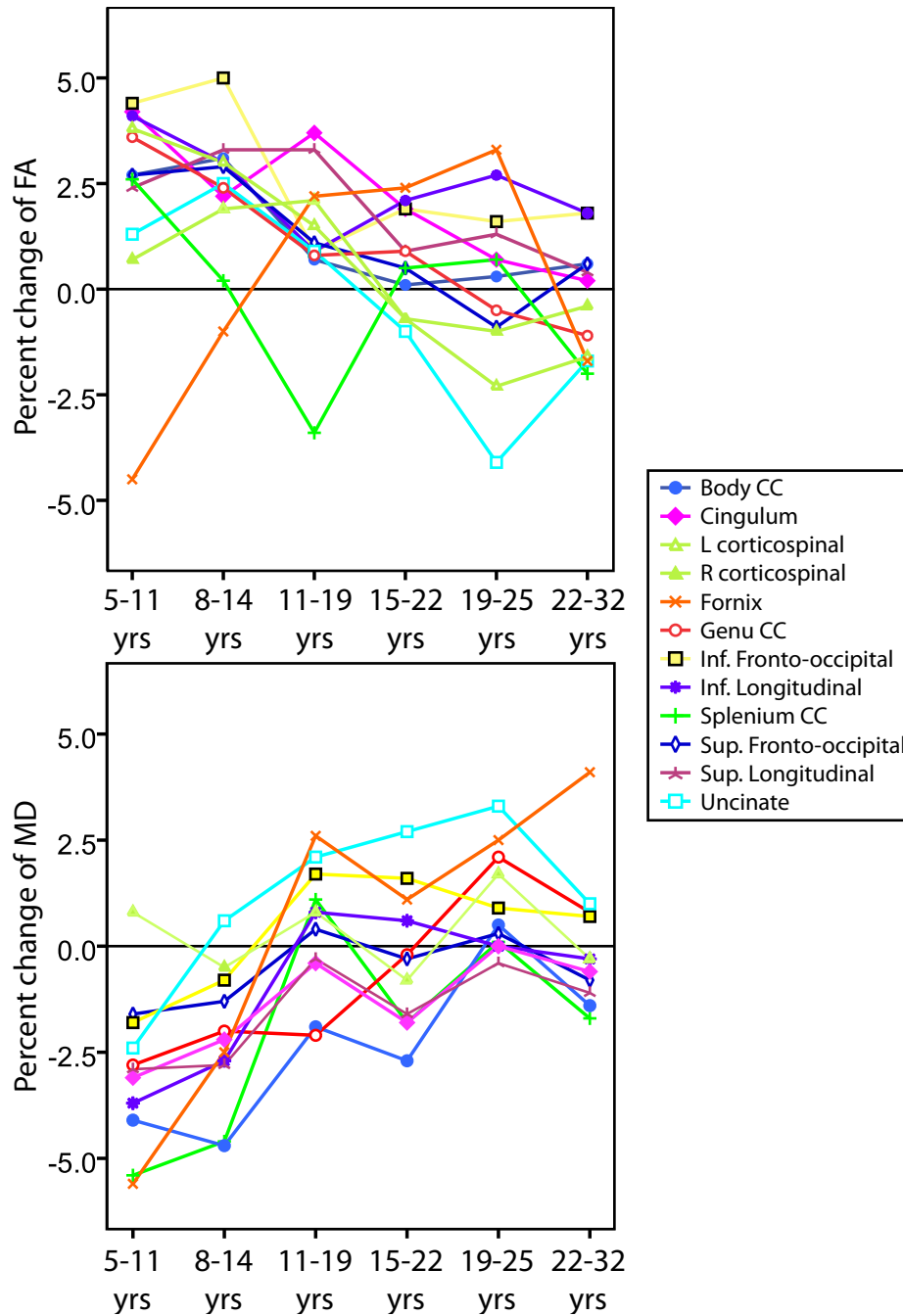


Figure 6.4: The average percent change between first and last scan is shown for each tract in each age group for FA (A) and MD (B). Note that in the youngest age group, all tracts have increasing FA and decreasing MD (except for a very slight MD increase in the corticospinal tract). In the oldest age group, approximately half of the tracts have decreasing FA and increasing MD.

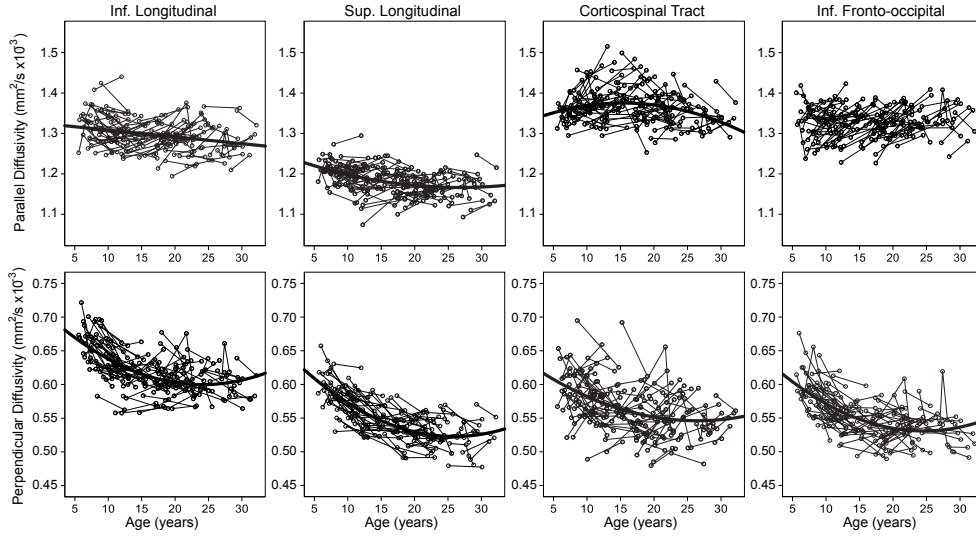


Figure 6.5: Examples of the two main different diffusivity patterns are shown, as well as the two exceptions. The inferior longitudinal fasciculus (shown), body of the corpus callosum, superior fronto-occipital fasciculus and uncinate fasciculus all had similar patterns with linear decreases of parallel diffusivity and quadratic decreases of perpendicular diffusivity. The superior longitudinal fasciculus (shown), cingulum, fornix, and genu and splenium of the corpus callosum all had quadratic decreases of both parallel and perpendicular diffusivity. The corticospinal tract exhibited a significant quadratic increase in parallel diffusivity at first, followed by decreasing parallel diffusivity, and a quadratic decrease of perpendicular diffusivity; the inferior fronto-occipital fasciculus had no significant changes of parallel diffusivity, but significant quadratic decreases in perpendicular diffusivity.

both  $\lambda_{\perp}$  and  $\lambda_{\parallel}$ , (cingulum, genu and splenium of the corpus callosum, superior longitudinal fasciculus). Two pathways did not fit these categories: the inferior fronto-occipital fasciculus, which had no significant changes in  $\lambda_{\parallel}$ , but quadratic trajectories of  $\lambda_{\perp}$ ; and the corticospinal tract, which showed initial increases of  $\lambda_{\parallel}$  followed by decreases, and a quadratic trajectory of  $\lambda_{\perp}$  with decreases than small increases. Figure 6.5 shows examples of each category of diffusivity changes. In all cases, the changes of  $\lambda_{\perp}$  were the primary cause of the observed FA changes. The MD changes in all tracts are a combination of both  $\lambda_{\perp}$  and  $\lambda_{\parallel}$ .

### 6.3.8 Brain Volumes

White matter increased significantly across the age range, with the rate of increase slowing at the upper end and showing a significant quadratic trend

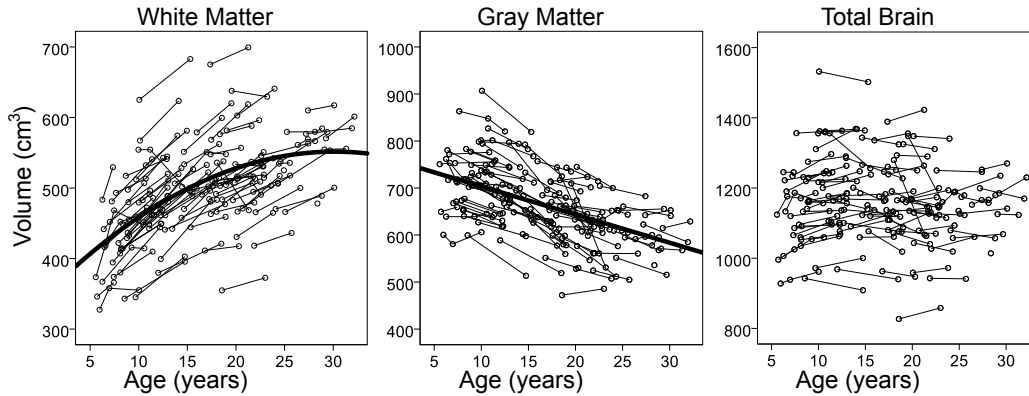


Figure 6.6: White matter volume increased significantly across the age range, and gray matter volume decreased. The white matter volume increase had a significant quadratic term, indicating slower increases at the upper end. The gray matter volume decreases, however, occurred linearly. Total brain volume did not change significantly at all.

(see Figure 6.6). Gray matter volume decreased linearly across the age range; its quadratic age term was not significant. Total brain volume (not including CSF) did not change significantly.

## 6.4 Discussion

Diffusion tensor tractography has demonstrated significant age-related changes of both FA and MD in all eleven white matter areas measured in this longitudinal study of 103 children, adolescents and young adults. Most changes were nonlinear, with FA increases occurring rapidly during childhood, and slowing during adolescence and young adulthood. In some cases, small decreases of FA were observed at the upper ends of the age range. MD changes occurred in an opposite pattern to those of FA, with most areas showing nonlinear trajectories with more rapid decreases at the beginning of the age range, then slower decreases or even increases at the upper end. The trajectories of both FA and MD (Figures 6.2 and 6.3) are in excellent agreement with many cross-sectional studies of children and adolescents (Ashtari et al., 2007; Barnea-Goraly et al., 2005b; Ben Bashat et al., 2005; Bonekamp et al., 2007; Eluvathingal et al., 2007; Mukherjee et al., 2001; Schmithorst et al., 2002), and one longitudinal study of adolescent development (Giorgio et al., 2010) showing robust FA in-

creases and MD decreases. In terms of the developmental trajectories, the relative timing of tract changes in this study supports timings obtained using exponential fits obtained in our previously published study, which was cross-sectional and included 94 of the current subjects (Lebel et al., 2008b). In both studies, the fronto-temporal connections (cingulum, uncinate fasciculus, superior longitudinal fasciculus) showed later development than other regions, while regions such as the genu and splenium of the corpus callosum had the earliest development. Unique to this study, however, is the significant FA increase observed in the fornix.

The group analysis of longitudinal changes within individuals revealed interesting results not necessarily evident in the mixed models trajectories. Although in most tracts, a progressively smaller portion of subjects had FA increases in each age group and subsequently more subjects experienced FA decreases (see Figure 6.2), some tracts showed very high proportions of subjects with increasing FA even in the older age groups. In the inferior longitudinal and fronto-occipital fasciculi, over 40% of subjects had increasing FA in the oldest group (22–32 years). For MD, the superior and inferior longitudinal, the superior fronto-occipital, and the cingulum had more than 40% of the oldest subjects with decreasing MD. Although the peaks in the longitudinal and fronto-occipital fasciculi seem to indicate early or intermediate development, the large proportion of subjects still changing in their 20s indicate that there is still considerable development after adolescence. Examination of Figure 6.4, with the average percent changes by group by tract also demonstrates considerable development in the oldest groups of the inferior longitudinal and fronto-occipital fasciculi. Changes within individuals were relatively small, averaging 2–5% for the youngest subjects and 0–2% in the oldest age group (Figure 6.4). Given that the majority of brain development occurs before the age of 5 years (Dubois et al., 2008; Hermoye et al., 2006), these fairly small changes are not surprising; however, they clearly indicate that significant brain changes occur within individuals throughout childhood and adolescence.

Examination of age-related parallel and perpendicular diffusivity trajectories revealed that changes of FA and MD were primarily driven by perpendicu-

lar diffusivity (Figure 6.5). Most tracts followed one of two diffusivity patterns: linearly decreasing parallel diffusivity with quadratic decreases of perpendicular diffusivity, and quadratic decreases of both parallel and perpendicular diffusivity. The corticospinal tract and inferior fronto-occipital fasciculus had slightly different trajectories for  $\lambda_{\parallel}$  (quadratic increases then decreases, and no change, respectively), but followed the same quadratically decreasing perpendicular diffusivity pattern of the other tracts. In all tracts, the changes of perpendicular diffusivity were driving the FA increases, and contributing to the slowing and eventual FA decrease observed in some tracts. MD changes appear to be influenced by both  $\lambda_{\parallel}$  and  $\lambda_{\perp}$ . While most previous DTI development studies describe decreasing perpendicular diffusivity as the driving force behind increasing FA (Bonekamp et al., 2007; Eluvathingal et al., 2007; Giorgio et al., 2008), some attribute FA increases to increased parallel diffusivity (Ashtari et al., 2007; Giorgio et al., 2010). Our results, with significantly decreasing perpendicular diffusivity in all regions except the fornix, suggest increasing myelination or fibre density during the childhood and adolescent periods.

Sex differences were observed in seven of eleven measured tracts; however, these differences were small. In the corticospinal tracts (left and right), superior longitudinal fasciculus, uncinate fasciculus, fornix and cingulum, males had significantly higher FA than females by 0.005–0.014 units. Females had higher FA in the splenium. These results support earlier findings of greater FA in boys in associative tracts including the superior longitudinal fasciculus, and higher FA in girls in the splenium of the corpus callosum in a study of 105 subjects aged 5–18 years (Schmithorst et al., 2008). MD values were significantly higher in females in the cingulum, corticospinal tracts, and superior fronto-occipital fasciculus (ranging from 0.008–0.012 $\times 10^{-3}$  mm<sup>2</sup>/s). Although significant, these sex differences were all less than 2.6%, compared to changes of 2–5% between scans within individuals. Furthermore, when compared to the standard deviations in the reliability analysis, the sex differences are smaller in all cases except the splenium. Perhaps the most convincing differences are those in the cingulum and corticospinal tracts, which have significantly dif-

ferent values for both FA and MD by 1.2–2.6%. A previous longitudinal DTI study of adolescents did not observe significant sex differences of FA; however, their small sample size of 24 subjects limits the power (Giorgio et al., 2010). Volumetric longitudinal studies suggest marked differences between boys and girls during adolescence (Giedd et al., 1999a; Lenroot et al., 2007), although the differences observed here by DTI are not as pronounced.

Previous studies report hemispheric asymmetry in several white matter pathways, including the cingulum (Bonekamp et al., 2007; Gong et al., 2005; Wilde et al., 2009), superior longitudinal fasciculus (Buchel et al., 2004; Lebel and Beaulieu, 2009; Niogi and McCandliss, 2006; Nucifora et al., 2005; Parker et al., 2005; Powell et al., 2006), uncinate fasciculus (Hasan et al., 2009a; Parker et al., 2005), inferior fronto-occipital fasciculus (Rodrigo et al., 2007), and superior fronto-occipital fasciculus (Bonekamp et al., 2007). In general, even significant lateralization findings are small compared to individual variation within the study or repeatability of measures between scans (Bonekamp et al., 2007). Here, we measured not absolute lateralization differences, but rather differences in developmental trajectories, which were only significantly different for FA values in the corticospinal tract, with the left increasing more than the right, and peaking slightly earlier. MD changes were not significantly different between hemispheres in the corticospinal tract or any other pathway.

Although overall brain volume did not change significantly, white matter volume increased and gray matter volume decreased significantly across this age range (Figure 6.6). Such volumetric changes are directly in line with many previous studies, both cross-sectional (Good et al., 2001b; Sowell et al., 2003) and longitudinal (Giedd et al., 1999a; Lenroot et al., 2007).

A potential limitation of this study is the use of deterministic tractography, which can be prone to error in low FA areas, such as regions with crossing fibres. This concern is mitigated, however, by the analysis of large, well-defined white matter pathways. Furthermore, the use of automated tractography for this study ensures an absence of operator bias during fibre tracking. The quadratic equation used to model development changes in this study may not be ideal for the non-linear FA and MD trajectories, and more complex

models (e.g., exponential, bi-exponential, Poisson) may provide improved fits. However, the quadratic model was used because it is compatible with a mixed models analysis, as was necessary for these longitudinal changes. Furthermore, a linear model is not appropriate since white matter development during adolescence is known to be nonlinear (Lebel et al., 2008b). Another potential issue is partial volume effects, especially in the fornix, which is directly above the CSF-filled ventricles. For this study, CSF-suppressed DTI was used to measure the fornix to alleviate these problems.

## **6.5 Conclusion**

This large, longitudinal DTI tractography study of white matter development demonstrates robust, nonlinear increases of FA and decreases of MD during childhood and adolescence. Minor gender and hemispheric differences were present, but were smaller than the 2–5% changes observed within individuals over time. These diffusion parameter changes are driven primarily by perpendicular diffusivity, suggesting increasing myelination and axonal packing through the childhood and adolescent periods.

# Chapter 7

## Age-Related Regional Variation of the Corpus Callosum Identified by Diffusion Tensor Tractography<sup>1</sup>

### Abstract

The corpus callosum is the largest white matter connection in the human brain, and an understanding of its evolution with age in healthy individuals is one crucial aspect for determining its role in cognition and disease. Diffusion tensor imaging (DTI) allows for investigation of age-related callosal changes since tractography can both virtually reconstruct the segments of the corpus callosum in vivo based on unique target cortical regions, and provide quantitative diffusion parameters reflecting tissue microstructure. DTI tractography was used to subdivide the corpus callosum into seven distinct sections based on unique target areas (i.e., orbital frontal, anterior frontal, superior frontal, superior parietal, posterior parietal, temporal, and occipital) in a very large number of healthy volunteers (n=315) across a wide age range (5–59 years). Both fractional anisotropy (FA) and mean diffusivity (MD) changes with respect to age were fit with Poisson curves, showing increasing FA and decreasing MD during childhood and adolescence and slightly slower decreases of FA and

---

<sup>1</sup>A version of this chapter has been published. C. Lebel, S. Caverhill-Godkewitsch, and C. Beaulieu, 2010. Age-Related Regional Variations of the Corpus Callosum Identified by Diffusion Tensor Tractography. *NeuroImage* 52: 20–31.

increases of MD at older ages. Age at peak FA values and minimum MD values varied from 21–44 years, and an overall “outer-to-inner” trend was observed in which the anterior and posterior regions peaked earlier than central areas. In addition to these maturational trends of diffusion parameters reflecting the microstructural changes in the healthy corpus callosum over a large age range spanning childhood to older adulthood, these results can provide a baseline for identifying the presence and timing of callosal abnormalities in various brain disorders.

## 7.1 Introduction

The corpus callosum, the largest white matter structure in the human brain, consists of millions of myelinated fibres and serves primarily to connect homologous regions across hemispheres. It is a complex, heterogeneous structure containing axons of different diameters and densities that vary by region (Aboitiz et al., 1992). Autopsy and neuroimaging studies have demonstrated important structural changes in the corpus callosum throughout life. During childhood, it undergoes myelination, increases in fibre density, and alterations of size and shape (Aboitiz et al., 1996; Giedd et al., 1999b; Kim et al., 2007; Rajapakse et al., 1996; Yakovlev and Lecours, 1967). Through adulthood and the aging process, reductions in size are noted (Allen et al., 1991; Smith et al., 2007). Furthermore, callosal size and area are associated with motor skills and numerous cognitive abilities (Fine et al., 2007; Hutchinson et al., 2009; Rademaker et al., 2004; van Kooij et al., 2008), and the corpus callosum is often malformed or absent in various conditions (Jeret et al., 1987).

Diffusion tensor imaging (DTI), a more sensitive measure of white matter microstructure than conventional imaging, has demonstrated increases of fractional anisotropy (FA) and decreases of mean diffusivity (MD) in the corpus callosum during childhood and adolescence (Barnea-Goraly et al., 2005b; Ben Bashat et al., 2005; Dubois et al., 2006; Hermoye et al., 2006; Lebel et al., 2008b; Mukherjee et al., 2001). The opposite trends occur during later adulthood, with MD rising and FA dropping (Abe et al., 2002; Bhagat and Beaulieu,

2004; Hsu et al., 2010; Ota et al., 2006; Pfefferbaum et al., 2000; Zhang et al., 2008b). DTI has also clearly shown relationships between callosal microstructure and cortical activation (Putnam et al., 2008), motor skills (Johansen-Berg et al., 2007), reading ability (Dougherty et al., 2007), and intelligence (Kontis et al., 2009).

Two previous groups used DTI to investigate diffusion parameter changes in the healthy corpus callosum across large age ranges (6–79 years) with sample sizes of 77–121 (Hasan et al., 2008a,b, 2009b; McLaughlin et al., 2007). These studies demonstrated age-related changes in diffusion parameters, with FA increasing and MD decreasing during childhood and adolescence, and then a reversal of trends during the aging process. Three of the previous studies segmented the corpus callosum into subregions based on geometric measures of length and distance, such as the Witelson method (Witelson, 1989); one study examined the corpus callosum as a whole without subdivision. Of these studies, three made diffusion measurements using two-dimensional regions of interest at or near the midline; one used tractography to examine the entire corpus callosum. To complicate matters, the corpus callosum is highly variable among individuals in terms of its size and shape, and has no characteristic anatomical landmarks, and thus these geometric parcellations may not reflect functionally distinct regions. Indeed, tractography studies have shown that geometric subdivisions of the corpus callosum do not always correspond to the functional subdivisions delineated based on the cortical areas to which the callosal fibres project, and have thus proposed a variety of tractography-based parcellation methods (Chao et al., 2009; Hofer and Frahm, 2006; Huang et al., 2005) that are more likely to relate to functionality. The purpose of this study was to use tractography-based segmentation of the corpus callosum to thoroughly examine its microstructural changes across a wide age range (5–59 years) in a very large number of healthy subjects (n=315).

## 7.2 Methods

### 7.2.1 Subjects

Subjects in this study were 315 healthy individuals (165 female/150 male, 292 right-handed/20 left-handed/3 no preference) aged 5–59 years (mean  $\pm$  standard deviation =  $22.4 \pm 13.6$  years). The distribution of subjects was: 129 individuals from 5–15 years old, 82 subjects from 16–25 years, 53 subjects between 26–35 years, 23 individuals 36–45 years, and 28 subjects from 46–59 years. Subjects had no self-reported history of neurological or psychiatric disease or brain injury. Informed consent was obtained from all subjects 18 years of age or older; parental consent and child assent were obtained from volunteers younger than 18 years. Of the 315 participants, 202 were included in a previous study of development limited from 5–30 years of age, in which development of only the genu and splenium of the corpus callosum was analyzed with semi-automated diffusion tractography, but not using manual cortical parcellation (Lebel et al., 2008b).

### 7.2.2 Image Acquisition

All scans were performed on the same 1.5T Siemens Sonata MRI scanner (Siemens, Erlangen, Germany) using identical methods. The imaging protocol included anatomical imaging as well as DTI and was approximately 26 minutes long. DTI was collected using a dual spin echo single shot echo-planar imaging sequence with forty 3 mm slices (no inter-slice gap), image matrix  $128 \times 128$  with 75% phase partial Fourier zero-filled to  $256 \times 256$ , field-of-view  $220 \times 220$  mm<sup>2</sup>, TE=88 ms, TR=6400 ms, b=1000 s/mm<sup>2</sup>, 8 averages, 6 directions. Total DTI acquisition time was 6:06 minutes. This DTI sequence yielded excellent quality FA maps, with average b0 image SNR=73.

### 7.2.3 Tractography

Deterministic streamline tractography of the corpus callosum was performed by manually drawing regions-of-interest in DTIStudio 2.4 (Jiang and Mori, Baltimore, MD) by the same operator (SCG) for each individual. The operator

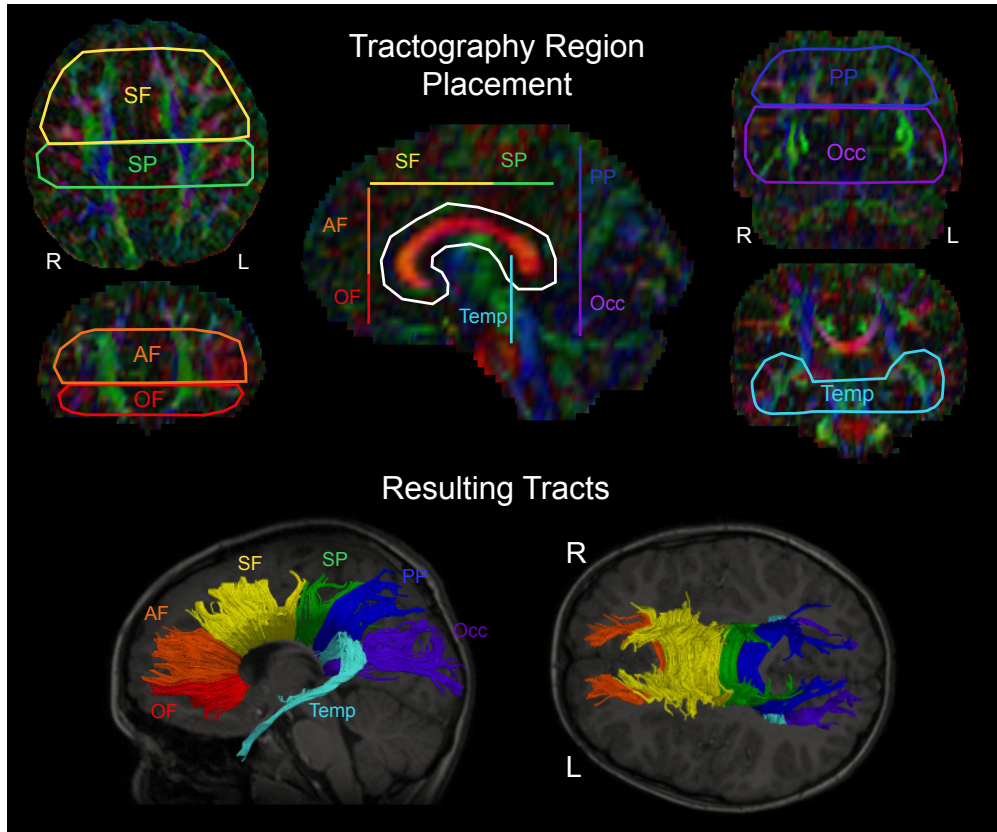


Figure 7.1: The corpus callosum was subdivided into seven separate sections using a two region-of-interest fibre tracking approach with one common area on a midsagittal slice, and seven distinct target regions, drawn bilaterally according to a priori determined rules and specific anatomical landmarks (Huang et al., 2005). The seven subsections are, in order from anterior to posterior: orbital frontal (OF), anterior frontal (AF), superior frontal (SF), superior parietal (SP), posterior parietal (PP), temporal (Temp) and occipital (Occ). All regions are shown here in a 9 year old male with the resulting tracts.

was blinded to subject age, gender, and handedness. FA thresholds to initiate and continue tracking were set to 0.25; the maximum angle threshold was 70°. Tractography was performed using the two region-of-interest approach (see Figure 7.1, top). One region was drawn on a midsagittal slice encompassing the entire corpus callosum, and seven separate regions-of-interest spanning both sides of the midline were used as target regions to segment the corpus callosum into distinct sections. All regions-of-interest were drawn according to specific anatomical landmarks and guidelines that were followed carefully and consistently for each individual; the tracking methods used were a modification of methods described by Huang et al. (2005). Ordered from front to back the seven sections delineated were: orbital frontal (OF), anterior frontal (AF), superior frontal (SF), superior parietal (SP), posterior parietal (PP), temporal (Temp), and occipital (Occ). As seen in Figure 7.1, one coronal slice was selected at approximately one third of the distance from the genu of the corpus callosum to the front of the head, and the OF and AF target regions were drawn on this slice, distinguished from each other using an axial slice at the level of the inferior edge of the splenium. The SF and SP target regions were drawn on either side of the central sulcus on the most inferior axial slice on which the central sulcus was still clearly visible. A coronal slice at the edge of the parietal-occipital sulcus was used to draw both the PP and occipital regions on either side of the parietal-occipital sulcus. Finally, the temporal target region was drawn on a coronal slice anterior to the splenium on which the temporal part of the corpus callosum (also known as the tapetum) could be clearly seen. Target regions for other tracts were used as exclusion areas (e.g., when tracking the AF portion, the OF and SF regions were used as exclusion regions). Other exclusion regions were rarely needed, but were used if necessary to eliminate fibres that were not part of the corpus callosum, according to a priori anatomical knowledge. This led to tracts identified for each subregion of the corpus callosum (shown in Figure 7.1, bottom) although the emphasis is on the medial aspects of the tracts as the lateral corpus callosum projections are not identified due to the limitations of deterministic tractography for crossing fibre areas.

Voxels were assigned to a particular callosal region based on tractography; voxels containing tracts from two or more callosal segments were not assigned to any section and were removed from further analysis. FA and MD were calculated for each region by averaging all voxels over the entire tract, counting each voxel only once.

#### **7.2.4 Tract Volume**

To check the consistency of segmentation techniques across the age range, the number of voxels in each subdivision and the total number of voxels were counted for each subject. Significant differences of volume between age groups were tested using a multivariate analysis of variance (MANOVA), with Bonferroni-corrected post-hoc tests for group differences.

#### **7.2.5 Curve Fitting**

Several types of curves were tried initially to model the age-related changes of FA and MD: linear, quadratic, exponential, bi-exponential, and Poisson. For all fits, the Poisson-type curve gave the best fits and parameter estimates in terms of  $R^2$  values and parameter significance. Furthermore, the Poisson fits had a minimal number of variables to fit (3) and allowed for different slopes on either side of the peak, permitting faster changes on the younger side of the peak and slower changes on the older side. Therefore, Poisson curves were used to represent changes of diffusion parameters with respect to age according to the following equation:  $FA \text{ (or MD)} = A * age * e^{-B * age} + C$ . Age of peak FA values and minimum MD values were calculated using the best fit equations for each tract in order to determine when a reversal of trends occurred (i.e. when FA increases changed to decreases, and when MD decreases changed to increases). Standard error intervals for each peak/minimum age were calculated using the standard errors of the initial fitting parameters. Significant differences between age at peak FA/minimum MD between regions were tested for using a t-test compensating for the correlations between regions. T-tests were also used to test significant differences between FA peak age and MD minimum age within regions.

### 7.2.6 Parallel and Perpendicular Diffusivity

To provide more information about what was driving any changes of FA or MD values, parallel ( $\lambda_{\parallel} = \lambda_1$ ) and perpendicular ( $\lambda_{\perp} = (\lambda_2 + \lambda_3)/2$ ) diffusivity were calculated for each corpus callosum subregion. Poisson curves were fit to the diffusivity data in the same way as for FA and MD, and the age at which minimum diffusivity was reached was calculated for each subdivision.

### 7.2.7 Gender and Handedness

Sex was included as an additional term in the original curve fitting equation: FA (or MD) =  $A * age * e^{-B * age} + C + D * sex$ . However, if the sex term was not significant (according to a t-test), it was removed from the equation for further analysis. There were not enough left-handers (20 of 315 were left-handed, 3 no preference) to reasonably include handedness as an additional term for curve fitting.

### 7.2.8 Midline Corpus Callosum DTI Analysis

Many other studies examine callosal diffusion parameters at or near the midline using two-dimensional regions of interest, or segmented tractography (Bhagat and Beaulieu, 2004; Dougherty et al., 2007; Hasan et al., 2008b). Therefore, to compare with other studies and to determine whether various parts of the corpus callosum were driving the age-related FA changes, at least coarsely, each callosal subregion was further divided into the midline (midsagittal slice plus 5mm on either side) and non-midline areas (the rest of the tract). These sections were analyzed separately in the same manner as previously described, using Poisson curve fitting. As MD is much more uniform across the brain, MD values were not analyzed in this way.

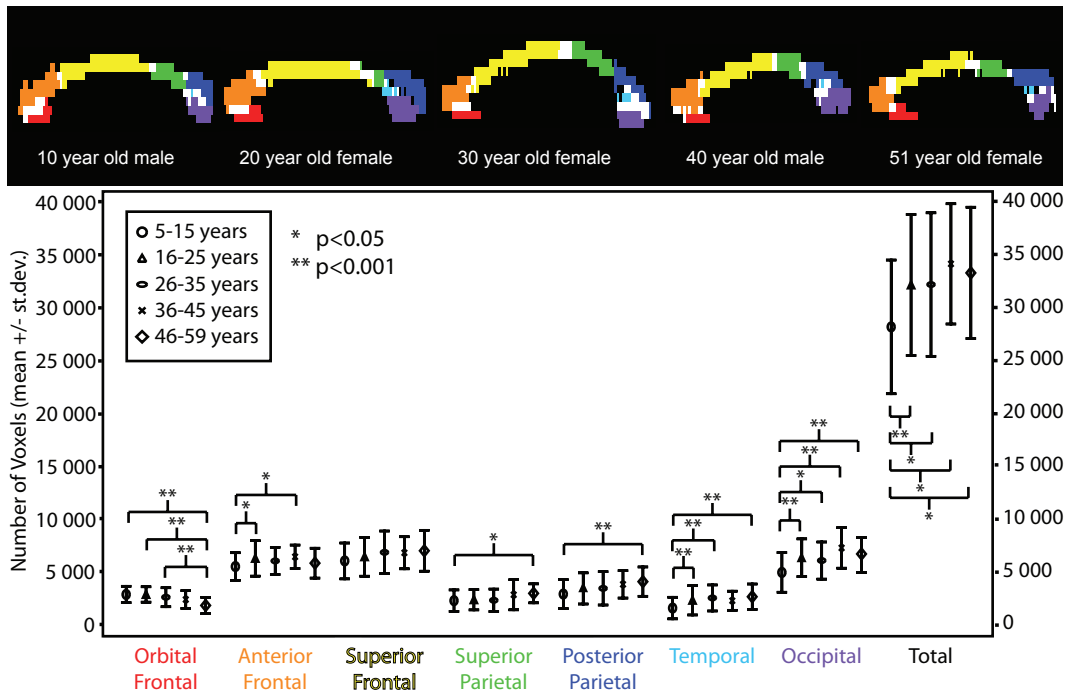


Figure 7.2: The midsagittal slice for 5 individual subjects across the age span is shown, with the seven subdivisions colour-coded (voxels with more than one tract are considered “overlap” and marked in white; these were not included in the analysis but are included in the total voxel count). The number of voxels contained in each callosal subdivision (for the entire tract) averaged across each age group is given, with the standard deviation shown as error bars. Significant differences between groups (corrected) are marked. The number of voxels in each region is significantly smaller for the youngest age group for five regions, while the older adults have significantly smaller orbital frontal regions. The total number of voxels is significantly smaller in the youngest group, but stable for the other ages.

## 7.3 Results

### 7.3.1 Tract Volume

Although tractography performance was qualitatively consistent across the wide age range in terms of tract shape, location, and ease of tracking, volume changes within each region were investigated. Figure 7.2 shows the mean and standard deviation for the number of voxels in each callosal subdivision for different age groups. In addition, examples of midsagittal slices with voxels colour-coded by tract are shown. For five of these regions (anterior frontal, superior parietal, posterior parietal, temporal, occipital), the youngest group (5–15 years) had a significantly smaller volume than one or more other groups. For the orbital frontal region, the oldest age group (46–59 years) has significantly smaller volume than three other age groups. The total volume of all corpus callosum regions was smaller in the youngest age group, but stable for the rest of the age range.

### 7.3.2 Fractional Anisotropy Changes with Age

Overall, the Poisson equation modeled the age-related FA changes well and the parameter estimates were stable, although the fit for FA versus age in the posterior parietal region did not reach significance (see Table 7.1, Figure 7.3A). Other than the posterior parietal area, all terms (linear term, exponential term and intercept) in each Poisson equation were highly significant ( $p=0.004$  for the temporal region intercept;  $p<0.001$  for all other terms) and R values were quite reasonable in the range of 0.21–0.37. As Figure 7.3A shows, FA increases during childhood and adolescence, peaks during early adulthood, and then decreases through later adulthood at a slightly slower rate than the increases during childhood and adolescence. Ages at which peak FA values were reached varied from 21 years for the orbital frontal region to 29 years for the temporal region (see Fig. 7.4). Significance values of differences between peak ages are shown in Table 7.2. Based on the peak ages and their significance values, the callosal regions can be divided into two groups: an early-peaking group (orbital and anterior frontal, occipital, peak at 20–23 years) and a later-peaking group

Table 7.1: Parameters for Poisson equations are shown, including intercept, linear and exponential terms for all seven regions of the corpus callosum (p value in parentheses). All terms were highly significant, except for the linear term for the posterior parietal area (the posterior parietal fit was not significant overall, either). The sex term, where significant, is also shown. Note that a positive sex term indicates higher values for males, where a negative term indicates lower values for males. MD units are  $\times 10^{-3}$  mm<sup>2</sup>/s.

FA	Intercept	Linear ( $\times 10^{-2}$ )	Exponential ( $\times 10^{-1}$ )	Sex ( $\times 10^{-2}$ )	R	p-value
Orbital Frontal	0.49	0.74	0.48	n.s.	0.34	<0.001
Anterior Frontal	0.50	0.57	0.44	n.s.	0.29	<0.001
Superior Frontal	0.49	0.43	0.36	0.78	0.37	<0.001
Superior Parietal	0.50	0.38	0.38	n.s.	0.23	0.001
Posterior Parietal	0.52	n.s.	n.s.	n.s.	n.s.	0.253
Temporal	0.52	0.42	0.35	n.s.	0.21	<0.001
Occipital	0.52	0.50	0.43	n.s.	0.24	0.002
MD	Intercept ( $\times 10^{-3}$ )	Linear ( $\times 10^{-4}$ )	Exponential ( $\times 10^{-4}$ )	Sex ( $\times 10^{-4}$ )	R	p-value
Orbital Frontal	0.91	-0.12	0.37	n.s.	0.44	<0.001
Anterior Frontal	0.85	-0.08	0.30	n.s.	0.53	<0.001
Superior Frontal	0.93	-0.10	0.25	-0.14	0.66	<0.001
Superior Parietal	0.90	-0.07	0.23	n.s.	0.36	<0.001
Posterior Parietal	0.90	-0.11	0.33	n.s.	0.31	<0.001
Temporal	1.03	-0.18	0.33	n.s.	0.53	<0.001
Occipital	0.92	-0.12	0.42	n.s.	0.39	<0.001

(temporal, superior frontal and parietal, peak at 26–29 years). Overall, the age of peak FA values occurred earliest in the more anterior and posterior regions of the corpus callosum and latest in the more central portions. Mean FA values for each region ranged from 0.53–0.56; they are lower than those obtained by measuring only the midline (which are 0.65–0.76), because the outer portions of the callosal tracts are also included in the averages. At the upper end of the age range, the frontal regions undergo a marked FA drop (0.027 and 0.021 units in the orbital and anterior frontal regions, respectively, over the last 30 years), much larger in magnitude than the drops experienced by other regions (which decrease by 0.002–0.018 units).

### 7.3.3 Mean Diffusivity Changes with Age

All Poisson fits of MD values versus age were excellent and yielded robust parameter estimates (see Fig. 7.3B, Table 7.1), even for the posterior parietal region whose FA fit was not significant. Significance values for all MD parameters were very low ( $p < 0.002$ ), and R values ranged from 0.31–0.66. MD followed a curve opposite to that of FA values, with MD decreasing through childhood, adolescence and young adulthood, reaching a minimum, and then increasing at a slower rate than its initial decreases (see Fig. 7.3B). Minimum MD values were reached between ages 24–44 years (see Fig. 7.4 and Table 7.2 for peaks and significance values). Overall, MD followed a similar pattern to FA values, with the outer portions of the tract (orbital frontal and occipital; minima at 24–27 years) reaching a minimum at younger ages than the central callosal areas (temporal, superior parietal, posterior parietal, anterior frontal, and superior frontal; minima at 30–44 years). Average MD values for each region varied from  $0.77\text{--}0.86 \times 10^{-3} \text{ mm}^2/\text{s}$ .

### 7.3.4 DTI Parameter Timing Differences

The differences between age at peak FA and age at minimum MD were significant within the four most anterior regions (orbital frontal, anterior frontal, superior frontal, superior parietal), where FA peaks were reached 6–18 years prior to MD minima (see Table 7.2). The differences in peak FA values and

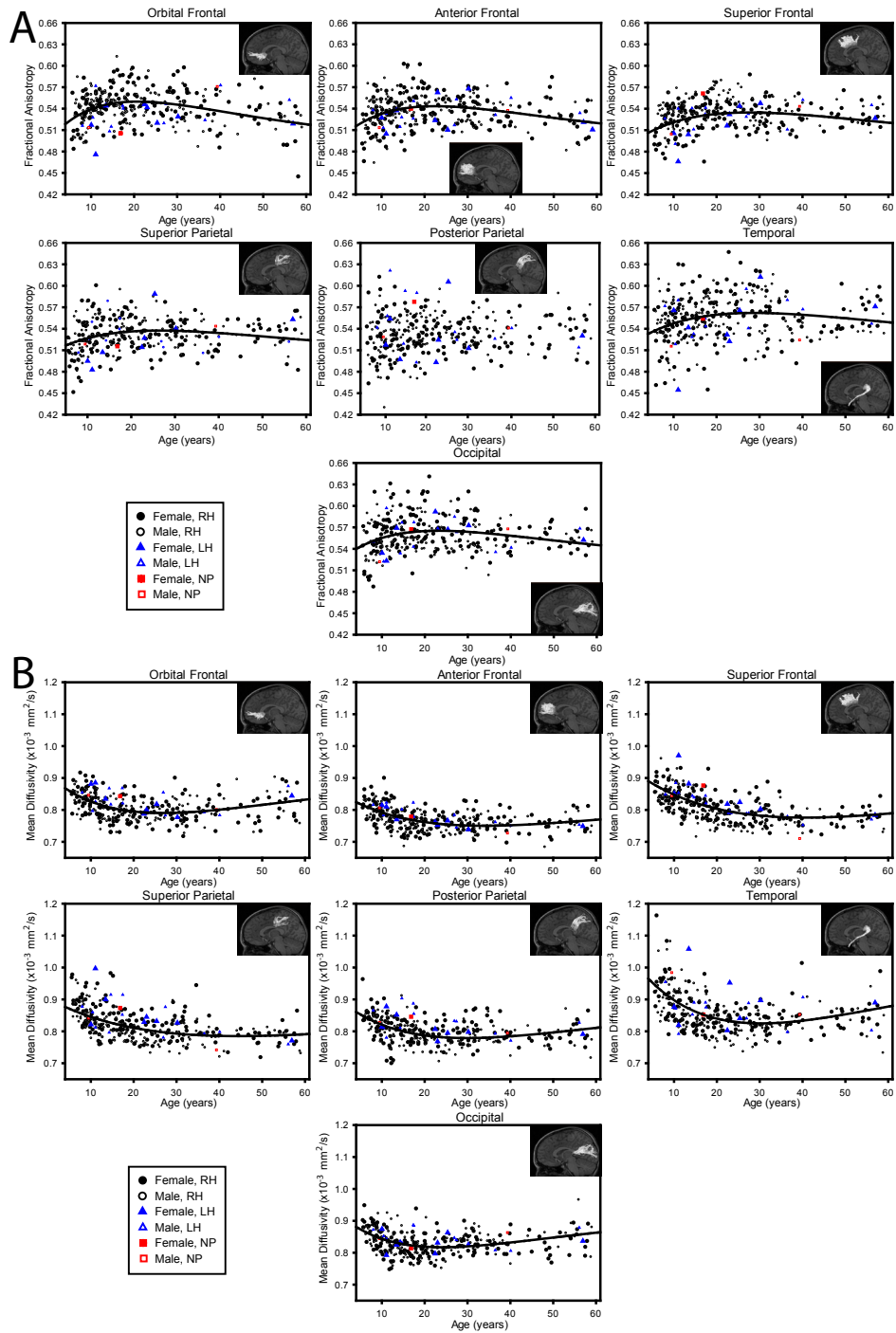


Figure 7.3: Fractional anisotropy (FA) (A) and mean diffusivity (MD) (B) versus age plots for all seven corpus callosum regions demonstrate FA increases followed by decreases, and conversely decreases of MD followed by increases. Best fit Poisson curves are given by the solid line. The FA vs. age fit for the posterior parietal region was not significant and is not shown; all other fits were highly significant. Gender and handedness are shown separately.

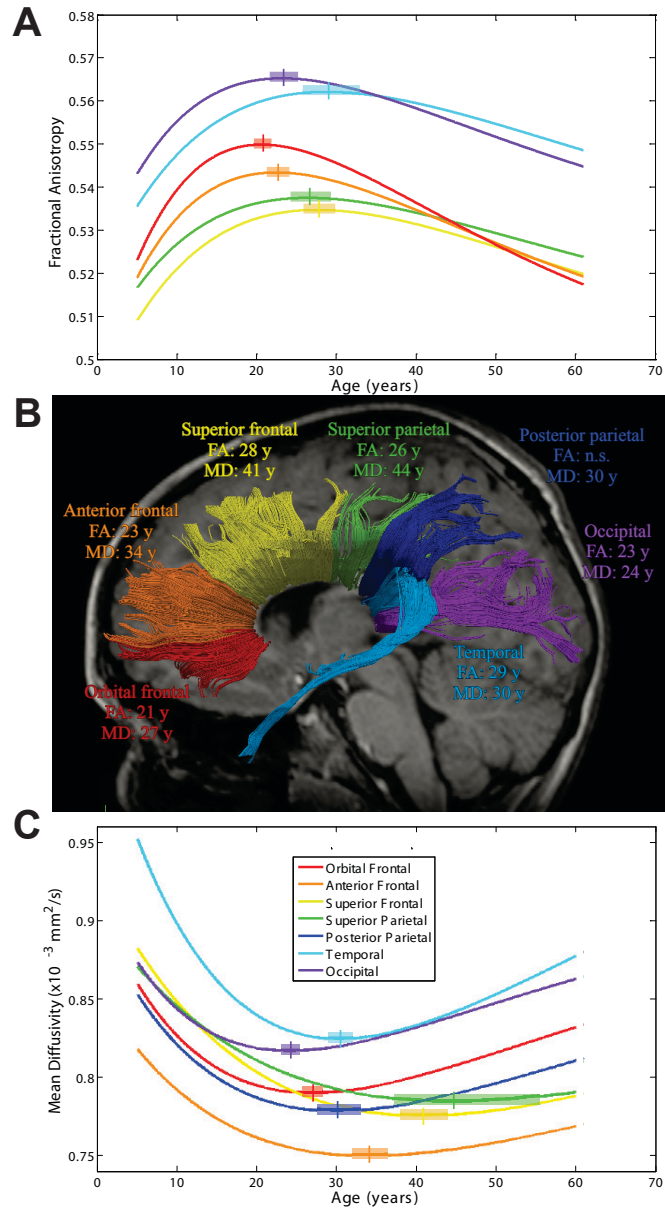


Figure 7.4: Poisson curves are shown for each section of the corpus callosum for both (A) fractional anisotropy (FA) and (C) mean diffusivity (MD). Ages of peak FA values and minimum MD values from the Poisson fits are listed (B) for all regions. The FA-age fit for the posterior parietal region was not significant, so it is not shown. The outer regions (orbital and anterior frontal, occipital) reach their peak FA values and minimum MD values earlier than more central regions such as the superior frontal and superior parietal regions; alternatively, peak values at younger ages can be seen as earlier degradation. Notably, the two most frontal regions (orbital and anterior frontal) show the steepest FA drops after the peak.

Table 7.2: Ages at peak FA value and minimum MD value are given for each region (upper/lower standard error bounds are in parentheses). The third line of the table presents the significance values for the t-test of differences between FA peak age and MD minimum within each region. The bottom section of the table lists p values for t-tests of the differences between FA peak age values and minimum MD ages among the seven regions. OF=orbital frontal, AF=anterior frontal, SF=superior frontal, SP=superior parietal, PP=posterior parietal, Temp=temporal, Occ=occipital.

Region	OF	AF	SF	SP	PP	Temp	Occ
Age at peak FA (yrs)	20.7 (19.6, 21.9)	22.5 (21.2, 24.0)	27.6 (25.8, 29.8)	26.5 (24.2, 29.2)	n.s.	28.8 (25.7, 32.8)	23.2 (21.6, 25.1)
Age at min MD (yrs)	26.9 (26.7, 28.2)	33.9 (31.8, 36.2)	40.7 (37.9, 43.8)	44.4 (37.2, 55.2)	29.9 (27.5, 32.9)	30.3 (28.9, 31.8)	24.1 (23.0, 25.3)
p-value (peak FA vs. min MD)	<0.000	<0.000	<0.000	0.002	- <sup>a</sup>	0.629	0.671
<b>Significance differences between callosal subregions for age at peak FA (top) and age at minimum MD (bottom)</b>							
OF	–	0.072 <0.001	<0.001 <0.001	0.003 <0.001	- <sup>a</sup> 0.164 0.164	0.002 0.008	0.092 0.008
AF		–	0.001 0.003	0.062 0.087	- <sup>a</sup> 0.156	0.019 0.037	0.688 <0.001
SF			–	0.603 0.574	- <sup>a</sup> 0.002	0.712 <0.001	0.056 <0.001
SP				–	- <sup>a</sup> 0.012	0.486 0.018	0.177 <0.001
PP					–	- <sup>a</sup> 0.887	- <sup>a</sup> 0.003
Temp						–	0.049 <0.001
Occ							–

<sup>a</sup> Because the posterior parietal FA fit was not significant, t-tests were not performed for the posterior parietal area's peak FA vs. minimum MD

minimum MD values between regions were also tested (Table 7.2). The central tracts had the largest gaps between FA peak ages and MD minimum ages (superior frontal=13 years, superior parietal=18 years), while the two most anterior regions had slightly smaller gap, but still significant separation (orbital frontal=6 years, anterior frontal=11 years), and the two posterior regions did not have significant separation between FA and MD peak/minimum ages. The posterior parietal did not have a significant FA peak, so differences between FA and MD could not be tested.

### 7.3.5 Diffusivities

The results for parallel and perpendicular diffusivity are presented in Figure 7.5. All fits followed Poisson curves similar to MD, decreasing initially, then reaching a minimum and then increasing. For the three frontal regions (occipital, anterior and superior), perpendicular diffusivity reached its minimum 8–11 years earlier than parallel diffusivity ( $p < 0.001$ ). This discrepancy between perpendicular and parallel diffusivity minima is the cause of the significant differences between FA peak age and MD minimum age for these regions. Notably, differences between perpendicular and parallel diffusivity minima were not significant for the four more posterior regions.

### 7.3.6 Sex Differences

A sex term was initially included in the equation to account for differences of FA or MD between males and females; this term was only significant in the superior frontal region. In that region, males had significantly higher FA values (0.008 higher, standard error=0.002,  $p=0.002$ ) and lower MD values ( $0.014 \times 10^{-3} \text{ mm}^2/\text{s}$  lower, standard error= $0.004 \times 10^{-3} \text{ mm}^2/\text{s}$ ,  $p=0.004$ ) than females. The sex term was retained in the equation for the superior frontal area, but removed from all other fits.

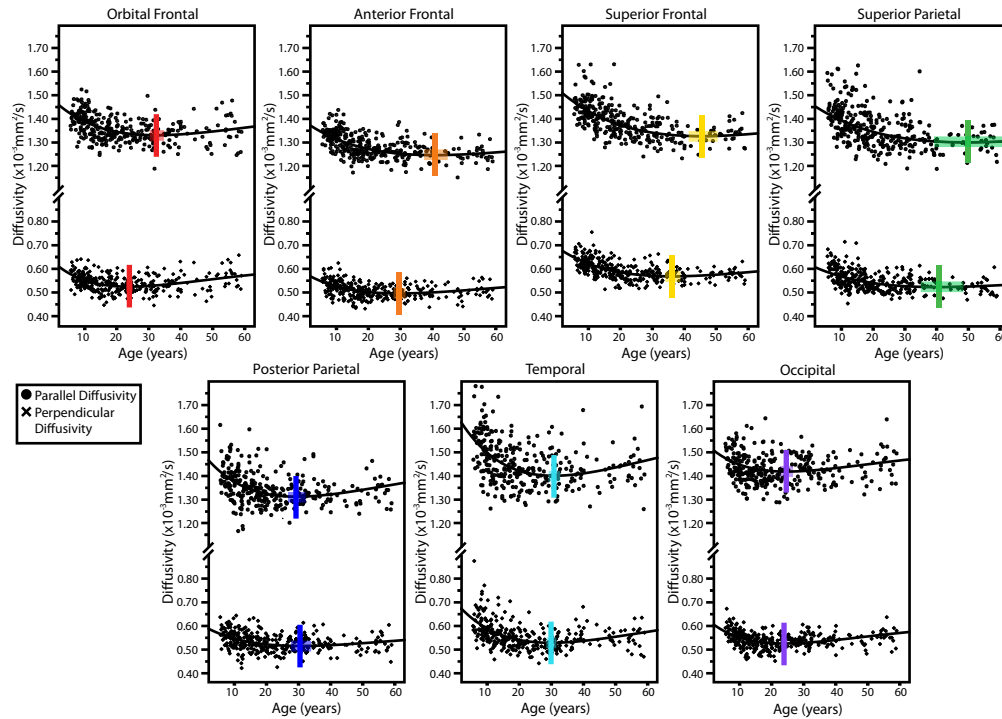


Figure 7.5: Parallel and perpendicular diffusivity vs. age plots are shown for each callosal subregion. The age at minimum diffusivity value is shown as a line, with the standard error of this estimate shown as a bar. Note that for all the frontal regions and even the superior parietal region, the minimum for perpendicular diffusivity occurs several years prior to the minimum for parallel diffusivity. In contrast, the more posterior regions such as the posterior parietal, temporal, and occipital regions, show minima for parallel and perpendicular diffusivity that occur at similar ages.

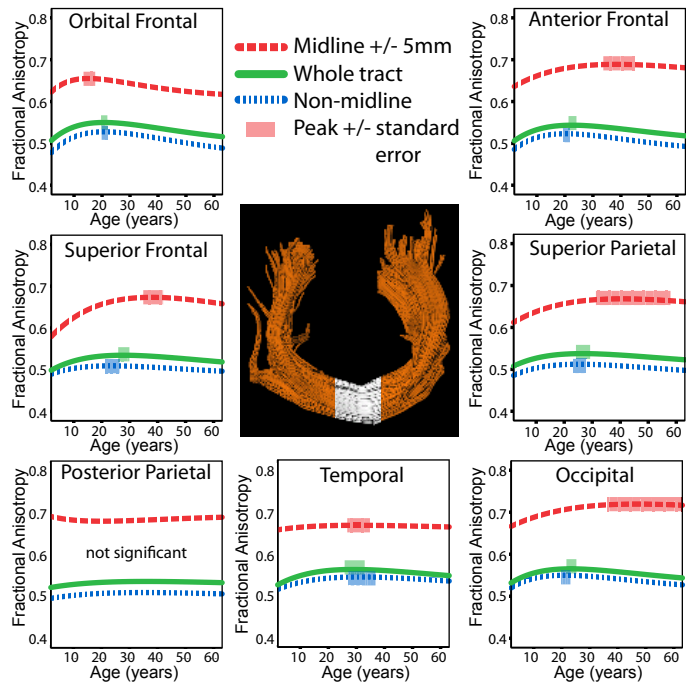


Figure 7.6: Best fit Poisson curves are shown for the whole tract (green solid curve), midsagittal slice  $\pm 5$  mm on either side shown as the white region on the tract insert (red dashed curve), and the non-midline area (whole tract except the midline  $\pm 5$  mm; blue dotted curve). The peak age  $\pm$  standard error is shown as a shaded box. Fits for the posterior parietal region were not significant. As expected, the FA values for the midline area are higher than those averaged over the remainder of the tract. Note that the fits for the midline follow those for the entire tract at the younger ages, but do not always show the same extent of declines at older ages.

### 7.3.7 Midline Corpus Callosum DTI Analysis

To determine whether changes of FA across the whole tract were similar to those of the more compact midline region (midsagittal slice  $\pm 5$  mm) alone, FA was measured in the midline region and the non-midline area, and fit to a Poisson curve for each callosal subdivision (Figure 7.6). All FA-age curves were significant, except that of the posterior parietal region. As can be seen in Figure 7.6, the midline curves follow the same trajectory as those of the whole tract nicely at the younger ages. At the older ages, however, the midline fits do not as closely follow the whole tract and do not demonstrate as large drops of FA as the whole tract.

## 7.4 Discussion

DTI tractography has demonstrated nonlinear trajectories of diffusion parameters within the corpus callosum across a wide age range of 5–59 years. The ages at peak FA value and minimum MD value for each region show an outer-to-inner pattern of trend reversal over this time frame, with peaks/minima reached between 21–44 years, depending on the callosal region and DTI parameter. FA values were modeled well with a Poisson curve, increasing during childhood, adolescence, and early adulthood, peaking, and then decreasing during later adulthood at a rate slower than that of the initial increases. MD follows a curve opposite to FA, although not necessarily in parallel timing, decreasing until middle adulthood and then increasing thereafter. The up/down trajectories are in general agreement with previous DTI studies of the corpus callosum showing U-shaped trajectories over 6–79 years using geometric parcellation of the corpus callosum (Hasan et al., 2008a,b, 2009b; McLaughlin et al., 2007); in our study, segmentation of the corpus callosum was based on target cortical regions, which provides subdivisions more likely to be functionally distinct and allows clearer separation of the posterior regions which otherwise would be difficult to identify individually. A previous DTI tractography study using geometric segmentation of the corpus callosum in 99 right handed 7–59 year olds showed significant quadratic fits in only 1 of 8 regions for FA and 4 of 8 regions for perpendicular diffusivity (Hasan et al., 2009b), making it impossible to draw meaningful conclusions about relative timing among regions. In contrast, our larger sample ( $n=315$ ) and the use of a Poisson equation, which permits differential slopes on either side of the peak/minimum, provided very robust fits and highly significant parameter estimates for 6 of 7 regions for FA (the posterior parietal region was not significant) and all 7 regions for MD,  $\lambda_{\parallel}$ , and  $\lambda_{\perp}$ , despite the inter-subject scatter clearly evident in Figure 7.3.

Previous non diffusion MRI studies have demonstrated a general anterior-to-posterior trend of maturation of the corpus callosum in children using mid-sagittal area measurements of the corpus callosum in 139 subjects (some with repeat scans) (Giedd et al., 1999b) and sophisticated tensor mapping of the

corpus callosum in 6 subjects scanned at multiple time points (Thompson et al., 2000). During the aging process in older adults, many DTI studies report larger FA declines in frontal regions (Bucur et al., 2008; Davis et al., 2009; Salat et al., 2005), and suggest that even more substantial decreases in the anterior corpus callosum are related to cognitive impairment and dementia (Chua et al., 2008). Although it is difficult to comment on maturation rates in a cross-sectional study, examining only the childhood or only the aging portions of the best fit FA-age curves appears to demonstrate similar anterior-to-posterior trends in this data. However, when the full age range is considered, an overall “outer-to-inner” trend is observed in terms of ages of peak FA and minimum MD (i.e. presumably when the brain is at its ‘best’ as far as DTI parameters are concerned). It must be noted that this trend results from two processes: development and degradation. Therefore, the FA peaks and MD minima may be dominated by either process, and longitudinal studies of diffusion parameter changes within the corpus callosum are needed to fully explore the question of maturation rates.

FA values drop off more sharply in anterior regions at older ages than in the posterior regions. The anterior regions of the corpus callosum had the lowest FA values at the upper end of the age range due to a sharp drop off, while more posterior regions showed higher FA values and a more gradual decline (see Fig. 7.4A). This marked drop in the anterior corpus callosum is in good agreement with previous studies reporting larger FA differences in the anterior corpus callosum than in the posterior region between younger and older adults (Bucur et al., 2008; Davis et al., 2009; Salat et al., 2005), and may suggest a gradient of change within the frontal lobe itself, as the orbital frontal region drops off most steeply, followed by the anterior and then superior frontal regions. The orbital frontal region is also the only region which had significantly smaller volume in the oldest subjects (see Figure 7.2), an observation noted by previous volumetric studies (Good et al., 2001b). The decreasing volume may potentially affect FA values in this region; however, given the stable volumes in other regions with decreasing FA, this concern is somewhat mitigated.

In the four most anterior callosal regions, MD minima lag significantly behind FA peaks, with minimum MD values occurring 6–18 years after FA peaks. An investigation of the eigenvalues revealed that the time lag is due to a prolonged decrease of parallel diffusivity ( $\lambda_{\parallel}$ ), even after perpendicular diffusivity ( $\lambda_{\perp}$ ) has begun to increase (see Figure 7.5). Initially, both parallel and perpendicular diffusivities decrease, although  $\lambda_{\perp}$  decreases more sharply than  $\lambda_{\parallel}$ ; this causes the increasing FA and decreasing MD values. Then, the perpendicular diffusivity reaches a minimum and begins to increase before the parallel diffusivity. This period of time, while  $\lambda_{\parallel}$  is decreasing but  $\lambda_{\perp}$  is increasing, causes both FA and MD values to decline. Then, once  $\lambda_{\parallel}$  begins to increase (but not to the same extent as  $\lambda_{\perp}$  increases), FA values continue to fall and MD values begin to rise. These various patterns of diffusivity may reflect different phases of physiological change (e.g., fibre organization, membrane proliferation, myelination), as proposed for infants (Dubois et al., 2008), although without histological evidence in this sample, it is impossible to be certain of the biological basis causing the diffusion changes. Nonetheless, animal studies indicate that increasing myelination and axonal packing would lead to decreased  $\lambda_{\perp}$  (Beaulieu, 2002; Song et al., 2005), and the subsequent increase of FA observed during childhood and adolescence, while the decreasing  $\lambda_{\parallel}$  that contributes to decreasing MD could be caused by reduced brain water content or increased prevalence of isotropic membranes (Neil et al., 2002; Song et al., 2003). At older ages, loss of myelinated fibres and decreased axonal density would lead to increasing  $\lambda_{\perp}$  and lower FA values (Moseley, 2002; Scheltens et al., 1995), while greater water content associated with atrophy in the aging brain could cause increased  $\lambda_{\parallel}$  and thus increasing MD (Moseley, 2002).

Notably, the three most posterior areas did not have significant differences between peak FA and minimum MD. From looking at the diffusivities (Figure 7.5), it is clear that the minima for parallel and perpendicular diffusivity occur almost at the same time (no significant differences), and the prolonged decline of  $\lambda_{\parallel}$  evident in the anterior corpus callosum does not occur in the posterior parietal, temporal, and occipital areas. As discussed above, the longer period of  $\lambda_{\parallel}$  decline in the frontal areas may be due to increased prevalence of

membranes or decreased water content that does not occur for as long in the posterior corpus callosum.

Sex differences were significant only in the superior frontal region for both the FA and MD curves; however, the absolute differences in this region were very small. Previous DTI studies of the corpus callosum have found mixed results with respect to gender differences; some studies observe higher FA in men (Sullivan et al., 2010; Westerhausen et al., 2003), another found higher FA in girls (Schmithorst et al., 2008), and many report no differences at all (Dougherty et al., 2007; Hasan et al., 2008a,b; Zarei et al., 2006).

Three of four previous corpus callosum lifespan DTI studies have measured diffusion values at or near the midline (Hasan et al., 2008a,b; McLaughlin et al., 2007). Many other DTI studies also measure only the medial portion of the corpus callosum (Bhagat and Beaulieu, 2004; Dougherty et al., 2007). Therefore, to facilitate comparisons and to determine whether there were differences between the central corpus callosum and the non-midline areas, additional analyses of FA versus age were conducted after further subdividing the callosal regions into midline and non-midline sections, containing the midsagittal slice plus 5 mm on either side and the rest of the tract, respectively. Figure 7.6 shows the best fit curves for the midline and non-midline regions, as well as fits for the whole tract (same as the curves in Figure 7.3A). The three posterior parietal curves were non-significant; all other fits were significant. During childhood and adolescence, the three curves follow very similar increasing trajectories, although FA is higher at the midline. For the orbital frontal and temporal regions, the midline and non-midline curves also look similar to that of the entire tract at older ages. For other regions, however (anterior and superior frontal, superior parietal, occipital), the declines at older ages are less in the midline section than in the whole tract or non-midline region. Since the midline data is averaged over approximately 200–1100 voxels (depending on the region) per subject, while the non-midline data contained approximately 2000–5000 voxels, the non-midline data is expected to more closely follow the whole tract curves since it has more overlapping voxels. The less substantial drops and earlier peaks in the midline data compared to the whole tract curves

suggest that it might be the more outer sections of the corpus callosum that are driving the declining FA at older ages, a fact that would be missed by studies measuring only midline data. The method of collapsing the data across an entire tract is advantageous because it reduces the numbers one must fit and report (which with this many subjects is already high), provides results that are robust across the entire tract, and improves the SNR; the disadvantage of this is ignoring the range of DTI parameters (particularly FA) along the tract and possibly missing regional differences. The more traditional measurement at the midline has its own limitations of assuming that mid-line results measured there are actually transferable to the entire tract and poorer SNR, although the FA is much higher.

Previous studies used quadratic models (Hasan et al., 2008a,b, 2009b) or interpolation (McLaughlin et al., 2007) to represent age-related diffusion parameters changes in the corpus callosum. While the quadratic model simplifies statistical testing, it is not necessarily the best model for age-related changes, as it assumes equal slopes on either side of the peak. However, a more rapid upslope for FA (or downslope for MD) has been suggested by previous studies examining diffusion changes during childhood and adolescence (Ben Bashat et al., 2005; Hermoye et al., 2006; Lebel et al., 2008b) than is predicted by a quadratic model. We originally used quadratic fits for this study, and obtained the same results in terms of development trends (outer-to-inner), although the ages at peak FA values and minimum MD values were approximately 6 years later with quadratic curves (Caverhill-Godkewitsch et al., 2009). The older peak ages obtained by quadratic fits are likely due to the constraints imposed by the quadratic that the development and the degradation slopes be the same; a constraint not present with Poisson fits. The Poisson fit was chosen for this study because it allowed for different rates of development and degradation (which would be expected due to different biological processes that occur), while maintaining the number of parameters quite low (only 3). It provided robust and significant parameter estimates and fits (which would not have been obtained using a fit with more parameters), but it is not necessarily the only model that could fit the DTI data. A model with separate “development”

and “degradation” terms may be ideal; however, the scatter in this data was too great to allow for fitting such a model, which would have at least 5 parameters. Furthermore, the largest developmental FA increases and MD decreases in the human brain occur before 5 years of age (Dubois et al., 2006; Hermoye et al., 2006), while the largest FA declines and MD increases occur after age 59 years (Hsu et al., 2010; Pfefferbaum et al., 2000). Although we demonstrate here that changes continue to occur between these two extremes, future studies with even larger sample sizes, wider age ranges and longitudinal data may be better able to assess the development and aging trends with more complex models.

Some limitations of this study must be acknowledged. First, DTI acquisition was performed using a six-direction diffusion encoding scheme with multiple averages. The use of more directions can provide more robust estimates of anisotropy (Jones, 2004); however, this is primarily a concern at low SNR values (such as 15 as presented in that paper), but SNR values were very high for our DTI scans (mean SNR was 73 on b0 images). Furthermore, the effects of different encoding schemes are minimal compared to the impact of SNR, and with SNR levels above  $\sim 30$ , FA estimates and power to detect group differences are comparable between acquisitions with six directions and those with more (Landman et al., 2007). Second, deterministic tractography, as used in this study, can be prone to error in areas of crossing fibres where FA values are often artificially low. This is evident in the lack of lateral projections present in the reconstruction of the corpus callosum, and in the sparseness of fibres in certain regions (e.g., the superior parietal region). Our data is therefore limited to the more medial projections of the corpus callosum, which provide reliable data. All tractography for this study was performed by the same investigator, blind to subject age and gender, according to a priori defined rules, to ensure consistency across subjects.

## 7.5 Conclusion

DTI and tractography in a very large group of 315 healthy subjects have shown that the various subregions of the corpus callosum undergo specific and significant age-related micro-structural changes reflecting development towards an apex and then subsequent degradation.

# Chapter 8

## Arcuate Fasciculus Lateralization and Cognition<sup>1</sup>

### Abstract

The arcuate fasciculus is a major white matter tract involved in language processing that has also been repeatedly implicated in intelligence and reasoning tasks. Language in the human brain is lateralized in terms of both function and structure, and while the arcuate fasciculus reflects this asymmetry, its pattern of lateralization is poorly understood in children and adolescents. We used diffusion tensor imaging (DTI) and tractography to examine arcuate fasciculus lateralization in a large (n=183) group of healthy right-handed volunteers aged 5–30 years; a subset of 68 children aged 5–13 years also underwent cognitive assessments. Fractional anisotropy and number of streamlines of the arcuate fasciculus were both significantly higher in the left hemisphere than the right hemisphere in most subjects, although a small number of subjects (10%) were right-lateralized. Age and gender effects on lateralization were not significant. Children receiving cognitive assessments were divided into three groups: a “left only” group in whom only the left side of the arcuate fasciculus could be tracked, a left-lateralized group, and a right-lateralized group. Scores on the Peabody Picture Vocabulary Test (PPVT) and NEPSY Phonological Processing task differed significantly among groups, with left-

---

<sup>1</sup>A version of this chapter has been published. C. Lebel and C. Beaulieu, 2009. Lateralization of the Arcuate Fasciculus from Childhood to Adulthood and its Relation to Cognitive Ability in Children. *Human Brain Mapping* 30: 3563–73.

only subjects outperforming the right-lateralized group on the PPVT, and the left-lateralized children scoring significantly better than the right-lateralized group on Phonological Processing. In summary, DTI tractography demonstrates leftward arcuate fasciculus lateralization in children, adolescents, and young adults, and reveals a relationship between structural white matter lateralization and specific cognitive abilities in children.

## 8.1 Introduction

It has long been known that language function in the human brain is lateralized, ever since Broca in 1861 and Wernicke in 1874 demonstrated that brain lesions associated with loss of language function are most often located in the left hemisphere (Broca, 1861; Wernicke, 1874). Many recent studies have reported functional language lateralization in adults (Binder et al., 2000; Wood et al., 2004), children (Balsamo et al., 2002; Gaillard et al., 2001; Spironelli et al., 2008), and infants (Dehaene-Lambertz et al., 2002). Structural lateralization of language areas, although not as well characterized as functional lateralization, also exists in the human brain. Several consistent structural asymmetries have been reported, including leftward lateralization of the planum temporale and the auditory cortex (Galaburda et al., 1978; Galuske et al., 2000; Geschwind and Levitsky, 1968; Good et al., 2001a; Penhune et al., 1996; Pujol et al., 2002), and white matter volume asymmetries in the frontal, parietal and temporal lobes (Galaburda et al., 1978; Good et al., 2001a; Gur et al., 1980; Pujol et al., 2002). Lesion, tumor, and epilepsy studies provide further evidence of left-lateralized language function and structure in humans (Davtian et al., 2008; Dronkers et al., 2007; Gazzaniga, 1995; Matsumoto et al., 2008; Rodrigo et al., 2008; Toga and Thompson, 2003).

The arcuate fasciculus, a subdivision of the superior longitudinal fasciculus, is a major white matter tract that is one of the primary fibre bundles involved in human language processing (Dejerine, 1895; Geschwind, 1970). This tract connects Broca's area in the frontal lobe, a region mainly involved in speech production (Broca, 1861), with Wernicke's area in the temporal lobe, a region

related to speech comprehension (Wernicke, 1874). The arcuate fasciculus is not only important in language function (Ashtari et al., 2007; Breier et al., 2008; Marslen-Wilson and Tyler, 2007), but it is also part of a network that has been repeatedly implicated in reasoning and intelligence tasks (Hoeft et al., 2007; Jung and Haier, 2007; Jung et al., 2005; Schmithorst et al., 2005; Turken et al., 2008). Structural asymmetry of the arcuate fasciculus has been reported in children, with the left arcuate demonstrating higher “white matter density” than the right side, based on T1-weighted MRI scans (Paus et al., 1999). Furthermore, the volumetric white matter asymmetries observed in adults (Galaburda et al., 1978; Good et al., 2001a; Gur et al., 1980; Pujol et al., 2002) suggest volumetric asymmetries of underlying white matter fibre bundles such as the arcuate fasciculus.

Diffusion tensor imaging (DTI) is an advanced MRI technique that is more sensitive to tissue microstructure than conventional imaging and is especially adept at virtually reconstructing white matter pathways in vivo, via tractography (Basser et al., 2000; Conturo et al., 1999; Jones et al., 1999; Mori et al., 1999). Using tractography, DTI parameters such as fractional anisotropy (FA), an indirect measure of myelination and/or axonal density within white matter (Beaulieu, 2002), can be measured along specific white matter tracts, including the arcuate fasciculus (Catani et al., 2002). DTI studies of the arcuate fasciculus have demonstrated leftward asymmetry in most adults for both structure (Glasser and Rilling, 2008; Hagmann et al., 2006; Parker et al., 2005) and diffusion parameters (Buchel et al., 2004; Nucifora et al., 2005; Powell et al., 2006; Upadhyay et al., 2008; Vernooij et al., 2007); however, these studies were generally small in size ( $n=4-43$ ), and focused solely on adults. One DTI study of 31 children aged 6–17 years reported overall leftward asymmetry of FA values across the group, and absence of the right arcuate in 29% of subjects (Eluvathingal et al., 2007). Further studies of children and adolescents are needed to get a full picture of lateralization during development and to investigate possible age or gender differences. Furthermore, a relationship between arcuate fasciculus asymmetry and language ability was reported in 40 young adults (Catani et al., 2007), but it is not known if a similar rela-

tionship exists in children. A thorough understanding of arcuate fasciculus asymmetry throughout childhood, adolescence, and young adulthood would help address the question of whether the structural asymmetry seen in adults develops over time or is present early in life, as well as providing further information about the relationship between lateralization and cognition. Here we use DTI and tractography to explore arcuate fasciculus asymmetry in a large group of healthy subjects ( $n=183$ ) ranging from 5–30 years of age. The goal of this study was to characterize lateralization of the arcuate fasciculus in children, adolescents and young adults, including an investigation of age- and gender-related changes, and to explore the relationship between arcuate fasciculus asymmetry and cognitive ability in a subgroup of children aged 5–13 years ( $n=68$ ).

## **8.2 Methods**

### **8.2.1 Subjects**

Subjects were 183 healthy, right-handed individuals (86 female/97 male) aged 5–30 years (mean  $\pm$  standard deviation:  $16.3 \pm 6.8$  years). Health was verified by asking participants a series of questions to ensure there was no history of neurological or psychiatric disease or brain injury. Subjects with a wide range of reading ability were recruited, as a broad spectrum of abilities was desired in order to better detect relationships between reading skill and brain structure. Subjects were not formally screening for reading disabilities, but were administered cognitive assessments associated with reading ability (Woodcock Word ID and Word Attack). Informed consent was obtained from all adult volunteers; child assent and parent/guardian consent were obtained for each subject under 18 years.

### **8.2.2 Cognitive Assessment**

Cognitive assessments were performed on a subset of 68 children aged 5–13 years (mean  $\pm$  standard deviation:  $9.4 \pm 2.0$  years, 30 female/38 male). NEPSY Phonological Processing, Word Identification and Word Attack (subtests of the

Table 8.1: Age-standardized score means, standard deviations, and ranges for cognitive assessments performed on a subset of 68 children aged 5–13 years.

Cognitive Assessment	n	Mean Score	Standard Deviation	Range
Phonological Processing	66	10.8	2.7	3–18
PPVT	67	116	13	90–154
TONI	65	112	14	82–142
Word Attack	66	107	13	74–134
Word ID	67	107	14	71–145

Woodcock Reading Mastery Test-Revised), the Peabody Picture Vocabulary Test (PPVT-III), and the Test of Nonverbal Intelligence (TONI) were used, although not all subjects completed all tests (see Table 8.1).

### 8.2.3 Image Acquisition

All imaging data was acquired on the exact same 1.5 T Siemens Sonata MRI scanner (Siemens, Erlangen, Germany) using identical methods. Total acquisition time was approximately 26 minutes and included anatomical imaging and DTI. DTI was acquired using a dual spin-echo, single shot echo-planar imaging sequence with the following parameters: 40 3 mm thick slices with no inter-slice gap, TR=6400 ms, TE=88 ms, 6 non-collinear diffusion sensitizing gradient directions with  $b=1000$  s/mm<sup>2</sup>, 8 averages, field-of-view 220×220 mm<sup>2</sup>, matrix of 128×128 with 75% phase partial Fourier, zero-filled to 256×256. Total DTI acquisition time was 6:06 minutes. Although anisotropic voxel size may be of some concern, a comparison of this sequence with an isotropic voxel size acquisition (2×2×2 mm<sup>3</sup> with the same 6 directions and 8 averages) in four volunteers demonstrated no differences of lateralization grouping and only minimal variation in key parameters derived from tractography of the arcuate fasciculus (standard deviation of FA=0.016 for each hemisphere, standard deviation of lateralization index=0.08). The SNR of b0 images in this study was quite high (average SNR=76, range 53–93), which should help mitigate concerns about the use of 6 directions as opposed to more.

## 8.2.4 Fibre Tracking Diffusion Measurements

Fibre tracking was performed in ExploreDTI (A. Leemans, Antwerp, Belgium), using a deterministic streamline method. FA thresholds were set to 0.25 to initiate and continue tracking, while the angle threshold was set to  $60^\circ$ . An FA threshold of 0.25 was chosen to avoid voxels that are not part of white matter tracts (cortex has FA of approximately 0.2), minimize the inclusion of voxels with a high degree of partial volume contamination, and limit the presence of spurious tracts. The arcuate fasciculus was delineated manually in each hemisphere for each subject. Semi-automated tracking, as we used in a previous study to delineate the superior longitudinal fasciculus (Lebel et al., 2008b), was not appropriate for this study due to the difficulty of isolating the fronto-temporal arcuate fasciculus from the frontal-parietal fibres of the superior longitudinal fasciculus. Superior longitudinal fibres (both fronto-temporal and frontal-parietal) can be obtained using seeding and target regions on coronal slices, a method well-suited to semi-automated tractography. However, obtaining only the arcuate fibres requires a target region on an axial slice in an area much more sensitive to small differences of region placement. Therefore, manual tracking was used to ensure accurate delineation of the entire arcuate fasciculus alone. The operator was not blind to left/right, but was blind to cognitive scores. In order to ensure accurate and unbiased tracking, a specific set of pre-defined rules was followed in the same way for each hemisphere. One seeding region was selected in each hemisphere on a coronal slice on which the arcuate fasciculus — appearing as a green (indicating anterior/posterior orientation) triangular shape — was seen to be largest (see Figure 8.1). Great care was taken to ensure that the seeding region was large enough in each hemisphere to encompass all possible fibres belonging to the arcuate fasciculus, and a margin of at least 5 mm around the tract on all sides was included. A target region was used on an axial slice through which the arcuate fasciculus passes in the inferior/superior direction (appears in blue/purple); again, this target region was drawn larger than the visible region corresponding to the tract to ensure that no fibres were missed. The seeding region was used to

initiate tracking, while the target region selected only fibres passing through both areas. Exclusion regions were used as necessary to eliminate spurious tracts, and were often required in the region of the internal capsules. Only individuals with more than five streamlines (total across hemispheres) were included in further analysis. Originally, 207 right-handed subjects were included in the study; 24 were excluded due to either motion artifacts or having too few streamlines. Average fractional anisotropy (FA) and number of streamlines were calculated for the arcuate fasciculus in each hemisphere for each subject. FA values were calculated by averaging across all voxels in the tract; it is important to note that each voxel was counted only once. Note that FA values were not calculated in hemispheres with no streamlines (63 individuals had no streamlines on the right; 6 had no streamlines on the left).

### 8.2.5 Statistical Analysis

Parametric tests were used for FA values; non-parametric tests were used for number of streamlines. Differences of FA values between hemispheres were tested in individuals having streamlines bilaterally (n=114) using a paired t-test; hemispheric differences of number of streamlines were tested across the population (n=183) using a Wilcoxon signed ranks test for two related samples (equivalent to a paired t-test for nonparametric data). To further characterize asymmetry, a lateralization index,  $LI = (\text{left-right})/(\text{left+right})$ , was calculated for the number of streamlines for each subject. Correlations of age with LI were calculated using Spearman's rho; sex differences were examined using an independent samples Mann-Whitney test. LI was compared to zero using a one-sample Kolmogorow-Smirnov test.

To analyze the relationship between cognitive ability and lateralization, the 68 children receiving cognitive assessments were divided into groups based on their lateralization scores. This was important to allow detection of differences that were not simply linear correlations. Children were divided into three groups: left-only (LI=1), left-lateralized ( $0 < LI < 1$ ), and right-lateralized (LI<0). Subjects were divided in this manner to produce logical groups with reasonably close sample sizes (although the left-lateralized group was larger).

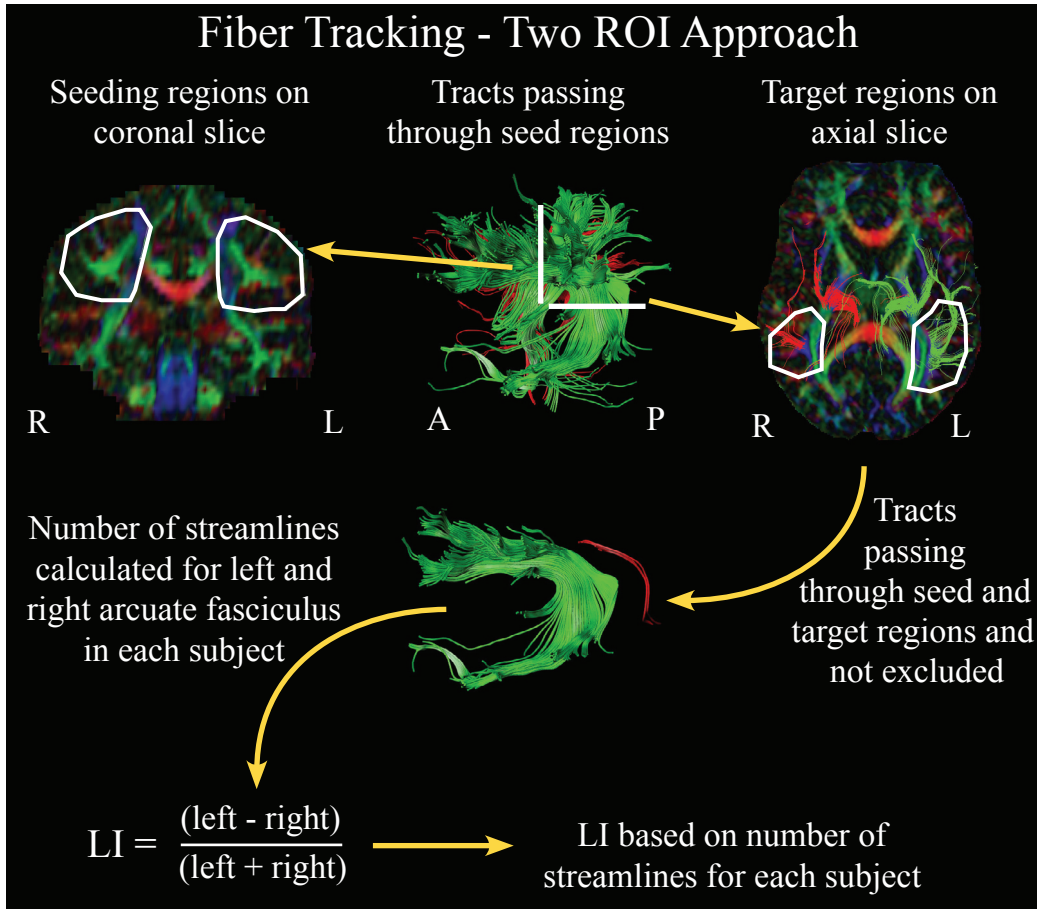


Figure 8.1: Schematic of tracking methods used to delineate the arcuate fasciculus. A manual two region-of-interest approach was used in which a seeding region was drawn on a coronal slice and a target region outlined on an axial slice in each hemisphere for each subject. Exclusion regions were used as need to eliminate spurious streamlines, and were often needed in the area of the internal capsule. Tracts passing through both the seeding and target regions, without passing through exclusion regions, were retained for calculation of the lateralization index (LI). LI was calculated for each subject based on the number of streamlines in each hemisphere.

Age-standardized test scores were compared among groups using a series of ANOVAs. Where the ANOVA test was significant, post-hoc tests (Tukey's honestly significantly different test) were used to determine where differences existed among groups, and Spearman's rho was used to test for correlations between LI and cognitive scores. Age and FA differences among these groups were tested using a series of ANOVAs; LI and number of streamline differences were assessed using the Kruskal-Wallis test, and Mann-Whitney tests with Bonferroni correction for multiple comparisons were used for post-hoc testing.

## 8.3 Results

### 8.3.1 Lateralization Indices

Across the entire group (n=183), individuals had a significantly higher number of streamlines in the left hemisphere than the right ( $p < 0.001$ ), and LI values were significantly different from zero ( $p < 0.001$ ), indicating overall leftward asymmetry in this group. Amongst individuals with streamlines bilaterally (n=114), FA values were significantly higher in the left arcuate fasciculus than the right (mean  $\pm$  standard deviation:  $FA_{left} = 0.52 \pm 0.03$ ,  $FA_{right} = 0.50 \pm 0.04$ ,  $p < 0.001$ ). Most individuals (n=153) were left-lateralized for number of streamlines ( $LI > 0$ ), while some subjects (n=30) were right-lateralized ( $LI < 0$ ); the median LI was 0.78. Across the group, the left arcuate was tracked in 177 individuals (out of 183), and the right was tracked in 120 subjects. In total, 34% of individuals had no detectable right arcuate, 3% showed no detectable left, and in the remaining subjects, both sides were tracked, to varying degrees. Even in hemispheres where the arcuate fasciculus was not able to be tracked, green anterior-posterior and blue superior-inferior sections of it were visible on the coronal and axial slices, respectively. If symmetry is defined as  $-0.2 < LI < 0.2$ , 81% of subjects are considered left-lateralized for number of streamlines, 9 are symmetric, and 10 are right-lateralized. Figure 8.2 shows examples of arcuate fasciculus arrangements for several subjects with a range of LI values.

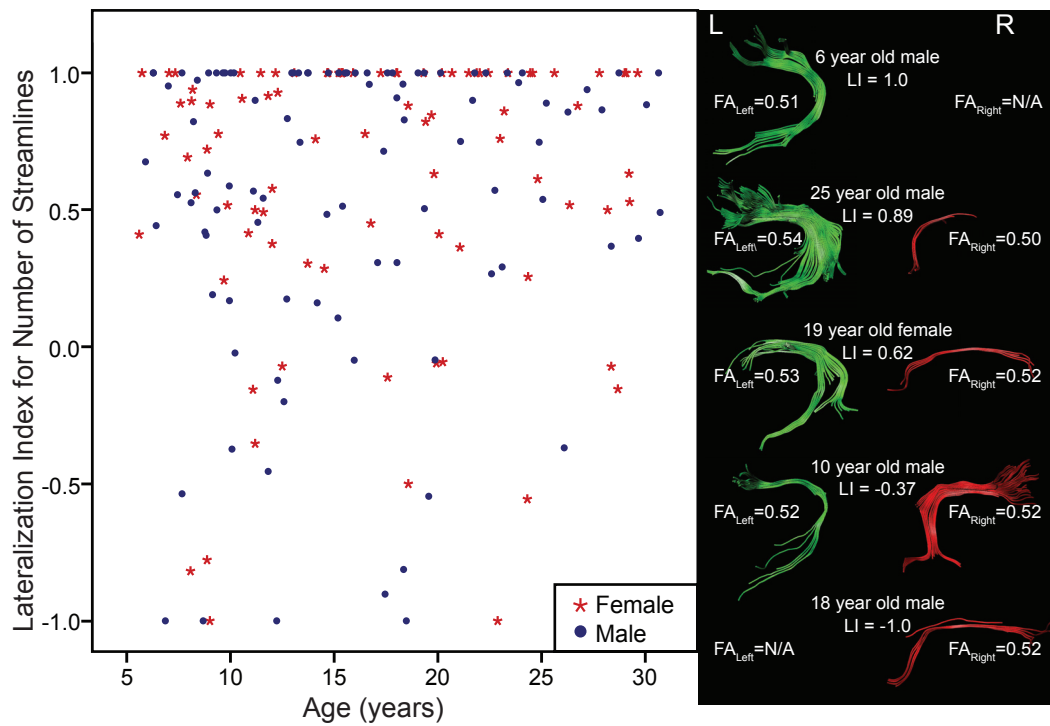


Figure 8.2: Lateralization index based on number of streamlines (LI) versus age graph for 183 right-handed subjects, as well as sample arrangements of the arcuate fasciculus with various values of LI. Most individuals are left-lateralized ( $LI > 0$ ), although there are some right-lateralized ( $LI < 0$ ) subjects. LI was not significantly correlated with age nor was it significantly different between males and females.

Table 8.2: Marginal group means and significance values for ANOVAs of group characteristics and standard test scores. Significantly different compared to right-lateralized group:  $*p_{corrected} < 0.05$ ,  $**p_{corrected} < 0.001$ . Significantly different compared to left-lateralized group:  $\dagger p_{corrected} < 0.05$ ,  $\dagger\dagger p_{corrected} < 0.001$ .

	Right-lateralized (n=15, 6f/9m)	Left-lateralized (n=36, 17f/19m)	Left only (n=17, 7f/10m)	ANOVA p value <sup>a</sup>
Age	10.2	9.1	9.3	0.180
Streamlines <sub>Left</sub>	15	47**	31**	0.000
Streamlines <sub>Right</sub>	34	11**	0** ††	0.000
LI	-0.45	0.58**	1.0** †	0.000
FA <sub>left</sub>	0.50 <sup>b</sup>	0.50	0.50	0.823
FA <sub>right</sub>	0.48	0.48	N/A <sup>c</sup>	0.717
<b>Cognitive assessments</b>				
Phonological Processing	9.2	11.5*	10.7	0.016
PPVT	111	115	123*	0.030
TONI	108	114	114	0.298
Word ID	100	108	110	0.089
Word Attack	104	109	107	0.215

<sup>a</sup> Non-parametric Kruskal-Wallis test used for number of streamlines and LI

<sup>b</sup> Mean of FA values for individuals with streamlines on both sides (11 subjects)

<sup>c</sup> No FA values obtained for right side

The 68 children receiving cognitive assessments were divided into three groups according to their LI scores: a “left-only” group containing subjects in whom only the left side of the arcuate fasciculus could be tracked (LI=1); a left-lateralized group containing subjects with streamlines bilaterally ( $0 < \text{LI} < 1$ ); and a right-lateralized group (LI<0). Subjects were divided in this way in order to produce logical groups relatively similar in size; there were not enough symmetric subjects to form a group. It is important to note that the left-lateralized group contains some individuals who are nearly symmetric (2 individuals with  $0 < \text{LI} < 0.2$ ), while the right-lateralized group contains subjects ranging from those with only the right segment (4 subjects) to those who are nearly symmetric (5 subjects with  $0 > \text{LI} > -0.2$ ). In total, 15 children (22%) were classified as right-lateralized (median LI = -0.45); 36 children (53%) were left-lateralized (median LI = 0.58), and 17 children (25%) were left-only (LI=1). See Table 8.2 for group characteristics.

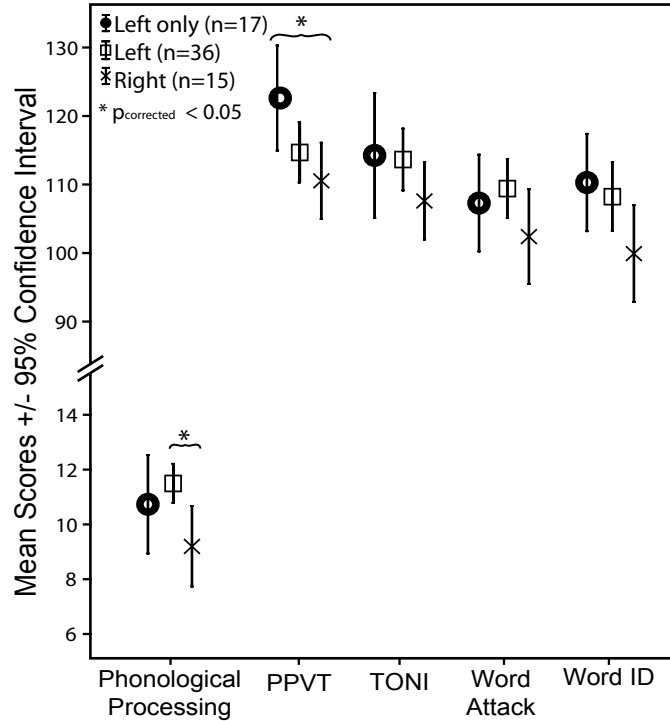


Figure 8.3: Mean scores ( $\pm$  95% confidence intervals) for each test for different lateralization groups of 68 children aged 5–13 years. The Peabody Picture Vocabulary Test (PPVT) and NEPSY Phonological Processing scores differed significantly among groups, with the left only group scoring significantly better than the right-lateralized group for the PPVT, and the left-lateralized group significantly outperforming the right-lateralized group for phonological processing.

### 8.3.2 Age and Gender Differences

Lateralization index (LI) was not significantly correlated with age ( $R=0.09$ ,  $p=0.214$ ), nor significantly different between males and females ( $p=0.456$ ). See Figure 8.2 for a plot of LI vs. age. Testing a similar lateralization index for tract volume also produced no significant differences of age or gender (data not shown).

### 8.3.3 Cognitive Assessments and Lateralization

Summary results for the cognitive assessments are shown in Table 8.1 and results of the ANOVA tests relating DTI-based lateralization to the age-standardized cognitive scores are presented in Table 8.2. Age did not differ significantly amongst groups and each group had approximately the same proportion of males and females. Scores on the PPVT and the NEPSY

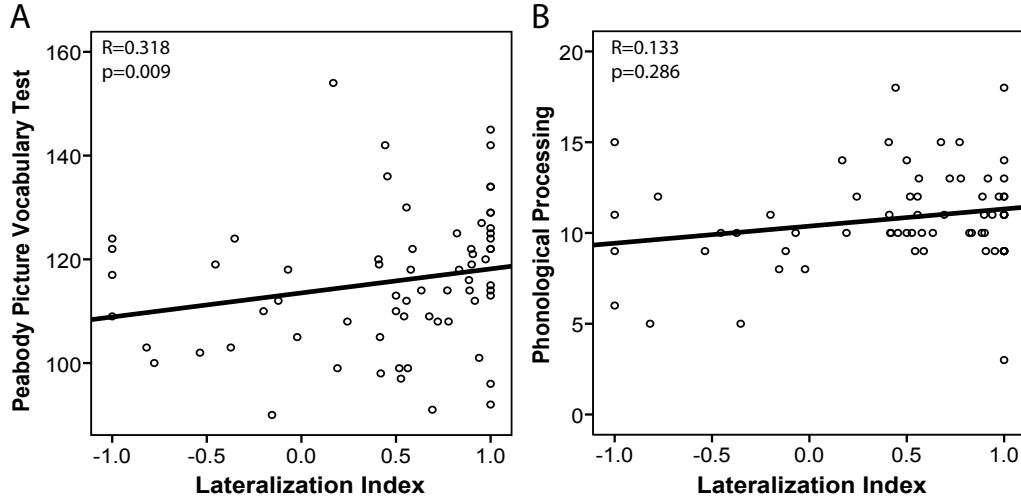


Figure 8.4: Plots of lateralization index (LI) vs. age-standardized scores for (A) Peabody Picture Vocabulary Test (PPVT) and (B) NEPSY Phonological Processing for the entire group of 68 children with cognitive assessments. There was a significant linear correlation between PPVT and LI, whereas the linear correlation between Phonological Processing and LI was not significant. Note the significant lateralization group findings shown in Figure 8.3.

Phonological Processing were significantly related to lateralization groupings ( $p=0.030$ ,  $p=0.016$ , respectively; see Table 8.2 and Figure 8.3). Post-hoc tests revealed that the left-only group significantly outperformed the right-lateralized group on the PPVT ( $p_{corrected}=0.028$ ) and PPVT scores were significantly linearly correlated with LI ( $R=0.32$ ,  $p=0.009$ ) across all children (see Figure 8.4 part A). For the NEPSY Phonological Processing task, the left-lateralized group performed significantly better than the right-lateralized group ( $p_{corrected}=0.012$ ), but the linear correlation with LI was not significant ( $R=0.13$ ,  $p=0.286$ , Figure 8.4B). The same results were observed when a lateralization index calculated based on tract volume was compared across groups (data not shown).

## 8.4 Discussion

Using DTI and tractography, we have characterized the lateralization of the arcuate fasciculus in children, adolescents and young adults, and have demonstrated a significant relationship between this asymmetry and specific cognitive

abilities in children. Across the entire group, number of streamlines and FA values were significantly higher in the left hemisphere than the right hemisphere, and most individuals were left-lateralized, in agreement with many previous DTI studies in healthy adult populations (Catani et al., 2007; Makris et al., 2005; Nucifora et al., 2005; Parker et al., 2005; Powell et al., 2006; Vernooij et al., 2007), healthy children (Eluvathingal et al., 2007), and adult patients (Matsumoto et al., 2008). Approximately 10% of individuals demonstrated rightward lateralization for number of streamlines ( $LI < -0.2$ ), while 34% had extreme leftward lateralization with no detectable streamlines in the right hemisphere. Previous adult studies have observed up to 4% of subjects to be right-lateralized, and anywhere from 0–62% to have streamlines in only the left hemisphere (Catani et al., 2007; Nucifora et al., 2005; Vernooij et al., 2007). The number of left-only arrangements observed in this study is well within the range of previous findings and is closest to observations in children, specifically that 29% of children have no detectable right streamlines (Eluvathingal et al., 2007). We observed more right-lateralized individuals than other studies; however, our sample size was considerably larger ( $n=183$  as opposed to  $n=20-40$ ), and therefore may be expected to contain a wider range of individuals. Interestingly, our findings are consistent with volumetric studies of the planum temporale, which have shown that while the majority of the population is left-lateralized, approximately 9–12% of right-handers exhibit rightward asymmetry of planum temporale volume (Dos Santos Sequeira et al., 2006; Pujol et al., 2002; Steinmetz, 1996).

There were no significant age or gender effects on lateralization. The consistent pattern of asymmetry observed suggests that arcuate fasciculus lateralization is present in early childhood and remains constant throughout adolescence into adulthood. Significant development of the arcuate and superior longitudinal fasciculi occurs during childhood and adolescence, as evidenced by increasing FA values (Barnea-Goraly et al., 2005b; Lebel et al., 2008b; Schmithorst et al., 2002) and “white matter density” (Paus et al., 1999); age-related changes of FA within this population were also significant (data not shown). Despite this development, however, lateralization does not change

with age in this cross-sectional cohort, suggesting that the relationship between hemispheres is maintained even as the brain develops. Similar observations of consistent lateralization have been made with regards to leftward asymmetry of the planum temporale, which exists in adults and is also observed in fetal and neonate brains (Chi et al., 1977; Witelson and Pallie, 1973). Increases of functional lateralization of language have been shown during childhood and adolescence (Everts et al., 2008; Holland et al., 2007; Ressel et al., 2008). However, these functional changes are believed to correspond to skill acquisition rather than more generalized brain development (Holland et al., 2007), a hypothesis supported by the lack of age-related structural lateralization changes in our study. Most previous DTI studies of the arcuate fasciculus do not comment on gender effects with respect to lateralization; however, one study reported gender differences of arcuate fibre density lateralization, with females having a more symmetric arrangement (Catani et al., 2007). Findings of gender differences in functional language lateralization and asymmetry of other brain structures have been mixed (Dos Santos Sequeira et al., 2006; Good et al., 2001a; Kansaku and Kitazawa, 2001; Pujol et al., 2002; Shaywitz et al., 1995; Sommer et al., 2004; Vikingstad et al., 2000).

Children with a greater number of arcuate fasciculus streamlines on the left performed significantly better on certain cognitive tasks than those with more on the right. The left-only group outperformed the right-lateralized group on the PPVT, and the left-lateralized group scored significantly better than the right-lateralized group on the NEPSY Phonological Processing task. Rightward lateralization was not associated with better scores on either task. Both the PPVT, a test of receptive vocabulary, and phonological processing tasks involve frontal and temporal brain areas (Burton et al., 2000; Dronkers et al., 2004; Shalom and Poeppel, 2008; Temple, 2002; Wells et al., 2008). Therefore, it is not surprising that the arcuate fasciculus, connecting the frontal and temporal regions, seems to play a role in both of these tasks. However, the Word ID and Word Attack tasks also involve frontal and temporal regions, yet performance on these tasks was not observed to be significantly different among lateralization groups. The relationship between lateralization of the ar-

uate fasciculus and cognitive skills is still unclear. Future studies on different populations will help to further elucidate the relationship between cognitive skills such as these and lateralization of white matter tracts.

One previous study found a significant correlation between arcuate fasciculus lateralization and a measure of word encoding and list retrieval in adults, with the more bilateral individuals performing best (Catani et al., 2007). Although these differ from our results, the tasks involved were quite different, as were the populations. Furthermore, the arcuate fasciculus is a complex fibre bundle, and is not the only pathway involved in language. Another, more ventral route has been implicated in language processing (Frey et al., 2008; Parker et al., 2005), and may play an additional role in cognitive tasks such as these. Future studies looking at lateralization of this and other brain pathways and their relationship to cognitive abilities may further elucidate the complex interplay between brain structure and language.

The arcuate fasciculus is part of a large, distributed network of brain systems implicated in intelligence tasks (Jung and Haier, 2007; Shaw, 2007). Based on changes in DTI parameters, this tract matures relatively slowly compared to other white matter fibre bundles (Lebel et al., 2008b; Zhang et al., 2007), and even appears to be absent in some children with global developmental delay (Sundaram et al., 2008). Furthermore, the arcuate fasciculus is much smaller or completely absent in other, non-human primates (Rilling et al., 2008), pointing to its advanced role in human cognition. FA values in the arcuate fasciculus correlate with various cognitive scores (Ashtari et al., 2007; Breier et al., 2008; Schmithorst et al., 2005; Turken et al., 2008), and arcuate lateralization is related to verbal recall in adults (Catani et al., 2007). Here, we provide further evidence of a key role for the arcuate fasciculus by demonstrating a correlation with verbal intelligence and phonological processing tasks.

For this study, a six direction diffusion encoding scheme with multiple averages was used for DTI acquisition. Although using more directions is advantageous for robust estimates of anisotropy (Jones, 2004), particularly at lower SNR values (such as 15 as presented in that paper), SNR values were

very high for our DTI scans (average SNR=76 on b0 images). It has been shown that the effects of different encoding schemes may be less of an issue compared to intra-session reliability and the impact of SNR, and that with SNR levels greater than  $\sim 30$ , a six direction acquisition scheme is comparable to those with more encoding directions in terms of FA estimates and power to detect group differences (Landman et al., 2007).

Deterministic tractography, as used in this study, aims to delineate white matter fibre tracts passing through specific regions, essentially creating a three-dimensional region of interest containing one specific tract. However, it is prone to errors in areas of crossing fibres where artificially low FA values are often obtained, such as the region where the arcuate fasciculus descends into the temporal lobe. To minimize errors in this study, a multiple region-of-interest approach was used with seeding and target regions for each tract placed according to a priori knowledge of tract location and trajectory (Makris et al., 2005; Wakana et al., 2004). Furthermore, all tracts were visually inspected to ensure that they conformed to known anatomical trajectories and did not contain spurious fibres. Crossing fibres, however, remain a limitation of deterministic tractography studies. Probabilistic tractography, on the other hand, takes into account the uncertainty in each voxel along the tract (Behrens et al., 2003; Jones and Pierpaoli, 2005; Lazar and Alexander, 2005) and helps overcome problems in crossing fibre regions by estimating all possible connections from a seeding region and their likelihood. Since the trajectory of the arcuate fasciculus is well-known (Catani et al., 2007; Makris et al., 2005; Wakana et al., 2004), and measurements of number of streamlines and FA along the entire length of the tract were desired, deterministic tractography was the appropriate method for this study, despite its limitations. Furthermore, previous studies of the arcuate fasciculus using both deterministic (Nucifora et al., 2005; Vernooij et al., 2007) and probabilistic (Powell et al., 2006) tractography are in agreement. Overall, diffusion tractography is a powerful technique able to virtually extract many of the major white matter connections of the brain, and evidence suggests that the trajectories of many major white matter tracts obtained via tractography agree with the results of postmortem studies

(Catani et al., 2002; Wakana et al., 2007).

## 8.5 Conclusion

DTI tractography has revealed a pattern of leftward asymmetry of the arcuate fasciculus in children, adolescents, and young adults that is consistent across both age and gender. In a subset of children aged 5–13 years, DTI has demonstrated a relationship between arcuate fasciculus lateralization and cognitive ability; extreme leftward lateralization was associated with better receptive vocabulary scores, while a phonological processing task was performed best by those with more moderate leftward lateralization. These findings suggest that the left-lateralized arrangement of the arcuate fasciculus is already present in childhood, and that this lateralization plays an important role in certain cognitive tasks. Future studies exploring the relationship between structural and functional lateralization and cognitive ability may further elucidate the interplay of brain lateralization and cognitive function.

# Chapter 9

## Brain Diffusion Abnormalities in Fetal Alcohol Spectrum Disorder<sup>1</sup>

### Abstract

Children with fetal alcohol spectrum disorder (FASD) have a variety of cognitive, behavioural, and neurological impairments, including structural brain damage. Despite the importance of white matter connections for proper brain function, little is known about how these connections, and the deep gray matter structures that act as relay stations, are affected in children with FASD. The purpose of this study was to use diffusion tensor imaging (DTI), an advanced magnetic resonance imaging technique, to examine microstructural differences of white and deep gray matter in children with FASD. Subjects in this study were 24 children aged 5–13 years previously diagnosed with FASD and 95 healthy children over the same age range. Diffusion tractography was used to delineate ten major white matter tracts in each individual, and region of interest analysis was used to assess four deep gray matter structures. Fractional anisotropy (FA) and mean diffusivity (MD) were assessed in all 14 brain structures. DTI revealed significant differences of diffusion parameters in several brain areas: the genu and splenium of the corpus callosum, cingulum,

---

<sup>1</sup>A version of this chapter has been published. C. Lebel, C. Rasmussen, K. Wyper, L. Walker, G. Andrew, J. Yager and C. Beaulieu, 2008. Brain Diffusion Abnormalities in Children with Fetal Alcohol Spectrum Disorder. *Alcohol Clinical and Experimental Research* 32: 1732–40.

corticospinal tracts, inferior fronto-occipital fasciculus, inferior and superior longitudinal fasciculi, globus pallidus, putamen, and thalamus. Reduced white and gray matter volumes, as well as total brain volume, were observed in the FASD group. These results demonstrate diffusion abnormalities in FASD beyond the corpus callosum, and suggest that multiple brain regions are sensitive to prenatal alcohol exposure.

## 9.1 Introduction

Prenatal alcohol exposure can lead to a variety of cognitive, behavioural and neurological deficits, including permanent structural damage to the brain (Barr and Streissguth, 2001; Jones and Smith, 1973; Lemoine et al., 1968; Mattson and Riley, 1998; Spadoni et al., 2007). Fetal alcohol spectrum disorder (FASD) is the umbrella term used to describe the various developmental disorders associated with maternal alcohol use during pregnancy (Chudley et al., 2005), and FASD is estimated to affect anywhere from 0.33–10 per 1000 live births in North America (Abel and Sokol, 1987, 1991; May and Gossage, 2001; Sampson et al., 1997). Children with FASD often have motor delays (Kalberg et al., 2006), and deficits in attention, learning and memory, executive functioning, mathematics, and language (Jacobson and Jacobson, 2002; Mukherjee et al., 2006). A thorough understanding of the structural brain abnormalities that underlie cognitive and behavioural deficits in FASD is needed, and it may provide insight into the relationship between structure and function in individuals with FASD.

Autopsy studies of children with severe prenatal alcohol exposure identified a host of brain abnormalities including agenesis of the corpus callosum, microcephaly, ventriculomegaly, a small cerebellum, and a variety of other malformations caused by neuronal and glial migration errors (Clarren et al., 1978; Jones and Smith, 1973; Peiffer et al., 1979); however, these studies did not reveal any consistent patterns of brain abnormalities (Roebuck et al., 1998). Although informative, autopsy studies are inevitably limited by the number of available subjects, and likely represent a skewed sample, since only

the most severely alcohol-affected subjects die during infancy. Magnetic resonance imaging (MRI) and spectroscopy make it possible to non-invasively assess the teratogenic effects of alcohol in vivo, and have demonstrated structural (Archibald et al., 2001; Autti-Ramo et al., 2002; Mattson et al., 1996), functional (Fryer et al., 2007; Sowell et al., 2007), and metabolic (Cortese et al., 2006; Fagerlund et al., 2006) abnormalities in individuals with prenatal alcohol exposure.

White matter forms the brain connections necessary for proper cognitive function, and although reduced white matter volume (Archibald et al., 2001) and abnormalities of the corpus callosum and anterior commissure (Bookstein et al., 2007; Peiffer et al., 1979) have been noted in FASD, relatively little is known about how specific brain white matter structures are affected. Diffusion tensor MRI (DTI) is an advanced imaging technique that provides a more sensitive measure of tissue microstructure than conventional MRI (Basser et al., 1994; Le Bihan, 2003) and is especially useful at virtually extracting white matter connections of the brain using tractography (Basser et al., 2000; Con-turo et al., 1999; Jones et al., 1999; Mori et al., 1999). Two previous DTI studies using two-dimensional region of interest analysis have reported callosal abnormalities in individuals with FASD, specifically reduced fractional anisotropy (FA) and increased mean diffusivity (MD) in the genu and splenium of the corpus callosum of severely alcohol-affected young adults (Ma et al., 2005), and increased MD in the isthmus of the corpus callosum of more mildly alcohol-affected children (Wozniak et al., 2006). These studies confirm consistent abnormalities of the corpus callosum in FASD; however, neither study investigated other brain regions. One recent study using voxel-based analysis of whole brain DTI in children and adolescents with FASD reported reduced FA in the regions of the lateral splenium, posterior cingulate white matter bilaterally, and the deep white matter of the right lateral temporal lobe (Sowell et al., 2008a); however, it did not examine specific white matter tracts, a task well suited for DTI tractography, nor did it report changes in mean diffusivity.

Given the variety of structural brain abnormalities and cognitive deficits

associated with FASD, other brain regions are likely to be affected and warrant investigation. Tractography allows for the examination of specific white matter fibre bundles as three-dimensional volumes, providing information about how specific brain connections are affected by prenatal alcohol exposure. In addition to white matter, deep gray matter structures show very large diffusion changes during neurodevelopment (Lebel et al., 2008b), yet DTI changes in deep gray matter have not yet been assessed in individuals with FASD. The purpose of our study was to determine the range of white and deep gray matter abnormalities in children with FASD using DTI and diffusion tractography.

## 9.2 Methods

### 9.2.1 Subjects

Subjects were 24 children aged 5–13 years (mean  $\pm$  st.dev:  $9.1 \pm 2.2$  years, 13 males/11 females, 19 right-handed/5 left-handed) with FASD recruited through a hospital FASD clinic. All children had confirmed prenatal alcohol exposure and a previous medical diagnosis of an alcohol-related disorder falling under the umbrella term FASD, according to the Diagnostic guide for Fetal Alcohol Spectrum Disorders: The 4-Digit Diagnostic Code (Astley, 2004). Two children were diagnosed with fetal alcohol syndrome (FAS) and the rest were diagnosed with other forms of FASD, including neurobehavioural disorder-alcohol exposed (6 subjects), static encephalopathy-alcohol exposed (3 subjects), and neurobehavioural disorder-alcohol exposed with sentinel physical findings (2 subjects). The remaining 11 subjects had a diagnosis of FASD without further specification. Control subjects were 95 healthy children aged 5–13 years (mean  $\pm$  st.dev:  $9.8 \pm 2.2$  years, 50 males/45 females, 88 right-handed/6 left-handed/1 no preference) with no self-reported history of neurological or psychiatric disease or brain injury, who were recruited and scanned as part of a separate study of healthy brain development (Lebel et al., 2008b). Child assent and parent/guardian consent were obtained from all participants. Of the children with FASD, approximately 30% were aboriginal, while the remaining subjects were primarily Caucasian. The majority of the

control participants were Caucasian. Unfortunately, specific information about quantity of alcohol use during pregnancy and possible use of other drugs was not available.

### **9.2.2 Cognitive Assessment**

A battery of cognitive assessments was performed on each child with FASD in order to compare cognitive scores with quantitative DTI parameters of specific brain regions. Executive functioning was assessed using the NEPSY: Tower, Auditory Attention and Response Set, Visuomotor Precision, Arrows, Memory for Names, and Narrative Memory subtests. The Working Memory Test Battery for Children (WMTB-C), Digit Recall and Block Recall subtests were used to measure working memory, and the Woodcock Johnson III (WJ-III) Tests of Achievement-Quantitative Concepts subtest assessed mathematical ability. The Woodcock Reading Mastery Test (WRMT) — Word ID, and the Comprehensive Receptive and Expressive Vocabulary Test (CREVT-2) tested reading achievement and vocabulary proficiency, respectively. Cognitive assessments were not performed on the control children.

### **9.2.3 Image Acquisition**

All data was acquired on the same 1.5 T Siemens Sonata MRI scanner using identical methods. Total acquisition time was approximately 18 minutes and included DTI, anatomical T1-weighted, T2-weighted and FLAIR imaging. DTI was acquired using a dual spin-echo, single shot echo-planar imaging sequence with the following parameters: 40 3 mm thick axial-oblique slices with no inter-slice gap, TR=6400 ms, TE=88 ms, 6 non-collinear diffusion sensitizing gradient directions with  $b=1000$  s/mm<sup>2</sup>, 8 averages, field-of-view 220×220 mm<sup>2</sup>, matrix of 128×128 zero-filled to 256×256, 75% phase partial Fourier. Total DTI acquisition time was 6:06 minutes and yielded excellent quality FA maps in the children (as shown in Figure 9.1). High resolution (1×1×1 mm<sup>3</sup>) T1-weighted images were acquired using MPRAGE with TE=4.38 ms, TR=1870 ms, TI=1100 ms, and a scan time of 4:29 minutes. Head motion was minimized using ear pads, but some children needed to be removed from

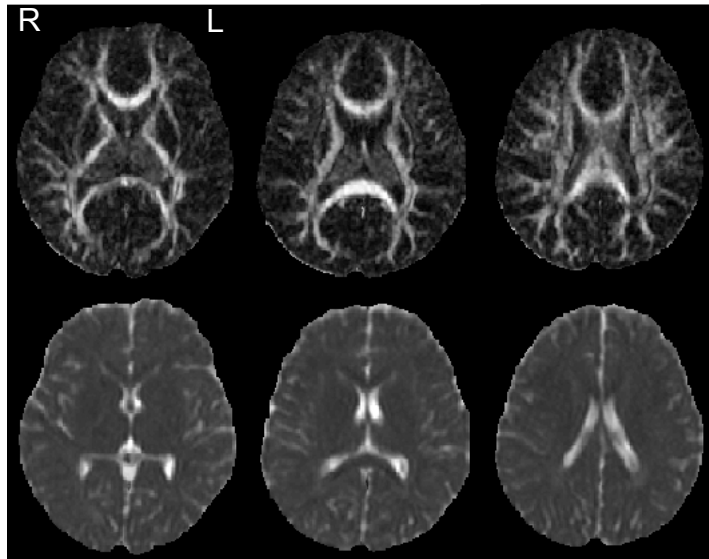


Figure 9.1: Several axial slices are shown from the fractional anisotropy (top) and mean diffusivity maps (bottom) of a 9 year old boy who was part of the FASD group.

the MRI scanner after the 6-minute DTI sequence, and therefore T1-weighted images were obtained in 20 of the 24 children with FASD, and 93 of the 95 control subjects. Conventional T2-weighted and FLAIR scans were obtained for 18 of the 24 FASD children to detect gross brain abnormalities.

#### 9.2.4 Region-of-Interest Diffusion Measurements

Average mean diffusivity (MD) and fractional anisotropy (FA) values were calculated for four deep gray matter structures (thalamus, globus pallidus, putamen, and head of the caudate nucleus) using region-of-interest (ROI) analysis by the same investigator (L.W.), according to previously described methods (Snook et al., 2005). A previous intra-rater reliability study by the individual who performed all of the ROI analysis in this paper showed good reliability of ROI measurements (LW is L. Snook from the previous study, with a change of surname) (Snook et al., 2005). For each structure, left and right measurements were made and analyzed separately. Diffusion eigenvalues were not analyzed for the regions measured using ROI analysis.

### 9.3 Fibre Tracking Diffusion Measurements

A novel, semi-automated tractography method was used to extract ten major white matter tracts in each individual. A template was created based on 20 DTI scans of one 25 year old male obtained on the same MRI scanner, which were normalized and averaged together. Non diffusion-weighted images ( $b=0$  s/mm<sup>2</sup>) were registered to the template using a non-affine transformation (SPM5, Wellcome Trust Centre for Neuroimaging, London, UK) to obtain warping parameters for each subject. For each tract, one seeding region and one target region known to contain the tract were selected on the template colour map according to a priori information on tract location (Wakana et al., 2004). Additional exclusion regions were used to eliminate spurious tracts. Seeding, target, and exclusion regions selected manually on the template colour map were un-warped to native space for each individual data set using the inverse of normalization parameters obtained from initial registration. The un-registered seeding and target regions were used to perform fibre tracking automatically within each individual in native space. Fibre tracking was performed in ExploreDTI (Antwerp, Belgium), using a deterministic streamline method. FA thresholds were set to 0.25 to initiate and continue tracking, while the angle threshold was set to 60° for the uncinate fasciculus and the superior longitudinal fasciculus and 30° for all other tracts. Ten major white matter fibre bundles with well-known anatomy were tracked: the genu, body and splenium of the corpus callosum, inferior and superior longitudinal fasciculi (ILF, SLF), inferior and superior fronto-occipital fasciculi (IFO, SFO), cingulum, uncinate fasciculus (UF), and corticospinal tracts (CST). FA and MD values were calculated by averaging all voxels over the entire tract for each individual. Note that each voxel was counted only once, regardless of the number of streamlines passing through it. Where appropriate, left and right tracts were measured and analyzed separately. Parallel and perpendicular diffusivity eigenvalues were measured for each white matter tract.

### **9.3.1 Volume Measurements**

T1-weighted MPRAGE images were segmented into gray and white matter using statistical parametric mapping software (SPM5, Wellcome Trust Centre for Neuroimaging, London, UK), after normalization to the ICBM-152 template. Total gray matter and white matter volumes were measured, and total brain volume was calculated. Cerebrospinal fluid was not included in total brain volume measurements.

### **9.3.2 Statistical Analysis**

Cognitive assessment scores for the FASD group were compared to standard values (a score of 100 WMTB-C, CREVT, WJ-III and WRMT tests, and a score of 10 for all NEPSY subtests) using a one sample t-test, with a significance level of 0.05. Diffusion parameters (FA and MD) for each tract were compared between control and FASD groups using a MANCOVA that accounted for the effects of age, since FA and MD are known to be age-dependent (Barnea-Goraly et al., 2005b; Ben Bashat et al., 2005; Lebel et al., 2008b). Tracts in the left and right hemispheres were assessed separately. Gray matter, white matter and total brain volume were also compared between groups using a MANCOVA controlling for age. Within the FASD group, partial correlations controlling for age, with Bonferroni correction for multiple comparisons, were used to examine the relationship of the DTI parameters, FA and MD, for each tract to the above mentioned raw cognitive scores. Male and female subjects were combined for all analyses, due to small sample size.

## **9.4 Results**

### **9.4.1 Cognitive Testing**

Standardized score means and standard deviations are shown in Table 9.1. Children with FASD performed significantly below average (based on general population averages for each test, not our control subjects) for almost all tests, except the NEPSY: Narrative Memory and Tower subtests. Children with

Table 9.1: Summary of cognitive scores, with mean and standard deviations for each score. Scores were tested against normal values (10 for all NEPSY subtests, 100 for all other assessments) using a one-sample t-test. Children with FASD performed significantly below average on most tests.

Cognitive Assessment	n	Mean	St.Dev.	p value
NEPSY: Narrative Memory	22	8.5	3.7	0.078
NEPSY: Memory for Names	22	7.1	3.7	0.002
NEPSY: Arrows	24	8.3	3.4	0.026
NEPSY: Visuomotor Precision	24	7.8	2.8	0.001
NEPSY: Auditory Attention and Response Set	17	8.1	3.3	0.026
NEPSY: Tower	24	8.9	4.0	0.185
Working Memory Test Battery — Children (WMTB-C): Digit Recall	23	83.6	12.0	0.000
Working Memory Test Battery — Children (WMTB-C): Block Recall	23	84.7	14.0	0.000
Comprehensive Receptive and Expressive Vocabulary Tests (CREVT): Composite Score	21	87.0	13.1	0.000
Woodcock-Johnson (WJ-III): Quantitative Concepts	21	87.1	16.5	0.002
Woodcock Reading Mastery Test (WRMT): Word Identification	21	93.1	10.1	0.005

FASD showed particular deficits in working memory, quantitative concepts, vocabulary, and some executive functioning measures. No correlations between cognitive measures and diffusion parameters of any of the ten tracts or four gray matter regions (left or right) were significant at the  $p=0.05$  level after Bonferroni correction for multiple comparisons.

#### 9.4.2 Structural Imaging and Volume

No gross brain abnormalities were observed on T2-weighted or FLAIR images for the FASD cohort. Gray matter, white matter, and total brain volume were significantly reduced in children with FASD compared to the control group (see Figure 9.2). White matter volume was slightly more affected and was reduced by 11.5% ( $57 \text{ cm}^3$ ) in FASD subjects, while gray matter was reduced by 6.8% ( $50 \text{ cm}^3$ ). Overall, total brain volume was reduced by 8.4% ( $107 \text{ cm}^3$ ) in the FASD group.

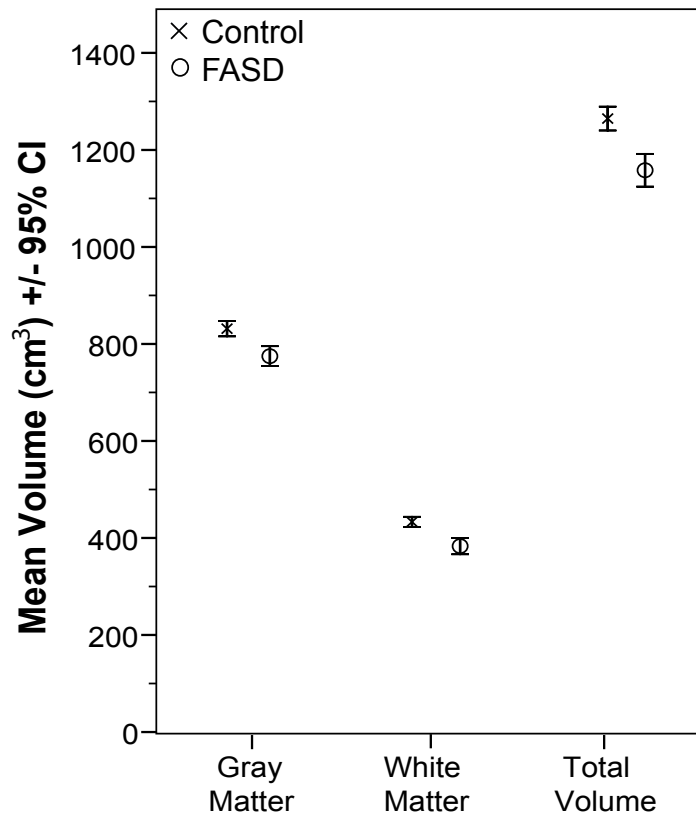


Figure 9.2: Children with FASD (n=20) showed a decrease in total volume ( $p < 0.001$ ) relative to controls (n=93) with a greater percent reduction of white matter (11.5%,  $p < 0.001$ ) than gray matter (6.8%,  $p = 0.002$ ).

Table 9.2: Summary of diffusion parameters, with mean FA and MD values for FASD (n=24) and control (n=95) subjects, and the significance of the between-groups comparison (p value from MANCOVA) for each of the ten white matter tracts and four deep gray matter regions.\*p<0.05

<b>Tractography Analysis</b>	FA			MD [ $10^{-3}$ mm <sup>2</sup> /s]		
	FASD	Control	p value	FASD	Control	p value
Genu CC	0.55	0.55	0.823	0.80	0.82	0.021*
Body CC	0.52	0.52	0.528	0.90	0.89	0.796
Splenium CC	0.56	0.58	0.001*	0.85	0.83	0.240
L Cingulum	0.47	0.47	0.855	0.81	0.81	0.792
R Cingulum	0.44	0.47	0.038*	0.81	0.80	1.000
L CST	0.49	0.51	0.058	0.85	0.84	0.792
R CST	0.50	0.51	0.435	0.87	0.84	0.001*
L IFO	0.49	0.49	0.348	0.84	0.82	0.015*
R IFO	0.49	0.50	0.964	0.85	0.82	0.001*
L ILF	0.42	0.45	0.000*	0.89	0.86	0.006*
R ILF	0.43	0.45	0.003*	0.88	0.87	0.090
L SFO	0.43	0.44	0.095	0.78	0.77	1.000
R SFO	0.44	0.45	0.477	0.77	0.76	0.217
L SLF	0.45	0.47	0.005*	0.80	0.78	0.106
R SLF	0.45	0.47	0.048*	0.79	0.78	0.087
L Uncinate	0.40	0.40	0.461	0.87	0.85	0.145
R Uncinate	0.41	0.40	0.218	0.87	0.85	0.055
<b>Region-of-Interest Analysis</b>						
L Caudate	0.18	0.18	0.720	0.75	0.73	0.484
R Caudate	0.18	0.18	0.493	0.74	0.73	0.059
L Globus pallidus	0.26	0.24	0.000*	0.80	0.77	0.000*
R Globus pallidus	0.26	0.24	0.007*	0.80	0.77	0.000*
L Putamen	0.15	0.15	0.093	0.76	0.74	0.327
R Putamen	0.15	0.16	0.193	0.76	0.74	0.001*
L Thalamus	0.28	0.30	0.034*	0.80	0.79	0.456
R Thalamus	0.29	0.29	0.817	0.80	0.78	0.043*

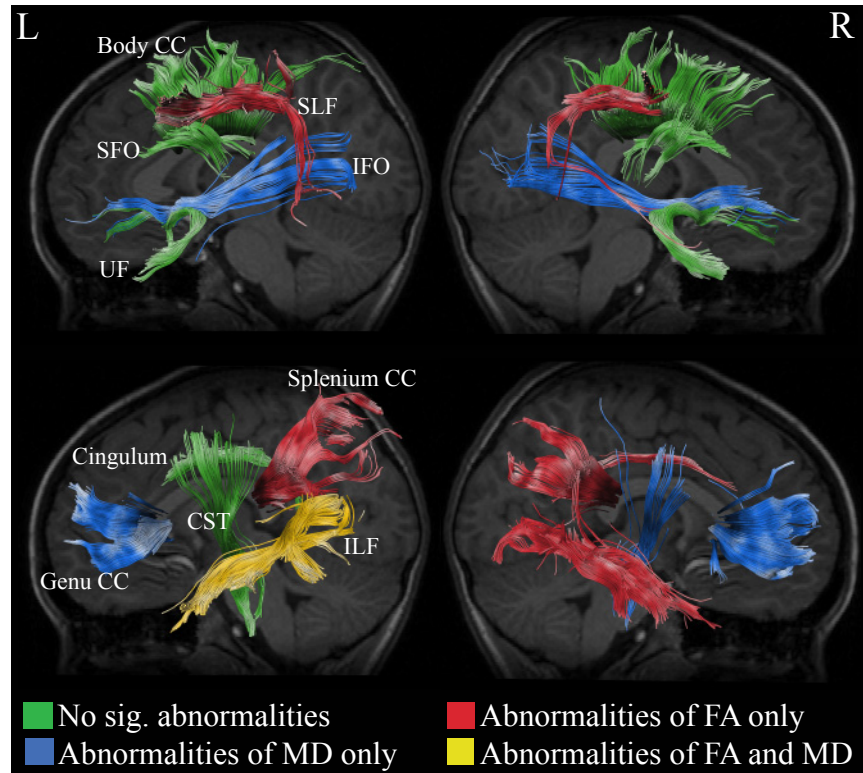


Figure 9.3: All ten tracts measured are shown in a healthy 8 year old male control. Seven of the ten tracts showed significant diffusion abnormalities in the FASD group, either bilaterally (FA in SLF, ILF, splenium, MD in IFO and genu) or unilaterally (FA in cingulum, MD in ILF, CST).

### 9.4.3 Diffusion Parameters

The MANCOVA test revealed abnormal diffusion parameters in children with FASD, either unilaterally or bilaterally, in 7 of 10 white matter tracts and 3 of 4 gray matter structures examined (see Table 9.2, Figures 9.3 and 9.4). The right cingulum, bilateral ILF and SLF, splenium of the corpus callosum, and left thalamus demonstrated FA reductions of 4–6% in children with FASD compared to controls; increased FA (8%) was observed in the globus pallidus. MD was increased by 1–4% in children with FASD compared to controls in the bilateral IFO, left ILF, right CST, globus pallidus, right putamen, and right thalamus. Mean diffusivity in the genu of the corpus callosum was reduced by 2% in children with FASD compared to controls.

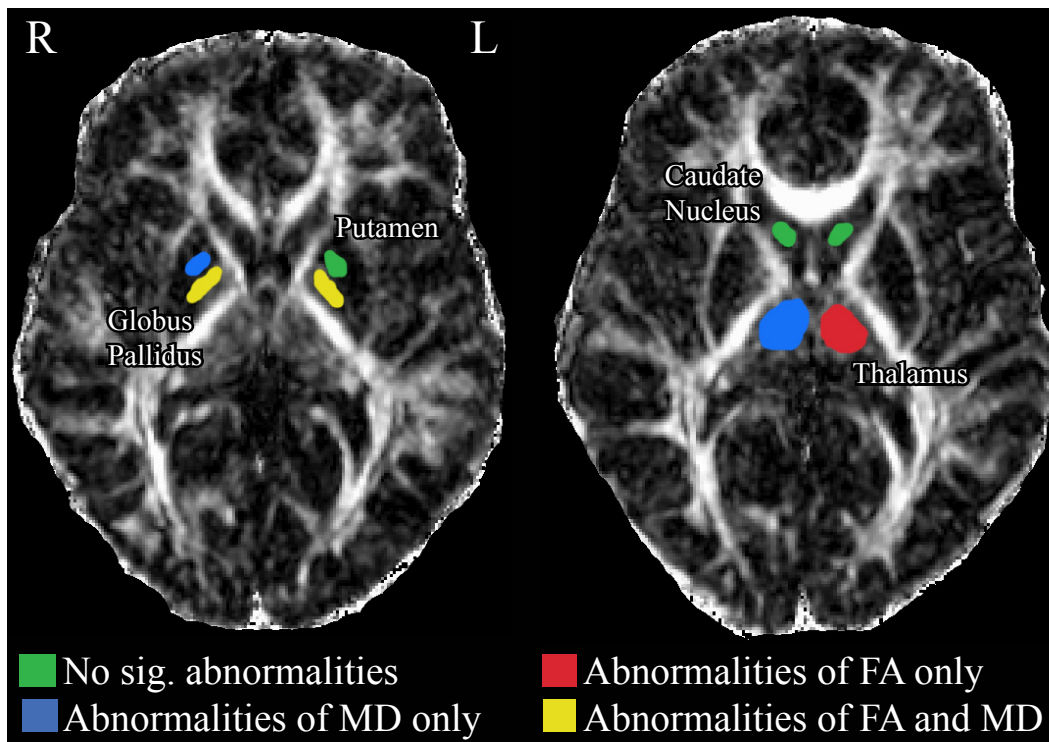


Figure 9.4: All four gray matter areas measured are shown in a healthy 6 year old male control. Three of the four structures showed diffusion parameter abnormalities either bilaterally (FA and MD in globus pallidus) or unilaterally (FA and MD in thalamus, MD in putamen).

## 9.5 Discussion

Tractography and region of interest analysis revealed diffusion abnormalities in seven of ten white matter tracts and three of four deep gray matter structures in children with FASD, as shown in Table 9.2 and Figures 9.3 and 9.4. Our results demonstrate widespread microstructural differences between children with FASD and healthy controls, and support previous DTI findings in the corpus callosum (Ma et al., 2005; Sowell et al., 2008a; Wozniak et al., 2006), posterior cingulate white matter bilaterally and right temporal white matter (Sowell et al., 2008a) in individuals with FASD.

Callosal abnormalities have been consistently reported in alcohol-affected individuals by studies using autopsy and various imaging techniques (Bookstein et al., 2007; Fagerlund et al., 2006; Peiffer et al., 1979), including DTI (Ma et al., 2005; Sowell et al., 2008a; Wozniak et al., 2006). Two DTI studies (Sowell et al., 2008a; Wozniak et al., 2006) found differences only in the posterior corpus callosum of children ( $n=17$  and  $n=14$ ) with FASD, while another study (Ma et al., 2005), demonstrated reduced FA and elevated MD in the frontal parts of the corpus callosum (genu) in addition to the splenium in nine alcohol-affected young adults. We examined a larger group of 24 children, and observed reduced FA in the splenium and reduced MD in the genu of the FASD group, confirming callosal abnormalities in individuals with prenatal alcohol exposure. Although we found reduced, rather than elevated, MD values in the genu, our subjects were younger and less severely alcohol-affected than those in the previous study (Ma et al., 2005) (who all had FAS), and therefore may be expected to have different structural brain abnormalities. Furthermore, our tractography method examines the tract volume as a whole, encompassing a much larger region than two-dimensional ROI analysis of a single slice.

Previous MRI studies have demonstrated a particular vulnerability of the temporal and parietal lobes to the teratogenic effects of alcohol, with these areas showing thicker cortices, perhaps implying less white matter, as well as greater volume reductions than other brain regions (Archibald et al., 2001; Sowell et al., 2008b). In addition, one study reported diffusion abnormalities

in children with FASD in the right temporal lobe, which is a region containing the inferior longitudinal and inferior fronto-occipital fasciculi (Sowell et al., 2008a). Consistent with these studies, we observed differences in the both of these tracts, and the largest differences between healthy children and those with FASD were in white matter fibres connecting to the temporal region of the brain. The bilateral superior longitudinal fasciculus, a temporal-parietal connection involved in language processing, the bilateral inferior longitudinal fasciculus, an occipital-temporal tract thought to be involved in secondary visual processing, and the right cingulum, a temporal connection projecting to the frontal lobe, all showed significant differences of FA and/or MD. Although the uncinate fasciculus, another fronto-temporal connection, was not significantly different between groups, there was a trend ( $p=0.055$ ) toward elevated MD in the right hemisphere.

The group differences we observed ranged from 0.02–0.03 for FA, or 4–8%, and  $0.02\text{--}0.03 \times 10^{-3}$  mm<sup>2</sup>/s for MD, or 1–4%. Previous studies have reported FA differences of 17–22% (Ma et al., 2005; Sowell et al., 2008a) and MD differences of 15–17% (Ma et al., 2005; Wozniak et al., 2006) in the corpus callosum, and FA changes of 6–11% in the right temporal lobe (Sowell et al., 2008a). Our percent differences of DTI parameters are somewhat lower than previous studies, particularly for the corpus callosum; however, we used tractography, which examines the entire white matter tract, rather than a smaller, more specific area. The other studies report differences from only a small portion of the tract, using either region-of-interest analysis, which examines only the central portion of the structure, or voxel-based methods that report differences from only voxels contained within the significant region. By averaging FA or MD values over a larger region, our differences are smaller, but demonstrate robust differences across an entire structure. Only two of the subjects in our study (8%) were diagnosed with FAS, the most severe diagnosis falling under the FASD umbrella, which is a much smaller percentage than two of the other studies, which had 24% (4 of 17 subjects) (Sowell et al., 2008a), and 100% of individuals (Ma et al., 2005) with FAS. The third study did not have any individuals with FAS (Wozniak et al., 2006). These differential diagnoses likely

also contribute to different magnitudes of changes between groups.

The eigenvalues of the diffusion tensor can provide detailed information about microstructural differences that might underlie changes of FA. An investigation of the eigenvalues for tracts with significant FA reductions revealed a consistent elevation of perpendicular diffusivity in children with FASD (data not shown). This suggests decreased barriers to diffusion across the axons, such as reduced myelination and/or axonal density (Beaulieu, 2002). Prenatal alcohol exposure is known to affect the glial cells of the brain (Guerra et al., 2001), and in particular, the oligodendrocytes that produce the myelin sheath surrounding axons (Ozer et al., 2000; Phillips and Krueger, 1992). Demyelination in the mouse brain is reflected by an increase of perpendicular diffusivity, whereas remyelination is characterized by decreases of perpendicular diffusivity (Song et al., 2005), suggesting that reduced myelination in the FASD group is a possible cause of the observed FA differences between groups.

Diffusion abnormalities were observed in the thalamus, putamen, and globus pallidus (Table 9.2, Figure 9.4). Deep gray matter structures are known to be affected by prenatal alcohol exposure, as demonstrated by decreased metabolic rates on positron emission tomography scans (Clark et al., 2000), reduced volume (Archibald et al., 2001; Cortese et al., 2006; Mattson et al., 1996), and abnormal metabolite ratios (Fagerlund et al., 2006). These deep gray matter structures also undergo large developmental changes (30–50% increase of FA) during childhood and adolescence (Lebel et al., 2008b). Although the interpretation of diffusion parameters in gray matter is not straightforward, the elevated MD indicates fewer barriers to diffusion, and reduced FA values may reflect a decreased level of organization, possibly indicating that children with FASD have less order in the thalamus and putamen, but increased organization in the globus pallidus. We did not observe any diffusion abnormalities in the caudate, perhaps indicating that its internal structure remains constant despite the overall volume decreases reported by other studies (Archibald et al., 2001; Cortese et al., 2006; Mattson et al., 1996).

Overall, there was good agreement between left and right hemispheres for changes of both FA and MD. However, the cingulum, corticospinal tracts,

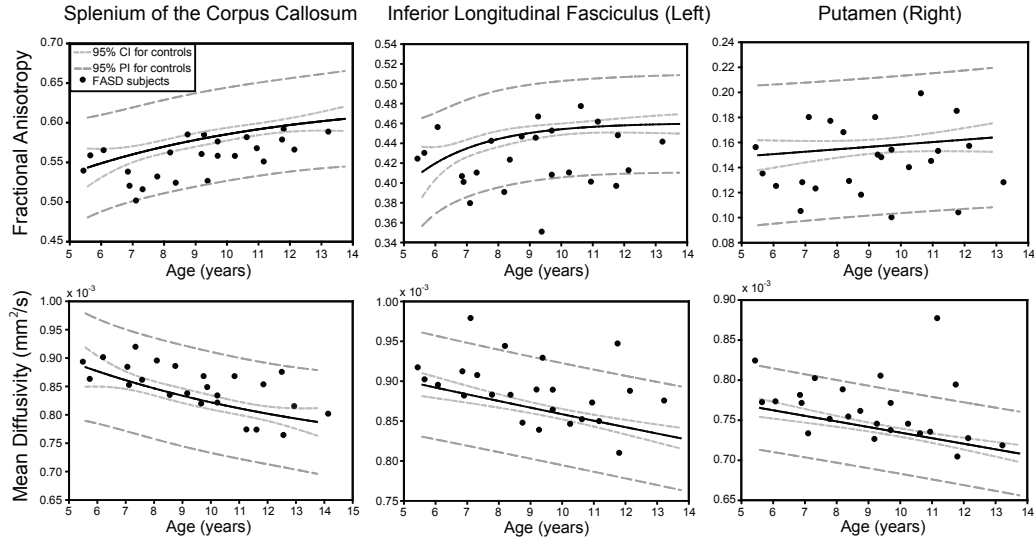


Figure 9.5: Three examples of age-related diffusion changes are shown with best fit curves for controls (solid line) and confidence/prediction intervals (dotted/dashed lines). Where there are significant group differences (FA in splenium, FA and MD in left ILF, MD in right putamen), most FASD subjects lie on one side of the fit line, but within the prediction interval.

inferior longitudinal fasciculus, putamen and thalamus demonstrated asymmetrical changes of FA and/or MD. Asymmetry of diffusion parameters in healthy subjects has been previously reported in the cingulum (Gong et al., 2005), putamen and thalamus (Fabiano et al., 2005), perhaps contributing to the hemispheric discrepancies for these structures. Asymmetric findings may also indicate different sensitivities of the right and left hemispheres to prenatal alcohol exposure.

As was expected and has been consistently described in the literature (Archibald et al., 2001; Autti-Ramo et al., 2006; Spadoni et al., 2007), we observed significantly reduced total brain volume, white matter and gray matter volume in the FASD group compared to controls (Figure 9.2). In our FASD group, white matter volume was slightly more reduced than gray matter volume compared to controls, supporting previous reports that white matter is more affected by prenatal alcohol exposure (Archibald et al., 2001). We did not examine regional volume differences, so are unable to determine whether any specific structures demonstrated volume changes.

During childhood, FA increases and MD decreases with age (Barnea-Goraly

et al., 2005b; Ben Bashat et al., 2005; Lebel et al., 2008b). Unfortunately, our sample was not large enough to examine age-related changes within the FASD group; however, it appears that differences between groups exist across our age range. For all structures, most children with FASD (>80%) fell within the 95% prediction interval for control subjects (see Figure 9.5). However, for structures with significant group differences, children with FASD were predominantly located on one side of the control development curve (within the 95% prediction interval, but outside the 95% confidence interval of the fit). For structures without significant differences, children with FASD are more evenly scattered about the control curve. A larger sample size over a wider age range is needed to compare the developmental trajectories of brain structures in FASD compared to healthy controls.

Many of the FASD children in this study showed deficits on cognitive tests, especially working memory, quantitative concepts, vocabulary, and some measures of executive functioning (see Table 9.1). One study has reported correlations between visuomotor integration test scores and FA in the splenium of the corpus callosum in subjects with FASD (Sowell et al., 2008a); however, we did not find any significant correlations between cognitive measures and DTI parameters. The robust cognitive deficits in our FASD subjects are indicative of underlying brain abnormalities; however, it may be overly simplistic to expect a one-to-one relationship between a single tract and a specific cognitive deficit. Furthermore, we had a diverse group of affected subjects, and did not have information regarding the degree of prenatal alcohol exposure. Although we did not find significant correlations between cognitive deficits and DTI parameters, that does not mean they are not related. In this regard, alcohol has been shown to increase fetal glutamate levels (Karl et al., 1995; Thomas et al., 1997) and reduce glutamate NMDA receptors (Hughes et al., 1998), which, during critical periods of development, may interfere with normal neuronal and glial migration. Others have found that exposure to alcohol during fetal life increases apoptotic neurodegeneration (Ikonomidou et al., 2001), again contributing to potential teratogenesis and neurobehavioural disturbances. However, it is clear that interruption of the normal excitation that

occurs in the immature nervous system, promoting neuronal survival, dendritic arborization, and synaptogenesis, results in abnormal cerebral growth and hence abnormal axonal growth (Ma et al., 2003; Mennerick and Zorumski, 2000; Olney, 2004). Further research examining more specific brain regions may help elucidate structure-function relationships.

Although a sensitive means of assessing tissue microstructure, diffusion tensor imaging and tractography do not accurately model all brain regions. In particular, the standard tensor model is not adequate to describe regions of crossing fibres within the brain, and can lead to artificially low FA values in these areas. Various techniques have been proposed for more accurately modeling voxels with crossing fibre populations (Anderson, 2005; Tuch, 2004); however, these require lengthy data acquisition times that are prohibitive to scanning children. In an attempt to avoid potentially problematic brain regions, we selected only major white matter tracts that have known trajectories and can be easily delineated using deterministic tractography. In addition, we chose a relatively high FA threshold for tracking of 0.25 and terminated any streamlines that reached voxels with FA values below 0.25, to minimize inclusion of white matter voxels with low FA due to crossing fibres or a high degree of partial volume contamination from cerebrospinal fluid or gray matter, and to avoid spurious tracts.

## 9.6 Conclusion

Diffusion abnormalities were observed across the brains of children with FASD, showing changes in projection, association and commissural white matter tracts, as well as deep gray matter structures. Diffusion tensor imaging demonstrates the widespread brain damage associated with prenatal alcohol exposure, and identifies key structural brain abnormalities that presumably underlie the cognitive, motor, behavioural and emotional difficulties associated with FASD.

# Chapter 10

## Brain Structure and Mathematical Ability in Fetal Alcohol Spectrum Disorder<sup>1</sup>

### Abstract

Children with fetal alcohol spectrum disorder (FASD) often demonstrate a variety of cognitive deficits, but mathematical ability seems to be particularly affected by prenatal alcohol exposure. Parietal brain regions have been implicated in both functional and structural studies of mathematical ability in healthy individuals, but little is known about the brain structure underlying mathematical deficits in children with FASD. The goal of this study was to use diffusion tensor imaging (DTI) to investigate the relationship between mathematical skill and brain white matter structure in children with FASD. Twenty-one children aged 5–13 years diagnosed with FASD underwent DTI and cognitive assessments including the Woodcock-Johnson Quantitative Concepts test. Voxel-based analysis was conducted by normalizing subject images to a template and correlating fractional anisotropy (FA) values across the brain white matter with age-standardized math scores. Voxel-based analysis revealed four clusters with significant correlations between FA and math scores: two positively-correlated clusters in the left parietal region, one positively-

---

<sup>1</sup>A version of this chapter has been published. C. Lebel, C. Rasmussen, K. Wyper, G. Andrew and C. Beaulieu, 2010. Brain Microstructure is Related to Math Ability in Children with Fetal Alcohol Spectrum Disorder. *Alcohol Clinical and Experimental Research* 34 (2): 354–363.

correlated cluster in the left cerebellum, and one negatively-correlated cluster in the bilateral brainstem. Diffusion tractography identified the specific white matter tracts passing through these clusters, namely the left superior longitudinal fasciculus, left corticospinal tract and body of the corpus callosum, middle cerebellar peduncle, and bilateral projection fibres including the anterior and posterior limbs of the internal capsule. These results identify four key regions related to mathematical ability and provide a link between brain microstructure and cognitive skills in children with FASD. Given previous findings in typically developing children and those with other abnormal conditions, our results highlight the consistent importance of the left parietal area for mathematical tasks across various populations, and demonstrate other regions that may be specific to mathematical processing in children with FASD.

## 10.1 Introduction

Fetal alcohol spectrum disorder (FASD) is the umbrella term used to describe the various developmental disorders associated with prenatal alcohol exposure (Chudley et al., 2005). FASD affects 0.3–10 individuals per 1000 live births (May and Gossage, 2001), and is the leading known cause of mental retardation (Abel and Sokol, 1986). Children with FASD show widespread structural brain abnormalities (Archibald et al., 2001; Fryer et al., 2009; Lebel et al., 2008a; Mattson et al., 1996), and may have various cognitive and behavioural impairments including motor delays, and deficits of attention, executive functioning, language, learning and memory (Jacobson and Jacobson, 2002; Kalberg et al., 2006; Mukherjee et al., 2006; Spadoni et al., 2007). Despite an array of intellectual impairments, individuals with FASD generally have greater difficulty with arithmetic than with other cognitive domains (Howell et al., 2006; Kopera-Frye et al., 1996; Rasmussen and Bisanz, 2009) and mathematical ability is more strongly correlated with amount of prenatal alcohol exposure than are other academic skills (Goldschmidt et al., 1996; Streissguth et al., 1994).

In healthy individuals, mathematical tasks activate frontal, precingulate and parietal gray matter areas, in particular the intraparietal sulcus (Ansari

and Dhital, 2006; Chochon et al., 1999; Dehaene et al., 1999, 2004; Eger et al., 2003; Kawashima et al., 2004). Lesion studies describe patients with left intraparietal strokes who subsequently developed acalculia (Ashkenazi et al., 2008; Takayama et al., 1994), and structural imaging has demonstrated reduced parietal gray matter (Isaacs et al., 2001; Rotzer et al., 2008) and abnormal intraparietal morphology (Molko et al., 2003) in individuals with calculation deficits. These studies show a clear relationship between intraparietal gray matter and mathematics; however, it is crucial to also understand the underlying brain connectivity.

Diffusion tensor imaging (DTI) is a powerful technique (Basser et al., 1994) that is excellent for studying white matter microstructure. DTI yields a quantitative diffusion parameter, fractional anisotropy (FA), that is related to axonal packing and myelination (Beaulieu, 2002). DTI has been used to study brain abnormalities in children with FASD (Fryer et al., 2009; Lebel et al., 2008a; Li et al., 2009; Sowell et al., 2008a; Wozniak et al., 2006, 2009), but only two studies reported correlations between cognitive tests and brain structure. Sowell et al. (2008a) observed a relationship between white matter integrity in the splenium of the corpus callosum and scores on a visuomotor integration task. Wozniak et al. (2009) observed a significant positive correlation between working memory and FA in the genu of the corpus callosum, and negative correlations between splenium MD and both perceptual organization and working memory. Another study reported correlations between FA and both intelligence and processing speed across a group of healthy controls and FASD youth, but these correlations were not significant in the FASD group alone (Ma et al., 2005), although the small sample size ( $n=9$ ) limits the power to detect correlations within the FASD group alone.

Two previous DTI studies correlated FA with mathematical abilities in children, one in a typically-developing cohort (van Eimeren et al., 2008) and one in a rare genetic disorder — velocardiofacial syndrome (Barnea-Goraly et al., 2005a). Both studies reported left parietal correlations; the former also implicated the left inferior temporal area. However, correlations between brain structure and mathematical abilities have never been reported in FASD.

Given the severity of mathematical deficits in FASD, there is likely to be a relationship between these difficulties and the underlying brain structure. The purpose of this study was to use DTI to examine the relationship between mathematical ability and white matter anisotropy in 21 children with FASD.

## 10.2 Methods

### 10.2.1 Subjects

Subjects were 21 children aged 5–13 years (mean  $\pm$  st.dev:  $9.2 \pm 2.2$  years, 12 males/9 females, 16 right-handed/5 left-handed) diagnosed with a condition falling under the umbrella term FASD, recruited through a hospital FASD clinic. Child assent and parent/guardian consent were obtained from all participants in the study. These subjects were a subset of the 24 children (the other three did not have math scores) examined in our previous study focusing on group comparisons of DTI parameters between children with FASD and a healthy cohort (Lebel et al., 2008a). All children had confirmed prenatal alcohol exposure validated by a social worker (prior to entry into the clinic) based on extensive review of birth records, Child and Youth Services documentation, and/or parental interview. All participants had a medical diagnosis of an alcohol-related disorder falling under the umbrella term FASD, made by a multidisciplinary team using the Diagnostic Guide for Fetal Alcohol Spectrum Disorders: The 4-Digit Diagnostic Code (Astley, 2004). The 4-Digit Diagnostic Code ranks diagnostic information in the areas of growth deficiency, facial phenotype, brain dysfunction, and alcohol use. The magnitude of expression of each diagnostic feature is ranked independently on a 4-point Likert scale, with 1 reflecting complete absence of the fetal alcohol syndrome (FAS) feature and 4 reflecting a strong “classic” presence of the FAS feature. To meet the criteria for FASD, all children must have a brain code of 2 or higher as well as confirmed alcohol exposure, as indicated by Alcohol Use scores of 3 (some risk) or 4 (high risk).

Table 10.1 presents subject characteristics for each participant. Two subjects were diagnosed with FAS, one with partial FAS, 10 had neurobehavioural

Table 10.1: Subject characteristics for each FASD child (ordered by Woodcock-Johnson III Quantitative Concepts age-standardized math score).

Subject	Age (years)	Dominant Hand	Sex	4-Digit Code <sup>a</sup>	Diagnosis <sup>b</sup>	Math Score
1	10.3	R	M	1124	NBD:AE	62
2	11.8	R	M	4433	FAS	62
3	8.4	R	F	1223	NBD:AE	70
4	8.2	R	F	1124	NBD:AE	72
5	9.3	L	M	1124	NBD:AE	73
6	6.7	R	M	1123	NBD:AE	74
7	11.0	R	F	1134	SE:AE	75
8	13.2	L	M	1233	SE:AE	75
9	11.2	L	F	3234	SP/SE:AE	79
10	8.8	R	M	1123	NBD:AE	82
11	10.6	R	F	1133	SE:AE	84
12	12.2	R	M	1134	SE:AE	88
13	7.3	R	F	4334	Partial FAS	90
14	7.1	R	M	1123	NBD:AE	100
15	9.7	R	M	4234	SP/SE:AE	100
16	9.7	R	F	4234	SP/SE:AE	101
17	11.8	R	F	2-23 <sup>c</sup>	NBD:AE	103
18	6.1	L	M	1323	SP/NBD:AE	105
19	5.7	R	M	1223	NBD:AE	106
20	9.2	L	M	1124	NBD:AE	113
21	5.4	R	F	- <sup>d</sup>	FAS	115

<sup>a</sup> The first digit represents growth deficiency, the second facial phenotype, third brain dysfunction and the fourth indicates prenatal alcohol exposure. A score of 1 indicates complete absence of the classic FAS feature, while 4 indicates its strong presence.

<sup>b</sup> NBD-AE: Neurobehavioural disorder — alcohol exposed, FAS: Fetal alcohol syndrome, SE-AE: static encephalopathy — alcohol exposed, SP: Sentinel physical findings.

<sup>c</sup> This subject was not assessed a facial score due to cleft palate.

<sup>d</sup> Code not available due to inaccessible file.

disorder-alcohol exposed, 4 had static encephalopathy-alcohol exposed, 3 had sentinel physical findings/static encephalopathy-alcohol exposed, and one had sentinel physical findings/neurobehavioural disorder-alcohol exposed. Specific information about quantity and timing of alcohol use during pregnancy was not available for most subjects; however, all children had confirmed significant alcohol exposure, as shown in Table 10.1. Exposure to other drugs in utero was reported for 13 subjects; substances included tobacco, marijuana and cocaine. Although this is a potential concern, the 13 subjects with other exposures were spread across the range of math scores; the children with the top 5 math scores and 5 of the 6 children with the lowest math scores all had exposure to other drugs. Gestational age of the 17 children for whom this information was available ranged from 36–41 weeks; 3 children were born preterm at 36–37 weeks. Birth weight and head circumference were within the normal range for most children: 8 children had birth weights below the 25<sup>th</sup> percentile and 4 were below the 10<sup>th</sup> percentile, but all head circumferences were above the 25<sup>th</sup> percentile, according to growth charts (Astley, 2004). Of the 17 children with recorded Apgar scores, one minute scores ranged from 4–9, with 12 children within the normal range of 7–10. At 5 minutes, all children were within the normal range.

### **10.2.2 Cognitive Assessment**

A battery of cognitive assessments was performed on each child including the Woodcock Johnson III (WJ-III) Tests of Achievement-Quantitative Concepts subtest to assess mathematical ability (listed in Table 10.1 per subject). For the full battery and mean scores for other cognitive tests, please refer to our previous study (Lebel et al., 2008a). The Quantitative Concepts subtest involves knowledge of math concepts, symbols, and vocabulary. Initial items involve counting, as well as identifying numbers, shapes, sequences, and identification of math operations and signs. Later items involve figuring out number patterns and identifying missing numbers in a series. Test scores were normalized based on participant age, and standardized Quantitative Concepts scores were compared to the typical mean score of 100 using a one sample t-test with

a significance level of 0.05.

### 10.2.3 Image Acquisition

All data was acquired on the same 1.5 T Siemens Sonata MRI scanner using identical methods. Total acquisition time was approximately 25 minutes and included DTI, and anatomical T1-weighted, T2-weighted and FLAIR imaging. DTI was acquired using a dual spin-echo, single shot echo-planar imaging sequence with the following parameters: 40 3 mm thick axial-oblique slices with no inter-slice gap, TR=6400 ms, TE=88 ms, 6 non-collinear diffusion sensitizing gradient directions with  $b=1000$  s/mm<sup>2</sup>, 8 averages, field-of-view 220×220 mm<sup>2</sup>, matrix of 128×128 zero-filled to 256×256, 75% phase partial Fourier, acquisition time 6:06 min. In the non diffusion-weighted ( $b=0$  s/mm<sup>2</sup>) images, SNR was quite high with a range of 67–88 (mean = 79) and thus yielded excellent quality FA maps (Figure 10.1). High resolution (1×1×1 mm<sup>3</sup>) T1-weighted images were acquired using MPRAGE with TE=4.38 ms, TR=1870 ms, TI=1100 ms, and a scan time of 4:29 minutes. Head motion was minimized using ear pads, but not all children were able to complete the entire 25 minute protocol. Therefore, T1-weighted images were obtained in 18 of the 21 children, while conventional T2-weighted and FLAIR scans were obtained for 17 children, and were used to ensure that there were no frank lesions.

### 10.2.4 Voxel-Based Image Analysis

Non diffusion weighted images ( $b=0$  s/mm<sup>2</sup>) were normalized to the ICBM EPI template using non-affine transformations in statistical parametric mapping software (SPM5, Wellcome Trust Centre for Neuroimaging, London, UK). The same transformation parameters were then used to normalize each individual's fractional anisotropy (FA) map to MNI space, and normalized FA maps were smoothed using a 4 mm kernel. Voxel-based correlation of FA with age-standardized math scores was performed in SPM5. Because FA values increase with age, age was controlled in the analysis by including it in the regression model in SPM5. In order to minimize inter-subject registration errors and to

avoid inclusion of voxels associated with cortical gray matter or cerebrospinal fluid in any one individual, only voxels with  $FA \geq 0.2$  (i.e. white matter) in all 21 subjects were included for further analysis. Due to the FA thresholding, many voxels are excluded from analysis and a false discovery rate correction across the brain is not appropriate. Monte Carlo simulations were conducted in AlphaSim (<http://afni.nimh.nih.gov/afni/doc/manual/AlphaSim>) to determine the probability that clusters of various sizes would randomly occur. These simulations showed that a p-value threshold of 0.05 per voxel and a cluster size threshold of 81 contiguous voxels produced an overall alpha value of 0.048. Therefore, these thresholds were used with an F-test to determine clusters with significant correlations between FA values and math scores. Clusters were overlaid on each individual subject's FA map and visualized in a movie loop to ensure adequate registration and that each cluster was within the same structure(s) in each individual.

A separate analysis was conducted on the 16 right-handed subjects using the exact same methods. Monte Carlo simulations for this data showed that a p-value threshold of 0.05 and a cluster threshold of 101 voxels gave an overall alpha value of 0.05.

### **10.2.5 Diffusivities**

To give an indication of the primary cause of any correlations between FA and math scores, the parallel and perpendicular diffusivities ( $\lambda_{\parallel}$  and  $\lambda_{\perp}$ ) were measured. Significant clusters from normalized space were warped back to native space for each individual using the inverse of the original template transformation parameters. FA, parallel and perpendicular diffusivities were averaged across each cluster for each individual and correlated with standardized math scores, controlling for age.

### **10.2.6 Tractography**

DTI tractography was used to evaluate which white matter tracts passed through the significant FA-math ability clusters. Inverse transformation parameters were calculated from the original non diffusion weighted image trans-

Table 10.2: Location and MNI coordinates are given for each cluster with significant correlations between fractional anisotropy (FA) and Woodcock-Johnson III Quantitative Concepts math scores. Correlation R value and significance shown is from correlation of FA with math scores, controlling for age, in the most correlated voxel of each cluster.

Cluster Size (number of voxels)	Anatomical Location	MNI Coordinates of Most Correlated Voxel	Correlation	Significance
186	Left cerebellum	12, -34, -42	0.74	<0.001
81	Left parietal lobe	-36, -16, 26	0.69	<0.001
114	Upper left parietal lobe	-22, -28, 50	0.64	<0.001
110	Brainstem (bilateral)	-6, -24, -20	-0.69	<0.001

formations to the EPI template. These parameters were used to transform significant math ability-FA clusters from MNI space to native space for each individual. Once in native space, each cluster was used separately as a seeding region for tractography. FA thresholds were set to 0.25 to initiate and continue tracking, while the angle threshold was set to  $60^\circ$ . Deterministic streamline tractography was performed in Matlab using code modified from ExploreDTI (A. Leemans, Utrecht, Netherlands). All tracts produced by each seeding region were retained (i.e. no target or exclusion regions were used).

## 10.3 Results

### 10.3.1 Quantitative Concepts Scores

The children with FASD in this study scored significantly below average (average normalized score in healthy children is  $100 \pm 15$ ) on the Woodcock-Johnson III (WJ-III) Tests of Achievement — Quantitative Concepts subtest of mathematical ability (mean  $\pm$  standard deviation =  $87 \pm 17$ ,  $p=0.002$ ). See Table 10.1 for individual scores.

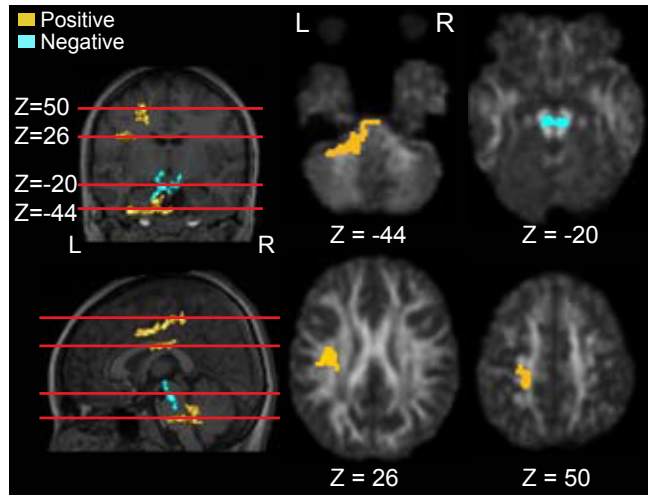


Figure 10.1: Locations of the four significantly correlated clusters are shown in yellow (positive correlations) and cyan (negative correlation). On the left, each cluster is shown with a backdrop of a coronal and a sagittal slice (T1-weighted images). On the right, one slice through each cluster is shown, with the significantly correlated voxels in that slice overlaid onto an individual FA map. The location of each axial slice is shown as a red line through the coronal and sagittal slices. MNI coordinates of each slice are given. All images shown are normalized images from a 10 year old girl with FASD who scored 75 on the WJ Quantitative Concepts test.

### 10.3.2 Correlations of FA with Math Scores

Voxel-based analysis revealed four clusters with significant correlations between FA and standardized Quantitative Concepts scores, after controlling for age (see Table 10.2 and Figure 10.1). Of these four clusters, three in the left hemisphere showed positive correlations between FA and math scores and one spanning both hemispheres was negatively correlated. The largest positively correlated cluster contained 186 voxels and was located in the left anterior cerebellum. The two other positively correlated clusters were located in the left parietal lobe, one in the lower parietal area (83 voxels), and the other more superiorly (114 voxels); both parietal clusters were close to the left intraparietal sulcus. The negatively correlated cluster was located in the brainstem bilaterally (110 voxels). Mean FA values in each cluster (averaged over all voxels in the cluster per individual) ranged from 0.31–0.51 for the cerebellar cluster, 0.38–0.54 for the brainstem, 0.29–0.56 for the lower parietal cluster, and 0.33–0.48 for the upper parietal cluster. The location of the most cor-

related voxel in each cluster is shown in Figure 10.2, along with plots of FA versus math score (both corrected for age) for that voxel. Correlations between math scores and FA were very high for these voxels, with R values of 0.74, 0.69, 0.64, and -0.69 ( $p < 0.001$ ).

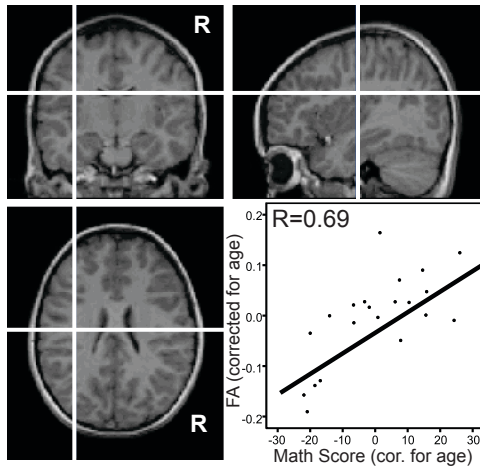
### 10.3.3 Right-handed Subjects Only

Excluding the five left-handed subjects, a repeat of the voxel-based analysis on right-handed subjects only ( $n=16$ ) revealed 5 significantly correlated clusters. Three clusters were in the same regions as the significant clusters from the analysis on all 21 subjects: a positively-correlated left cerebellum cluster (290 voxels), a positively-correlated lower left parietal cluster (124 voxels), and a positively-correlated upper left parietal cluster (142 voxels). Two additional clusters were observed: a negatively-correlated left occipital cluster (154 voxels) and a positively correlated left splenium cluster (322 voxels).

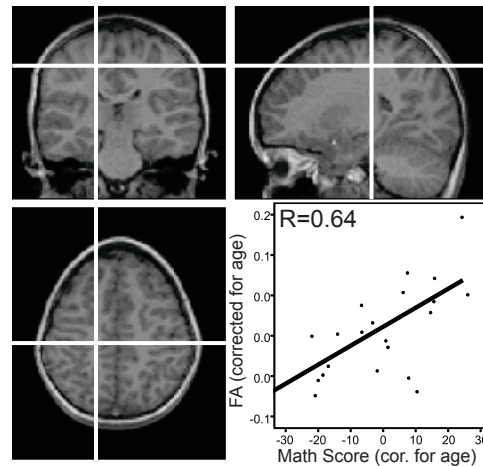
### 10.3.4 Diffusivities

Average FA values, as measured across the entire cluster in native space for each individual, were strongly and significantly correlated with standardized math scores (after age correction), as expected. Correlations of FA, parallel diffusivity ( $\lambda_{\parallel}$ ), and perpendicular diffusivity ( $\lambda_{\perp}$ ) with math scores (both age-corrected) are shown in Figure 10.3. Note that these correlations are slightly different from those shown in Figure 10.2, since FA is not taken only from the most significantly correlated voxel (as it was for Figure 10.2), but has been averaged across the entire cluster. For the lower and upper left parietal clusters, parallel diffusivity ( $\lambda_{\parallel}$ ) was also correlated with math scores ( $p=0.001$ ,  $<0.001$ ;  $R=0.68$ ,  $0.75$ , respectively). Perpendicular diffusivity in the parietal clusters was not significantly correlated with math scores. In contrast, perpendicular diffusivity was the primary cause of FA-math score correlations in the cerebellum and brainstem clusters ( $p=0.005$ ,  $R=-0.58$ ;  $p=0.002$ ,  $R=0.64$ , respectively), while parallel diffusivity in these regions was not significantly correlated with math scores.

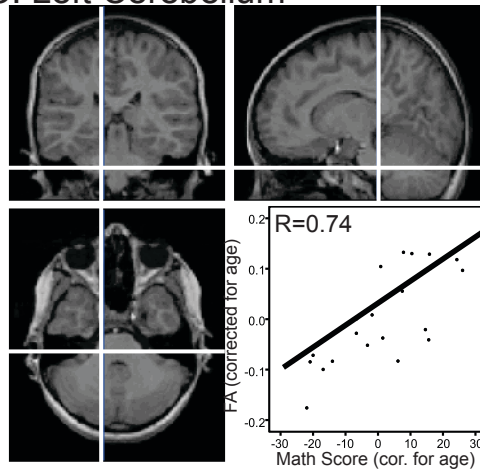
A: Lower Left Parietal Lobe



B: Upper Left Parietal Lobe



C: Left Cerebellum



D: Bilateral Brainstem

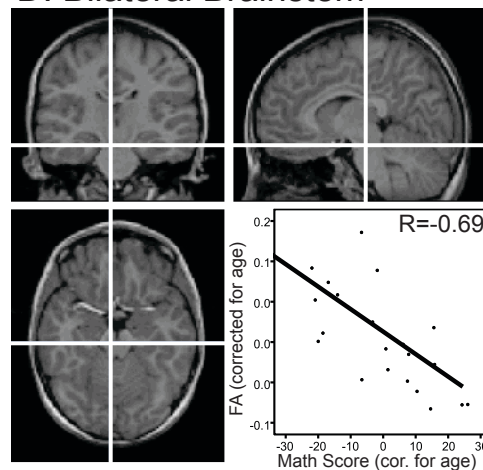


Figure 10.2: Math scores were highly correlated with fractional anisotropy (FA) in four clusters: two in the left parietal lobe (A, B), one in the left cerebellum (C), and one in the bilateral brainstem (D). The most correlated voxel for each cluster is shown with a plot of FA vs. standardized math score (Woodcock Johnson Quantitative Concepts), after controlling for age (residuals of age correlations are shown). For all four correlations,  $p < 0.001$ .

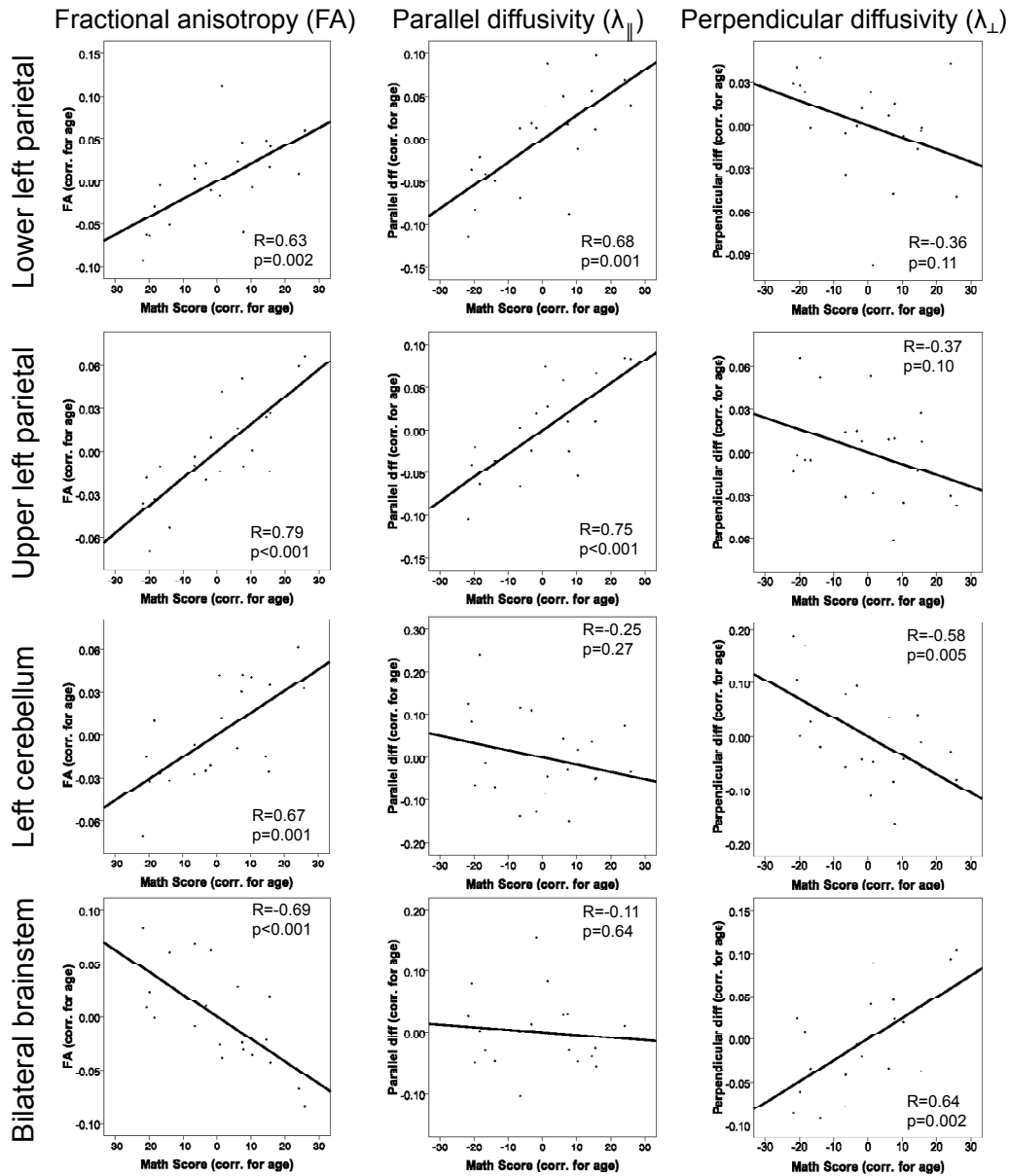


Figure 10.3: Correlations of fractional anisotropy (FA) and parallel and perpendicular diffusivities with math scores (all corrected for age) are shown for all voxels averaged over each of the four significant clusters. For the cerebellum and brainstem clusters, changes of perpendicular diffusivity were the primary cause of the FA-math correlations, while for the two left parietal clusters, it was parallel diffusivity driving the FA-math score correlations.

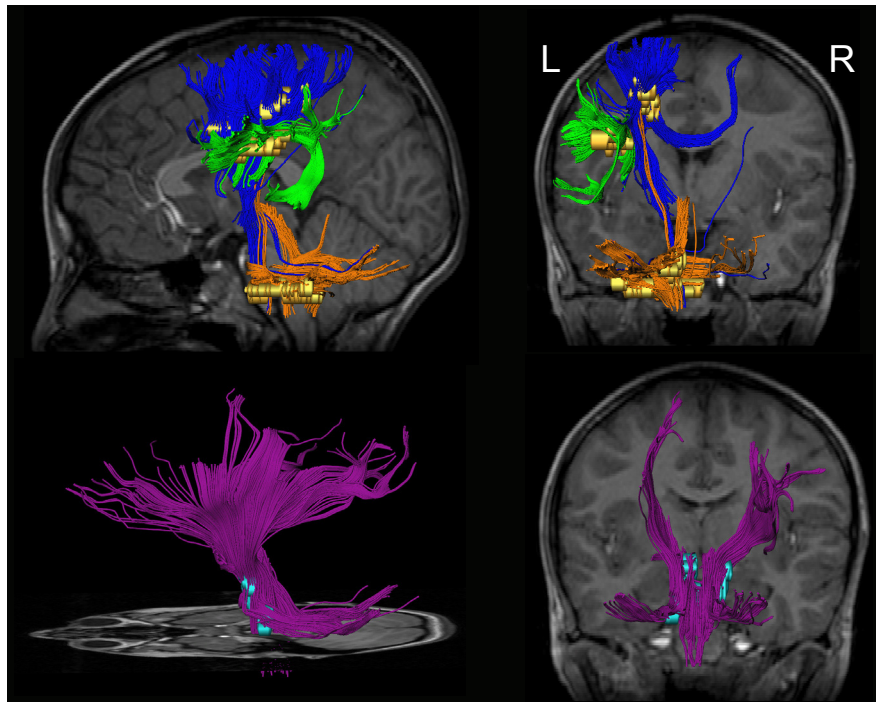


Figure 10.4: White matter tracts passing through significant fractional anisotropy (FA)-math score clusters are shown. Each of the four clusters with significant correlations between FA and Quantitative Concepts math scores was used as a seeding region for tractography. All tracts produced from each cluster in a 9-year-old boy with fetal alcohol spectrum disorder and a math score of 100 are shown above in native space. Three positive clusters (top) were observed: an upper left parietal cluster (tracts in blue) that produced corticospinal tracts and part of the corpus callosum; a lower parietal cluster (tracts in green) that contained the superior longitudinal fasciculus; and a cerebellar cluster (tracts in orange) whose tracts are part of the middle cerebellar peduncle. The negative cluster (bottom) produced projection fibres (tracts in purple).

### 10.3.5 White Matter Tracts Passing Through Clusters

Diffusion tractography was used to determine which white matter tracts were contained within each of the four significant clusters (see Figure 10.4). The cerebellar cluster produced tracts from the middle cerebellar peduncle, a white matter tract connecting the cerebellum and the pontine nuclei. Although the entire cerebellar cluster was located in the left hemisphere, middle cerebellar peduncle tracts cross the midline so fibre tracking yielded streamlines in both hemispheres. Using the lower left parietal cluster as a seeding region gave tracts belonging to the left superior longitudinal fasciculus, a frontal-parietal-temporal connection. The upper left parietal cluster revealed tracts belonging to both the body of the corpus callosum and the left corticospinal tracts. The negatively correlated cluster in the brainstem produced projection fibres bilaterally, including the anterior and posterior limbs of the internal capsule, as well as some cerebellar tracts. Tractography results were consistent from subject to subject, with each cluster demonstrating the same major white matter pathway or pathways in all FASD individuals.

## 10.4 Discussion

Diffusion tensor imaging has demonstrated correlations between mathematics scores and fractional anisotropy (FA) in white matter of the left parietal lobe, left cerebellum, and bilateral brainstem in children with FASD for the first time. Brain structure in the left parietal region seems to be consistently involved in mathematics across both healthy and abnormal populations, as it has been previously implicated in both healthy individuals (van Eimeren et al., 2008) and those with a rare genetic disorder (Barnea-Goraly et al., 2005a). The observed positive correlations in the cerebellar region and the negative correlations in the brainstem are new findings that may or may not be specific to children with FASD.

Parietal gray matter bilaterally has been consistently implicated in mathematical abilities by both functional (Ansari and Dhital, 2006; Chochon et al., 1999; Dehaene et al., 1999; Eger et al., 2003; Kucian et al., 2006; Molko et al.,

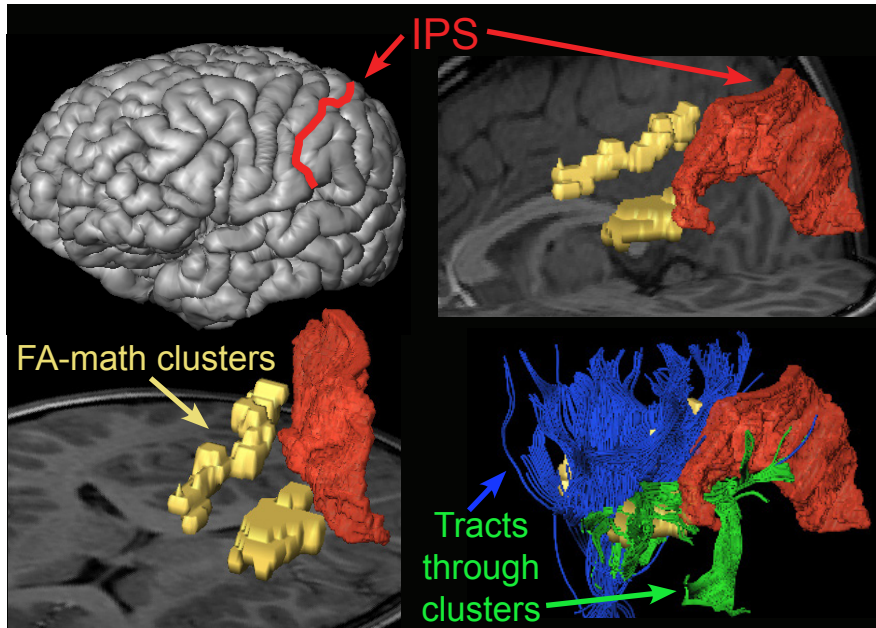


Figure 10.5: Parietal fractional anisotropy (FA)-math clusters are shown in relation to the left intraparietal sulcus. The two left parietal clusters (yellow) that showed significant correlations between FA and mathematics scores are in very close proximity to the left intraparietal sulcus shown in red. The tracts passing through each cluster are also shown: the left corticospinal tracts and part of the corpus callosum pass through the upper parietal cluster (tracts in blue), while the superior longitudinal fasciculus (tracts in green) passes through the lower parietal cluster. All structures shown are in native space in a 9-year-old boy with fetal alcohol spectrum disorder (math score = 100).

2003; Price et al., 2007) and structural (Isaacs et al., 2001; Molko et al., 2003; Rotzer et al., 2008) imaging studies. The entire parietal area is important for mathematical processing, but the horizontal segment of the intraparietal sulcus (IPS), in particular, seems to be specific to the number domain. The horizontal IPS, on both the left and right sides, is activated by the great majority of functional imaging studies of mathematics and number processing, and shows increased activation with more quantitative tasks (Dehaene et al., 2003). It is also the left horizontal IPS region that has been implicated in lesion studies showing that strokes there are associated with subsequent acalculia (Ashkenazi et al., 2008; Takayama et al., 1994). While the underlying white matter has not been as extensively examined, two DTI studies, one in healthy children and one in children with the genetic-based velocardiofacial syndrome, showed correlations between left parietal white matter anisotropy and math ability (Barnea-Goraly et al., 2005a; van Eimeren et al., 2008). Here we show that left parietal white matter microstructure directly underlying the horizontal IPS is related to mathematical skills in children with FASD. Figure 10.5 demonstrates the proximity of the two left parietal clusters with significant FA-math correlations to the left horizontal IPS. Both clusters are adjacent to the horizontal IPS, and the tracts passing through them surround the sulcus. Clearly, there is consistent involvement of the intraparietal region, both gray matter and white matter, in mathematical processing tasks. This study provides further evidence that this area is crucial to mathematical tasks across both typically-developing and abnormal populations, given the previously observed DTI correlations in healthy children and those with a genetic condition. Interestingly, however, we (and the other two DTI math studies) find that only the left white matter is correlated with mathematical ability, in contrast to the bilateral activation of the IPS region shown by the majority of functional imaging studies.

We identified using tractography which specific white matter connections are contained in these parietal clusters, namely the superior longitudinal fasciculus, corticospinal tracts, and body of the corpus callosum (see Figures 10.4 and 10.5). The superior longitudinal fasciculus, the tract containing the

lower left parietal cluster observed in this study, is a frontal-parietal-temporal connection known to be involved in language and intelligence tasks (Marslen-Wilson and Tyler, 2007). FA in the superior longitudinal fasciculus has been correlated with IQ (Schmithorst et al., 2005), language (Ashtari et al., 2007), and processing speed (Turken et al., 2008); here we show that a portion of it is also correlated with math ability in children with FASD. The second, upper parietal cluster contained left corticospinal tracts and part of the body of the corpus callosum. This region has been previously implicated in DTI studies of reading ability in children (Beaulieu et al., 2005; Deutsch et al., 2005; Niogi and McCandliss, 2006) and adults (Klingberg et al., 2000), suggesting that it is an important region for a variety of cognitive tasks. Structurally, the parietal brain regions are known to be abnormal in children with FASD, having thicker cortices (Sowell et al., 2008b), smaller volumes (Archibald et al., 2001), and abnormal diffusion parameters (Fryer et al., 2009; Lebel et al., 2008a) compared to typically-developing children, and previous studies have speculated that abnormal parietal function in children with FASD may lead to their mathematical deficits (Riikonen et al., 1999).

A third positively correlated cluster was observed in the left anterior region of the cerebellum, suggesting that this area is also related to math ability in FASD. The fibre tracts that contain this cluster belong to the middle cerebellar peduncle, the largest of the cerebellar peduncles, and connect the cerebellum with the pontine nuclei. The cerebellum is one of the regions most affected by prenatal alcohol exposure (Archibald et al., 2001; Jones and Smith, 1973; Spadoni et al., 2007), particularly the anterior portion (Sowell et al., 1996). Although the cerebellum is traditionally thought to regulate motor coordination and balance, recent studies have suggested it also plays a role in higher cognition. Cerebellar volume correlates positively with intelligence measures in healthy young adults (Andreasen et al., 1993) and preterm adolescents (Parker et al., 2008), cerebellar abnormalities are associated with a variety of intellectual deficits (Steinlin, 2008), and the cerebellum is often activated during cognitive tasks (Baillieux et al., 2008). The cerebellum plays an important role in learning processes, and it is hypothesized that the earlier

abnormalities are present, the more severe the deficits (Steinlin, 2008). This region was not observed to correlate with math ability in either of the previous DTI math studies on healthy controls and velocardiofacial syndrome, and therefore may be unique to children with FASD. Further studies comparing diffusion parameter-math score correlations between individuals with FASD and control subjects may help address this question.

One negatively correlated cluster was observed in the brainstem, located on both sides of the midline. This is in contrast to the three positively correlated clusters, which were all found in the left hemisphere. Tracts from this cluster were primarily projection fibres, including both the anterior and posterior limbs of the internal capsule (see Figure 10.4). Although the observed negative correlations may seem counter-intuitive, negative relationships have been observed previously between cognitive scores and brain structure, in healthy children (Dougherty et al., 2007), dyslexic adults (Frye et al., 2008), and adults with Williams Syndrome, a neurodevelopment disorder (Hoeft et al., 2007). Negative correlations may also be related to changes in crossing fibre areas. The standard tensor model attributes artificially low FA values to areas in which two or more fibre bundles intersect. Therefore, degradation of one of the fibre bundles in the crossing area would actually lead to higher FA values in that region, and it is possible that negative correlations between FA and math scores may actually still represent lower white matter integrity in that region of children who are poorer at math.

Analysis of the parallel and perpendicular diffusivities gives insight into the cause of the FA-math score correlations observed (see Figure 10.3). For the two left parietal clusters, parallel diffusivity was significantly positively correlated with math scores, after correcting for age, but perpendicular diffusivity was not. Parallel diffusivity is often associated with axonal integrity, and axonal damage has been linked to decreases of parallel diffusivity (Song et al., 2003). In the cerebellar and brainstem clusters, the FA-math score correlations were driven by the perpendicular diffusivity, while the parallel diffusivity-math score correlations were not significant. Perpendicular diffusivity in the cerebellar cluster was negatively correlated with math scores, while

it was positively correlated in the brainstem cluster. Perpendicular diffusivity is generally associated with myelination and axonal packing, and studies have shown that demyelination and remyelination lead to increases and decreases of perpendicular diffusivity, respectively (Song et al., 2002, 2005).

Although both functional and structural brain lateralization exist for language tasks, lateralization and handedness in mathematics have been less well studied. Although our left-handed subjects were spread across the range of math scores, grouping both left- and right-handed subjects together for analysis is a potential concern. To address this concern, a separate analysis was conducted in exactly the same way on the 16 right-handed subjects only. This analysis revealed 5 significantly-correlated clusters, three of which corresponded to the left cerebellar and two left parietal clusters observed within the whole group. These results should increase confidence in those three particular clusters, since those results were consistent whether or not left-handers were included. The discrepancies between the results with right-handers only versus the entire group, specifically the absence of the brainstem cluster in the right-handers, and the appearance of two other clusters in the left occipital area and left splenium, may be due to handedness and lateralization differences, or may simply be caused by a slightly different subject group. Due to the small number ( $n=5$ ) of left-handers, a left-hander only analysis was not feasible. Nonetheless, there were strong similarities between the right-hander only results and the entire group, suggesting robust correlations between FA and math scores in the parietal and cerebellar regions.

Although gender differences have not been examined by most brain imaging studies of mathematical abilities (Ansari and Dhital, 2006; Barnea-Goraly et al., 2005a; Dehaene et al., 1999; Eger et al., 2003; van Eimeren et al., 2008), they are a potential concern. With our relatively small sample size, it was not feasible to further subdivide our group into males ( $n=12$ ) and females ( $n=9$ ) for separate analyses. Males and females are plotted separately in Figure 10.3, and it appears as though they both follow the same relationships between diffusion parameters and math scores. Furthermore, including gender as an additional covariate for correlations between math scores and diffusion

parameters averaged across each cluster produced exactly the same results as not including gender, suggesting that gender differences are minimal. Future studies with larger sample sizes will be better able to investigate gender (and handedness) differences and may help determine the consistency of the clusters and their dependence on these variables.

Alcohol exposure during fetal development affects secondary calcium signaling pathways (Kumada et al., 2007), alters glutamate NMDA receptor function (Hughes et al., 1998), increases apoptotic neurodegeneration (Ikonomidou et al., 2001), and impairs neuronal proliferation and migration (Miller, 1986). These disruptions to the developing nervous system can result in abnormal cerebral and axonal growth (Ma et al., 2003; Mennerick and Zorumski, 2000; Olney, 2004), leading to brain malformations caused by neuronal and glial migration errors (Clarren et al., 1978; Jones and Smith, 1973; Peiffer et al., 1979). Clearly, the many cognitive deficits observed in FASD (Jacobson and Jacobson, 2002; Mukherjee et al., 2006) are related to the widespread structural brain abnormalities (Fryer et al., 2009; Lebel et al., 2008a; Li et al., 2009; Sowell et al., 2008a; Wozniak et al., 2006, 2009), and here DTI measures of tissue microstructure have yielded four select white matter regions related to math ability.

## 10.5 Conclusion

Future studies combining DTI with other techniques such as functional MRI or shape and thickness measurements of various brain structures in children with FASD would be useful for linking mathematical abilities with functional, cortical, and underlying white matter abnormalities. Ultimately, a better understanding of the brain structures related to cognitive skills such as mathematics may lead to earlier diagnoses and more effective treatment of such difficulties, not only in children with FASD, but also in the wider population.

# Chapter 11

## Ongoing Projects

### 11.1 Brain White Matter Changes Across the Lifespan<sup>1</sup>

#### 11.1.1 Introduction

Lifespan studies of the normal human brain provide the necessary link between the developmental processes of childhood and the degenerative processes of old age. Postmortem lifespan studies of the human brain demonstrate a variety of structural changes, including overall brain weight (Dekaban, 1978), myelination (Benes et al., 1994; Yakovlev and Lecours, 1967), and synaptic density (Huttenlocher, 1979; Huttenlocher and de Courten, 1987). Imaging studies have shown changes in brain tissue volumes (Hasan et al., 2007) and cortical thickness (Sowell et al., 2003). In general, these studies show rapid development during infancy and childhood, slower rates of development during adolescence and young adulthood, then an eventual reversal of the developmental processes at some point during adulthood and degradation in later life.

Diffusion tensor imaging (DTI) gives measures of tissue microstructure and DTI studies of healthy development show robust increases of fractional anisotropy (FA) and decreases of mean diffusivity (MD) during childhood and adolescence in most brain white matter regions (Barnea-Goraly et al., 2005b; Lebel et al., 2008b; Schmithorst et al., 2002). DTI studies of healthy aging

---

<sup>1</sup>A version of this section has been published. C. Lebel, M. Gee, R. Camicioli, M. Wieler, W. Martin, C. Beaulieu, 2010. Diffusion Tensor Imaging of Brain White Matter Changes Across the Lifespan, Abstract #112. Proceedings of the International Society for Magnetic Resonance in Medicine, 18th Annual Meeting, Stockholm, Sweden.

demonstrate the opposite trends, with FA decreasing and MD increasing during old age, again in most white matter areas (Abe et al., 2002; Hsu et al., 2010; Ota et al., 2006; Pfefferbaum et al., 2000). However, only a handful of DTI studies have examined microstructural white matter changes across the lifespan. Three very recent DTI studies have examined multiple brain white matter regions across a wide age range: one looked at 119 subjects aged 7-68 years using tractography of the inferior longitudinal and fronto-occipital, arcuate, and uncinate fasciculi, the corticospinal tract, somatosensory pathways, and eight subdivisions of the corpus callosum (Hasan et al., 2010); another examined 430 subjects aged 8-85 using tract-based spatial statistics (TBSS) (Westlye et al., 2009), and the third analyzed 831 subjects aged 11-90 years also using TBSS (Kochunov et al., 2010). These studies all demonstrated U-shaped trajectories and regional variation in the timing of development, with increasing FA and decreasing MD during childhood and adolescence, followed by decreasing FA and increasing MD later in life. It is important to note that none of these previous studies, nor our current one presented here, analyze infants or very young children, and therefore miss a period of very rapid brain development. Nonetheless, these studies provide valuable information about the regional variation of age-related brain changes across a wide age range. The previous studies used a quadratic fit to model age-related changes (Hasan et al., 2010; Kochunov et al., 2010; Westlye et al., 2009), although one study also used locally weighted polynomial regression (Westlye et al., 2009). While quadratic equations provide a reasonable fit in many cases, they are not ideal because they restrict the slopes on either side of the peak or minimum in the curve to be the same. This is not desirable because the initial slope reflects developmental processes, while the slope after the peak/minimum reflects degradation and there is no particular reason why these two processes should occur at the same rate. Therefore, less restrictive fits, such as a Poisson curve, are beneficial because they allow differential slopes, while still maintaining a small number of estimation parameters. DTI tractography is an excellent way of studying white matter changes because it provides robust estimates of diffusion parameters across the entire tract, does not rely on spatial normalization,

and is more reliable than region-of-interest analysis (Kanaan et al., 2006). The goal of this study was to use DTI tractography to provide a comprehensive analysis of age-related microstructural changes in brain white matter in a large number of healthy subjects (n=403) across a very wide age range (5-83 years).

### **11.1.2 Methods**

#### **Subjects**

In total, 403 healthy volunteers (195 males/208 females) aged 5 to 83 years (mean age  $\pm$  standard deviation:  $31.3 \pm 21.5$ , 374 right-handed/26 left-handed/3 no preference) participated in this study. All subjects had no self-reported history of neurological or psychiatric disease or brain injury. All volunteers gave informed consent; both child assent and parent/guardian consent was obtained for volunteers under 18 years. Two previous studies have been published looking at subsets of these subjects: one examined development of white matter tracts from age 5–30 in 202 of the same subjects using similar methods (Lebel et al. 2008b and Chapter 5 of this thesis); another study used manual tractography to examine development of corpus callosum subdivision in 315 of these subjects, aged 5–59 years (Lebel et al. 2010 and Chapter 7). This study is distinct in that it includes a larger number of subjects across a much wider age range, and examines all major white matter fibre bundles across the brain.

#### **Image Acquisition**

All data was acquired on the exact same 1.5 T Siemens Sonata MRI scanner using identical methods. Total acquisition time was approximately 25 minutes and included anatomical imaging and DTI. The DTI acquisition protocol used a dual spin-echo, single shot echo-planar imaging sequence with the following parameters: 35 or 40 3 mm thick slices with no inter-slice gap, TR=6400 ms, TE=88 ms, 6 non-collinear diffusion sensitizing gradient directions with  $b=1000$  s/mm<sup>2</sup>, 8 averages, field-of-view 220×220 mm<sup>2</sup>, matrix of 128×128 zero-filled to 256×256, with 75% phase partial Fourier. Total DTI acquisition time was approximately 6 minutes. Most data was acquired with 40 slices,

as this is our standard imaging protocol and the one used throughout this thesis; additional data with only 35 slices was obtained from control subjects participating in a separate study of Parkinson’s disease and was identical in all sequence parameters other than number of slices. T1-weighted images were also acquired using MPRAGE. Two different sequences were used, depending on the subject. The first sequence (297 subjects) had resolution  $1 \times 1 \times 1$  mm<sup>3</sup> interpolated to  $0.5 \times 0.5 \times 1$  mm<sup>3</sup>, 144 slices TE=4.38 ms, TR=1870 ms, TI=1100 ms, and scan time of 4:29 minutes. The second sequence (60 subjects) used voxel size  $0.9 \times 0.9 \times 1$  mm<sup>3</sup> interpolated to  $0.45 \times 0.45 \times 1$  mm<sup>3</sup>, 176 slices, TE=3.9 ms, TR=2120 ms, TI=1100 ms. The remaining 46 subjects either did not receive MPRAGE imaging due to time constraints, or the MPRAGE was not of suitable quality for automated volume segmentation.

### **Fibre Tracking Diffusion Measurements**

A semi-automated tractography method was used to extract twelve major white matter pathways in each individual. This method has been previously described (Lebel et al., 2008a), and uses seeding, target, and exclusion regions drawn on a template that are subsequently warped back to native space for automated tracking in each individual. Fibre tracking was performed with modified code from ExploreDTI (A. Leemans, Utrecht, Netherlands), using a deterministic streamline method. FA thresholds were set to 0.25 to initiate and continue tracking, and the angle threshold was set to 60° for all tracts. Tractography was used to delineate the inferior and superior longitudinal fasciculi (ILF/SLF), inferior and superior fronto-occipital fasciculi (IFO/SFO), fornix, cingulum, corticospinal tracts, anterior limb of the internal capsule (ALIC), genu, body, and splenium of the corpus callosum (gCC, bCC, sCC), and the uncinate fasciculus (UF), according to a priori information on tract location (Catani et al., 2002; Wakana et al., 2004). Corpus callosum subdivisions were examined previously in another study containing many of the same subjects using manual tractography of seven regions (Lebel et al., 2010). The three corpus callosum subdivisions that are easily analyzed using semi-automated tractography (genu, body, splenium) were included here for completeness and

in order to examine the additional ~90 subjects in the older age range (60–83 years). For each tract and each subject, FA and MD values were averaged across all voxels in the entire tract; each voxel was counted only once. Where appropriate (i.e. for all tracts except the fornix and corpus callosum), FA and MD values were calculated separately for left and right hemispheres.

### **Curve Fitting**

FA and MD values for each tract were fit to Poisson-type curves according to the following equation:  $FA \text{ (or MD)} = C + A * age * \exp^{-B * age}$ . Each fitting parameter, as well as the fit as a whole, was assessed for significance using F-tests. From the best fit equation, age of peak FA and minimum MD values were calculated for each tract using the derivative of the best fit equation:  $FA \text{ peak (or MD min)} = 1/B$ . Error of the peak/minimum age estimates were calculated using the standard error of the exponential fitting parameter, by recalculating the peak/minimum age using  $B \pm SE$ . In addition, the absolute and percent changes of FA and MD values from 5 years to peak/minimum and from peak/minimum to 83 years were calculated for each tract.

### **Left-right Asymmetry**

Initially, left-right differences were tested using a paired t-test. However, as this only provides information about absolute asymmetries, separate fits were performed for the left and right tracts, where appropriate. The fitting parameters were compared using t-tests to determine if the fits were significantly different between left and right hemispheres. If fits were not significantly different, left and right were combined by averaging and a fit was performed on the averaged values.

### **Sex Differences**

Sex differences were tested by fitting male and female curves separately and using t-tests to check for significant differences of fitting parameters. If there were no significant differences of age parameters, genders were combined for

further analysis, but a sex term was included in the overall fitting equation to test for possible absolute differences between genders.

### **11.1.3 Results**

#### **Age-related FA Changes**

All tracts followed Poisson-type development trajectories, with FA increasing initially from childhood to adulthood, reaching a peak, and then decreasing at a rate slightly slower than the initial increases (see Figure 11.1). All fitting parameters and overall fits were highly significant ( $p < 0.004$ ; see Table 11.1).

#### **Age-related MD Changes**

All tracts followed Poisson-type development curves for MD change, with MD decreasing from childhood to adulthood, reaching a minimum and then increasing slightly slower (see Figure 11.2). All fitting parameters and overall fits were highly significant ( $p < 0.001$ ; see Table 11.1).

#### **Left-right Asymmetry**

Paired t-tests between left and right hemispheres for each tract revealed significant differences in most tracts. FA values were significantly different between hemispheres in the ALIC, IFO, ILF (right-lateralized by 0.007, 0.007, 0.003 units, respectively), and the SLF (left-lateralized by 0.003). MD values were significantly different for ALIC, cingulum, SFO, and SLF (left-lateralized by  $0.003\text{--}0.014 \times 10^{-3} \text{ mm}^2/\text{s}$ ), and the IFO and ILF (right-lateralized by 0.007 and  $0.004 \times 10^{-3} \text{ mm}^2/\text{s}$ , respectively).

Despite many absolute differences of FA and MD, the fitting parameters (linear and exponential terms) were only significantly different for the FA fits in the anterior limb of the internal capsule, for the exponential term ( $L=0.031$ ,  $R=0.037$ ,  $p < 0.001$ ). Therefore, all other tracts were combined across hemispheres by averaging left and right values, while the left and right ALIC remained separate for FA fits.

Table 11.1: Fitting parameters for each parameter in the best fit equation are shown, with significance values in parentheses. The sex term was omitted where not significant. Equation used to model age-related changes: FA (or MD) = C + A\*age\*e<sup>B\*age</sup> + D\*sex. Positive values for the sex term indicate higher values in males. MD units are mm<sup>2</sup>/s. \*p<0.001; n.s.=not significant

<b>Fractional Anisotropy</b>					
Tract	Intercept (C)	Linear (A) ( $\times 10^{-2}$ )	Exponential (B)	Sex (D) ( $\times 10^{-2}$ )	R
ALIC — Left	0.40 *	0.60 *	0.031 *	n.s.	0.50
ALIC — Right	0.41 *	0.57 *	0.037 *	n.s.	0.40
bCC	0.49 *	0.36 *	0.029 *	0.60 (0.001)	0.40
Cingulum	0.42 *	0.59 *	0.024 *	n.s.	0.56
CST	0.47 *	0.37 *	0.027 *	1.1 *	0.41
Fornix	0.38 *	0.45 *	0.050 *	n.s.	0.35
gCC	0.48 *	0.89 *	0.048 *	n.s.	0.59
IFO	0.43 *	0.92 *	0.036 *	n.s.	0.58
ILF	0.41 *	0.49 *	0.040 *	-0.47 *	0.43
sCC	0.54 *	0.34 *	0.040 *	n.s.	0.21
SFO	0.41 *	0.40 *	0.036 *	0.38 (0.04)	0.36
SLF	0.41 *	0.75 *	0.035 *	0.48 (0.02)	0.55
UF	0.36 *	0.57 *	0.028 *	0.91 *	0.49
<b>Mean Diffusivity</b>					
Tract	Intercept (C) ( $\times 10^{-3}$ )	Linear (A) ( $\times 10^{-4}$ )	Exponential (B)	Sex (D) ( $\times 10^{-5}$ )	R
ALIC	0.87 *	-0.12 *	0.035 *	n.s.	0.61
bCC	1.01 *	-0.19 *	0.034 *	n.s.	0.61
Cingulum	0.88 *	-0.09 *	0.025 *	-0.50 (0.024)	0.74
CST	0.90 *	-0.07 *	0.031 *	-1.8 *	0.30
Fornix	1.42 *	-0.40 *	0.057 *	n.s.	0.50
gCC	0.91 *	-0.13 *	0.031 *	n.s.	0.56
IFO	0.90 *	-0.11 *	0.037 *	n.s.	0.54
ILF	0.94 *	-0.11 *	0.036 *	n.s.	0.48
sCC	0.93 *	-0.14 *	0.034 *	n.s.	0.47
SFO	0.84 *	-0.10 *	0.031 *	n.s.	0.58
SLF	0.85 *	-0.09 *	0.028 *	n.s.	0.62
UF	0.92 *	-0.11 *	0.032 *	n.s.	0.47

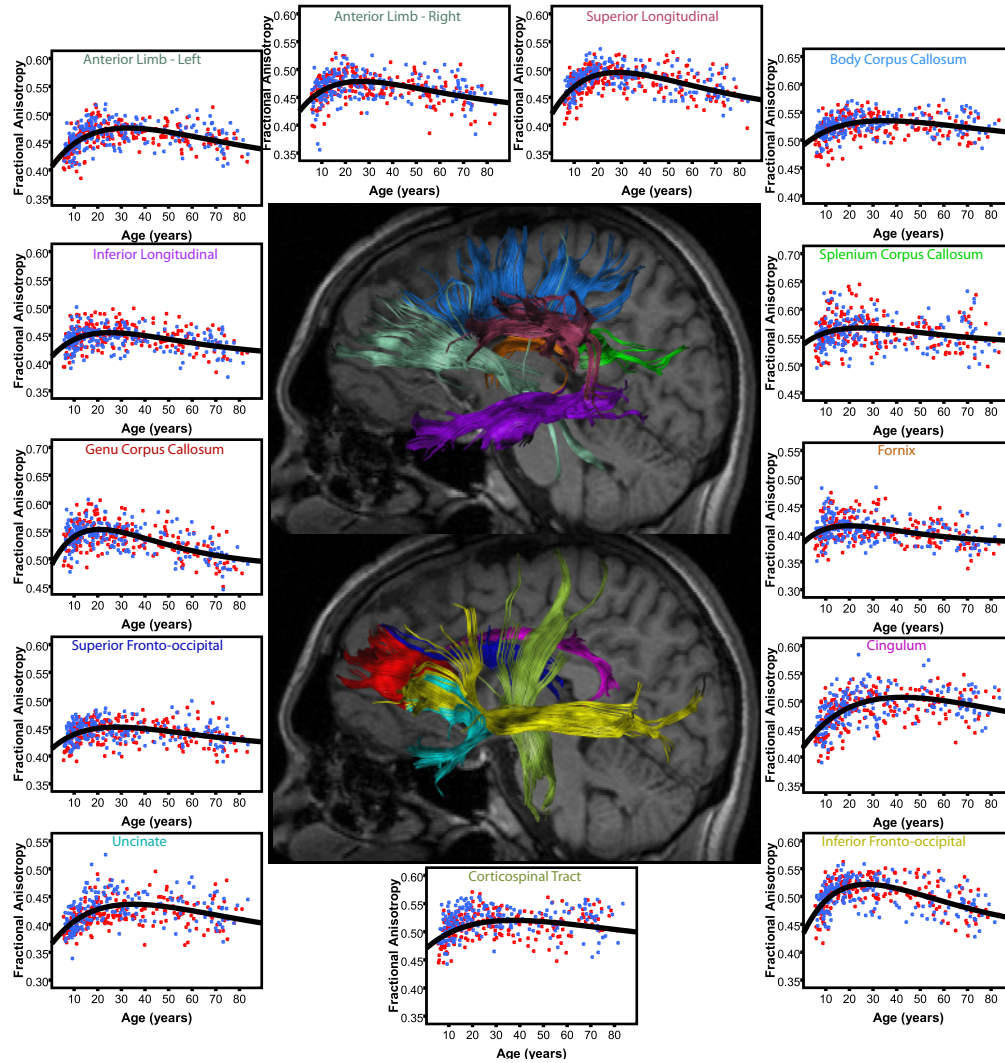


Figure 11.1: Fractional anisotropy (FA)-age plots are shown for each tract measured, along with the best fit curve. Males and females are shown separately, although there were significant differences in curve shape for only the uncinatus fasciculus (two curves shown). For the body of the corpus callosum, cingulum, inferior and superior longitudinal fasciculi, and the posterior limb of the internal capsule, there were small absolute sex differences; the male curve is shown for these tracts. All tracts are shown in a healthy 22 year old male.

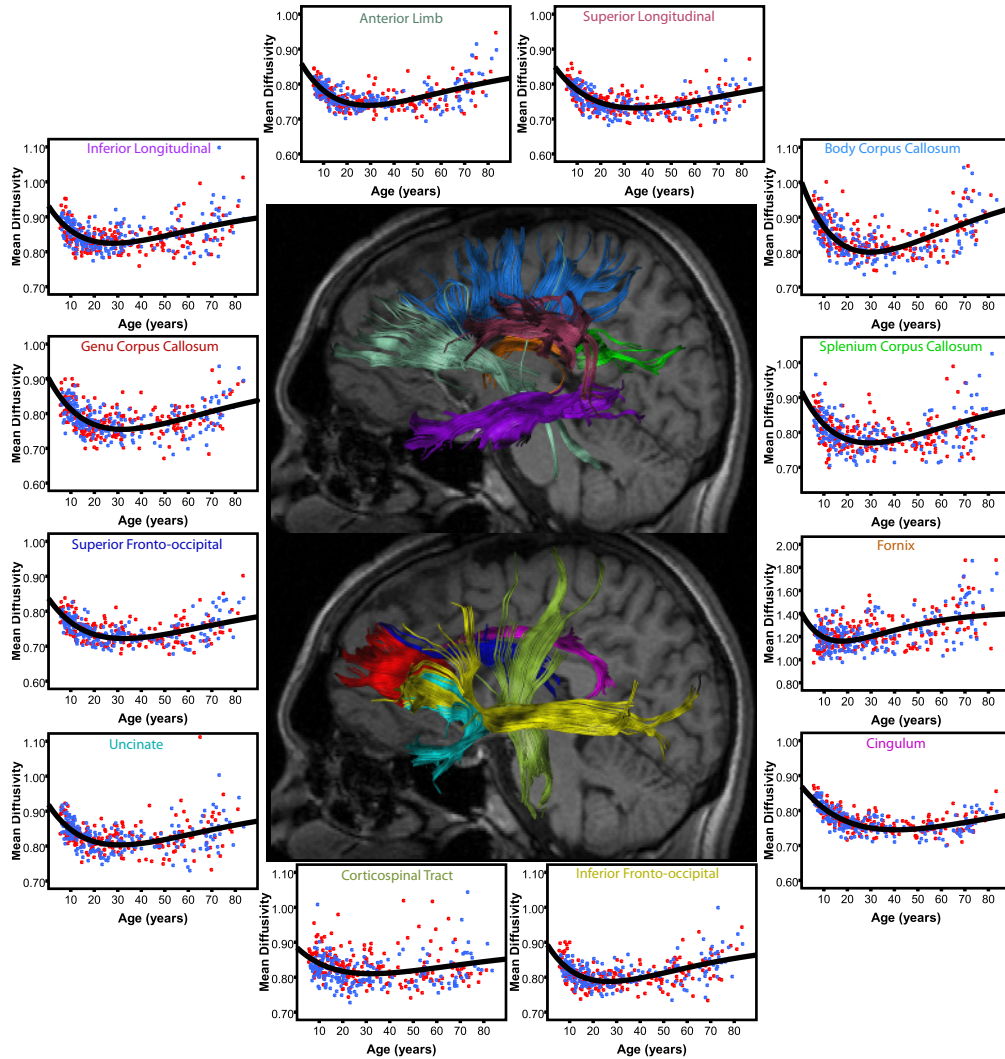


Figure 11.2: Mean diffusivity (MD)-age plots are shown for each tract measured, along with the best fit curve. Males and females are shown separately, although there were significant differences in curve shape for only the cingulum (two curves shown). For the superior longitudinal fasciculus and the posterior limb of the internal capsule, there were small absolute sex differences; the male curve is shown for these tracts. All tracts are shown in a healthy 22 year old male.

## Sex Differences

For fitting parameters (linear and exponential terms), no tracts had significant differences, so the sexes were combined and a sex term was included in the fitting equation. This sex term was significant at  $p < 0.05$  for seven tracts: the bCC, corticospinal tract, superior longitudinal and fronto-occipital fasciculi, and the uncinate fasciculus showed higher FA values in males than females (by 0.004–0.011 units); the inferior longitudinal fasciculus had lower FA by 0.005 units in males (see Table 11.1). For MD, the cingulum and corticospinal tract had significant sex terms, with females having higher MD values than males (by  $0.5\text{--}1.8 \times 10^{-5} \text{ mm}^2/\text{s}$ ).

## Timing and Magnitude of FA Changes

Age of peak FA values ranged from 20 years for the fornix to 42 years for the cingulum (see Figure 11.3A). In general, the tracts could be grouped into those that peaked early, those that peaked at intermediate ages, and those that peaked later than the rest. In addition to the fornix, the inferior longitudinal fasciculus, and genu and splenium of the corpus callosum peaked early (<25 years). Intermediate developing tracts (peak age between 27–30 years) were the inferior and superior fronto-occipital fasciculi, superior longitudinal fasciculus, and left and right anterior limbs of the internal capsule. The corticospinal tract, body of the corpus callosum, and uncinate fasciculus all developed late (peaking >35 years). The amount of FA change from age 5 years to peak FA ranged from 3% for the splenium to 13% for the cingulum, while the FA drop after peak ranged from 3% in the body of the corpus callosum and the corticospinal tract to an 11% drop in the inferior fronto-occipital fasciculus.

## Timing and Magnitude of MD Changes

Ages at which the minimum MD values were reached ranged from 18 years (fornix) to 41 (cingulum; see Figure 11.3B). Most tracts reached their minimum MD values between 26–33 years, with only the fornix reaching its min-

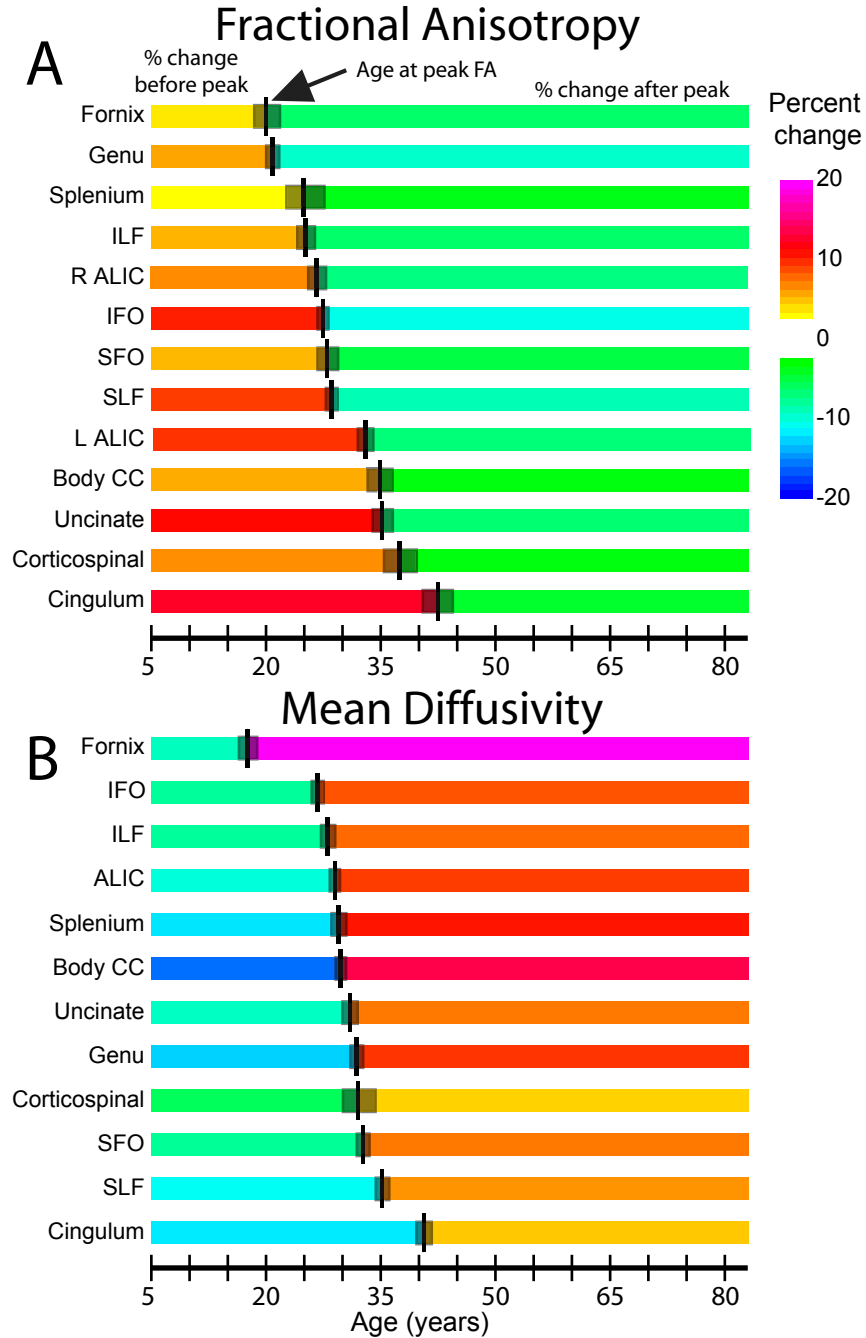


Figure 11.3: Age of peak fractional anisotropy (FA) and minimum mean diffusivity (MD) values are shown for each tract, with the magnitude of changes before/after the peak. For each tract, the black vertical line is the age at FA peak or MD minimum, and the gray bar is the standard error of the estimate. The colour of the long bars on each side of the peak represents the magnitude of change before (left) and after (right) the peak/minimum value.

inum earlier and the superior longitudinal fasciculus and cingulum reaching their minima at 25 and 41 years, respectively. The smallest MD decline before reaching the minimum was 6% in the corticospinal tracts, while the body of the corpus callosum experienced the largest drop at 16%. MD increases after the minimum values ranged from 4% in the cingulum to almost 20% in the fornix.

#### **11.1.4 Discussion**

Diffusion tensor imaging and tractography have shown development trajectories in major white matter tracts of the human brain that are nonlinear and regionally varying. Poisson-type fits were robust and demonstrated FA increases and MD decreases during childhood and adolescence in all tracts, followed by FA decreases and MD increases during adulthood and the aging process. Ages at which the FA and MD trends reversed varied from 17–42 years, depending on the region. In general, a trend was observed where frontal-temporal connections, including the uncinate fasciculus, superior longitudinal fasciculus and cingulum, had longer periods of development before trend reversals and shorter periods of decline afterward than other tracts. The fornix, inferior longitudinal fasciculus, and corpus callosum tended to have the shortest periods of development and the earliest trend reversals. It is important to note that both development and aging processes influence the peak/minimum age for each tract, and these are difficult to separate. Therefore, late peaks may be interpreted as prolonged maturation or delayed aging, or most likely a combination of the two.

The findings presented here are in excellent agreement with the two large previous DTI lifespan studies in terms of the relative timing of development (Kochunov et al., 2010; Westlye et al., 2009). Both of these studies report peak FA values between ages 23-39, and the most prolonged maturation is observed in the cingulum, with relatively late development in the uncinate fasciculus (the fronto-occipital region in the Kochunov paper), corticospinal tracts (the internal capsule in the Kochunov paper, which includes the corticospinal tracts as well as the anterior limb), and superior longitudinal fasciculus. One of the

unique aspects of our results is that we observe greater spread between early-developing regions and late-developing regions than reported previously. This is likely due in part to the use of the Poisson fits, which are more flexible in terms of development and degradation slopes and therefore is likely less restrictive the location of the peak values than a quadratic fit.

The late-maturing frontal-temporal connections are involved in a variety of cognitive tasks, including reading and memory. The superior longitudinal fasciculus connects Broca's area in the frontal lobe with Wernicke's area in the temporal lobe. The superior longitudinal fasciculus has been consistently shown to be involved in language and intelligence tasks (Catani et al., 2007; Jung and Haier, 2007), and matures more slowly than other tracts during childhood and adolescence (Zhang et al., 2007). Interestingly, the uncinate fasciculus is thought to provide an additional, ventral language pathway in the brain (Parker et al., 2005). The cingulum is part of the limbic system, a group of brain structures involved in tasks such as memory and emotion.

In contrast to the late development/declines in frontal-temporal pathways, the fornix, corpus callosum and inferior longitudinal fasciculus showed early trend reversals. These results are in good agreement with several previous reports describing early maturation of the fornix and inferior longitudinal fasciculus compared to other brain areas (Dubois et al., 2008; Hermoye et al., 2006). An additional report describes early maturation of the anterior corpus callosum (genu) (Thompson et al., 2000).

Increases of FA before peak ranged from 3–13%, while reductions of FA after the peak ranged from 3–11%. The IFO and genu of the corpus callosum experienced the largest drops. In general, the regions with the biggest increases and declines of FA were frontal connections (genu, inferior fronto-occipital, superior longitudinal fasciculi). The cingulum is a frontal connection that did not experience large FA declines; however, with its late peak, it does not have as long to undergo declines as the other regions. It was also frontal connections (cingulum and uncinate), which underwent the greatest percent increases of FA before their peaks (10–13%).

Sex differences were observed in seven of twelve tracts measured in this

study, but even where significant, they were small in magnitude. Sex differences are controversial, with smaller age range studies reporting very mixed results (Abe et al., 2002; Hsu et al., 2008; Ota et al., 2006; Schmithorst et al., 2008; Schneiderman et al., 2007). The previous DTI lifespan studies either did not examine sex differences (Westlye et al., 2009; McLaughlin et al., 2007), did not report any significant findings (Hasan et al., 2009a,b), or found only very minimal differences (Hasan et al., 2010; Kochunov et al., 2010).

Hemispheric asymmetry is known to exist in the brain, and has been reported by many studies (Buchel et al., 2004; Gong et al., 2005; Hasan et al., 2009a; Rodrigo et al., 2007; Wilde et al., 2009), although as with gender differences, the results are not always consistent. For example, both leftward (Ardekani et al., 2007; Hasan et al., 2009a) and rightward (Park et al., 2004; Yasmin et al., 2009) asymmetry have been reported in the anterior limb of the internal capsule and uncinate fasciculus. In general, even significant lateralization findings are small compared to individual variation within the study or repeatability of measures between scans (Bonekamp et al., 2007). In this study, many of the white matter pathways measured — the anterior limb, cingulum, inferior and superior fronto-occipital and longitudinal fasciculi — had significant hemispheric differences of FA or MD. Most of these showed rightward lateralization, although some were left-lateralized (superior longitudinal fasciculus for FA, anterior limb and superior fronto-occipital and longitudinal fasciculi for MD). However, it is important to note that although these differences were significant, they were very small ( $<0.01$  for FA;  $<0.014 \times 10^{-3}$  mm<sup>2</sup>/s for MD). The leftward lateralization of FA in the superior longitudinal fasciculus is consistent with many other studies (Buchel et al., 2004; Catani et al., 2007; Powell et al., 2006). Although many reports have examined absolute differences of diffusion parameters between hemispheres, few studies have examined asymmetry of development trends. In this study, we found significantly different trajectories of FA in the anterior limb of the internal capsule, with the right side reaching a peak earlier than the left. Both demonstrated similar FA declines after the peak, although the left side had a larger percent increase of FA before the peak. There were no significant hemisphere

differences of MD curves in the anterior limb. The discrepancies between lateralization differences in this study and others may be due to the wide age range and large sample size in this study. A small degree of lateralization may be present in small populations or across narrow age ranges that are not apparent in a large group. Similarly, the large group used in this study may permit detection of previous unobserved asymmetries.

Although a variety of nonlinear development models have been used by previous studies, including quadratic (Hasan et al., 2009b), cubic (Hsu et al., 2010), monoexponential (Ben Bashat et al., 2005), and biexponential (Mukherjee et al., 2001), the Poisson-type fit was chosen for this study because of several advantages. The Poisson curve accounts for the known FA increases/MD decreases during childhood and FA decreases/MD increases during aging, but allows for different rates of development and aging, unlike a quadratic model that has equal slopes on either side of the peak. Furthermore, the Poisson fit uses only three parameters, unlike a biexponential model that requires at least 5, and a smaller number of fitting parameters is desirable for robust fitting. For this study, the Poisson fits gave robust fits and highly significant parameter estimates and provided developmental trajectories that were intuitive. However, other, more complex models may offer equivalent or even better fits. Longitudinal studies in particular will be better able to assess the development and aging trends and may have sufficient subject numbers to use more complex models.

Deterministic tractography can be prone to error in crossing fibre areas where FA values may be particularly low, such as parietal regions where the superior longitudinal fasciculus, corticospinal tracts, and lateral projections of the corpus callosum intersect. However, the tracts examined for this study are well-known pathways that were drawn according to a priori anatomical knowledge (Catani et al., 2002; Wakana et al., 2004) and verified to ensure accuracy.

In conclusion, DTI tractography of twelve major white matter structures over a wide age range of 5 to 83 years in a large sample of 403 healthy subjects has demonstrated significant age-related changes of diffusion parameters with

regional variation in the timing and magnitude of changes. Deterministic tractography revealed development trajectories for all structures that, if compared to those in a patient population, could highlight the presence and timing of specific brain abnormalities associated with a particular disease.

### **11.1.5 Future Directions**

When measuring diffusion parameters in white matter, it is important to understand potential contributions to any observed FA or MD changes. One way of doing this is to measure the eigenvalues (parallel and perpendicular diffusivity), similar to what was done in many of the previous chapters. For this study, diffusivity will be measured in each tract, and the patterns of change with age will provide clues for the potential driving causes behind FA and MD increases/decreases. In addition, volume measurements may provide interesting information. Total brain volume, gray matter and white matter volumes are more global measures of brain structure, and they are useful for providing an overall picture of the brain changes. Three global volumes (total, gray matter, white matter) will be assessed in each subject using automated software called FreeSurfer (Charlestown, MA) (Fischl et al., 2002). Curves will then be fit to the brain volume data to determine the patterns of change across the age range.

Another parameter that will be examined is the volume of individual white matter tracts. This can be done quite simply by counting the number of voxels included in the result of tractography. Tract volume is usually strongly correlated with FA and may even influence FA measurements via partial voluming. An examination of tract volumes in this study will be conducted to determine how they relate to FA and MD measurements and whether they provide additional information or confound measurements.

## 11.2 Reading Ability and Brain Structure in Typically-Developing Children and Adolescents and Those with Fetal Alcohol Spectrum Disorder<sup>2</sup>

### 11.2.1 Introduction

Diffusion tensor imaging (DTI) studies of reading ability consistently highlight left temporal-parietal white matter in healthy individuals (Beaulieu et al., 2005; Nagy et al., 2004; Qiu et al., 2008) and dyslexia (Deutsch et al., 2005; Klingberg et al., 2000; Niogi and McCandliss, 2006; Odegard et al., 2009; Rimrodt et al., 2010); the corpus callosum is also implicated by DTI (Dougherty et al., 2007; Frye et al., 2008; Odegard et al., 2009). Studies have also investigated DTI white matter-reading relationships in traumatic brain injury (n=41) (Ewing-Cobbs et al., 2008) and preterm children (n=19) (Andrews et al., 2009), demonstrating correlations in callosal areas. Individuals with fetal alcohol spectrum disorder (FASD), where brain injury is associated with prenatal alcohol exposure, often have cognitive deficits including reading (Spadoni et al., 2007). DTI abnormalities in the corpus callosum and temporal lobe (Lebel et al., 2008a; Sowell et al., 2008a) are observed in FASD, yet their link to reading is unknown. The purpose of this study was to determine if white matter microstructure, measured by fractional anisotropy (FA), correlates with reading ability in subjects with FASD and how that relates to a healthy cohort of volunteers.

### 11.2.2 Methods

Subjects were 40 volunteers aged 5–19 years (22 males, 18 females; mean age  $\pm$  standard deviation:  $10.7 \pm 3.4$  years) with FASD and 40 age- and gender-matched controls. Some of the control subjects were part of earlier studies of

---

<sup>2</sup>A version of this section has been published. C. Lebel, C. Rasmussen, K. Wyper, G. Andrew and C. Beaulieu, 2010. White Matter Structure Correlates with Reading Ability in Healthy Subjects and Those with Fetal Alcohol Spectrum Disorder, Abstract #3431. Proceedings of the International Society for Magnetic Resonance in Medicine, 18th Annual Meeting, Stockholm, Sweden.

reading ability in healthy children aged 5–8 (Beaulieu et al., 2006) and 9–12 years (Beaulieu et al., 2005). All subjects were assessed with the Woodcock Reading Mastery Word ID test. The Word ID test is a sight word reading test where participants are shown words and asked to pronounce them aloud. An independent samples t-test evaluated group differences. DTI was performed on a 1.5T Siemens Sonata scanner using dual spin echo EPI, 40 3mm slices (no gap), image matrix  $128 \times 128$  with 75% phase partial Fourier zero-filled to  $256 \times 256$ , TE/TR=98ms/6400ms, b=1000 s/mm<sup>2</sup>, 8 averages and 6 directions, 6:06 minutes. Non diffusion weighted images were normalized to the ICBM EPI template with non-affine transformations in SPM8; FA maps were normalized with the same parameters and smoothed with a 4 mm kernel. Voxel-based correlation of FA, controlling for age, with age-normalized Word ID scores was performed in SPM8 for each group separately; to exclude CSF, cortical gray matter, and most deep gray matter (with the exception of the thalamus), only voxels with  $FA \geq 0.2$  in all individuals were included in the analysis. Positive and negative t-tests with  $p < 0.025$  per voxel and cluster size  $> 84$  were used to determine significant clusters (overall alpha was  $< 0.049$ ). Cluster size threshold was determined using Monte Carlo simulations conducted in AlphaSim (<http://afni.nimh.nih.gov/afni/doc/manual/AlphaSim>).

### 11.2.3 Results

Subjects with FASD had lower Word ID scores than controls (FASD mean =  $92 \pm 13$ ; control mean =  $107 \pm 13$ ;  $p < 0.001$ ). In the FASD group, 6 clusters with positive Word ID-FA correlations were observed: brainstem (595 voxels, MNI coordinates of most correlated voxel in cluster: [24, -22, -8]), two bilateral parietal (left: 103 voxels [-22, -16, 40], right: 102 voxels [26, -16, 38]), right internal capsule (137 voxels [18, -6, 10]), and two left temporal (148 [-24, -28, -8] and 150 voxels [-36, -24, -14]). Three clusters in the FASD group had negative correlations: the right frontal/parietal (192 voxels [16, 12, 26]) and two bilateral cerebellum (left: 210 voxels [-18, -60, -34], right: 227 voxels [28, -52, -36]). In the control group, no negative clusters and four positive clusters were observed: three in left temporal/parietal (209 [-18, -42, 54], 206 [-32, -8,

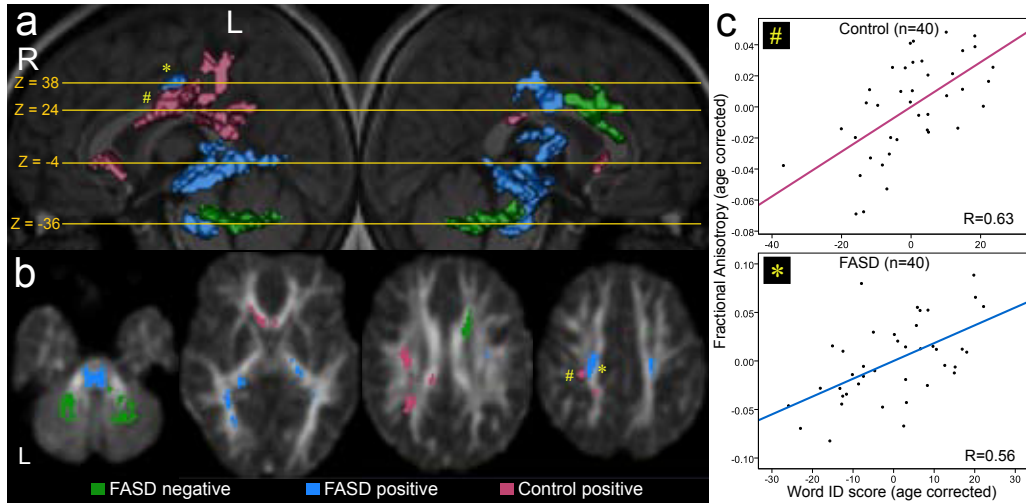


Figure 11.4: a: Clusters with significant fractional anisotropy (FA)-Word ID correlations are shown for controls (n=40) and FASD subjects (n=40). b: Clusters overlaid on normalized, smoothed FA maps. c: FA averaged across a left parietal cluster from each group (# for controls, \* for FASD) is shown plotted against Word ID scores, both corrected for age.

24], 136 voxels[-32, -52, 28] ), and one in genu of corpus callosum (92 voxels [-4, 18, 0]). Figure 11.4 shows all clusters and plots of FA averaged over a left parietal cluster for each group (marked by \*, #). There was no overlap between FASD and control clusters.

### 11.2.4 Discussion

Significant FA-Word ID correlations in controls were focused in the left temporal-parietal region, with one cluster in the genu, supporting earlier findings in healthy individuals and dyslexia (Beaulieu et al., 2005; Deutsch et al., 2005; Klingberg et al., 2000; Niogi and McCandliss, 2006; Odegard et al., 2009; Qiu et al., 2008; Rimrodt et al., 2010). An additional study observed FA changes in the left anterior centrum semiovale in 8-10 year old poor readers that correlated with improvements in reading skill after remediation (Keller and Just, 2009). Similar left temporal-parietal clusters were observed in FASD, suggesting consistent involvement of this brain region despite known brain damage of this area in FASD. However, correlations in FASD differed in that they were more widespread than in controls, including right hemisphere white matter, and that there were 3 clusters with negative correlations. The more

widespread, and notably symmetric correlations, in FASD individuals may be due to atypical brain development or compensation for the limited capacity of other brain regions. Some FASD clusters may simply reflect coincidental brain damage and poor general cognitive performance in the disorder rather than direct involvement in reading.

Brain structure-reading correlations in FASD are reported for the first time, highlighting the consistent involvement of the left temporal-parietal area for reading ability in healthy and abnormal populations, albeit with more widespread regions in FASD children/adolescents.

### **11.2.5 Future Directions**

One of the major limitations of voxel-based analysis is normalization of the images to a template. Some regions are well normalized and one can be reasonably confident that any correlations or group differences are the result of actual diffusion parameter differences. For example, the left parietal cluster observed to be significant in control subjects (see Figure 11.5) seems to be in a well normalized area, and it is located in the same structure in all subjects. However, other regions may be poorly registered and lead to false results, particularly if they are near structure edges or crossing fibre regions with artificially low FA. Suboptimal normalization is evident in the right frontal cluster shown in Figure 11.6, which is at the edge of the corpus callosum and adjacent to some crossing fibre regions. This cluster had negative correlations in subjects with FASD, and may be a product of poor normalization rather than a real reflection of structural differences.

Two approaches to reduce normalization errors are to use an improved template and/or a better normalization algorithm. For example a subject-specific template may produce better normalization than using a pre-made one, especially with children, who have smaller brains and heads than adults. The images shown in Figure 11.6 were normalized to the ICBM-152 template that is provided as part of the SPM software package. However, normalization of the same subjects to a template made based on the control subjects in this study yielded a similar right frontal cluster with negative correlations (data

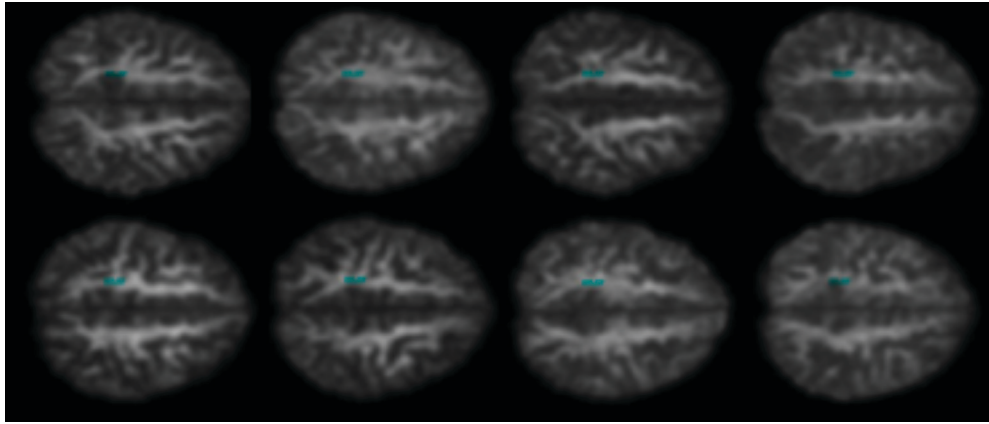


Figure 11.5: One of the left parietal clusters found to have significant Word ID-FA correlations in controls is overlaid on smoothed, normalized FA maps from 8 random control subjects. It is clear that this cluster is located consistently in a left parietal white matter region in all subjects.

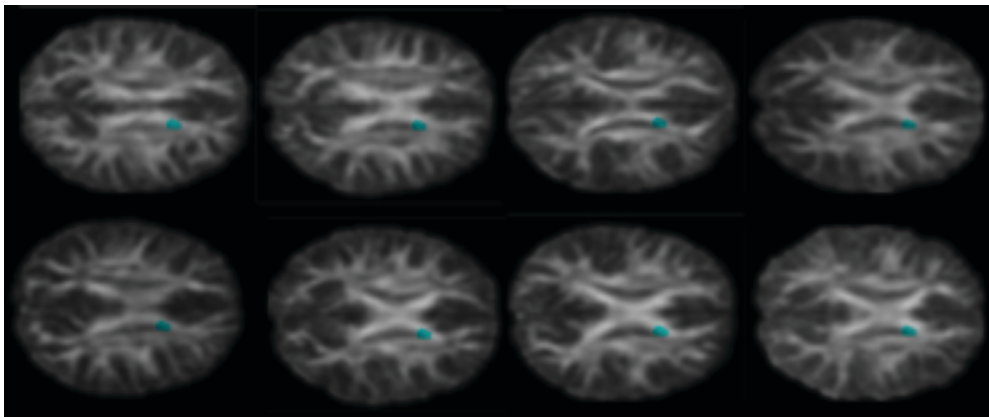


Figure 11.6: The negatively correlated right frontal cluster observed in subjects with FASD is overlaid on smoothed, normalized FA maps from 8 random FASD subjects. It is clear that this cluster is located near an edge and not in the same region for all individuals.

not shown), so changing the template may not have much impact for this study. A means of reducing spurious correlations is to set a very high FA threshold, ensuring that regions with poor normalization (which tend to have lower FA values in at least some individuals) are not analyzed. The major drawback of this approach, however, is that regions with adequate registration but naturally low FA values may be missed. For example, average FA values in the left parietal cluster ranged from 0.21–0.48, meaning that an FA threshold of 0.3 would exclude some voxels there.

Different combinations of templates, normalization techniques and FA thresholds will be explored for this data to better understand the observed correlations and ensure that they are plausibly attributed to diffusion differences.

# Chapter 12

## Limitations and Future Directions

While they are powerful and informative, the techniques used in this thesis have, as have all methods, inherent limitations. These limitations begin with the imaging techniques themselves. Single-shot echo-planar imaging (EPI) is by far the most commonly used sequence for DTI because of its speed and efficiency. However, EPI (and especially single-shot EPI) has limited resolution and is prone to several types of artifacts that can degrade image quality. Susceptibility differences within the brain (e.g. at air/tissue interfaces around the sinuses) lead to field inhomogeneities and cause off-resonance effects. Because of its acquisition, EPI is very sensitive to these effects in the phase-encoding direction, and they result in image distortions, as seen in Figure 12.1. BThese phase encoding direction is usually set to be anterior-posterior because of these distortions, to avoid introducing asymmetry into images. Other artifacts common in EPI sequences include ghosting caused by a phase or amplitude mismatch between odd and even echoes (the so-called “N/2 ghost”), chemical shift artifacts caused by fat (which has a different resonant frequency from water), and eddy-current distortions. Most of these artifacts can be reduced or eliminated by careful protocol selection. For example, a fat saturation pulse can be added to the sequence and is designed to fully dephase any magnetization contribution from fat and eliminate its contribution to the image. Eddy currents may be reduced using special DTI sequences like the twice-refocussed spin echo sequence used throughout this thesis (Reese et al., 2003), or they may be

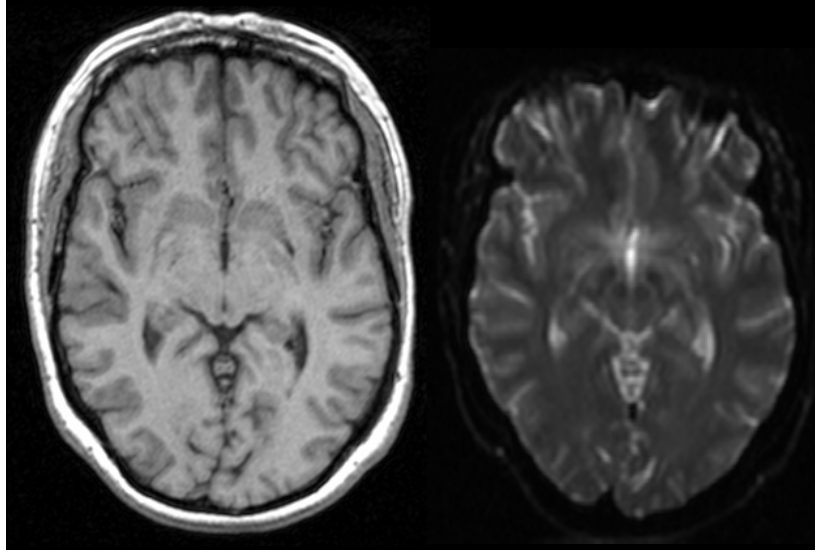


Figure 12.1: In areas of susceptibility difference, such as the air/tissue interfaces around the sinuses, EPI leads to distortions such as those seen here at the anterior end of the brain. A T1-weighted image is shown on the left, compared to a non-diffusion-weighted image on the right at the same axial position (although slice thickness differs between these images). These distortions occur in the phase-encoding direction, which is generally set to be anterior-posterior.

removed during post-processing with a variety of tools available in packages such as DTIStudio or FSL. Proper calibration of gradients, alignment of echoes and reduction of eddy currents should all help reduce or eliminate ghosting.

A further limitation of EPI is its spatial resolution. Image resolution of MRI in general is limited by the available signal, and rapid acquisitions like single-shot EPI must compromise resolution to achieve adequate signal and are even more limited. Typical image resolution in DTI acquisitions is approximately 8-16 mm<sup>3</sup> per voxel, acquired either isotropically (say 2.2×2.2×2.2 mm<sup>3</sup>) or anisotropically (for example, 1.72×1.72×3 mm<sup>3</sup>, as used in this thesis). These voxel sizes are much larger than the typical diameter of axons, which is on the order of several microns. DTI, however, is able to probe the microstructural properties of tissues because signal loss results from hindered diffusion even at scales much smaller than a voxel. However, the resolution of DTI images will limit the fibres that can be identified and easily reconstructed. For fibre tracking, one is limited to fibres that are at least 2-3 voxels across in order to achieve accurate measures and reliable tracking (see below

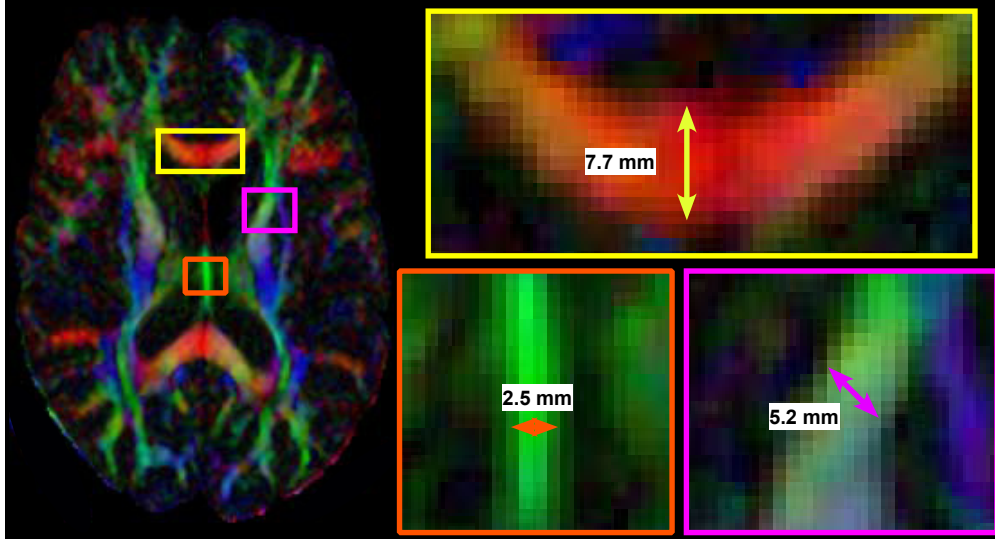


Figure 12.2: A colour map axial slice is shown, along with zoomed-in sections of several tracts, and the tract width is given for a specific point. Note that the fornix (bottom left) can be quite narrow at some points, while other tracts such as the genu of the corpus callosum (top) and the anterior limb of the internal capsule (bottom right) are wider at 5-10 mm. This colour map is obtained from the 6-direction data used throughout this thesis (interpolated data).

for a brief discussion of partial voluming problems). The major fibre bundles measured in this thesis have diameters that range from approximately 5-15 mm, although the fornix is thinner (see Figure 12.2 for some examples). This width makes the fibres easily identifiable on 2-dimensional images, and makes it possible to assess them using DTI, since they will fully occupy at least 2-3 voxels in any direction. However, many other interesting white matter fibre bundles are too small to assess using typical resolution DTI methods. Better imaging techniques and increased resolution would allow for a more thorough study of brain white matter.

The narrowest tract examined in this thesis was the fornix, which can be only 2-3 mm wide in some parts (see Figure 12.2), leading to partial voluming problems. Partial voluming with CSF, in the case of the fornix, can lead to drastically reduced FA values, elevated MD values, and difficulty tracking. For this reason, CSF-suppressed DTI is often used to measure the fornix, as it helps reduce partial voluming (Concha et al., 2005b). This technique was used to assess the fornix in both Chapter 5 and 6; however, the CSF-suppressed

acquisition takes considerably longer to acquire than standard DTI and is not always possible in young subjects. In the data used here, standard DTI data was acquired in 6 minutes and provided almost complete brain coverage (part of the cerebellum was missed in subjects with medium to large heads). However, the CSF-suppressed DTI lasted over 8 minutes and covered an area only 65% as large as the standard DTI. In young children or uncooperative subjects, those types of differences in timing are important; however, for measurements of the fornix in particular, CSF-suppressed data is very beneficial.

Partial voluming may be a problem for other tracts as well. Since many tracts are adjacent to gray matter regions (those adjacent to other white matter fibre tracts may have crossing fibre issues as discussed below), gray and white matter may both be present in voxels around the edges of the tracts. This lowers the FA values at the edges of the tracts, and one concern is that it may cause larger tracts to have artificially higher FA values because the proportion of voxels with partial voluming (and lower FA values) is smaller. This is likely a problem for many DTI studies, particularly those using tractography. One method that might help to further understand the partial volume problem within white matter tracts is to test correlations between volume and FA within tracts. This is something that will be interesting to explore, particularly within the healthy development data, to determine if partial voluming is affecting the relative developmental timing of regions. This will be examined using the already collected data, as discussed in Chapter 11.1.

Deterministic tractography, the main analysis tool used throughout this thesis, uses the FA and primary diffusion direction within each voxel to trace fibre pathways in the brain. It is often criticized because it does not provide any measure of uncertainty for the streamlines it produces, though there is often a range of possible trajectories, each with a certain likelihood. Probabilistic tractography is one way to handle uncertainty in fibre estimates, and it provides probabilities for numerous pathways originating from a single seed region (Behrens et al., 2003; Parker et al., 2003). However, probabilistic tractography algorithms have their own drawbacks, such as the propagation of uncertainty along the length of the tract (Jones, 2008), and they are not designed for ac-

quisitions with only six diffusion encoding directions (and are therefore not well-suited for the six direction DTI data used through this thesis).

One of the main limitations of deterministic tractography comes not from the tracking algorithm, but from the tensor itself, which is not sufficient to accurately model regions where two or more fibre bundles intersect in a crossing or in a “kissing” pattern. Since the tensor can only handle one primary diffusion direction per voxel, these intersections produce oblate, rather than elongated, ellipsoids, and result in artificially low FA values, which may terminate deterministic tracking algorithms. An example of this problem occurs in parietal brain regions, where lateral projections of the corpus callosum cross with corticospinal tracts and the superior longitudinal fasciculus; this is why the lateral projections of the corpus callosum are effectively absent in the work presented in Chapter 7. A variety of more sophisticated models and new DTI acquisition methods using high angular resolution are capable of representing multiple fibre orientations per voxel, and thus can better cope with crossing fibre areas (Alexander, 2005; Hess et al., 2006; Tuch, 2004; Wedeen et al., 2005). It would be interesting to investigate additional brain regions using more sophisticated methods capable of reconstructing additional white matter pathways that are not easily assessed using classic deterministic tractography.

Voxel-based morphometry (VBM) is a useful method for investigating structure-function correlations that are not necessarily apparent when an entire white matter tract is examined. However, VBM is limited by the normalization methods used, and may produce errors in regions where normalization is poor (see Section 11.2.5). Misregistration may be reduced using study-specific templates or improved normalization algorithms. For example, while the VBM data presented here used non-affine registration in SPM to the ICBM-152 template, some studies use higher-dimensional warping techniques (Ashtari et al., 2007; Park et al., 2004), or homemade templates (Kubicki et al., 2005; Lee et al., 2010) that may provide improved registration. Since normalization problems are likely to persist even with improved templates and registration, some methods of mitigating their effects are to use a more stringent statistical threshold to reduce the chance of false positives or to mask corre-

lations/group differences with a more strict threshold (i.e.  $FA > 0.3$  or higher, instead of the more standard  $FA > 0.2$ ). These modifications may have other consequences; for example, higher statistical or masking thresholds greatly increase the chances of finding false negative results and true differences may be missed. VBM is sensitive to the normalization, smoothing, and analysis parameters chosen, including template, statistical thresholds, and the size and shape of the smoothing kernel (Jones et al., 2005; Van Hecke et al., 2010). Parameters should be carefully selected and consistently applied to minimize the potential for error. A promising new voxel-based method is tract-based spatial statistics (TBSS), which uses an FA skeleton and measures FA only along the middle of tracts (Smith et al., 2006). This method may provide a more robust analysis of white matter differences, including additional information about correlations between brain structure and cognition in both the FASD and typically developing populations studied here. However, one of the disadvantages of TBSS is that it misses non-central white matter regions and non white matter regions such as the thalamus, which may provide interesting information. Moreover, like other voxel-based approaches, TBSS suffers from statistical difficulties in controlling for multiple comparisons while maintaining adequate power to detect differences.

In addition to DTI, there are many other imaging techniques useful for assessing brain structure. Methods such as volumetric analysis and cortical thickness measurement will help further elucidate both healthy age-related changes and the abnormalities present in fetal alcohol spectrum disorder (FASD).

MRI volumetrics can be done by manually tracing regions and structures; however, this is very time-consuming and not feasible for very large subject groups such as those presented here. Fortunately, there are also a number of software packages providing automated methods of brain segmentation (e.g., FreeSurfer (Fischl et al., 2002)). These packages identify and delineate brain structures by labelling each voxel, then provide volume measurements for each structure. Typically, a software package can provide measures of lobe volumes for both gray and white matter, and the volumes of most major gray matter structures. Cortical thickness analysis is also able to give gray matter thick-

ness at multiple points along the cortical surface (Aganj et al., 2009; Hutton et al., 2008; MacDonald et al., 2000), providing specific information about areas with age-related changes or group differences. Volumetric and cortical thickness analyses have previously been conducted in a variety of studies of both healthy individuals (Lerch et al., 2006; Sowell et al., 2003; Walhovd et al., 2009) and subjects with FASD (Archibald et al., 2001; Astley et al., 2009a; Sowell et al., 2008b), providing valuable information. Using these techniques in conjunction with DTI in the same subjects may highlight patterns of regional development or abnormalities that are consistent across both white and gray matter, and will provide opportunities for examining correlations between DTI and other structural. Relationships between thickness, volume, cognition or behaviour indices, and DTI-derived parameters will give an even clearer overall picture of brain development and various abnormalities. Much of the healthy development and FASD data presented here has already been processed through FreeSurfer and cortical thickness analysis programs; analysis of the results is likely to provide additional interesting information about brain structure (e.g. cortical thinning in FASD subjects (Zhou et al., 2010)).

The two completed studies of FASD presented here provide information about brain abnormalities in children with FASD. It has been suggested that the gap in cognitive performance between individuals with FASD and their peers widens during adolescence compared to childhood, and it would be interesting to investigate whether brain development curves show similar results with increasing age. In that regard, additional subjects with FASD have been and continue to be recruited to fill in the age range of 13–30 years, as the studies described in Chapters 9 and 10 only examined children aged 5–13 years. Furthermore, as longitudinal studies provide increased sensitivity compared to cross-sectional designs and increase the power to detect differences or age-related changes, the initial participants in the FASD study are being asked to return for a follow-up scan. The longitudinal data already collected on typically developing children, adolescents, and young adults gives valuable information about healthy brain changes; longitudinal data on children and adolescents with FASD will provide a better understanding of differences in

developmental trajectories rather than just abnormalities at a particular point in time. With additional FASD subjects, it may also be possible to investigate brain differences among diagnostic categories of FASD (i.e. FAS, pFAS, SE, NBD) rather than simply between individuals with FASD and control subjects. The four-digit diagnostic code for FASD allows for even further separation of individuals, and correlations can be analyzed between each element of the diagnostic code (i.e. brain dysfunction, growth deficits, facial abnormalities, and alcohol exposure) and diffusion parameters. This allows for investigation of whether the brain abnormalities detected in subjects with FASD scale with the severity of the diagnosis.

In total, there are many additional methods that offer promise to detect previously unseen abnormalities or normal age-related changes in the data presented here. Ultimately, a combination of methods for DTI analysis, volumetrics and correlations with cognitive and behavioural measures will provide the most complete picture of structural brain development in both healthy individuals and abnormal conditions.

# Chapter 13

## Conclusions

Magnetic resonance imaging (MRI) provides a safe, non-invasive tool for investigation of normal, healthy brain changes. Diffusion tensor imaging (DTI) in particular, is an advanced MRI technique and a useful method for studying white matter microstructure because of its sensitivity. The data presented in this thesis demonstrate, using DTI, that healthy age-related changes vary regionally throughout the brain in both magnitude and rate of development. These changes occur non-linearly across the age span and the patterns of change are consistent in both cross-sectional and longitudinal studies. In general, the age-related trajectories are similar across hemispheres and between genders. The normative data provided here will be useful to identify brain abnormalities in various disease populations and developmental disorders.

One such developmental disorder is fetal alcohol spectrum disorder (FASD). FASD has considerable consequences for the individuals diagnosed with this condition, their caregivers and families, and in society. Yet, despite its prevalence ( $\sim 1\%$ ), it is relatively poorly understood. DTI has proven useful for studying this disorder, and was used here to demonstrate widespread brain abnormalities in children with FASD that presumably underlie the extensive cognitive, behavioural, and emotional abnormalities experienced by those with FASD. Understanding the brain differences in this disorder may ultimately help lead to earlier diagnoses, improved treatments, and better outcomes.

In addition to understanding brain structure itself and its age- or condition-related variations, it is useful to relate brain structure to cognition within both

typical and abnormal populations. Thus, an additional focus of this thesis was to examine correlations between a variety of cognitive abilities and diffusion parameters reflecting brain structure in both the healthy and FASD groups. Brain lateralization correlated with picture vocabulary and phonological processing performance in healthy children, while correlations between mathematical ability and white matter structure were observed in children with FASD. Another study of reading ability and brain structure across both populations is ongoing and preliminary results were described. These types of studies provide insight into the brain structure underlying intellectual abilities in the general population and in FASD, and may someday lead to advanced methods of evaluating treatments and interventions to improve cognitive performance.

In conclusion, DTI has allowed us to describe, in detail, healthy development across the lifespan as well as brain abnormalities in FASD. The results highlight regional patterns of change, as well as relationships between cognition and brain structure in both populations. When combined, behavioural, cognitive, and imaging data help provide a thorough understanding of both typical brain changes from childhood to old age, and abnormalities present in FASD — a serious, acquired brain disorder.

# Bibliography

- Abe, O, Aoki, S, Hayashi, N, Yamada, H, Kunimatsu, A, Mori, H, Yoshikawa, T, Okubo, T, and Ohtomo, K. Normal aging in the central nervous system: quantitative MR diffusion-tensor analysis. *Neurobiol Aging*, 23:433–41 (2002).
- Abel, EL and Sokol, RJ. Fetal alcohol syndrome is now leading cause of mental retardation. *Lancet*, 2:1222 (1986).
- Abel, EL and Sokol, RJ. Incidence of fetal alcohol syndrome and economic impact of FAS-related anomalies. *Drug Alcohol Depend*, 19:51–70 (1987).
- Abel, EL and Sokol, RJ. A revised conservative estimate of the incidence of FAS and its economic impact. *Alcohol Clin Exp Res*, 15:514–24 (1991).
- Aboitiz, F and Montiel, J. One hundred million years of interhemispheric communication: the history of the corpus callosum. *Braz J Med Biol Res*, 36:409–20 (2003).
- Aboitiz, F, Rodriguez, E, Olivares, R, and Zaidel, E. Age-related changes in fibre composition of the human corpus callosum: sex differences. *Neuroreport*, 7:1761–4 (1996).
- Aboitiz, F, Scheibel, AB, Fisher, RS, and Zaidel, E. Fiber composition of the human corpus callosum. *Brain Res*, 598:143–53 (1992).
- Aganj, I, Sapiro, G, Parikshak, N, Madsen, SK, and Thompson, PM. Measurement of cortical thickness from MRI by minimum line integrals on soft-classified tissue. *Hum Brain Mapp*, 30:3188–99 (2009).
- Alexander, AL, Lee, JE, Lazar, M, Boudos, R, DuBray, MB, Oakes, TR, Miller, JN, Lu, J, Jeong, EK, McMahon, WM, Bigler, ED, and Lainhart, JE. Diffusion tensor imaging of the corpus callosum in Autism. *Neuroimage*, 34:61–73 (2007a).
- Alexander, AL, Lee, JE, Lazar, M, and Field, AS. Diffusion tensor imaging of the brain. *Neurotherapeutics*, 4:316–29 (2007b).
- Alexander, DC. Multiple-fiber reconstruction algorithms for diffusion MRI. *Ann N Y Acad Sci*, 1064:113–33 (2005).
- Allen, LS, Richey, MF, Chai, YM, and Gorski, RA. Sex differences in the corpus callosum of the living human being. *J Neurosci*, 11:933–42 (1991).
- Anderson, AW. Measurement of fiber orientation distributions using high angular resolution diffusion imaging. *Magn Reson Med*, 54:1194–206 (2005).

- Andreasen, NC, Flaum, M, Swayze, n, V., O'Leary, DS, Alliger, R, Cohen, G, Ehrhardt, J, and Yuh, WT. Intelligence and brain structure in normal individuals. *Am J Psychiatry*, 150:130–4 (1993).
- Andrews, JS, Ben-Shachar, M, Yeatman, JD, Flom, LL, Luna, B, and Feldman, HM. Reading performance correlates with white-matter properties in preterm and term children. *Dev Med Child Neurol* (2009).
- Ansari, D and Dhital, B. Age-related changes in the activation of the intraparietal sulcus during nonsymbolic magnitude processing: an event-related functional magnetic resonance imaging study. *J Cogn Neurosci*, 18:1820–8 (2006).
- Archibald, SL, Fennema-Notestine, C, Gamst, A, Riley, EP, Mattson, SN, and Jernigan, TL. Brain dysmorphology in individuals with severe prenatal alcohol exposure. *Dev Med Child Neurol*, 43:148–54 (2001).
- Ardekani, S, Kumar, A, Bartzokis, G, and Sinha, U. Exploratory voxel-based analysis of diffusion indices and hemispheric asymmetry in normal aging. *Magn Reson Imaging*, 25:154–67 (2007).
- Ashburner, J and Friston, KJ. Voxel-based morphometry—the methods. *Neuroimage*, 11:805–21 (2000).
- Ashkenazi, S, Henik, A, Ifergane, G, and Shelef, I. Basic numerical processing in left intraparietal sulcus (IPS) acalculia. *Cortex*, 44:439–48 (2008).
- Ashtari, M, Cervellione, KL, Hasan, KM, Wu, J, McIlree, C, Kester, H, Ardekani, BA, Roofeh, D, Szeszko, PR, and Kumra, S. White matter development during late adolescence in healthy males: a cross-sectional diffusion tensor imaging study. *Neuroimage*, 35:501–10 (2007).
- Assaf, Y and Pasternak, O. Diffusion tensor imaging (DTI)-based white matter mapping in brain research: a review. *J Mol Neurosci*, 34:51–61 (2008).
- Astley, SJ. *Diagnositc Guide for Fetal Alcohol Spectrum Disorders: The 4-Digit Diagnostic Code*. Fetal Alcohol Syndrome Diagnostic and Prevention Network, University of Washington, Seattle (2004).
- Astley, SJ, Aylward, EH, Olson, HC, Kerns, K, Brooks, A, Coggins, TE, Davies, J, Dorn, S, Gendler, B, Jirikowic, T, Kraegel, P, Maravilla, K, and Richards, T. Magnetic Resonance Imaging Outcomes From a Comprehensive Magnetic Resonance Study of Children With Fetal Alcohol Spectrum Disorders. *Alcohol Clin Exp Res* (2009a).
- Astley, SJ, Olson, HC, Kerns, K, Brooks, A, Aylward, EH, Coggins, TE, Davies, J, Dorn, S, Gendler, B, Jirikowic, T, Kraegel, P, Maravilla, K, and Richards, T. Neuropsychological and behavioral outcomes from a comprehensive magnetic resonance study of children with fetal alcohol spectrum disorders. *Can J Clin Pharmacol*, 16:e178–201 (2009b).
- Astley, SJ, Richards, T, Aylward, EH, Olson, HC, Kerns, K, Brooks, A, Coggins, TE, Davies, J, Dorn, S, Gendler, B, Jirikowic, T, Kraegel, P, and Maravilla, K. Magnetic resonance spectroscopy outcomes from a comprehensive magnetic resonance study of children with fetal alcohol spectrum disorders. *Magn Reson Imaging*, 27:760–78 (2009c).

- Autti-Ramo, I, Autti, T, Korkman, M, Kettunen, S, Salonen, O, and Valanne, L. MRI findings in children with school problems who had been exposed prenatally to alcohol. *Dev Med Child Neurol*, 44:98–106 (2002).
- Autti-Ramo, I, Fagerlund, A, Ervalahti, N, Loimu, L, Korkman, M, and Hoyme, HE. Fetal alcohol spectrum disorders in Finland: clinical delineation of 77 older children and adolescents. *Am J Med Genet A*, 140:137–43 (2006).
- Baer, JS, Sampson, PD, Barr, HM, Connor, PD, and Streissguth, AP. A 21-year longitudinal analysis of the effects of prenatal alcohol exposure on young adult drinking. *Arch Gen Psychiatry*, 60:377–85 (2003).
- Baillieux, H, De Smet, HJ, Paquier, PF, De Deyn, PP, and Marien, P. Cerebellar neurocognition: insights into the bottom of the brain. *Clin Neurol Neurosurg*, 110:763–73 (2008).
- Balsamo, LM, Xu, B, Grandin, CB, Petrella, JR, Braniecki, SH, Elliott, TK, and Gaillard, WD. A functional magnetic resonance imaging study of left hemisphere language dominance in children. *Arch Neurol*, 59:1168–74 (2002).
- Barnea-Goraly, N, Eliez, S, Menon, V, Bammer, R, and Reiss, AL. Arithmetic ability and parietal alterations: a diffusion tensor imaging study in velocardiocardiofacial syndrome. *Brain Res Cogn Brain Res*, 25:735–40 (2005a).
- Barnea-Goraly, N, Menon, V, Eckert, M, Tamm, L, Bammer, R, Karchemskiy, A, Dant, CC, and Reiss, AL. White matter development during childhood and adolescence: a cross-sectional diffusion tensor imaging study. *Cereb Cortex*, 15:1848–54 (2005b).
- Barr, HM, Bookstein, FL, O'Malley, KD, Connor, PD, Huggins, JE, and Streissguth, AP. Binge drinking during pregnancy as a predictor of psychiatric disorders on the Structured Clinical Interview for DSM-IV in young adult offspring. *Am J Psychiatry*, 163:1061–5 (2006).
- Barr, HM and Streissguth, AP. Identifying maternal self-reported alcohol use associated with fetal alcohol spectrum disorders. *Alcohol Clin Exp Res*, 25:283–7 (2001).
- Basser, PJ, Mattiello, J, and LeBihan, D. MR diffusion tensor spectroscopy and imaging. *Biophys J*, 66:259–67 (1994).
- Basser, PJ, Pajevic, S, Pierpaoli, C, Duda, J, and Aldroubi, A. In vivo fiber tractography using DT-MRI data. *Magn Reson Med*, 44:625–32 (2000).
- Beaulieu, C. The basis of anisotropic water diffusion in the nervous system - a technical review. *NMR Biomed*, 15:435–55 (2002).
- Beaulieu, C, Plewes, C, Paulson, LA, Roy, D, Snook, L, Concha, L, and Phillips, L. Imaging brain connectivity in children with diverse reading ability. *Neuroimage*, 25:1266–71 (2005).
- Beaulieu, C, Plewes, C, Snook, L, Roy, D, Concha, L, and Phillips, L. Reading Ability Correlates with White Matter Anisotropy in Elementary School Children. In *Proceedings of the International Society for Magnetic Resonance in Medicine*. Seattle, Washington (2006).

- Behrens, TE, Woolrich, MW, Jenkinson, M, Johansen-Berg, H, Nunes, RG, Clare, S, Matthews, PM, Brady, JM, and Smith, SM. Characterization and propagation of uncertainty in diffusion-weighted MR imaging. *Magn Reson Med*, 50:1077–88 (2003).
- Ben Bashat, D, Ben Sira, L, Graif, M, Pianka, P, Hendler, T, Cohen, Y, and Assaf, Y. Normal white matter development from infancy to adulthood: comparing diffusion tensor and high b value diffusion weighted MR images. *J Magn Reson Imaging*, 21:503–11 (2005).
- Benes, FM. Myelination of cortical-hippocampal relays during late adolescence. *Schizophr Bull*, 15:585–93 (1989).
- Benes, FM, Turtle, M, Khan, Y, and Farol, P. Myelination of a key relay zone in the hippocampal formation occurs in the human brain during childhood, adolescence, and adulthood. *Arch Gen Psychiatry*, 51:477–84 (1994).
- Bhagat, YA and Beaulieu, C. Diffusion anisotropy in subcortical white matter and cortical gray matter: changes with aging and the role of CSF-suppression. *J Magn Reson Imaging*, 20:216–27 (2004).
- Binder, JR, Frost, JA, Hammeke, TA, Bellgowan, PS, Springer, JA, Kaufman, JN, and Possing, ET. Human temporal lobe activation by speech and nonspeech sounds. *Cereb Cortex*, 10:512–28 (2000).
- Bonekamp, D, Nagae, LM, Degaonkar, M, Matson, M, Abdalla, WM, Barker, PB, Mori, S, and Horska, A. Diffusion tensor imaging in children and adolescents: reproducibility, hemispheric, and age-related differences. *Neuroimage*, 34:733–42 (2007).
- Bookstein, FL, Connor, PD, Huggins, JE, Barr, HM, Pimentel, KD, and Streissguth, AP. Many infants prenatally exposed to high levels of alcohol show one particular anomaly of the corpus callosum. *Alcohol Clin Exp Res*, 31:868–79 (2007).
- Bookstein, FL, Sampson, PD, Streissguth, AP, and Connor, PD. Geometric morphometrics of corpus callosum and subcortical structures in the fetal-alcohol-affected brain. *Teratology*, 64:4–32 (2001).
- Brass, SD, Chen, NK, Mulkern, RV, and Bakshi, R. Magnetic resonance imaging of iron deposition in neurological disorders. *Top Magn Reson Imaging*, 17:31–40 (2006).
- Breier, JI, Hasan, KM, Zhang, W, Men, D, and Papanicolaou, AC. Language dysfunction after stroke and damage to white matter tracts evaluated using diffusion tensor imaging. *AJNR Am J Neuroradiol*, 29:483–7 (2008).
- Broca, P. Remarques sur le siege de la faculte du langage articule, suivies d’une observation d’aphemie (perte de la parole). *Bull Soc Anthropol*, 6:330–357 (1861).
- Brown, R. A brief account of microscopical observations made in the months of June, July, and August, 1827, on the particles contained in the pollen of plants; and on the general existence of active molecules in organic and inorganic bodies. *Philosophical Magazine NS*, 4:161–173 (1828).
- Brown, R. Additional remarks on active molecules. *Philosophical Magazine NS*, 6:161–166 (1829).

- Buchel, C, Raedler, T, Sommer, M, Sach, M, Weiller, C, and Koch, MA. White matter asymmetry in the human brain: a diffusion tensor MRI study. *Cereb Cortex*, 14:945–51 (2004).
- Bucur, B, Madden, DJ, Spaniol, J, Provenzale, JM, Cabeza, R, White, LE, and Huettel, SA. Age-related slowing of memory retrieval: contributions of perceptual speed and cerebral white matter integrity. *Neurobiol Aging*, 29:1070–9 (2008).
- Burton, MW, Small, SL, and Blumstein, SE. The role of segmentation in phonological processing: an fMRI investigation. *J Cogn Neurosci*, 12:679–90 (2000).
- Carr, HY and Purcell, EM. Effects of Diffusion on Free Precession in Nuclear Magnetic Resonance Experiments. *Physical Review*, 94:630–638 (1954).
- Catani, M, Allin, MP, Husain, M, Pugliese, L, Mesulam, MM, Murray, RM, and Jones, DK. Symmetries in human brain language pathways correlate with verbal recall. *Proc Natl Acad Sci U S A*, 104:17163–8 (2007).
- Catani, M, Howard, RJ, Pajevic, S, and Jones, DK. Virtual in vivo interactive dissection of white matter fasciculi in the human brain. *Neuroimage*, 17:77–94 (2002).
- Catani, M, Jones, DK, Donato, R, and Ffytche, DH. Occipito-temporal connections in the human brain. *Brain*, 126:2093–107 (2003).
- Caverhill-Godkewitsch, S, Lebel, C, and Beaulieu, C. Diffusion Tensor Tractography of Corpus Callosum Development Across the Lifespan. In *Proceedings of the International Society for Magnetic Resonance in Medicine*. Honolulu, Hawaii (2009).
- Chao, YP, Cho, KH, Yeh, CH, Chou, KH, Chen, JH, and Lin, CP. Probabilistic topography of human corpus callosum using cytoarchitectural parcellation and high angular resolution diffusion imaging tractography. *Hum Brain Mapp*, 30:3172–87 (2009).
- Chenevert, TL, Brunberg, JA, and Pipe, JG. Anisotropic diffusion in human white matter: demonstration with MR techniques in vivo. *Radiology*, 177:401–5 (1990).
- Chi, JG, Dooling, EC, and Gilles, FH. Left-right asymmetries of the temporal speech areas of the human fetus. *Arch Neurol*, 34:346–8 (1977).
- Chochon, F, Cohen, L, van de Moortele, PF, and Dehaene, S. Differential contributions of the left and right inferior parietal lobules to number processing. *J Cogn Neurosci*, 11:617–30 (1999).
- Chua, TC, Wen, W, Slavin, MJ, and Sachdev, PS. Diffusion tensor imaging in mild cognitive impairment and Alzheimer’s disease: a review. *Curr Opin Neurol*, 21:83–92 (2008).
- Chudley, AE, Conry, J, Cook, JL, Loock, C, Rosales, T, and LeBlanc, N. Fetal alcohol spectrum disorder: Canadian guidelines for diagnosis. *Cmaj*, 172:S1–S21 (2005).

- Clark, CM, Li, D, Conry, J, Conry, R, and Loock, C. Structural and functional brain integrity of fetal alcohol syndrome in nonretarded cases. *Pediatrics*, 105:1096–9 (2000).
- Clarren, SK, Alvord, J, E. C., Sumi, SM, Streissguth, AP, and Smith, DW. Brain malformations related to prenatal exposure to ethanol. *J Pediatr*, 92:64–7 (1978).
- Cloak, CC, Ernst, T, Fujii, L, Hedemark, B, and Chang, L. Lower diffusion in white matter of children with prenatal methamphetamine exposure. *Neurology*, 72:2068–75 (2009).
- Concha, L, Beaulieu, C, and Gross, DW. Bilateral limbic diffusion abnormalities in unilateral temporal lobe epilepsy. *Ann Neurol*, 57:188–96 (2005a).
- Concha, L, Gross, DW, and Beaulieu, C. Diffusion tensor tractography of the limbic system. *AJNR Am J Neuroradiol*, 26:2267–74 (2005b).
- Concha, L, Livy, DJ, Beaulieu, C, Wheatley, BM, and Gross, DW. In vivo diffusion tensor imaging and histopathology of the fimbria-fornix in temporal lobe epilepsy. *J Neurosci*, 30:996–1002 (2010).
- Conturo, TE, Lori, NF, Cull, TS, Akbudak, E, Snyder, AZ, Shimony, JS, McKinstry, RC, Burton, H, and Raichle, ME. Tracking neuronal fiber pathways in the living human brain. *Proc Natl Acad Sci U S A*, 96:10422–7 (1999).
- Cortese, BM, Moore, GJ, Bailey, BA, Jacobson, SW, Delaney-Black, V, and Hannigan, JH. Magnetic resonance and spectroscopic imaging in prenatal alcohol-exposed children: preliminary findings in the caudate nucleus. *Neurotoxicol Teratol*, 28:597–606 (2006).
- Davis, SW, Dennis, NA, Buchler, NG, White, LE, Madden, DJ, and Cabeza, R. Assessing the effects of age on long white matter tracts using diffusion tensor tractography. *Neuroimage*, 46:530–41 (2009).
- Davtian, M, Ulmer, JL, Mueller, WM, Gaggl, W, Mulane, MP, and Krouwer, HG. The superior longitudinal fasciculus and speech arrest. *J Comput Assist Tomogr*, 32:410–4 (2008).
- Dehaene, S, Molko, N, Cohen, L, and Wilson, AJ. Arithmetic and the brain. *Curr Opin Neurobiol*, 14:218–24 (2004).
- Dehaene, S, Piazza, M, Pinel, P, and Cohen, L. Three Parietal Circuits for Number Processing. *Cogn Neuropsychol*, 20:487–506 (2003).
- Dehaene, S, Spelke, E, Pinel, P, Stanescu, R, and Tsivkin, S. Sources of mathematical thinking: behavioral and brain-imaging evidence. *Science*, 284:970–4 (1999).
- Dehaene-Lambertz, G, Dehaene, S, and Hertz-Pannier, L. Functional neuroimaging of speech perception in infants. *Science*, 298:2013–5 (2002).
- Deipolyi, AR, Mukherjee, P, Gill, K, Henry, RG, Partridge, SC, Veeraraghavan, S, Jin, H, Lu, Y, Miller, SP, Ferriero, DM, Vigneron, DB, and Barkovich, AJ. Comparing microstructural and macrostructural development of the cerebral cortex in premature newborns: diffusion tensor imaging versus cortical gyration. *Neuroimage*, 27:579–86 (2005).

- Dejerine, J. *Anatomie des centres nerveux*. Masson, Paris (1895).
- Dekaban, AS. Changes in brain weights during the span of human life: relation of brain weights to body heights and body weights. *Ann Neurol*, 4:345–56 (1978).
- Deutsch, GK, Dougherty, RF, Bammer, R, Siok, WT, Gabrieli, JD, and Wandell, B. Children’s reading performance is correlated with white matter structure measured by diffusion tensor imaging. *Cortex*, 41:354–63 (2005).
- Doran, M, Hajnal, JV, Van Bruggen, N, King, MD, Young, IR, and Bydder, GM. Normal and abnormal white matter tracts shown by MR imaging using directional diffusion weighted sequences. *J Comput Assist Tomogr*, 14:865–73 (1990).
- Doron, KW and Gazzaniga, MS. Neuroimaging techniques offer new perspectives on callosal transfer and interhemispheric communication. *Cortex*, 44:1023–9 (2008).
- Dos Santos Sequeira, S, Woerner, W, Walter, C, Kreuder, F, Lueken, U, West-erhausen, R, Wittling, RA, Schweiger, E, and Wittling, W. Handedness, dichotic-listening ear advantage, and gender effects on planum temporale asymmetry—a volumetric investigation using structural magnetic resonance imaging. *Neuropsychologia*, 44:622–36 (2006).
- Douek, P, Turner, R, Pekar, J, Patronas, N, and Le Bihan, D. MR color mapping of myelin fiber orientation. *J Comput Assist Tomogr*, 15:923–9 (1991).
- Dougherty, RF, Ben-Shachar, M, Deutsch, GK, Hernandez, A, Fox, GR, and Wandell, BA. Temporal-callosal pathway diffusivity predicts phonological skills in children. *Proc Natl Acad Sci U S A*, 104:8556–61 (2007).
- Dronkers, NF, Plaisant, O, Iba-Zizen, MT, and Cabanis, EA. Paul Broca’s historic cases: high resolution MR imaging of the brains of Leborgne and Lelong. *Brain*, 130:1432–41 (2007).
- Dronkers, NF, Wilkins, DP, Van Valin, J, R. D., Redfern, BB, and Jaeger, JJ. Lesion analysis of the brain areas involved in language comprehension. *Cognition*, 92:145–77 (2004).
- Dubois, J, Dehaene-Lambertz, G, Perrin, M, Mangin, JF, Cointepas, Y, Duchesnay, E, Le Bihan, D, and Hertz-Pannier, L. Asynchrony of the early maturation of white matter bundles in healthy infants: quantitative landmarks revealed noninvasively by diffusion tensor imaging. *Hum Brain Mapp*, 29:14–27 (2008).
- Dubois, J, Hertz-Pannier, L, Dehaene-Lambertz, G, Cointepas, Y, and Le Bihan, D. Assessment of the early organization and maturation of infants’ cerebral white matter fiber bundles: a feasibility study using quantitative diffusion tensor imaging and tractography. *Neuroimage*, 30:1121–32 (2006).
- Egaas, B, Courchesne, E, and Saitoh, O. Reduced size of corpus callosum in autism. *Arch Neurol*, 52:794–801 (1995).
- Eger, E, Sterzer, P, Russ, MO, Giraud, AL, and Kleinschmidt, A. A supramodal number representation in human intraparietal cortex. *Neuron*, 37:719–25 (2003).

- Einstein, A. Über die von der molekularkinetischen Theorie der Wärme geforderte Bewegung von in ruhenden Flüssigkeiten suspendierten Teilchen. *Annalen der Physik*, 4:549–60 (1905).
- Eluvathingal, TJ, Hasan, KM, Kramer, L, Fletcher, JM, and Ewing-Cobbs, L. Quantitative diffusion tensor tractography of association and projection fibers in normally developing children and adolescents. *Cereb Cortex*, 17:2760–8 (2007).
- Everts, R, Lidzba, K, Wilke, M, Kiefer, C, Mordasini, M, Schroth, G, Perrig, W, and Steinlin, M. Strengthening of laterality of verbal and visuospatial functions during childhood and adolescence. *Hum Brain Mapp* (2008).
- Ewing-Cobbs, L, Prasad, MR, Swank, P, Kramer, L, Cox, J, C. S., Fletcher, JM, Barnes, M, Zhang, X, and Hasan, KM. Arrested development and disrupted callosal microstructure following pediatric traumatic brain injury: relation to neurobehavioral outcomes. *Neuroimage*, 42:1305–15 (2008).
- Fabiano, AJ, Horsfield, MA, and Bakshi, R. Interhemispheric asymmetry of brain diffusivity in normal individuals: a diffusion-weighted MR imaging study. *AJNR Am J Neuroradiol*, 26:1089–94 (2005).
- Fagerlund, A, Heikkinen, S, Autti-Ramo, I, Korkman, M, Timonen, M, Kuusi, T, Riley, EP, and Lundbom, N. Brain metabolic alterations in adolescents and young adults with fetal alcohol spectrum disorders. *Alcohol Clin Exp Res*, 30:2097–104 (2006).
- Fine, JG, Semrud-Clikeman, M, Keith, TZ, Stapleton, LM, and Hynd, GW. Reading and the corpus callosum: an MRI family study of volume and area. *Neuropsychology*, 21:235–41 (2007).
- Fischl, B, Salat, DH, Busa, E, Albert, M, Dieterich, M, Haselgrove, C, van der Kouwe, A, Killiany, R, Kennedy, D, Klaveness, S, Montillo, A, Makris, N, Rosen, B, and Dale, AM. Whole brain segmentation: automated labeling of neuroanatomical structures in the human brain. *Neuron*, 33:341–55 (2002).
- Frey, S, Campbell, JS, Pike, GB, and Petrides, M. Dissociating the human language pathways with high angular resolution diffusion fiber tractography. *J Neurosci*, 28:11435–44 (2008).
- Frye, RE, Hasan, K, Xue, L, Strickland, D, Malmberg, B, Liederman, J, and Papanicolaou, A. Splenium microstructure is related to two dimensions of reading skill. *Neuroreport*, 19:1627–31 (2008).
- Fryer, SL, Schweinsburg, BC, Bjorkquist, OA, Frank, LR, Mattson, SN, Spadoni, AD, and Riley, EP. Characterization of White Matter Microstructure in Fetal Alcohol Spectrum Disorders. *Alcohol Clin Exp Res*, 33:514–21 (2009).
- Fryer, SL, Tapert, SF, Mattson, SN, Paulus, MP, Spadoni, AD, and Riley, EP. Prenatal alcohol exposure affects frontal-striatal BOLD response during inhibitory control. *Alcohol Clin Exp Res*, 31:1415–24 (2007).
- Gaillard, WD, Pugliese, M, Grandin, CB, Braniecki, SH, Kondapaneni, P, Hunter, K, Xu, B, Petrella, JR, Balsamo, L, and Basso, G. Cortical localization of reading in normal children: an fMRI language study. *Neurology*, 57:47–54 (2001).

- Galaburda, AM, LeMay, M, Kemper, TL, and Geschwind, N. Right-left asymmetries in the brain. *Science*, 199:852–6 (1978).
- Galuske, RA, Schlote, W, Bratzke, H, and Singer, W. Interhemispheric asymmetries of the modular structure in human temporal cortex. *Science*, 289:1946–9 (2000).
- Gazzaniga, MS. Principles of human brain organization derived from split-brain studies. *Neuron*, 14:217–28 (1995).
- Geschwind, N. The organization of language and the brain. *Science*, 170:940–4 (1970).
- Geschwind, N and Levitsky, W. Human brain: left-right asymmetries in temporal speech region. *Science*, 161:186–7 (1968).
- Giedd, JN, Blumenthal, J, Jeffries, NO, Castellanos, FX, Liu, H, Zijdenbos, A, Paus, T, Evans, AC, and Rapoport, JL. Brain development during childhood and adolescence: a longitudinal MRI study. *Nat Neurosci*, 2:861–3 (1999a).
- Giedd, JN, Blumenthal, J, Jeffries, NO, Rajapakse, JC, Vaituzis, AC, Liu, H, Berry, YC, Tobin, M, Nelson, J, and Castellanos, FX. Development of the human corpus callosum during childhood and adolescence: a longitudinal MRI study. *Prog Neuropsychopharmacol Biol Psychiatry*, 23:571–88 (1999b).
- Giorgio, A, Watkins, KE, Chadwick, M, James, S, Winmill, L, Douaud, G, De Stefano, N, Matthews, PM, Smith, SM, Johansen-Berg, H, and James, AC. Longitudinal changes in grey and white matter during adolescence. *Neuroimage*, 49:94–103 (2010).
- Giorgio, A, Watkins, KE, Douaud, G, James, AC, James, S, De Stefano, N, Matthews, PM, Smith, SM, and Johansen-Berg, H. Changes in white matter microstructure during adolescence. *Neuroimage*, 39:52–61 (2008).
- Glasser, MF and Rilling, JK. DTI Tractography of the Human Brain’s Language Pathways. *Cereb Cortex* (2008).
- Golabchi, FN, Brooks, DH, Hoge, WS, De Girolami, U, and Maier, SE. Pixel-based comparison of spinal cord MR diffusion anisotropy with axon packing parameters. *Magn Reson Med*, 63:1510–9 (2010).
- Goldschmidt, L, Richardson, GA, Stoffer, DS, Geva, D, and Day, NL. Prenatal alcohol exposure and academic achievement at age six: a nonlinear fit. *Alcohol Clin Exp Res*, 20:763–70 (1996).
- Gong, G, Jiang, T, Zhu, C, Zang, Y, He, Y, Xie, S, and Xiao, J. Side and handedness effects on the cingulum from diffusion tensor imaging. *Neuroreport*, 16:1701–5 (2005).
- Good, CD, Johnsrude, I, Ashburner, J, Henson, RN, Friston, KJ, and Frackowiak, RS. Cerebral asymmetry and the effects of sex and handedness on brain structure: a voxel-based morphometric analysis of 465 normal adult human brains. *Neuroimage*, 14:685–700 (2001a).
- Good, CD, Johnsrude, IS, Ashburner, J, Henson, RN, Friston, KJ, and Frackowiak, RS. A voxel-based morphometric study of ageing in 465 normal adult human brains. *Neuroimage*, 14:21–36 (2001b).

- Guerri, C, Pascual, M, and Renau-Piqueras, J. Glia and fetal alcohol syndrome. *Neurotoxicology*, 22:593–9 (2001).
- Gulani, V, Webb, AG, Duncan, ID, and Lauterbur, PC. Apparent diffusion tensor measurements in myelin-deficient rat spinal cords. *Magn Reson Med*, 45:191–5 (2001).
- Gur, RC, Packer, IK, Hungerbuhler, JP, Reivich, M, Obrist, WD, Amarnek, WS, and Sackeim, HA. Differences in the distribution of gray and white matter in human cerebral hemispheres. *Science*, 207:1226–8 (1980).
- Hagmann, P, Cammoun, L, Martuzzi, R, Maeder, P, Clarke, S, Thiran, JP, and Meuli, R. Hand preference and sex shape the architecture of language networks. *Hum Brain Mapp*, 27:828–35 (2006).
- Hahn, EL. Spin Echoes. *Physical Review*, 77:746–746 (1950).
- Hasan, KM, Ewing-Cobbs, L, Kramer, LA, Fletcher, JM, and Narayana, PA. Diffusion tensor quantification of the macrostructure and microstructure of human midsagittal corpus callosum across the lifespan. *NMR Biomed*, 21:1094–101 (2008a).
- Hasan, KM, Iftikhar, A, Kamali, A, Kramer, LA, Ashtari, M, Cirino, PT, Papanicolaou, AC, Fletcher, JM, and Ewing-Cobbs, L. Development and aging of the healthy human brain uncinate fasciculus across the lifespan using diffusion tensor tractography. *Brain Res*, 1276:67–76 (2009a).
- Hasan, KM, Kamali, A, Abid, H, Kramer, LA, Fletcher, JM, and Ewing-Cobbs, L. Quantification of the spatiotemporal microstructural organization of the human brain association, projection and commissural pathways across the lifespan using diffusion tensor tractography. *Brain Struct Funct*, 214:361–73 (2010).
- Hasan, KM, Kamali, A, Iftikhar, A, Kramer, LA, Papanicolaou, AC, Fletcher, JM, and Ewing-Cobbs, L. Diffusion tensor tractography quantification of the human corpus callosum fiber pathways across the lifespan. *Brain Res*, 1249:91–100 (2009b).
- Hasan, KM, Kamali, A, Kramer, LA, Papanicolaou, AC, Fletcher, JM, and Ewing-Cobbs, L. Diffusion tensor quantification of the human midsagittal corpus callosum subdivisions across the lifespan. *Brain Res*, 1227:52–67 (2008b).
- Hasan, KM, Sankar, A, Halphen, C, Kramer, LA, Brandt, ME, Juranek, J, Cirino, PT, Fletcher, JM, Papanicolaou, AC, and Ewing-Cobbs, L. Development and organization of the human brain tissue compartments across the lifespan using diffusion tensor imaging. *Neuroreport*, 18:1735–9 (2007).
- Hermoye, L, Saint-Martin, C, Cosnard, G, Lee, SK, Kim, J, Nassogne, MC, Menten, R, Clapuyt, P, Donohue, PK, Hua, K, Wakana, S, Jiang, H, van Zijl, PC, and Mori, S. Pediatric diffusion tensor imaging: normal database and observation of the white matter maturation in early childhood. *Neuroimage*, 29:493–504 (2006).
- Hess, CP, Mukherjee, P, Han, ET, Xu, D, and Vigneron, DB. Q-ball reconstruction of multimodal fiber orientations using the spherical harmonic basis. *Magn Reson Med*, 56:104–17 (2006).

- Hoefft, F, Barnea-Goraly, N, Haas, BW, Golarai, G, Ng, D, Mills, D, Korenberg, J, Bellugi, U, Galaburda, A, and Reiss, AL. More is not always better: increased fractional anisotropy of superior longitudinal fasciculus associated with poor visuospatial abilities in Williams syndrome. *J Neurosci*, 27:11960–5 (2007).
- Hofer, S and Frahm, J. Topography of the human corpus callosum revisited—comprehensive fiber tractography using diffusion tensor magnetic resonance imaging. *Neuroimage*, 32:989–94 (2006).
- Holland, SK, Vannest, J, Mecoli, M, Jacola, LM, Tillema, JM, Karunanayaka, PR, Schmithorst, VJ, Yuan, W, Plante, E, and Byars, AW. Functional MRI of language lateralization during development in children. *Int J Audiol*, 46:533–51 (2007).
- Hoon, J, A. H., Stashinko, EE, Nagae, LM, Lin, DD, Keller, J, Bastian, A, Campbell, ML, Levey, E, Mori, S, and Johnston, MV. Sensory and motor deficits in children with cerebral palsy born preterm correlate with diffusion tensor imaging abnormalities in thalamocortical pathways. *Dev Med Child Neurol*, 51:697–704 (2009).
- Hourani, R, El-Hajj, T, Barada, WH, Hourani, M, and Yamout, BI. MR imaging findings in autosomal recessive hereditary spastic paraplegia. *AJNR Am J Neuroradiol*, 30:936–40 (2009).
- Howell, KK, Lynch, ME, Platzman, KA, Smith, GH, and Coles, CD. Prenatal alcohol exposure and ability, academic achievement, and school functioning in adolescence: a longitudinal follow-up. *J Pediatr Psychol*, 31:116–26 (2006).
- Hsu, JL, Leemans, A, Bai, CH, Lee, CH, Tsai, YF, Chiu, HC, and Chen, WH. Gender differences and age-related white matter changes of the human brain: a diffusion tensor imaging study. *Neuroimage*, 39:566–77 (2008).
- Hsu, JL, Van Hecke, W, Bai, CH, Lee, CH, Tsai, YF, Chiu, HC, Jaw, FS, Hsu, CY, Leu, JG, Chen, WH, and Leemans, A. Microstructural white matter changes in normal aging: a diffusion tensor imaging study with higher-order polynomial regression models. *Neuroimage*, 49:32–43 (2010).
- Huang, H, Zhang, J, Jiang, H, Wakana, S, Poetscher, L, Miller, MI, van Zijl, PC, Hillis, AE, Wytik, R, and Mori, S. DTI tractography based parcellation of white matter: application to the mid-sagittal morphology of corpus callosum. *Neuroimage*, 26:195–205 (2005).
- Hughes, PD, Kim, YN, Randall, PK, and Leslie, SW. Effect of prenatal ethanol exposure on the developmental profile of the NMDA receptor subunits in rat forebrain and hippocampus. *Alcohol Clin Exp Res*, 22:1255–61 (1998).
- Hutchinson, AD, Mathias, JL, Jacobson, BL, Ruzic, L, Bond, AN, and Banich, MT. Relationship between intelligence and the size and composition of the corpus callosum. *Exp Brain Res*, 192:455–64 (2009).
- Huttenlocher, PR. Synaptic density in human frontal cortex - developmental changes and effects of aging. *Brain Res*, 163:195–205 (1979).
- Huttenlocher, PR and de Courten, C. The development of synapses in striate cortex of man. *Hum Neurobiol*, 6:1–9 (1987).

- Hutton, C, De Vita, E, Ashburner, J, Deichmann, R, and Turner, R. Voxel-based cortical thickness measurements in MRI. *Neuroimage*, 40:1701–10 (2008).
- Ikonomidou, C, Bittigau, P, Koch, C, Genz, K, Hoerster, F, Felderhoff-Mueser, U, Tenkova, T, Dikranian, K, and Olney, JW. Neurotransmitters and apoptosis in the developing brain. *Biochem Pharmacol*, 62:401–5 (2001).
- Isaacs, EB, Edmonds, CJ, Lucas, A, and Gadian, DG. Calculation difficulties in children of very low birthweight: a neural correlate. *Brain*, 124:1701–7 (2001).
- Jacobsen, LK, Picciotto, MR, Heath, CJ, Frost, SJ, Tsou, KA, Dwan, RA, Jackowski, MP, Constable, RT, and Mencl, WE. Prenatal and adolescent exposure to tobacco smoke modulates the development of white matter microstructure. *J Neurosci*, 27:13491–8 (2007).
- Jacobson, JL and Jacobson, SW. Effects of prenatal alcohol exposure on child development. *Alcohol Res Health*, 26:282–6 (2002).
- Jeret, JS, Serur, D, Wisniewski, KE, and Lubin, RA. Clinicopathological findings associated with agenesis of the corpus callosum. *Brain Dev*, 9:255–64 (1987).
- Johansen-Berg, H, Della-Maggiore, V, Behrens, TE, Smith, SM, and Paus, T. Integrity of white matter in the corpus callosum correlates with bimanual co-ordination skills. *Neuroimage*, 36 Suppl 2:T16–21 (2007).
- Jones, DK. The effect of gradient sampling schemes on measures derived from diffusion tensor MRI: a Monte Carlo study. *Magn Reson Med*, 51:807–15 (2004).
- Jones, DK. Studying connections in the living human brain with diffusion MRI. *Cortex*, 44:936–52 (2008).
- Jones, DK and Pierpaoli, C. Confidence mapping in diffusion tensor magnetic resonance imaging tractography using a bootstrap approach. *Magn Reson Med*, 53:1143–9 (2005).
- Jones, DK, Simmons, A, Williams, SC, and Horsfield, MA. Non-invasive assessment of axonal fiber connectivity in the human brain via diffusion tensor MRI. *Magn Reson Med*, 42:37–41 (1999).
- Jones, DK, Symms, MR, Cercignani, M, and Howard, RJ. The effect of filter size on VBM analyses of DT-MRI data. *Neuroimage*, 26:546–54 (2005).
- Jones, KL and Smith, DW. Recognition of the fetal alcohol syndrome in early infancy. *Lancet*, 2:999–1001 (1973).
- Jung, RE and Haier, RJ. The Parieto-Frontal Integration Theory (P-FIT) of intelligence: converging neuroimaging evidence. *Behav Brain Sci*, 30:135–54; discussion 154–87 (2007).
- Jung, RE, Haier, RJ, Yeo, RA, Rowland, LM, Petropoulos, H, Levine, AS, Sibbitt, WL, and Brooks, WM. Sex differences in N-acetylaspartate correlates of general intelligence: an 1H-MRS study of normal human brain. *Neuroimage*, 26:965–72 (2005).

- Kail, R. Processing time decreases globally at an exponential rate during childhood and adolescence. *J Exp Child Psychol*, 56:254–65 (1993).
- Kalberg, WO, Provost, B, Tollison, SJ, Tabachnick, BG, Robinson, LK, Eugene Hoyne, H, Trujillo, PM, Buckley, D, Aragon, AS, and May, PA. Comparison of motor delays in young children with fetal alcohol syndrome to those with prenatal alcohol exposure and with no prenatal alcohol exposure. *Alcohol Clin Exp Res*, 30:2037–45 (2006).
- Kanaan, RA, Shergill, SS, Barker, GJ, Catani, M, Ng, VW, Howard, R, McGuire, PK, and Jones, DK. Tract-specific anisotropy measurements in diffusion tensor imaging. *Psychiatry Res*, 146:73–82 (2006).
- Kansaku, K and Kitazawa, S. Imaging studies on sex differences in the lateralization of language. *Neurosci Res*, 41:333–7 (2001).
- Karl, PI, Kwun, R, Slonim, A, and Fisher, SE. Ethanol elevates fetal serum glutamate levels in the rat. *Alcohol Clin Exp Res*, 19:177–81 (1995).
- Kawashima, R, Taira, M, Okita, K, Inoue, K, Tajima, N, Yoshida, H, Sasaki, T, Sugiura, M, Watanabe, J, and Fukuda, H. A functional MRI study of simple arithmetic—a comparison between children and adults. *Brain Res Cogn Brain Res*, 18:227–33 (2004).
- Keller, TA and Just, MA. Altering cortical connectivity: remediation-induced changes in the white matter of poor readers. *Neuron*, 64:624–31 (2009).
- Kier, EL, Staib, LH, Davis, LM, and Bronen, RA. MR imaging of the temporal stem: anatomic dissection tractography of the uncinate fasciculus, inferior occipitofrontal fasciculus, and Meyer’s loop of the optic radiation. *AJNR Am J Neuroradiol*, 25:677–91 (2004).
- Kim, EY, Kim, DH, Yoo, E, Park, HJ, Golay, X, Lee, SK, Kim, DJ, Kim, J, and Kim, DI. Visualization of maturation of the corpus callosum during childhood and adolescence using T2 relaxometry. *Int J Dev Neurosci*, 25:409–14 (2007).
- Klingberg, T, Hedehus, M, Temple, E, Salz, T, Gabrieli, JD, Moseley, ME, and Poldrack, RA. Microstructure of temporo-parietal white matter as a basis for reading ability: evidence from diffusion tensor magnetic resonance imaging. *Neuron*, 25:493–500 (2000).
- Kochunov, P, Williamson, DE, Lancaster, J, Fox, P, Cornell, J, Blangero, J, and Glahn, DC. Fractional anisotropy of water diffusion in cerebral white matter across the lifespan. *Neurobiol Aging* (2010).
- Kontis, D, Catani, M, Cuddy, M, Walshe, M, Nosarti, C, Jones, D, Wyatt, J, Rifkin, L, Murray, R, and Allin, M. Diffusion tensor MRI of the corpus callosum and cognitive function in adults born preterm. *Neuroreport*, 20:424–8 (2009).
- Kopera-Frye, K, Dehaene, S, and Streissguth, AP. Impairments of number processing induced by prenatal alcohol exposure. *Neuropsychologia*, 34:1187–96 (1996).
- Kretschmann, HJ. Localisation of the corticospinal fibres in the internal capsule in man. *J Anat*, 160:219–25 (1988).

- Kubicki, M, Park, H, Westin, CF, Nestor, PG, Mulkern, RV, Maier, SE, Niznikiewicz, M, Connor, EE, Levitt, JJ, Frumin, M, Kikinis, R, Jolesz, FA, McCarley, RW, and Shenton, ME. DTI and MTR abnormalities in schizophrenia: analysis of white matter integrity. *Neuroimage*, 26:1109–18 (2005).
- Kubicki, M, Westin, CF, Maier, SE, Frumin, M, Nestor, PG, Salisbury, DF, Kikinis, R, Jolesz, FA, McCarley, RW, and Shenton, ME. Uncinate fasciculus findings in schizophrenia: a magnetic resonance diffusion tensor imaging study. *Am J Psychiatry*, 159:813–20 (2002).
- Kucian, K, Loenneker, T, Dietrich, T, Dosch, M, Martin, E, and von Aster, M. Impaired neural networks for approximate calculation in dyscalculic children: a functional MRI study. *Behav Brain Funct*, 2:31 (2006).
- Kumada, T, Jiang, Y, Cameron, DB, and Komuro, H. How does alcohol impair neuronal migration? *J Neurosci Res*, 85:465–70 (2007).
- Kyriakopoulos, M, Bargiotas, T, Barker, GJ, and Frangou, S. Diffusion tensor imaging in schizophrenia. *Eur Psychiatry*, 23:255–73 (2008).
- Landman, BA, Farrell, JA, Jones, CK, Smith, SA, Prince, JL, and Mori, S. Effects of diffusion weighting schemes on the reproducibility of DTI-derived fractional anisotropy, mean diffusivity, and principal eigenvector measurements at 1.5T. *Neuroimage*, 36:1123–38 (2007).
- Lazar, M and Alexander, AL. Bootstrap white matter tractography (BOOT-TRAC). *Neuroimage*, 24:524–32 (2005).
- Le Bihan, D. Looking into the functional architecture of the brain with diffusion MRI. *Nat Rev Neurosci*, 4:469–80 (2003).
- Lebel, C and Beaulieu, C. Lateralization of the arcuate fasciculus from childhood to adulthood and its relation to cognitive abilities in children. *Hum Brain Mapp*, 30:3563–73 (2009).
- Lebel, C, Caverhill-Godkewitsch, S, and Beaulieu, C. Age-related regional variations of the corpus callosum identified by diffusion tensor tractography. *Neuroimage*, 52:20–31 (2010).
- Lebel, C, Rasmussen, C, Wyper, K, Walker, L, Andrew, G, Yager, J, and Beaulieu, C. Brain diffusion abnormalities in children with fetal alcohol spectrum disorder. *Alcohol Clin Exp Res*, 32:1732–40 (2008a).
- Lebel, C, Walker, L, Leemans, A, Phillips, L, and Beaulieu, C. Microstructural maturation of the human brain from childhood to adulthood. *Neuroimage*, 40:1044–55 (2008b).
- Lee, B, Park, JY, Jung, WH, Kim, HS, Oh, JS, Choi, CH, Jang, JH, Kang, DH, and Kwon, JS. White matter neuroplastic changes in long-term trained players of the game of "Baduk" (GO): a voxel-based diffusion-tensor imaging study. *Neuroimage*, 52:9–19 (2010).
- Lemoine, P, Harousseau, H, Borteyru, J, and Menuet, J. Les enfants de parents alcooliques. Anomalies observees. A propos de 127 cas. *Ouest Med*, 21:476–82 (1968).

- Lemons, D. *An introduction to stochastic processes in physics*. Johns Hopkins University Press, Baltimore (2002).
- Lenroot, RK, Gogtay, N, Greenstein, DK, Wells, EM, Wallace, GL, Clasen, LS, Blumenthal, JD, Lerch, J, Zijdenbos, AP, Evans, AC, Thompson, PM, and Giedd, JN. Sexual dimorphism of brain developmental trajectories during childhood and adolescence. *Neuroimage*, 36:1065–73 (2007).
- Lerch, JP, Worsley, K, Shaw, WP, Greenstein, DK, Lenroot, RK, Giedd, J, and Evans, AC. Mapping anatomical correlations across cerebral cortex (MACACC) using cortical thickness from MRI. *Neuroimage*, 31:993–1003 (2006).
- Li, L, Coles, CD, Lynch, ME, and Hu, X. Voxelwise and skeleton-based region of interest analysis of fetal alcohol syndrome and fetal alcohol spectrum disorders in young adults. *Hum Brain Mapp* (2009).
- Luders, E, Narr, KL, Hamilton, LS, Phillips, OR, Thompson, PM, Valle, JS, Del’Homme, M, Strickland, T, McCracken, JT, Toga, AW, and Levitt, JG. Decreased callosal thickness in attention-deficit/hyperactivity disorder. *Biol Psychiatry*, 65:84–8 (2009).
- Luna, B, Garver, KE, Urban, TA, Lazar, NA, and Sweeney, JA. Maturation of cognitive processes from late childhood to adulthood. *Child Dev*, 75:1357–72 (2004).
- Ma, W, Li, BS, Maric, D, Zhao, WQ, Lin, HJ, Zhang, L, Pant, HC, and Barker, JL. Ethanol blocks both basic fibroblast growth factor- and carbachol-mediated neuroepithelial cell expansion with differential effects on carbachol-activated signaling pathways. *Neuroscience*, 118:37–47 (2003).
- Ma, X, Coles, CD, Lynch, ME, Laconte, SM, Zurkiya, O, Wang, D, and Hu, X. Evaluation of corpus callosum anisotropy in young adults with fetal alcohol syndrome according to diffusion tensor imaging. *Alcohol Clin Exp Res*, 29:1214–22 (2005).
- MacDonald, D, Kabani, N, Avis, D, and Evans, AC. Automated 3-D extraction of inner and outer surfaces of cerebral cortex from MRI. *Neuroimage*, 12:340–56 (2000).
- Makris, N, Kennedy, DN, McInerney, S, Sorensen, AG, Wang, R, Caviness, J, V. S., and Pandya, DN. Segmentation of subcomponents within the superior longitudinal fascicle in humans: a quantitative, in vivo, DT-MRI study. *Cereb Cortex*, 15:854–69 (2005).
- Marslen-Wilson, WD and Tyler, LK. Morphology, language and the brain: the decompositional substrate for language comprehension. *Philos Trans R Soc Lond B Biol Sci*, 362:823–36 (2007).
- Matsumoto, R, Okada, T, Mikuni, N, Mitsueda-Ono, T, Taki, J, Sawamoto, N, Hanakawa, T, Miki, Y, Hashimoto, N, Fukuyama, H, Takahashi, R, and Ikeda, A. Hemispheric asymmetry of the arcuate fasciculus : A preliminary diffusion tensor tractography study in patients with unilateral language dominance defined by Wada test. *J Neurol* (2008).
- Mattson, SN and Riley, EP. A review of the neurobehavioral deficits in children with fetal alcohol syndrome or prenatal exposure to alcohol. *Alcohol Clin Exp Res*, 22:279–94 (1998).

- Mattson, SN, Riley, EP, Sowell, ER, Jernigan, TL, Sobel, DF, and Jones, KL. A decrease in the size of the basal ganglia in children with fetal alcohol syndrome. *Alcohol Clin Exp Res*, 20:1088–93 (1996).
- May, PA and Gossage, JP. Estimating the prevalence of fetal alcohol syndrome. A summary. *Alcohol Res Health*, 25:159–67 (2001).
- McKinstry, RC, Mathur, A, Miller, JH, Ozcan, A, Snyder, AZ, Schefft, GL, Almlı, CR, Shiran, SI, Conturo, TE, and Neil, JJ. Radial organization of developing preterm human cerebral cortex revealed by non-invasive water diffusion anisotropy MRI. *Cereb Cortex*, 12:1237–43 (2002).
- McLaughlin, NC, Paul, RH, Grieve, SM, Williams, LM, Laidlaw, D, DiCarlo, M, Clark, CR, Whelihan, W, Cohen, RA, Whitford, TJ, and Gordon, E. Diffusion tensor imaging of the corpus callosum: a cross-sectional study across the lifespan. *Int J Dev Neurosci*, 25:215–21 (2007).
- Mennerick, S and Zorumski, CF. Neural activity and survival in the developing nervous system. *Mol Neurobiol*, 22:41–54 (2000).
- Mielke, MM, Kozauer, NA, Chan, KC, George, M, Toroney, J, Zerrate, M, Bandeen-Roche, K, Wang, MC, Vanzijl, P, Pekar, JJ, Mori, S, Lyketsos, CG, and Albert, M. Regionally-specific diffusion tensor imaging in mild cognitive impairment and Alzheimer’s disease. *Neuroimage*, 46:47–55 (2009).
- Miller, MW. Effects of alcohol on the generation and migration of cerebral cortical neurons. *Science*, 233:1308–11 (1986).
- Mills, R. Self-Diffusion in Normal and Heavy-Water in Range 1-45 Degrees. *Journal of Physical Chemistry*, 77:685–688 (1973).
- Molko, N, Cachia, A, Riviere, D, Mangin, JF, Bruandet, M, Le Bihan, D, Cohen, L, and Dehaene, S. Functional and structural alterations of the intraparietal sulcus in a developmental dyscalculia of genetic origin. *Neuron*, 40:847–58 (2003).
- Mori, S, Crain, BJ, Chacko, VP, and van Zijl, PC. Three-dimensional tracking of axonal projections in the brain by magnetic resonance imaging. *Ann Neurol*, 45:265–9 (1999).
- Morriss, MC, Zimmerman, RA, Bilaniuk, LT, Hunter, JV, and Haselgrove, JC. Changes in brain water diffusion during childhood. *Neuroradiology*, 41:929–34 (1999).
- Moseley, M. Diffusion tensor imaging and aging - a review. *NMR Biomed*, 15:553–60 (2002).
- Mukherjee, P, Miller, JH, Shimony, JS, Conturo, TE, Lee, BC, Almlı, CR, and McKinstry, RC. Normal brain maturation during childhood: developmental trends characterized with diffusion-tensor MR imaging. *Radiology*, 221:349–58 (2001).
- Mukherjee, P, Miller, JH, Shimony, JS, Philip, JV, Nehra, D, Snyder, AZ, Conturo, TE, Neil, JJ, and McKinstry, RC. Diffusion-tensor MR imaging of gray and white matter development during normal human brain maturation. *AJNR Am J Neuroradiol*, 23:1445–56 (2002).

- Mukherjee, RA, Hollins, S, and Turk, J. Fetal alcohol spectrum disorder: an overview. *J R Soc Med*, 99:298–302 (2006).
- Nagy, Z, Westerberg, H, and Klingberg, T. Maturation of white matter is associated with the development of cognitive functions during childhood. *J Cogn Neurosci*, 16:1227–33 (2004).
- Neil, J, Miller, J, Mukherjee, P, and Huppi, PS. Diffusion tensor imaging of normal and injured developing human brain - a technical review. *NMR Biomed*, 15:543–52 (2002).
- Nelson, E. *Dynamical theories of Brownian motion*. Princeton University Press, Princeton, 2 edition (2001).
- Ni, H, Kavcic, V, Zhu, T, Ekholm, S, and Zhong, J. Effects of number of diffusion gradient directions on derived diffusion tensor imaging indices in human brain. *AJNR Am J Neuroradiol*, 27:1776–81 (2006).
- Niogi, SN and McCandliss, BD. Left lateralized white matter microstructure accounts for individual differences in reading ability and disability. *Neuropsychologia*, 44:2178–88 (2006).
- Nucifora, PG, Verma, R, Melhem, ER, Gur, RE, and Gur, RC. Leftward asymmetry in relative fiber density of the arcuate fasciculus. *Neuroreport*, 16:791–4 (2005).
- Odegard, TN, Farris, EA, Ring, J, McColl, R, and Black, J. Brain connectivity in non-reading impaired children and children diagnosed with developmental dyslexia. *Neuropsychologia*, 47:1972–7 (2009).
- O'Donnell, LJ and Westin, CF. Automatic tractography segmentation using a high-dimensional white matter atlas. *IEEE Trans Med Imaging*, 26:1562–75 (2007).
- Olney, JW. Fetal alcohol syndrome at the cellular level. *Addict Biol*, 9:137–49; discussion 151 (2004).
- Ota, M, Obata, T, Akine, Y, Ito, H, Ikehira, H, Asada, T, and Suhara, T. Age-related degeneration of corpus callosum measured with diffusion tensor imaging. *Neuroimage*, 31:1445–52 (2006).
- Ozer, E, Sarioglu, S, and Gure, A. Effects of prenatal ethanol exposure on neuronal migration, neuronogenesis and brain myelination in the mice brain. *Clin Neuropathol*, 19:21–5 (2000).
- Park, HJ, Westin, CF, Kubicki, M, Maier, SE, Niznikiewicz, M, Baer, A, Frumin, M, Kikinis, R, Jolesz, FA, McCarley, RW, and Shenton, ME. White matter hemisphere asymmetries in healthy subjects and in schizophrenia: a diffusion tensor MRI study. *Neuroimage*, 23:213–23 (2004).
- Parker, GJ, Haroon, HA, and Wheeler-Kingshott, CA. A framework for a streamline-based probabilistic index of connectivity (PICO) using a structural interpretation of MRI diffusion measurements. *J Magn Reson Imaging*, 18:242–54 (2003).
- Parker, GJ, Luzzi, S, Alexander, DC, Wheeler-Kingshott, CA, Ciccarelli, O, and Lambon Ralph, MA. Lateralization of ventral and dorsal auditory-language pathways in the human brain. *Neuroimage*, 24:656–66 (2005).

- Parker, J, Mitchell, A, Kalpakidou, A, Walshe, M, Jung, HY, Nosarti, C, Santosh, P, Rifkin, L, Wyatt, J, Murray, RM, and Allin, M. Cerebellar growth and behavioural and neuropsychological outcome in preterm adolescents. *Brain*, 131:1344–51 (2008).
- Partridge, SC, Mukherjee, P, Berman, JI, Henry, RG, Miller, SP, Lu, Y, Glenn, OA, Ferriero, DM, Barkovich, AJ, and Vigneron, DB. Tractography-based quantitation of diffusion tensor imaging parameters in white matter tracts of preterm newborns. *J Magn Reson Imaging*, 22:467–74 (2005).
- Paul, LK, Brown, WS, Adolphs, R, Tyszka, JM, Richards, LJ, Mukherjee, P, and Sherr, EH. Agenesis of the corpus callosum: genetic, developmental and functional aspects of connectivity. *Nat Rev Neurosci*, 8:287–99 (2007).
- Paus, T, Zijdenbos, A, Worsley, K, Collins, DL, Blumenthal, J, Giedd, JN, Rapoport, JL, and Evans, AC. Structural maturation of neural pathways in children and adolescents: in vivo study. *Science*, 283:1908–11 (1999).
- Peiffer, J, Majewski, F, Fischbach, H, Bierich, JR, and Volk, B. Alcohol embryo- and fetopathy. Neuropathology of 3 children and 3 fetuses. *J Neurol Sci*, 41:125–37 (1979).
- Penhune, VB, Zatorre, RJ, MacDonald, JD, and Evans, AC. Interhemispheric anatomical differences in human primary auditory cortex: probabilistic mapping and volume measurement from magnetic resonance scans. *Cereb Cortex*, 6:661–72 (1996).
- Pfefferbaum, A, Sullivan, EV, Hedehus, M, Lim, KO, Adalsteinsson, E, and Moseley, M. Age-related decline in brain white matter anisotropy measured with spatially corrected echo-planar diffusion tensor imaging. *Magn Reson Med*, 44:259–68 (2000).
- Phillips, DE and Krueger, SK. Effects of combined pre- and postnatal ethanol exposure (three trimester equivalency) on glial cell development in rat optic nerve. *Int J Dev Neurosci*, 10:197–206 (1992).
- Powell, HW, Parker, GJ, Alexander, DC, Symms, MR, Boulby, PA, Wheeler-Kingshott, CA, Barker, GJ, Noppeney, U, Koepp, MJ, and Duncan, JS. Hemispheric asymmetries in language-related pathways: a combined functional MRI and tractography study. *Neuroimage*, 32:388–99 (2006).
- Price, GR, Holloway, I, Rasanen, P, Vesterinen, M, and Ansari, D. Impaired parietal magnitude processing in developmental dyscalculia. *Curr Biol*, 17:R1042–3 (2007).
- Provenzale, JM, Liang, L, DeLong, D, and White, LE. Diffusion tensor imaging assessment of brain white matter maturation during the first postnatal year. *AJR Am J Roentgenol*, 189:476–86 (2007).
- Pujol, J, Lopez-Sala, A, Deus, J, Cardoner, N, Sebastian-Galles, N, Conesa, G, and Capdevila, A. The lateral asymmetry of the human brain studied by volumetric magnetic resonance imaging. *Neuroimage*, 17:670–9 (2002).
- Putnam, MC, Wig, GS, Grafton, ST, Kelley, WM, and Gazzaniga, MS. Structural organization of the corpus callosum predicts the extent and impact of cortical activity in the nondominant hemisphere. *J Neurosci*, 28:2912–8 (2008).

- Qiu, D, Tan, LH, Zhou, K, and Khong, PL. Diffusion tensor imaging of normal white matter maturation from late childhood to young adulthood: voxel-wise evaluation of mean diffusivity, fractional anisotropy, radial and axial diffusivities, and correlation with reading development. *Neuroimage*, 41:223–32 (2008).
- Rademaker, KJ, Lam, JN, Van Haastert, IC, Uiterwaal, CS, Lieftink, AF, Groenendaal, F, Grobbee, DE, and de Vries, LS. Larger corpus callosum size with better motor performance in prematurely born children. *Semin Perinatol*, 28:279–87 (2004).
- Rajapakse, JC, Giedd, JN, Rumsey, JM, Vaituzis, AC, Hamburger, SD, and Rapoport, JL. Regional MRI measurements of the corpus callosum: a methodological and developmental study. *Brain Dev*, 18:379–88 (1996).
- Rasmussen, C and Bisanz, J. Exploring mathematics difficulties among children with prenatal alcohol exposure. *Child Development Perspectives*, 3:125–30 (2009).
- Reese, TG, Heid, O, Weisskoff, RM, and Wedeen, VJ. Reduction of eddy-current-induced distortion in diffusion MRI using a twice-refocused spin echo. *Magn Reson Med*, 49:177–82 (2003).
- Ressel, V, Wilke, M, Lidzba, K, Lutzenberger, W, and Krageloh-Mann, I. Increases in language lateralization in normal children as observed using magnetoencephalography. *Brain Lang* (2008).
- Riikonen, R, Salonen, I, Partanen, K, and Verho, S. Brain perfusion SPECT and MRI in foetal alcohol syndrome. *Dev Med Child Neurol*, 41:652–9 (1999).
- Riley, EP and McGee, CL. Fetal alcohol spectrum disorders: an overview with emphasis on changes in brain and behavior. *Exp Biol Med (Maywood)*, 230:357–65 (2005).
- Rilling, JK, Glasser, MF, Preuss, TM, Ma, X, Zhao, T, Hu, X, and Behrens, TE. The evolution of the arcuate fasciculus revealed with comparative DTI. *Nat Neurosci*, 11:426–8 (2008).
- Rimrodt, SL, Peterson, DJ, Denckla, MB, Kaufmann, WE, and Cutting, LE. White matter microstructural differences linked to left perisylvian language network in children with dyslexia. *Cortex*, 46:739–49 (2010).
- Rodrigo, S, Naggara, O, Oppenheim, C, Golestani, N, Poupon, C, Cointepas, Y, Mangin, JF, Le Bihan, D, and Meder, JF. Human subinsular asymmetry studied by diffusion tensor imaging and fiber tracking. *AJNR Am J Neuroradiol*, 28:1526–31 (2007).
- Rodrigo, S, Oppenheim, C, Chassoux, F, Hodel, J, de Vanssay, A, Baudoin-Chial, S, Devaux, B, and Meder, JF. Language lateralization in temporal lobe epilepsy using functional MRI and probabilistic tractography. *Epilepsia* (2008).
- Roebuck, TM, Mattson, SN, and Riley, EP. A review of the neuroanatomical findings in children with fetal alcohol syndrome or prenatal exposure to alcohol. *Alcohol Clin Exp Res*, 22:339–44 (1998).

- Rotzer, S, Kucian, K, Martin, E, von Aster, M, Klaver, P, and Loenneker, T. Optimized voxel-based morphometry in children with developmental dyscalculia. *Neuroimage*, 39:417–22 (2008).
- Salat, DH, Tuch, DS, Greve, DN, van der Kouwe, AJ, Hevelone, ND, Zaleta, AK, Rosen, BR, Fischl, B, Corkin, S, Rosas, HD, and Dale, AM. Age-related alterations in white matter microstructure measured by diffusion tensor imaging. *Neurobiol Aging*, 26:1215–27 (2005).
- Sampson, PD, Streissguth, AP, Bookstein, FL, Little, RE, Clarren, SK, Dehaene, P, Hanson, JW, and Graham, J, J. M. Incidence of fetal alcohol syndrome and prevalence of alcohol-related neurodevelopmental disorder. *Teratology*, 56:317–26 (1997).
- Santhanam, P, Li, Z, Hu, X, Lynch, ME, and Coles, CD. Effects of prenatal alcohol exposure on brain activation during an arithmetic task: an fMRI study. *Alcohol Clin Exp Res*, 33:1901–8 (2009).
- Scheltens, P, Barkhof, F, Leys, D, Wolters, EC, Ravid, R, and Kamphorst, W. Histopathologic correlates of white matter changes on MRI in Alzheimer’s disease and normal aging. *Neurology*, 45:883–8 (1995).
- Schmithorst, VJ, Holland, SK, and Dardzinski, BJ. Developmental differences in white matter architecture between boys and girls. *Hum Brain Mapp*, 29:696–710 (2008).
- Schmithorst, VJ, Wilke, M, Dardzinski, BJ, and Holland, SK. Correlation of white matter diffusivity and anisotropy with age during childhood and adolescence: a cross-sectional diffusion-tensor MR imaging study. *Radiology*, 222:212–8 (2002).
- Schmithorst, VJ, Wilke, M, Dardzinski, BJ, and Holland, SK. Cognitive functions correlate with white matter architecture in a normal pediatric population: a diffusion tensor MRI study. *Hum Brain Mapp*, 26:139–47 (2005).
- Schneider, JF, Il’yasov, KA, Hennig, J, and Martin, E. Fast quantitative diffusion-tensor imaging of cerebral white matter from the neonatal period to adolescence. *Neuroradiology*, 46:258–66 (2004).
- Schneiderman, JS, Buchsbaum, MS, Haznedar, MM, Hazlett, EA, Brickman, AM, Shihabuddin, L, Brand, JG, Torosjan, Y, Newmark, RE, Tang, C, Aronowitz, J, Paul-Oudouard, R, Byne, W, and Hof, PR. Diffusion tensor anisotropy in adolescents and adults. *Neuropsychobiology*, 55:96–111 (2007).
- Shalev, RS. Developmental dyscalculia. *J Child Neurol*, 19:765–71 (2004).
- Shalom, DB and Poeppel, D. Functional anatomic models of language: assembling the pieces. *Neuroscientist*, 14:119–27 (2008).
- Shaw, P. Intelligence and the developing human brain. *Bioessays*, 29:962–73 (2007).
- Shaywitz, BA, Shaywitz, SE, Pugh, KR, Constable, RT, Skudlarski, P, Fulbright, RK, Bronen, RA, Fletcher, JM, Shankweiler, DP, Katz, L, and et al. Sex differences in the functional organization of the brain for language. *Nature*, 373:607–9 (1995).

- Smith, CD, Chebrolu, H, Wekstein, DR, Schmitt, FA, and Markesbery, WR. Age and gender effects on human brain anatomy: a voxel-based morphometric study in healthy elderly. *Neurobiol Aging*, 28:1075–87 (2007).
- Smith, SM, Jenkinson, M, Johansen-Berg, H, Rueckert, D, Nichols, TE, Mackay, CE, Watkins, KE, Ciccarelli, O, Cader, MZ, Matthews, PM, and Behrens, TE. Tract-based spatial statistics: voxelwise analysis of multi-subject diffusion data. *Neuroimage*, 31:1487–505 (2006).
- Snook, L, Paulson, LA, Roy, D, Phillips, L, and Beaulieu, C. Diffusion tensor imaging of neurodevelopment in children and young adults. *Neuroimage*, 26:1164–73 (2005).
- Sommer, IE, Aleman, A, Bouma, A, and Kahn, RS. Do women really have more bilateral language representation than men? A meta-analysis of functional imaging studies. *Brain*, 127:1845–52 (2004).
- Song, SK, Sun, SW, Ju, WK, Lin, SJ, Cross, AH, and Neufeld, AH. Diffusion tensor imaging detects and differentiates axon and myelin degeneration in mouse optic nerve after retinal ischemia. *Neuroimage*, 20:1714–22 (2003).
- Song, SK, Sun, SW, Ramsbottom, MJ, Chang, C, Russell, J, and Cross, AH. Dysmyelination revealed through MRI as increased radial (but unchanged axial) diffusion of water. *Neuroimage*, 17:1429–36 (2002).
- Song, SK, Yoshino, J, Le, TQ, Lin, SJ, Sun, SW, Cross, AH, and Armstrong, RC. Demyelination increases radial diffusivity in corpus callosum of mouse brain. *Neuroimage*, 26:132–40 (2005).
- Sotak, CH. The role of diffusion tensor imaging in the evaluation of ischemic brain injury - a review. *NMR Biomed*, 15:561–9 (2002).
- Sowell, ER, Jernigan, TL, Mattson, SN, Riley, EP, Sobel, DF, and Jones, KL. Abnormal development of the cerebellar vermis in children prenatally exposed to alcohol: size reduction in lobules I-V. *Alcohol Clin Exp Res*, 20:31–4 (1996).
- Sowell, ER, Johnson, A, Kan, E, Lu, LH, Van Horn, JD, Toga, AW, O'Connor, MJ, and Bookheimer, SY. Mapping white matter integrity and neurobehavioral correlates in children with fetal alcohol spectrum disorders. *J Neurosci*, 28:1313–9 (2008a).
- Sowell, ER, Lu, LH, O'Hare, ED, McCourt, ST, Mattson, SN, O'Connor, MJ, and Bookheimer, SY. Functional magnetic resonance imaging of verbal learning in children with heavy prenatal alcohol exposure. *Neuroreport*, 18:635–9 (2007).
- Sowell, ER, Mattson, SN, Kan, E, Thompson, PM, Riley, EP, and Toga, AW. Abnormal cortical thickness and brain behavior correlation patterns in individuals with heavy prenatal alcohol exposure. *Cereb Cortex*, 18:136–44 (2008b).
- Sowell, ER, Peterson, BS, Thompson, PM, Welcome, SE, Henkenius, AL, and Toga, AW. Mapping cortical change across the human life span. *Nat Neurosci*, 6:309–15 (2003).
- Sowell, ER, Thompson, PM, and Toga, AW. Mapping changes in the human cortex throughout the span of life. *Neuroscientist*, 10:372–92 (2004).

- Spadoni, AD, Bazinet, AD, Fryer, SL, Tapert, SF, Mattson, SN, and Riley, EP. BOLD Response During Spatial Working Memory in Youth With Heavy Prenatal Alcohol Exposure. *Alcohol Clin Exp Res* (2009).
- Spadoni, AD, McGee, CL, Fryer, SL, and Riley, EP. Neuroimaging and fetal alcohol spectrum disorders. *Neurosci Biobehav Rev*, 31:239–45 (2007).
- Spironelli, C, Penolazzi, B, and Angrilli, A. Dysfunctional hemispheric asymmetry of theta and beta EEG activity during linguistic tasks in developmental dyslexia. *Biol Psychol*, 77:123–31 (2008).
- Spohr, HL, Willms, J, and Steinhausen, HC. Fetal alcohol spectrum disorders in young adulthood. *J Pediatr*, 150:175–9, 179 e1 (2007).
- Stade, B, Ali, A, Bennett, D, Campbell, D, Johnston, M, Lens, C, Tran, S, and Koren, G. The burden of prenatal exposure to alcohol: revised measurement of cost. *Can J Clin Pharmacol*, 16:e91–102 (2009).
- Steinlin, M. Cerebellar disorders in childhood: cognitive problems. *Cerebellum*, 7:607–10 (2008).
- Steinmetz, H. Structure, functional and cerebral asymmetry: in vivo morphometry of the planum temporale. *Neurosci Biobehav Rev*, 20:587–91 (1996).
- Streissguth, AP, Barr, HM, Olson, HC, Sampson, PD, Bookstein, FL, and Burgess, DM. Drinking during pregnancy decreases word attack and arithmetic scores on standardized tests: adolescent data from a population-based prospective study. *Alcohol Clin Exp Res*, 18:248–54 (1994).
- Streissguth, AP, Bookstein, FL, Barr, HM, Sampson, PD, O'Malley, K, and Young, JK. Risk factors for adverse life outcomes in fetal alcohol syndrome and fetal alcohol effects. *J Dev Behav Pediatr*, 25:228–38 (2004).
- Streissguth, AP and Dehaene, P. Fetal alcohol syndrome in twins of alcoholic mothers: concordance of diagnosis and IQ. *Am J Med Genet*, 47:857–61 (1993).
- Suganthi, J, Raghuram, L, Antonisamy, B, Vettivel, S, Madhavi, C, and Koshi, R. Gender- and age-related differences in the morphology of the corpus callosum. *Clin Anat*, 16:396–403 (2003).
- Sullivan, EV, Rohlfing, T, and Pfefferbaum, A. Quantitative fiber tracking of lateral and interhemispheric white matter systems in normal aging: Relations to timed performance. *Neurobiol Aging*, 31:464–81 (2010).
- Sundaram, SK, Sivaswamy, L, Makki, MI, Behen, ME, and Chugani, HT. Absence of arcuate fasciculus in children with global developmental delay of unknown etiology: a diffusion tensor imaging study. *J Pediatr*, 152:250–5 (2008).
- Takayama, Y, Sugishita, M, Akiguchi, I, and Kimura, J. Isolated acalculia due to left parietal lesion. *Arch Neurol*, 51:286–91 (1994).
- Temple, E. Brain mechanisms in normal and dyslexic readers. *Curr Opin Neurobiol*, 12:178–83 (2002).

- Thanh, NX and Jonsson, E. Costs of fetal alcohol spectrum disorder in Alberta, Canada. *Can J Clin Pharmacol*, 16:e80–90 (2009).
- Thomas, JD, Weinert, SP, Sharif, S, and Riley, EP. MK-801 administration during ethanol withdrawal in neonatal rat pups attenuates ethanol-induced behavioral deficits. *Alcohol Clin Exp Res*, 21:1218–25 (1997).
- Thompson, PM, Giedd, JN, Woods, RP, MacDonald, D, Evans, AC, and Toga, AW. Growth patterns in the developing brain detected by using continuum mechanical tensor maps. *Nature*, 404:190–3 (2000).
- Toga, AW and Thompson, PM. Mapping brain asymmetry. *Nat Rev Neurosci*, 4:37–48 (2003).
- Toga, AW, Thompson, PM, and Sowell, ER. Mapping brain maturation. *Trends Neurosci*, 29:148–59 (2006).
- Torrey, HC. Bloch Equations with Diffusion Terms. *Physical Review*, 104:563 LP – 565 (1956).
- Tuch, DS. Q-ball imaging. *Magn Reson Med*, 52:1358–72 (2004).
- Turken, A, Whitfield-Gabrieli, S, Bammer, R, Baldo, JV, Dronkers, NF, and Gabrieli, JD. Cognitive processing speed and the structure of white matter pathways: convergent evidence from normal variation and lesion studies. *Neuroimage*, 42:1032–44 (2008).
- Upadhyay, J, Hallock, K, Ducros, M, Kim, DS, and Ronen, I. Diffusion tensor spectroscopy and imaging of the arcuate fasciculus. *Neuroimage*, 39:1–9 (2008).
- van Eimeren, L, Niogi, SN, McCandliss, BD, Holloway, ID, and Ansari, D. White matter microstructures underlying mathematical abilities in children. *Neuroreport*, 19:1117–21 (2008).
- Van Hecke, W, Leemans, A, De Backer, S, Jeurissen, B, Parizel, PM, and Sijbers, J. Comparing isotropic and anisotropic smoothing for voxel-based DTI analyses: A simulation study. *Hum Brain Mapp*, 31:98–114 (2010).
- van Kooij, B, M, MvH, Uiterwaal., C, Groenendaal, F, Nivelstein, R, Rademaker, K, Jongmans, M, and Vries, LD. Corpus callosum size in relation to motor performance in 9- to 10-year-old children with neonatal encephalopathy. *Pediatr Res*, 63:103–8 (2008).
- Vernooij, MW, Smits, M, Wielopolski, PA, Houston, GC, Krestin, GP, and van der Lugt, A. Fiber density asymmetry of the arcuate fasciculus in relation to functional hemispheric language lateralization in both right- and left-handed healthy subjects: a combined fMRI and DTI study. *Neuroimage*, 35:1064–76 (2007).
- Vikingstad, EM, George, KP, Johnson, AF, and Cao, Y. Cortical language lateralization in right handed normal subjects using functional magnetic resonance imaging. *J Neurol Sci*, 175:17–27 (2000).
- Wakana, S, Caprihan, A, Panzenboeck, MM, Fallon, JH, Perry, M, Gollub, RL, Hua, K, Zhang, J, Jiang, H, Dubey, P, Blitz, A, van Zijl, P, and Mori, S. Reproducibility of quantitative tractography methods applied to cerebral white matter. *Neuroimage*, 36:630–44 (2007).

- Wakana, S, Jiang, H, Nague-Poetscher, LM, van Zijl, PC, and Mori, S. Fiber tract-based atlas of human white matter anatomy. *Radiology*, 230:77–87 (2004).
- Walhovd, KB, Westlye, LT, Amlien, I, Espeseth, T, Reinvang, I, Raz, N, Agartz, I, Salat, DH, Greve, DN, Fischl, B, Dale, AM, and Fjell, AM. Consistent neuroanatomical age-related volume differences across multiple samples. *Neurobiol Aging* (2009).
- Walterfang, M, Yung, A, Wood, AG, Reutens, DC, Phillips, L, Wood, SJ, Chen, J, Velakoulis, D, McGorry, PD, and Pantelis, C. Corpus callosum shape alterations in individuals prior to the onset of psychosis. *Schizophr Res*, 103:1–10 (2008).
- Warner, TD, Behnke, M, Eyler, FD, Padgett, K, Leonard, C, Hou, W, Garvan, CW, Schmalfluss, IM, and Blackband, SJ. Diffusion tensor imaging of frontal white matter and executive functioning in cocaine-exposed children. *Pediatrics*, 118:2014–24 (2006).
- Wedeen, VJ, Hagmann, P, Tseng, WY, Reese, TG, and Weisskoff, RM. Mapping complex tissue architecture with diffusion spectrum magnetic resonance imaging. *Magn Reson Med*, 54:1377–86 (2005).
- Wells, CT, Mahone, EM, Matson, MA, Kates, WR, Hay, T, and Horska, A. Relationship of temporal lobe volumes to neuropsychological test performance in healthy children. *Brain Cogn* (2008).
- Wernicke, C. *Der aphasische Symptomenkomplex: eine psychologische Studie auf anatomischer Basis*. Cohn und Wegert, Breslau (1874).
- Westerhausen, R, Walter, C, Kreuder, F, Wittling, RA, Schweiger, E, and Wittling, W. The influence of handedness and gender on the microstructure of the human corpus callosum: a diffusion-tensor magnetic resonance imaging study. *Neurosci Lett*, 351:99–102 (2003).
- Westerhausen, R, Woerner, W, Kreuder, F, Schweiger, E, Hugdahl, K, and Wittling, W. The role of the corpus callosum in dichotic listening: a combined morphological and diffusion tensor imaging study. *Neuropsychology*, 20:272–9 (2006).
- Westlye, LT, Walhovd, KB, Dale, AM, Bjornerud, A, Due-Tonnessen, P, Engvig, A, Grydeland, H, Tamnes, CK, Ostby, Y, and Fjell, AM. Life-Span Changes of the Human Brain White Matter: Diffusion Tensor Imaging (DTI) and Volumetry. *Cereb Cortex* (2009).
- White, T, Nelson, M, and Lim, KO. Diffusion tensor imaging in psychiatric disorders. *Top Magn Reson Imaging*, 19:97–109 (2008).
- Whitford, TJ, Rennie, CJ, Grieve, SM, Clark, CR, Gordon, E, and Williams, LM. Brain maturation in adolescence: concurrent changes in neuroanatomy and neurophysiology. *Hum Brain Mapp*, 28:228–37 (2007).
- Wilde, EA, McCauley, SR, Chu, Z, Hunter, JV, Bigler, ED, Yallampalli, R, Wang, ZJ, Hanten, G, Li, X, Ramos, MA, Sabir, SH, Vasquez, AC, Menefee, D, and Levin, HS. Diffusion tensor imaging of hemispheric asymmetries in the developing brain. *J Clin Exp Neuropsychol*, 31:205–18 (2009).

- Witelson, SF. Hand and sex differences in the isthmus and genu of the human corpus callosum. A postmortem morphological study. *Brain*, 112 ( Pt 3):799–835 (1989).
- Witelson, SF and Pallie, W. Left hemisphere specialization for language in the newborn. Neuroanatomical evidence of asymmetry. *Brain*, 96:641–6 (1973).
- Wood, AG, Harvey, AS, Wellard, RM, Abbott, DF, Anderson, V, Kean, M, Saling, MM, and Jackson, GD. Language cortex activation in normal children. *Neurology*, 63:1035–44 (2004).
- Wozniak, JR, Mueller, BA, Chang, PN, Muetzel, RL, Caros, L, and Lim, KO. Diffusion tensor imaging in children with fetal alcohol spectrum disorders. *Alcohol Clin Exp Res*, 30:1799–806 (2006).
- Wozniak, JR, Muetzel, RL, Mueller, BA, McGee, CL, Freerks, MA, Ward, EE, Nelson, ML, Chang, PN, and Lim, KO. Microstructural Corpus Callosum Anomalies in Children With Prenatal Alcohol Exposure: An Extension of Previous Diffusion Tensor Imaging Findings. *Alcohol Clin Exp Res* (2009).
- Yakovlev, P and Lecours, AR. The myelogenetic cycles of regional maturation of the brain. In A Minkowski, ed., *Regional development of the brain early in life.*, pages 3–70. Blackwell Scientific Publications Inc., Boston, Massachusetts (1967).
- Yasmin, H, Aoki, S, Abe, O, Nakata, Y, Hayashi, N, Masutani, Y, Goto, M, and Ohtomo, K. Tract-specific analysis of white matter pathways in healthy subjects: a pilot study using diffusion tensor MRI. *Neuroradiology*, 51:831–40 (2009).
- Zarei, M, Johansen-Berg, H, Smith, S, Ciccarelli, O, Thompson, AJ, and Matthews, PM. Functional anatomy of interhemispheric cortical connections in the human brain. *J Anat*, 209:311–20 (2006).
- Zhang, J, Evans, A, Hermoye, L, Lee, SK, Wakana, S, Zhang, W, Donohue, P, Miller, MI, Huang, H, Wang, X, van Zijl, PC, and Mori, S. Evidence of slow maturation of the superior longitudinal fasciculus in early childhood by diffusion tensor imaging. *Neuroimage*, 38:239–47 (2007).
- Zhang, W, Olivi, A, Hertig, SJ, van Zijl, P, and Mori, S. Automated fiber tracking of human brain white matter using diffusion tensor imaging. *Neuroimage*, 42:771–7 (2008a).
- Zhang, Y, Du, AT, Hayasaka, S, Jahng, GH, Hlavin, J, Zhan, W, Weiner, MW, and Schuff, N. Patterns of age-related water diffusion changes in human brain by concordance and discordance analysis. *Neurobiol Aging*, (in press). doi:10.1016/j.neurobiolaging.2008.10.009. (2008b).
- Zhou, D, Lebel, C, Lepage, C, Evans, A, Rasmussen, C, Wyper, K, Pei, J, Andrew, G, Massey, A, Massey, D, and Beaulieu, C. Developmental Cortical Thinning in Fetal Alcohol Spectrum Disorder. In *Proceedings of the Organization for Human Brain Mapping*. Barcelona, Spain (2010).

# Appendix A

## Template Creation

The fibre tracking presented in Chapters 5, 6, and 9, and Section 11.1 was done using a semi-automated method described in Appendix C. This semi-automated tracking method uses a homemade template to which images are normalized. This template was created by scanning a healthy 25-year old male subject 20 times with the standard 6-direction DTI protocol used through this thesis (see any of the “Research” chapters for details). The images from all 20 scans were normalized to each other using affine transformations and then averaged together to create the template. As all of the DTI data presented in this thesis, the template has 40 3 mm thick slices. All 40 slices are shown in Figure A.1.

Note that this is not the same template used for the voxel-based analysis described in Chapter 10 and Section 11.2; those studies used the ICBM-152 template provided as part of the SPM software package. The fibre tracking for Chapters 7 and 8 was done manually and did not require a template.

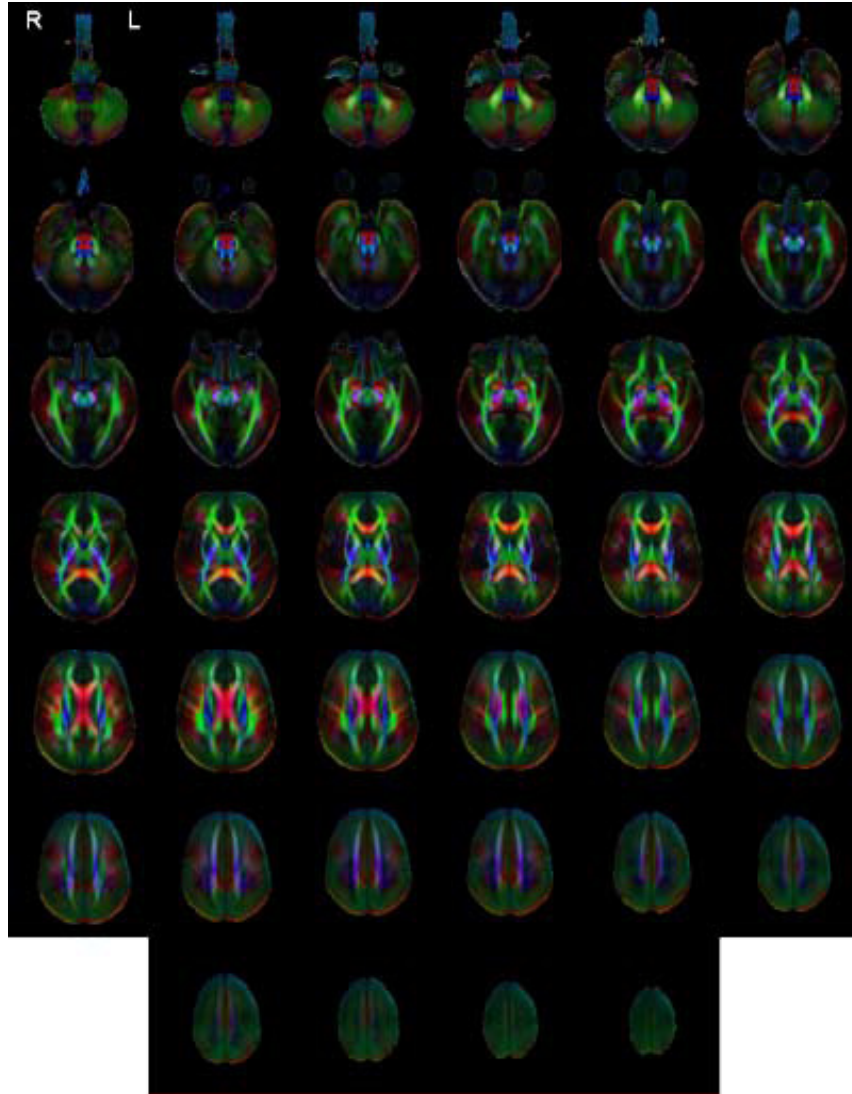


Figure A.1: Colour maps for all 40 slices from the homemade template used for semi-automated tractography are shown. The bottom slice is located in the upper left corner; slice numbers increase left-to-right across the page and down across the rows. Green indicates that the primary diffusion direction is anterior/posterior, blue indicates inferior/superior, and red indicates left/right.

# Appendix B

## Tracking Fibres

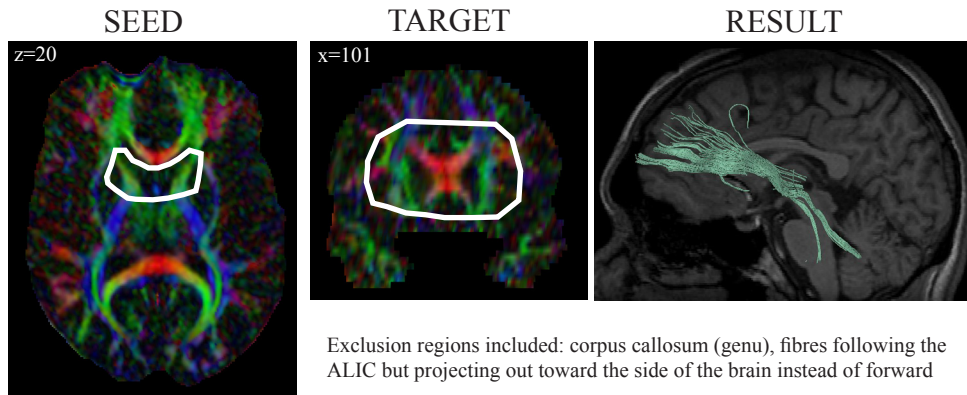
This section demonstrates the locations of seeding and target regions to delineate the major white matter tracts. These regions are the ones used for the semi-automated and automated tractography presented in Appendices C and D, so they are drawn considerably larger than would be necessary for manual tracking in individual subjects. Furthermore, it must be noted that both the colour maps and the tracking results will vary greatly from subject to subject and will not be identical to those presented here. Slices shown here are given for the homemade DTI template described in Appendix A and are based on data that is  $256 \times 256 \times 40$  slices, with voxel sizes of  $0.86 \times 0.86 \times 3$  mm<sup>3</sup>. Tracts shown are those from a healthy 22 year old male.

Additional tools that will help with tractography include:

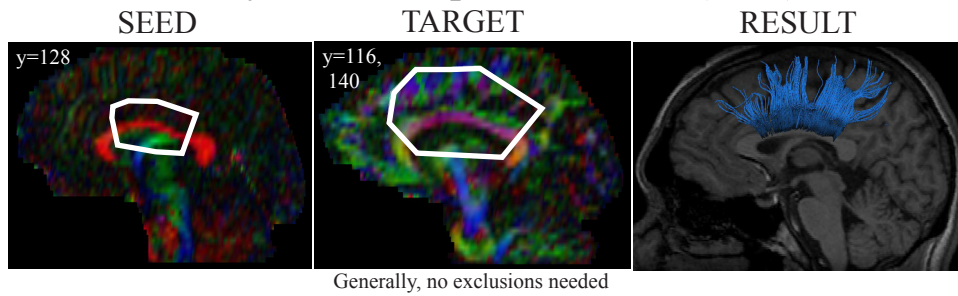
- (Catani et al., 2002): a paper demonstrating some major white matter tracts and how to delineate them using a multiple region-of-interest approach.
- (Wakana et al., 2004): a paper showing most major white matter tracts, what they look like and where they are located on both 2-dimensional colour and FA maps.
- [www.dtiatlas.org](http://www.dtiatlas.org): a good website showing an atlas of tracts and describing the function of each tract

Tracking of the fornix for Chapters 5 and 6 was done using CSF-suppressed DTI data. An additional template was constructed for the CSF-suppressed

## Anterior Limb of the Internal Capsule (ALIC)



## Body of the Corpus Callosum (bCC)



## Cingulum (cg)

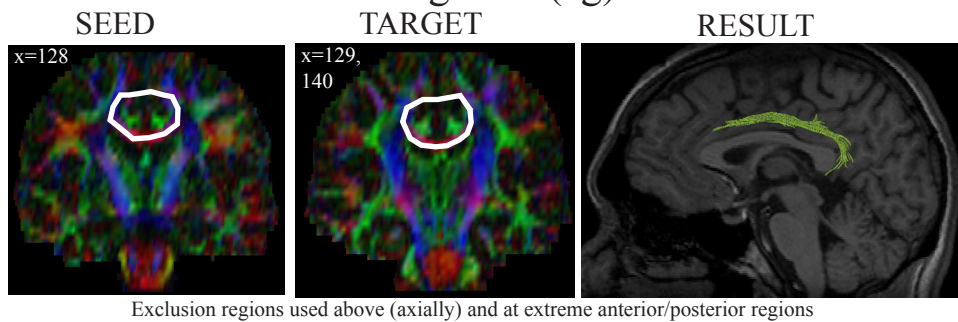
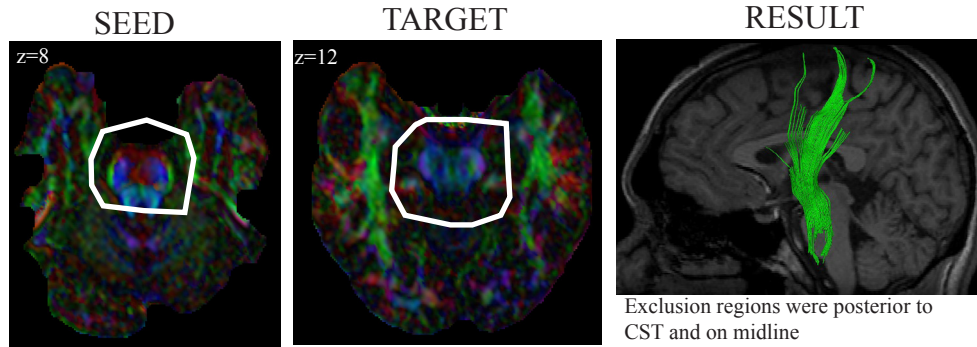
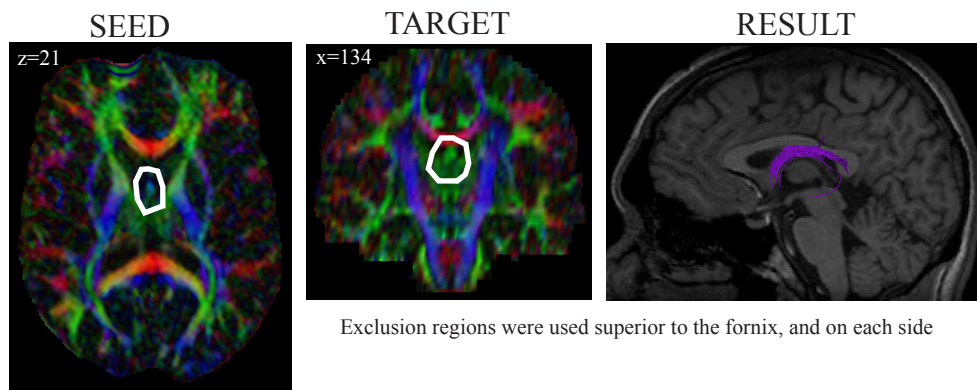


Figure B.1: Fibre tracking of the anterior limb of the internal capsule, body of the corpus callosum and cingulum.

## Corticospinal Tracts (CST)



## Fornix (fx)



## Genu Corpus Callosum (gCC)

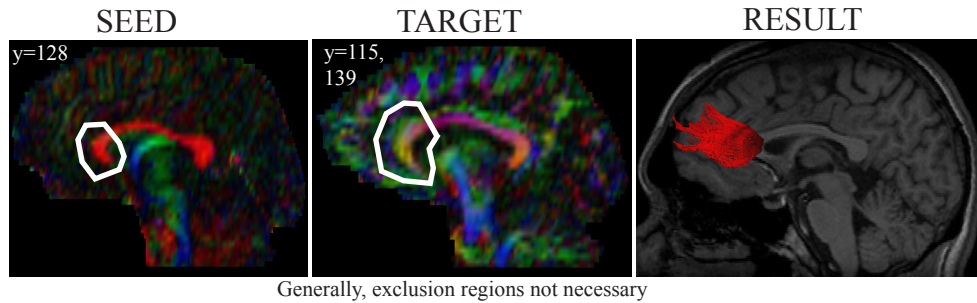
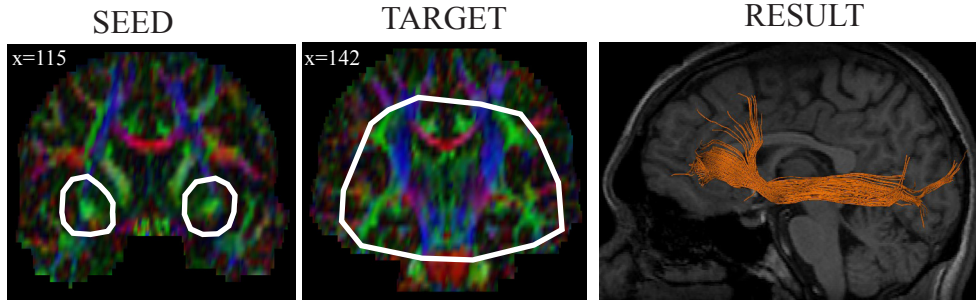


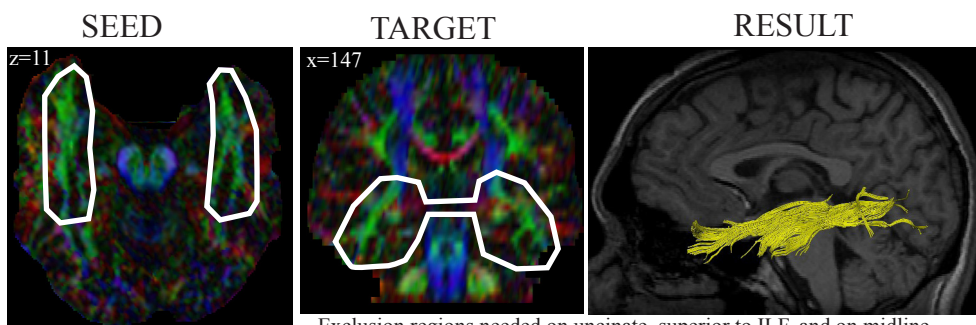
Figure B.2: Fibre tracking of the corticospinal tracts, fornix, and genu of the corpus callosum.

### Inferior Fronto-occipital Fasciculus (IFO)



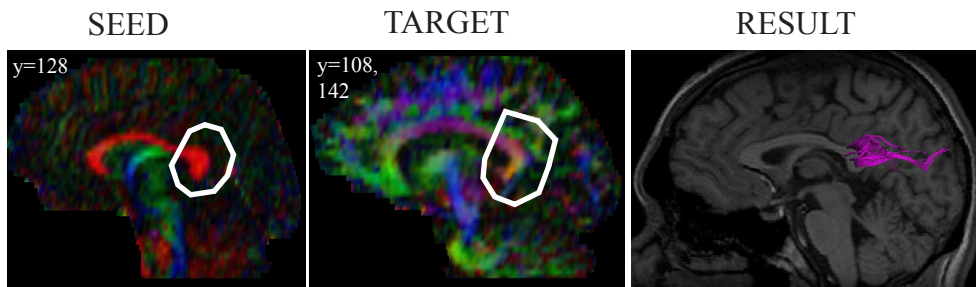
Exclusion regions sometimes needed above/below tract to eliminate superior/inferiorly oriented fibers

### Inferior Longitudinal Fasciculus (ILF)



Exclusion regions needed on uncinate, superior to ILF, and on midline

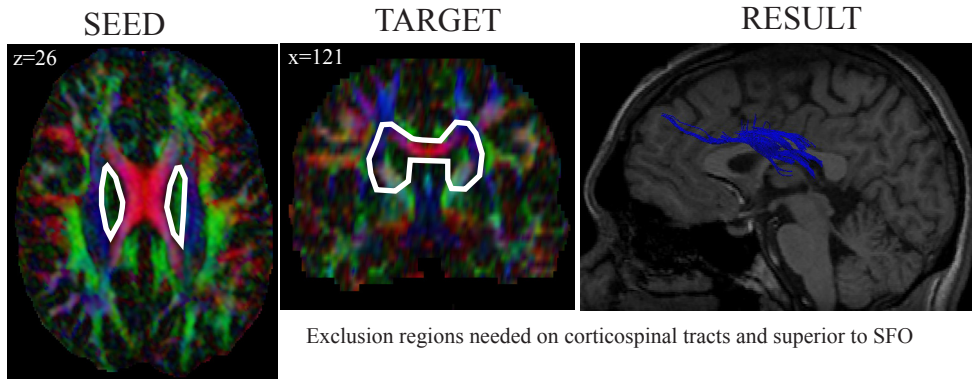
### Splenium of the Corpus Callosum (sCC)



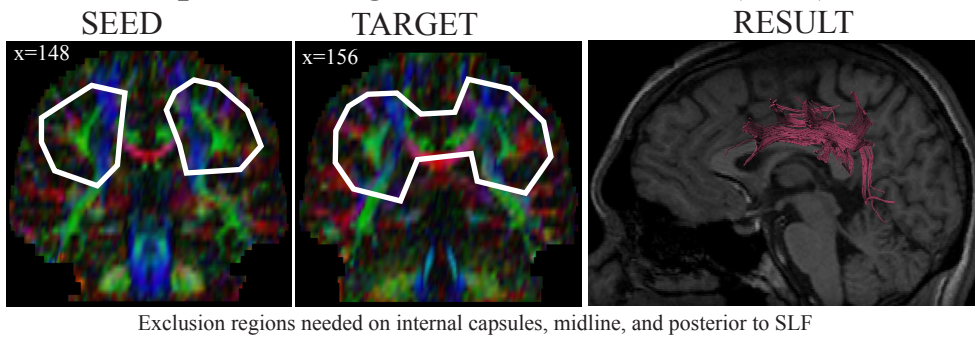
Exclusion regions needed to eliminate temporal CC (tapetum), if desired

Figure B.3: Fibre tracking of the inferior fronto-occipital fasciculus, inferior longitudinal fasciculus, and splenium of the corpus callosum.

### Superior Fronto-occipital Fasciculus (SFO)



### Superior Longitudinal Fasciculus (SLF)



### Uncinate Fasciculus (UF)

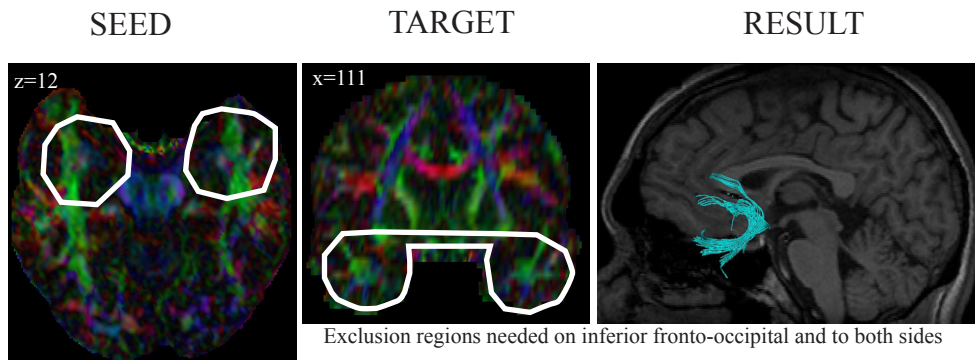


Figure B.4: Fibre tracking of the superior fronto-occipital fasciculus, superior longitudinal fasciculus, and uncinate fasciculus.

data and it is shown below. In comparison to the reconstructed fornix from the standard DTI data, this tract has a longer crus section extending extension toward the hippocampi in either hemisphere. The fornix here appears somewhat thinner than the fornix reconstructed from the standard DTI data, but this will vary from person to person.

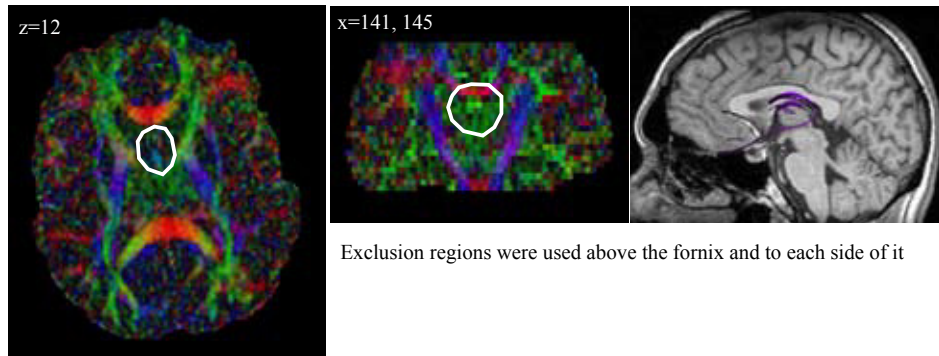


Figure B.5: Fibre tracking of the fornix using CSF-suppressed data is shown.

# Appendix C

## Semi-Automated Tractography: A step-by-step tutorial

Semi-automated tractography is useful for quick analysis of large data sets. Subject images (generally, the non diffusion-weighted images ( $b=0$  s/mm<sup>2</sup>), but fractional anisotropy (FA) images could be used instead) are normalized to a template using a non-affine transformation in SPM. Seeding, target, and exclusion regions for each fibre tract are drawn on a template colour map and then warped back to native space for each individual using the inverse of the original transformation parameters. Fibre tracking is then done in native space for each individual using a deterministic streamline algorithm and the warped seeding, target, and exclusion regions.

Semi-automated tractography is done in four stages: preparation of files; selection of seeding, target and exclusion regions; fibre tracking; and analysis. Instructions and figures shown in this appendix are taken from SPM8, but the semi-automated tractography code is compatible with both SPM8 and SPM5.

### C.1 Preparation of Files

1. Create \*.mat files for each subject in ExploreDTI. There is code provided with the ExploreDTI package (Calculate\_Mat\_File\_For\_ExploreDTI.m) that must be modified to include the proper gradient table and b-value; a version that works for the 6-direction DTI sequence off the Siemens 1.5T scanner is available. Once the \*.mat files have been created for

each subject, put all files into the same folder. These are the native space images.

2. Create deformation matrices in SPM:

- (a) Create \*.nii files for the images you wish to normalize (either b0 or FA images). This can be done using the generate\_nii\_list.m Matlab code. To use generate\_nii\_list.m, just make sure parameters for voxel size and dimensions are correct. Furthermore, ensure that the origin of the \*.nii native images created and the template image are close together or normalization will not work.
- (b) Use the **Normalise:Estimate** function in SPM to normalize the b0 or FA images to a template image (see Figure C.1). Subject images in \*.nii format are selected under **Source Image**, and the template is selected under **Template Image**. The template image must also be in NIfTI (\*.nii) or Analyze (\*.hdr, \*.img) format. Several templates are provided by SPM in MNI space (EPI, T1, T2, etc), or you may use a homemade template, for example the Atlas\_AL.nii template. A homemade template is easier because you will have DTI data (including a colour map and a \*.mat file) on which to draw the seeding regions.

You may select **Normalise: Estimate & Write** instead of **Normalise: Estimate** if you wish. **Estimate** will create the necessary \*\_sn.mat file, while **Estimate & Write** will create both the \*\_sn.mat file and a saved normalized image. The normalized image is not necessary for semi-automated tractography but may be useful for other applications (such as voxel-based analysis, see Section E). Multiple subjects can be normalized at one time to template image. Simply add additional subjects under **Data**, and select the b0 or FA \*.nii file for each subject under **Source Image**. Generally, the other default SPM parameters are okay.

- (c) Create the deformation maps to warp images from template back

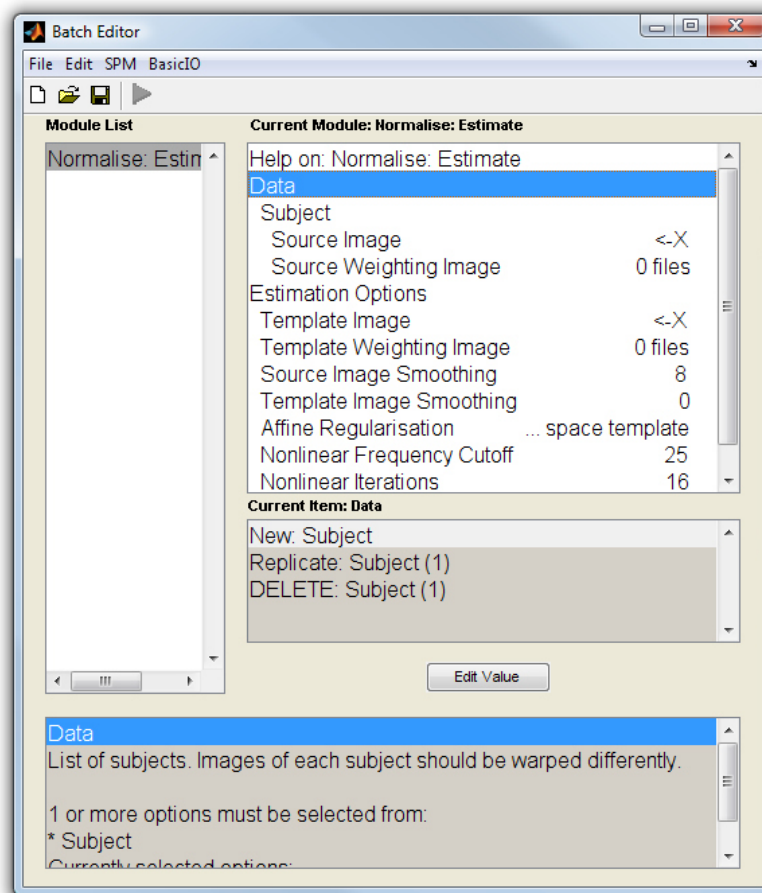


Figure C.1: SPM: Normalise: Estimate

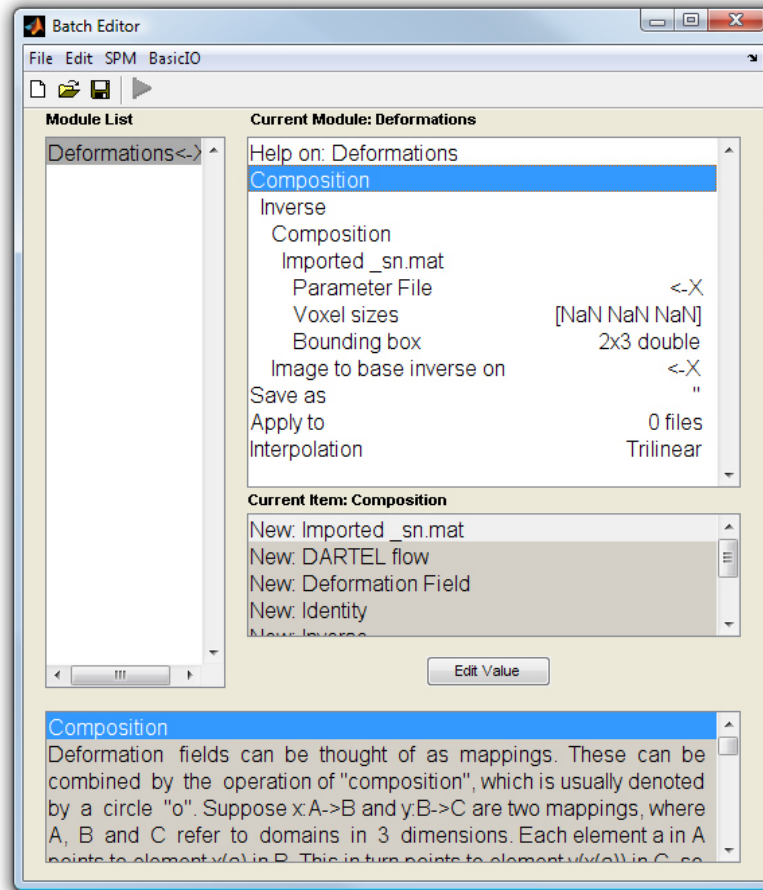


Figure C.2: SPM: Deformations

to native space for each individual.

Use SPM Deformations to create maps, (in the batch editor, under SPM > Util; see Fig. C.2). Under **Composition**, choose **New:Inverse**, then under the next **Composition**, choose **New:Imported\_sn.mat**. Select the parameter file (\*\_sn.mat) from normalization.

Under **Save as**, put the subject's name. The name of this file must be the same as the native \*.mat file for the tracking code to work.

**Apply to** can be used if you want to apply the deformations to something (for example to the normalized image to test if the deformation is correct), but it is not necessary to fill in this field.

**Apply to** is also the code to be used for normalization of FA maps

for voxel-based morphometry, for example. Multiple subjects may be run in one batch by creating additional deformation modules. Save all deformations in the same folder.

## C.2 Selection of Seeding, Target, and Exclusion Regions

1. Load the template image (\*.mat file) into ExploreDTI. You can display it as either a colour map, FA map or non diffusion-weighted image. This must have the same dimensions as the native space images for each subject, or the semi-automated tractography will not work.
2. Draw the seeding region in the desired area (see Appendix B for guidelines for drawing seeding and target regions). Seeding region should be drawn considerably larger than the structure desired to ensure that no fibres are missed due to normalization errors; however, the size of the seeding region must be balanced against attempts not to include other fibres in the seeding region.
3. Save the seeding region or regions. Go to **Data > Save mask of ROIs (\*.mat)**, and save the mask. Each mask is a logical matrix in Matlab, the same size as the DTI data.
4. Repeat steps 2 and 3 for the target (AND) and exclusion (NOT) regions. It makes things easier later if the regions are all saved in the same folder. Note that the selection of these regions is an iterative process. You must try your seeding, target and exclusion regions on a few subjects to see if they work, and you then may need to go back and modify later.

## C.3 Tracking the Fibres

This will do the tracking of the fibres in native space for each individual, saving the tracts as a Matlab workspace. The file can then be loaded into ExploreDTI

for analysis, into the Matlab workspace for examining the variables, or used with `analyse_nonaffine_Tractography_Results` (see section C.4).

1. Run `nonaffine_Tractography_Analysis.m` by typing it into the Matlab command line.
2. Set the tracking parameters in dialog box:

- Minimum FA for seed point selection is usually 0.15–0.3; this parameter is a trade-off between getting all the fibres you want and minimizing spurious fibres.
- Maximum FA for seed point selection should always be 1, unless you want to avoid seeding in regions of high FA (but I do not know why you would want this).
- Minimum FA to allow tracking should generally be the same as the minimum FA for seed point selection.
- Maximum angle is usually 30–70°, although I have found it does not make a large difference to the tracking results.
- Step size is usually 1 mm.
- Minimum fibre length is usually 10 mm.
- Maximum fibre length is usually 400 mm.
- The seed point supersampling factor can be used to compensate for anisotropic voxels by seeding more points in one direction. For example, when using sagittal or coronal seeding regions, I use `[0 0 2]` to compensate for the fact that my slices are thicker (3 mm) than the in-plane resolution (0.85 mm after interpolation). The supersampling seeds  $2n+1$  points in each direction, so `[0 0 2]` seeds  $1 \times 1 \times 5$  points.

3. Select the folders to be used:

Each folder should have all of the subject files in it, without other files. The `*.nii` deformation files must have the same name as the native space `*.mat` files, with the exception of the “y\_” at the front.

4. Select the seed, and, not masks (seeding, target, exclusion):

These are the Matlab files (\*.mat) with the same dimensions as the native images. They are logical format, with ones in the voxels selected and zeros elsewhere. The workspace variable must be named ROIMask. You may decide whether you want to use AND or NOT masks; generally, these are needed for accurate tracking.

The program will keep track of its progress by outputting the current subject number to the workspace. Fortunately, each subject's tracts area saved to the file after completion, so if the program crashes partway through you will not need to resume it from the beginning, but only from the subject it was working on when it crashed. To do this, simply remove the files of subjects who have been completed from the deformation folder (put into a temporary folder; do not delete them) and the program will skip them.

## C.4 Analyzing the Tracts

This analysis uses the tracts calculated using `nonaffine_Tractography_Analysis` to extract FA values, eigenvalues, and MD for the tract for each subject. Other variables such as number of streamlines, tract volume, and tract length may be saved. Depending on the version of `ExploreDTI` being run, line 98 may need to be changed from loading the `TractsMask` variable to loading the `TractMask` variable.

1. Run `analyse_nonaffine_Tractography_Results` by typing it into Matlab command line.
2. Select the appropriate folders and the name for the resulting file.
3. Select slice range. This can be used to analyze tracts only in a specific region (e.g., left only or right only). You must be careful, though, because this selects the region in native space, so it may be slightly different for

different individuals (left/right is fine for clearly separated tracts because there is enough empty space between tracts, though).

This program will save two files — a Matlab file and a text file; they will both have the same name. You can load the Matlab file into the workspace and examine the variables. The text file can then be imported into SPSS or Excel for statistical analysis.

## C.5 Rejection of Tracts

Throughout the process of selecting seeding, target, and exclusion regions for semi-automated tractography, the resulting tracts should be examined to ensure that they are accurate. Selection of the seeding, target, and exclusion regions is iterative and should be refined until almost all tracts obtained are deemed acceptable. However, it is likely that some tracts will continue to be inadequately traced. Some individuals may have no streamlines found for a particular tract, while others may result in incorrect tracts that may be necessary to exclude. When no streamlines are found, Matlab outputs a message into the command window, and the values output for FA, MD, and the eigenvalues will be zero; these values should be removed from the spreadsheet so as not to skew results.

Incorrect tracts may be more difficult to spot, and it is important to conduct a random check for each analysis by examining each tract in several individuals to ensure they follow the desired pathway. Another easy way to check for incorrect tracts is to examine the FA and MD values output by the `analyse_nonaffine_Tractography_Results` code. Tracts that have particularly high or low FA or MD values should be looked at to determine whether they follow the correct trajectory.

For this thesis, cases where tracts were clearly not what was desired or cases where no streamlines were produced were excluded from further analysis of that tract. Fortunately, the large sample sizes permitted removal of one subject from part of the analysis without significantly altering the power or sensitivity of the results. In the lifespan development study (Section 11.1),

which contained 403 subjects, the following number of cases were excluded for each tract: 1 fornix, 3 splenium, 2 cingulum, 1 corticospinal tract, 5 inferior fronto-occipital fasciculus, 1 superior fronto-occipital fasciculus, 1 uncinate, and no cases were excluded for the anterior limb, inferior or superior longitudinal fasciculi, or the genu or body of the corpus callosum. Removal of tracts which did not work with the semi-automated tractography method ensured that no bias was introduced by using manual tracking in only some subjects. Interestingly, however, even manual tractography was unsuccessful for most of the cases in which the semi-automated method failed to reconstruct the proper pathway.

# Appendix D

## Automated Tractography

In addition to the step-by-step process presented in Appendix C, I have written two pieces of code which will do the preprocessing in one step, then the fibre tracking in another, completely automatically. This code works for data acquired on the Siemens scanner using 35 or 40 slices and uses my prepared tractography masks, so data should be similar to the acquisition scheme used throughout this thesis or it is unlikely to produce accurate results. The seeding, inclusion and exclusion regions used for this automated tracking are very similar to those shown in Appendix B.

To run this software, you must have downloaded (ExploreDTI (current version at time of writing was v4.6.8), and SPM (Statistical Parametric Mapping)). You will also need to place the “Automated Tractography” folder somewhere in the Matlab path.

### D.1 Preparation of Files

1. Put all the DTI DICOM files into one folder for each subject, and put all subject folders into the same directory. Make sure there are no other files or folders in these directories. For this code to work, SPM must be initialized. This is done within the code, but SPM must be closed manually.
2. Run “Preprocess\_For\_ExploreDTI\_batch.m” in Matlab, by typing “Preprocess\_For\_ExploreDTI\_batch” into the command window.

3. Press “okay” and then quit SPM by pressing “quit”.
4. Select the directory of the DICOM data for all subjects.
5. Input the sequence parameters: b-value, voxel dimensions, matrix dimensions, gradient table (the default is the Siemens 1.5T 6-direction protocol). The default parameters can be changed in the code itself, if desired.

For the 6-direction Siemens data used through this thesis, the parameters are:

b-value:  $1000 \text{ s/mm}^2$

Voxel dimensions: [0.86 0.86 3]

Matrix dimensions: [256 256 40]

Gradient table: [(1,0,1), (-1,0,1), (0,1,1), (0,1,-1), (1,1,0), (-1,1,0)]

6. Select the template to use for normalization — this should be either the Atlas.nii file (for 40 slice data), or the Atlas35.nii file (for 35 slice data). If using other data, a different template and new tractography masks would need to be created.
7. Select the location to save the processed files. The files will be saved using the Patient ID field from the DICOM header. If the Patient ID is the scanner-input default (which contains a very long string of numbers and dots), a dummy label “subject\_x” will be used instead. If you later change the name of any subject, make sure to change the name of that subject for all associated files produced by this preprocessing code.

You should now have 6 files for each subject (5 will be in sub-folders):

1. In the main folder (overall directory with DICOMs in it), there will be a \*.mat file for each subject called subID.mat, which contains all diffusion parameters and can be loaded into ExploreDTI to view the FA, colour map, do additional tracking, etc.

2. In the folder “b0 maps”, there are b0 images NIFTI format for each subject, called subIDb0.nii. These are the non diffusion-weighted images in native space and they can be loaded into SPM or MRICro for viewing. These are the images used for normalization.
3. In the folder “FA maps”, there are FA maps for each subject in native space, called subIDFA.nii. As with the b0 images, these can be loaded into SPM, MRICro, etc. to view.
4. The folder “Parameter files” contains the normalization parameters used to warp the b0 images to the template selected at the beginning of the code (should be the AL template for either 35 or 40 slices).
5. The “Normalized FA maps” folder contains the normalized FA maps, called wsubIDFA.nii. The FA maps are normalized using the parameters in “Parameter files” to create these normalized FA maps.
6. “Deformation maps” contains the un-warping parameters created by taking the inverse of the normalization parameters in “Parameter files”.

The mat files and deformation maps are the only ones necessary for tracking. The other files are useful for checking raw data or normalization, or possibly for later use in other analysis (see Appendix E).

## D.2 Tracking of Fibres

The tracking is done using pre-made seeding, inclusion, and exclusion masks selected specifically for the 6-direction protocol. If you are using other data, or warping to a different template (not the AL template), you will need to create new masks. This code can take a while, depending on how many subjects and how many tracts measured. Plan on it taking approximately 1–3 minutes per subject per tract, depending on the computer.

To run the tracking:

1. Run the file “Track\_fibres\_automatically.m” in Matlab by typing into the command window: “Track\_fibres\_automatically”.

2. Select the tracts you wish to delineate and measure.
3. Select the appropriate folders containing the \*.mat files, deformation maps, and the tracking masks.
4. Name the file in which to save all parameters.

Now, you should have a folder for each tract, which contains mat files of the tracts for each subject. These can be loaded into ExploreDTI to view, and should be examined to make sure they are correct. There is also a text file for each tract, containing the FA, MD, and eigenvalues averaged across the entire tract. These text files can be loaded directly into SPSS or Excel for analysis. Finally, there is a Matlab file (called the name specified when running the code) containing all parameters that can be easily loaded into Matlab.

# Appendix E

## Voxel-Based Analysis

Voxel-based analysis (or voxel-based morphometry, VBM) is useful for examining all of the brain white matter at once in an automated way. Images for each subject are normalized to a template and compared voxel-by-voxel across the whole brain to examine for group differences or correlations with another variable (e.g., age or a cognitive score). VBM is done in three stages: normalization of images, smoothing of images, and voxel-by-voxel statistical analysis.

### E.1 Normalization of Images

1. Create \*.nii files for each subject. This can be done using the generate\_nii\_list.m Matlab code (as in Section 2a). If using the b0 images for normalization to a template, create \*.nii files for both b0 and FA images (FA images will be normalized later using b0 parameters); if normalizing the FA images to a template directly, only FA \*.nii files need to be created.
2. Use the **Normalise:Estimate & Write** function in SPM to normalize subject images (either b0 or FA) to a template (see Figure E.1). Select image to normalize (either b0 or FA image) as **Source Image**, and select the FA map under **Images to Write**. Multiple subjects can be normalized at one time to template image by adding additional subjects under **Data** and selecting the appropriate images to normalize and write.

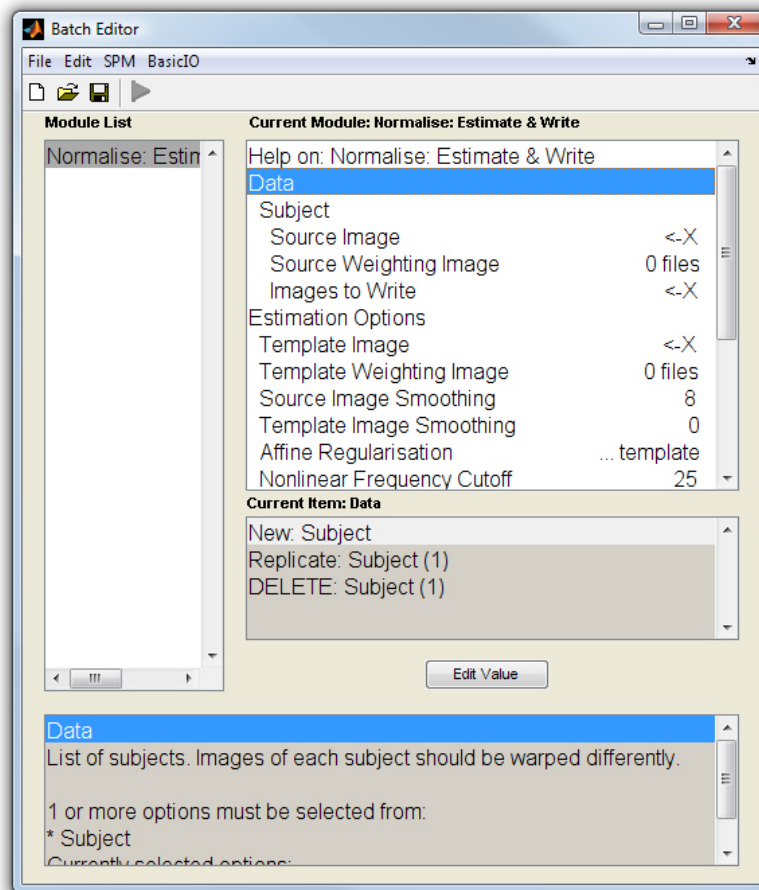


Figure E.1: SPM Normalise: Estimate & Write

The template is selected under **Template Image** and must also be in NIfTI (\*.nii) or Analyze (\*.hdr, \*.img) format. There are several templates provided by SPM (EPI, T1, T2, etc), or you can make one of your own from your subject data. The template image should be of similar contrast (b0 or FA map) to the images being normalized.

**Normalise: Estimate & Write** will create both the \*\_sn.mat file and a saved normalized image (which will have the same name as the original image, with a 'w' appended to the front).

## E.2 Smoothing of Images

To smooth images, select **Smooth** in SPM (see Figure E.2). Select all of the files to smooth (normalized FA maps) under **Images to Smooth** and set the

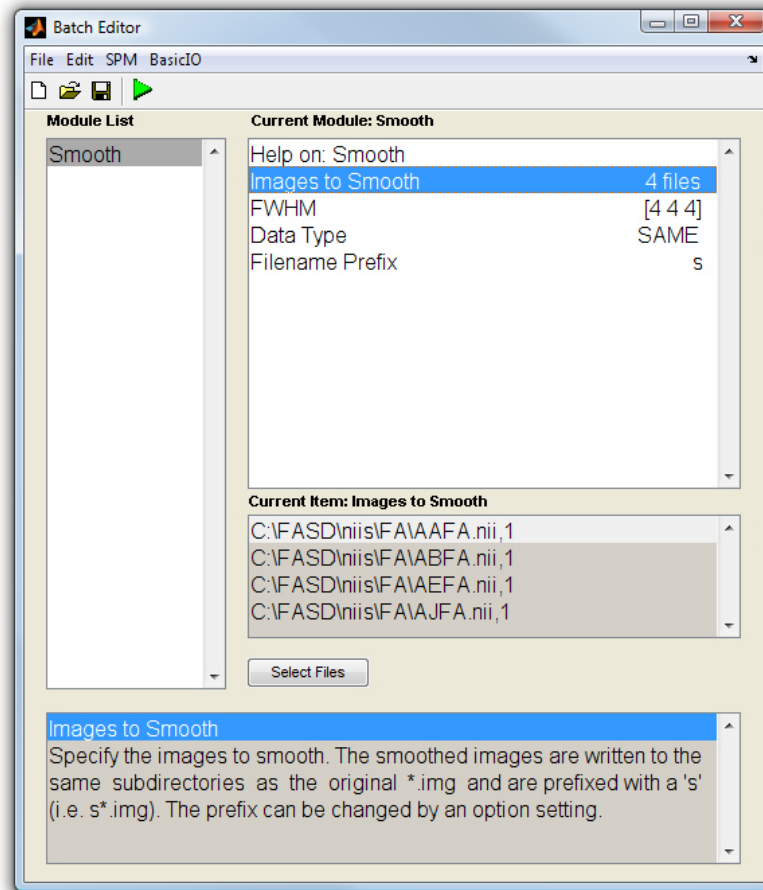


Figure E.2: SPM: Smooth

appropriate full width half-maximum under **FWHM**. The value for FWHM should be chosen with consideration of the original resolution of the data. Smoothed images will be saved with an 's' appended to the front of the name of the original (normalized) file. Many subjects can be run at once simply by selecting all files under **Images to Smooth**.

### E.3 Statistical Analysis

Statistical analysis for VBM in SPM is done in three parts. First, the analysis is set up, then the contrasts are estimated, and then the results can be explored.

1. Select **Specify 2nd-level** in SPM. The type of statistical test is selected under **Design**, for example, **Two-sample t-test** can be used to

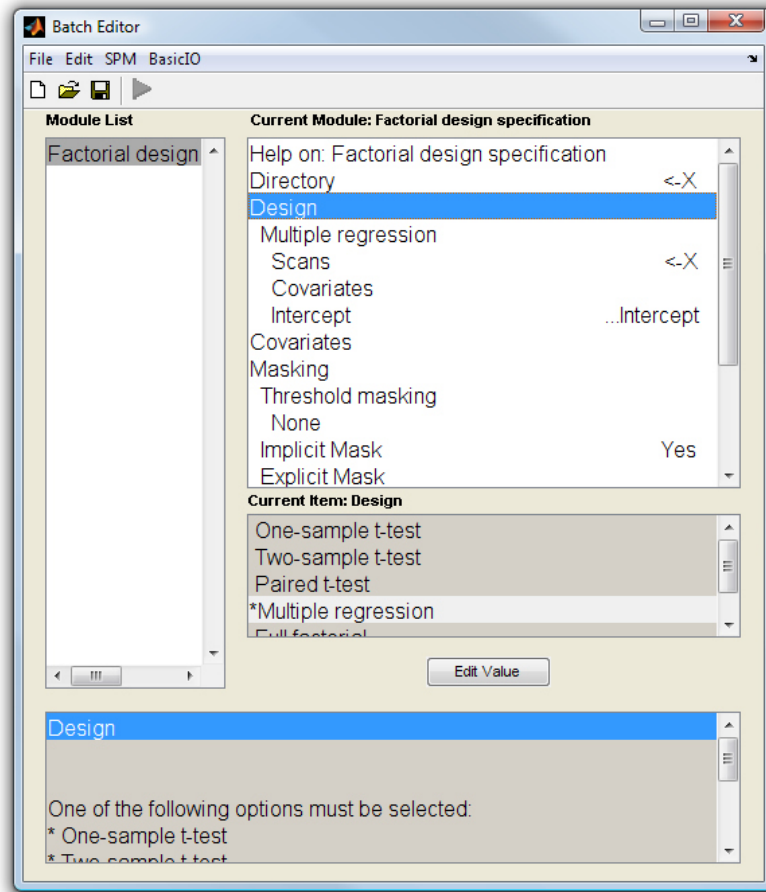


Figure E.3: SPM: Specify 2nd-level

test for group differences, or **Multiple regression** can be used to test correlations with another variable. After selecting the type of test, the scans are selected, under **Scans**. Covariates (e.g., age, reading score, etc) can be added under **Covariates**, but must be in the same order as the selected scans. **Threshold masking** can be used to test only white matter, by including an absolute threshold of 0.2 (for example) for FA. This means that if a particular voxel has a value  $\leq 0.2$  in any subject, it will be excluded from the analysis. This ensures that only white matter is analyzed. **Directory** is where the results of the analysis will be saved.

2. Once the second-level analysis has been specified and run, the **Estimate** function must be used. Simply open **Estimate** and select the SPM.mat file created by running the second-level analysis.

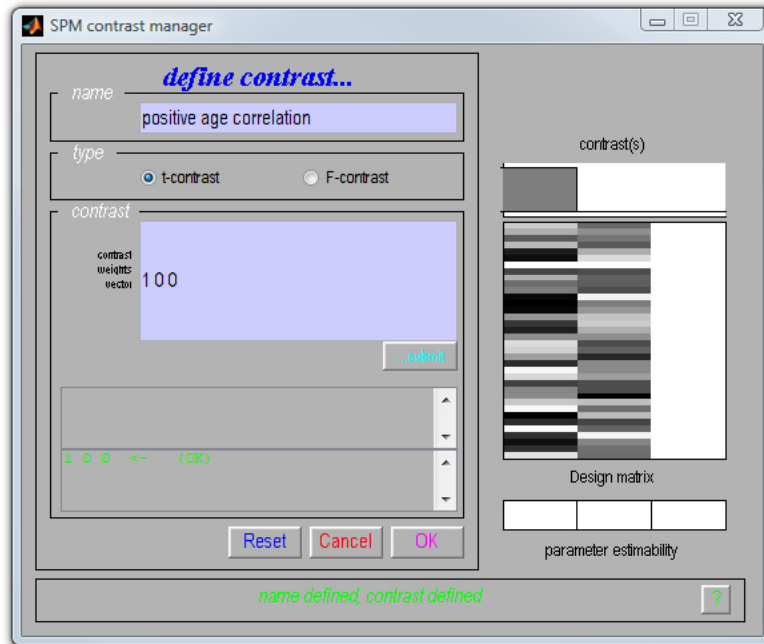


Figure E.4: SPM Results: Contrast

3. After running **Estimate**, the results can be explored. Select **Results** in SPM and select the SPM file created by second-level analysis and previously estimated. After selecting the file, contrasts must be defined. This is the tricky part, but advice on how to best select contrast matrices can be found on the SPM website in the documentation section at <http://www.fil.ion.ucl.ac.uk/spm/doc/>.

For example, in a multiple regression analysis with two variables, you may be interested in correlations with age (Figure E.4). A t-contrast can be created to test for positive correlations with age. This contrast will be a 1x3 vector,  $[1\ 0\ 0]$ . A negative correlation with age would be  $[-1\ 0\ 0]$ . A t-test will test significance in one direction only (e.g., positive correlation, Group A > Group B), while an F-test will examine significance in both directions (positive and negative correlations, Group A different from Group B). An F-test for correlations with age would look like  $[1\ 0\ 0; -1\ 0\ 0]$ .

After designing a contrast, you will go through a few SPM options. You can **mask with other contrast(s)**, although it is unlikely that this will

be useful.

Since many voxels across the brain are compared at once, multiple comparisons are a concern. There are several ways to correct for this, including SPM's built-in family-wise error (FWE) correction. This is very stringent, especially if you are only examining white matter, so I prefer to choose **none** and use other methods for multiple comparison correction (see section 10.2.4 for details). The **threshold** is the per voxel statistical threshold for significance, and the **extent threshold** is the number of significant voxels that must be adjacent (forming a cluster) to be considered significant overall. This helps to prevent spurious results.

Once the parameters are chosen for displaying results, the significant brain regions will appear in the SPM window. They can be overlaid on FA or T1 maps and explored (see Figure E.5). Results can also be displayed in numeric form (with cluster size, location, and significance) using the **whole brain** button under **p-values**. Clusters can also be saved using **save** for later use or display in Matlab, MRICro or other programs.

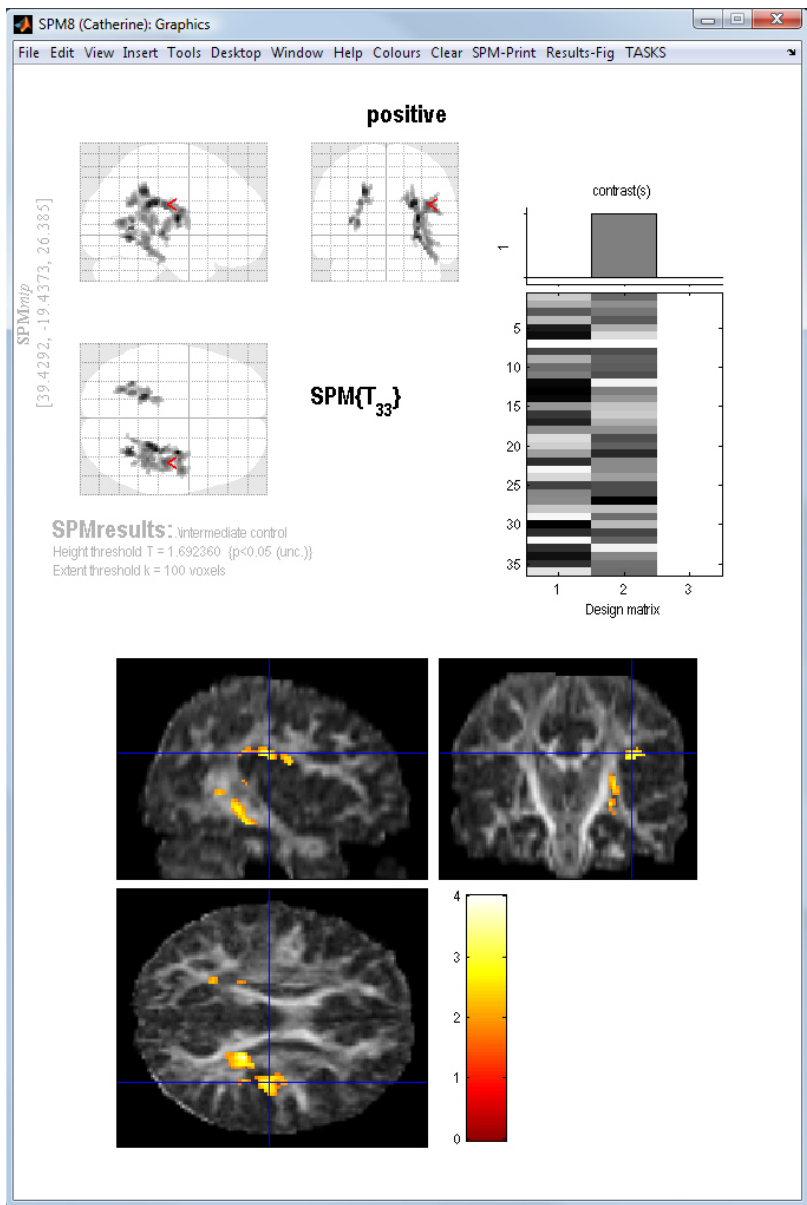


Figure E.5: SPM Results

# Appendix F

## Stereograms

Similar to Magic Eyes, stereograms provide depth to an image - try these out and see what you can see! To view, cross your eyes until you see four images, then adjust your eyes and allow middle two images to overlap, forming three total, and focus on the centre image.

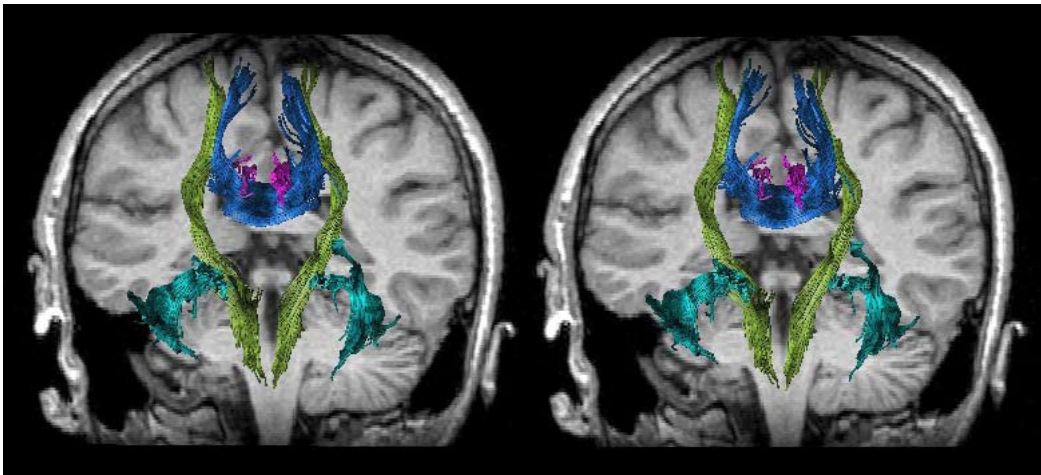


Figure F.1: Tracts on a coronal brain slice: corticospinal tracts (green), uncinate fasciculus (cyan), body of the corpus callosum (blue), and cingulum (pink). Front of brain is out of page toward you.

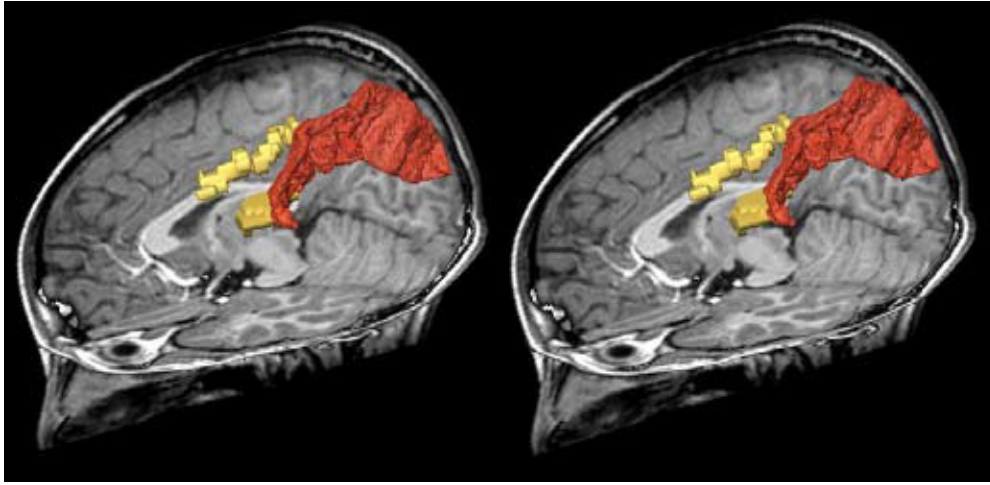


Figure F.2: Clusters with significant FA-math correlations in the left parietal lobe (from Chapter 10). The intraparietal sulcus (IPS) is shown in red.

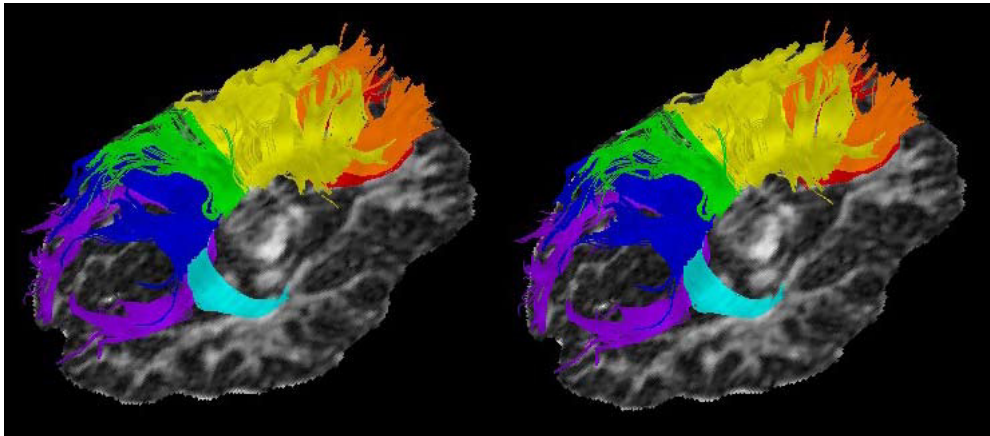


Figure F.3: The seven subdivisions of the corpus callosum shown on an axial FA map. Colours follow the rainbow (red to purple) from front to back: orbital frontal, anterior frontal, superior frontal, superior parietal, posterior parietal, temporal, and occipital sections.

